Aspects of the Invariant Spin Field for High Energy Polarized Proton Beams

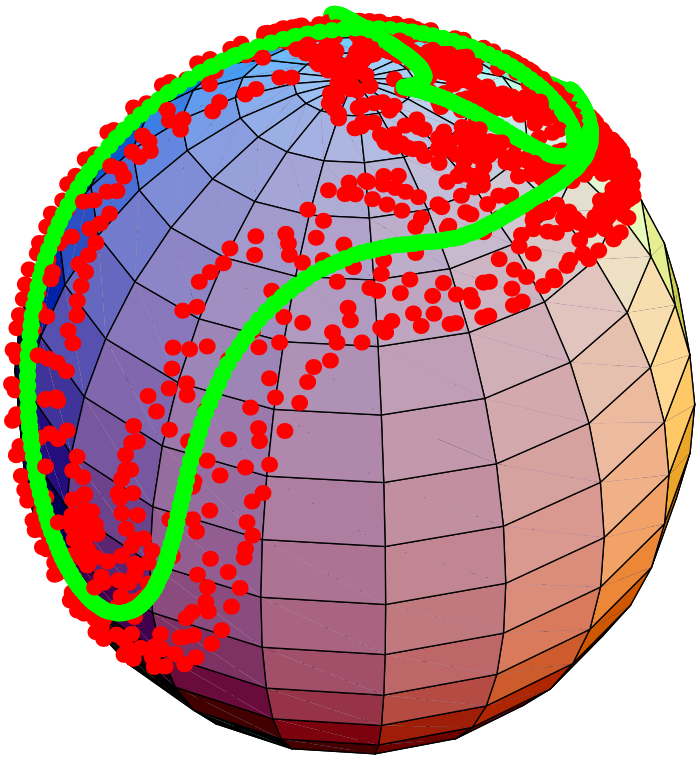

Aspects of the Invariant Spin Field for High Energy Polarized Proton Beams

Dem Fachbereich Physik der Technischen Universität Darmstadt

als

Habilitationsschrift

vorgelegt von

Georg Heinz Hoffstätter

Januar 2000

ABSTRACT

ASPECTS OF THE INVARIANT SPIN FIELD FOR HIGH ENERGY POLARIZED PROTON BEAMS

By

Georg Heinz Hoffstätter

So far polarized proton beams have never been accelerated to energies higher than about 25GeV. Up to these energies the beam polarization is quite undisturbed when the accelerator is well adjusted, except at special energies where resonances occur. In particular, it has not been necessary to study the variation of the protons' spin direction across the phase space of the beam. Taking the pre–accelerators of HERA–p at DESY as an example, methods will be described which have already been established in the AGS at the Brookhaven National Laboratory and which could therefore be used to avoid a reduction of the polarization at resonance energies. But when accelerating to energies of several hundred GeV as in RHIC, TEVATRON, or HERA–p, new phenomena can occur which can lead to a significantly diminished beam polarization. For these high energies, it is necessary to look in more detail at the spin motion at each point in phase space and the *invariant spin field* will prove to be a useful tool. This is a vector field over the phase space of the proton beam which describes a polarization state that is periodic from turn to turn, and it is already widely used for the description of high energy electron beams which become polarized by the emission of spin–flip synchrotron radiation.

It will be proven that this field gives rise to an adiabatic invariant of spin–orbit motion and that it defines the maximum time average polarization that is usable in a particle physics experiment. Furthermore, the invariant spin field allows the amplitude dependent spin tune to be defined and computed and thereby opens the way to a clear evaluation of the effects of higher–order spin–orbit resonances. In particular the strengths and the depolarizing effects of these resonances can only be determined once the amplitude dependent spin tune has been computed.

These concepts make it possible to optimize HERA–p for acceleration and storage of a polarized proton beam. For example, it will be shown that schemes with 4 and 8 Siberian Snakes can be so chosen that the influence of higher–order spin–orbit resonances, the spread of the spin tune over the particle amplitudes in the beam, and the variation of the invariant spin field over orbital phase space are reduced and then polarization can be maintained for a significantly increased region of the beam while accelerating to high energy and therefore more polarization can be delivered for particle physics experiments.

The utility of the invariant spin field will be illustrated by simulations of spin motion up to 920GeV in HERA–p and various methods for computing the invariant spin field, the adiabatic spin invariant, and the amplitude dependent spin tune will be presented. Moreover, several high energy spin–orbit dynamical effects will be discussed which go beyond conventional models of spin dynamics and were observed with these novel methods.

Contents

Chapter 1

Introduction

This report describes phenomena which occur when accelerating polarized proton beams to energies of several hundred GeV. In addition to introducing concepts and techniques which are relevant to all very high energy rings, this report will illustrate them by a study of the feasibility of obtaining very high energy polarized protons in HERA, the "Hadron–Electron–Ring–Anlage" at DESY in Hamburg. HERA has an $e^{\pm}$ ring (HERA–e) and a proton ring (HERA–p) and they are contained in the same 6335m long tunnel. HERA–p stores protons at 920GeV and HERA–e stores $e^{\pm}$ at 27.5GeV for typically about 10 hours. The tunnel of HERA contains the proton ring as well as a 27.5GeV electron ring. Both rings have 4 straight sections and 4 arcs which bend the beams by $\pi/2$. Proton and electron beams are brought to collision in two experimental detectors, H1 in the North and ZEUS in the South. The East straight section contains HERMES, a fixed target experiment for the electron beam and the West straight section contains HERA–B, a fixed target experiment for the proton beam. This layout is sketched in figure 1.1.

The electron or positron beam in HERA–e becomes polarized by spin–flip synchrotron radiation [1, 2]. When the disturbing effects of misalignments are compensated, a polarization of 60% can routinely be obtained. Around the HERMES experiment, spin rotators consisting of interleaved vertical and horizontal bends have been installed, which disturb the orbit only marginally but orient the polarization parallel to the beam direction in the HERMES experiment while it remains vertical in the arcs. Installing such spin rotators in a high energy storage ring while keeping a high degree of the self–polarizing mechanism was only possible after spin matching of spin–orbit motion [3, 4, 5, 6, 7]. This has not been achieved in any other laboratory and the attainment of longitudinally polarized electron or positron beams in HERA–e was, and still is, a unique achievement.

The HERMES experiment studies interactions of the polarized electron or positron beam with polarized nuclei in an internal gas target. The center of mass energy of these collisions is approximately 7GeV. A 920GeV polarized proton beam in HERA–p would allow measurements at center of mass energies of up to 318GeV for collisions between polarized protons and polarized electrons in the detectors H1 and ZEUS to be made. In a future experiment, collisions of the polarized protons with a polarized gas target at 42GeV center of mass energy could also be investigated. A

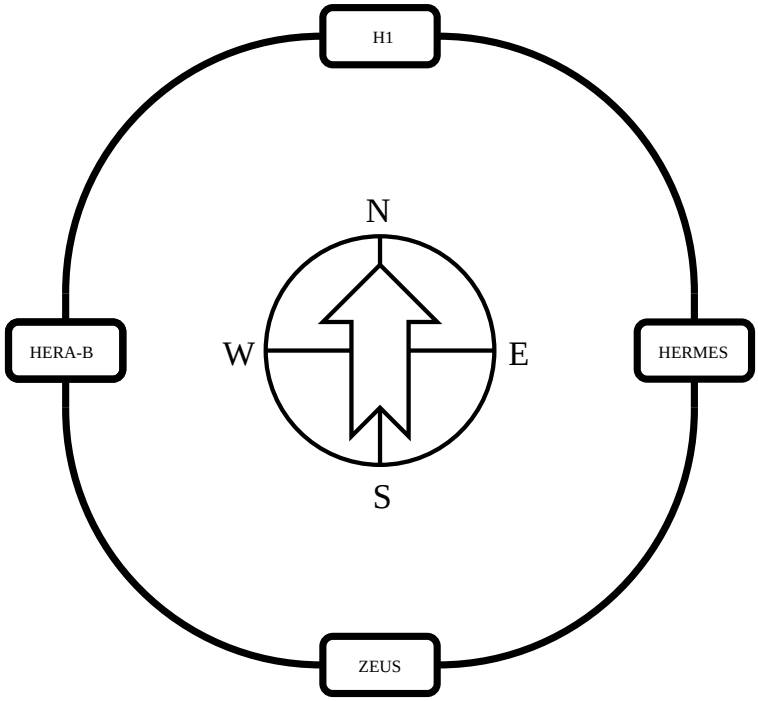

Figure 1.1: Schematic view of the HERA ring.

very active group of many high energy physicists has already been studying which experiments could be performed with polarized protons and electrons at HERA energies [8, 9, 10, 11].

The spin flip synchrotron radiation leads to a typical polarization buildup time of roughly $\tau = \tau_{ST}\frac{2\pi\rho}{L}$ [12, 13]

$$\frac{1}{\tau_{ST}} = C\frac{1}{\rho^3}\frac{E^5}{(mc^2)^7} \tag{1.1}$$

with the constant $C = 0.92214 \cdot 10^{-7}(\mathrm{eV})^2\mathrm{m}^3\mathrm{s}^{-1}$. The fraction between the bending radius ρ of the main dipoles and the length $L = 6335\mathrm{m}$ of the ring takes the absence of synchrotron radiation between the dipoles into account. With the bending radius of $\rho = 608\mathrm{m}$ for the main dipoles of the electron ring HERA–e, the characteristic buildup time is 38 minutes. The energies in modern proton accelerators are still too low to produce a sufficient amount of synchrotron radiation for polarization buildup. For protons in HERA–p with $\rho = 583\mathrm{m}$, the corresponding buildup time would be $7 \cdot 10^{10}$ years. For this reason, the energy of polarized proton beams has not increased along with the achievement of higher and higher energies for unpolarized proton beams. So far no polarized proton beam with momentum above 25GeV/c has been produced [14, 15, 16, 17]. But theoretical and numerical studies of very high energy polarized proton acceleration have been undertaken for high energy rings, namely for RHIC (250GeV/c) [18], TEVATRON (900GeV/c) [19], and HERA–p (920GeV/c) [20, 21, 22, 23, 24, 25, 26, 27]. The study presented here will add to the studies for HERA–p.

Since the protons in HERA–p do not become polarized by spin flip synchrotron radiation, methods for obtaining polarized proton beams will be completely different from the well established methods of obtaining polarized electron beams. Various ideas for creating a polarized high energy proton beam have been discussed:

- Resonance excitation by the Stern–Gerlach Effect. This method has not been tested and requires very difficult phase space manipulations [28, 29, 30, 31, 32].
- Spin flipping by scattering the proton beam on a polarized electron beam. The polarization buildup would be too slow [33, 34] and protons would get lost due to the scattering process.
- Spin filtering with a polarized internal target. This method has been tested and is understood for low energies [35, 36]. For high energies the polarization buildup would be too slow.
- Acceleration of polarized protons after creation in a polarized source. This method has been tested at several accelerators [37, 14].

Here I concentrate on the last possibility since all of these ideas except the last are currently either too difficult or not very promising. In this scenario polarized protons are produced in a polarized H^- source. A proton beam at DESY is then accelerated by an RFQ to 750keV, then by the LINAC III to 50MeV, by the DESY III synchrotron to a momentum of 7.5GeV/c, by the PETRA synchrotron to 40GeV/c and then by HERA–p to 920GeV/c. This accelerator chain is shown in figure 1.2. The 4 main challenges for the DESY polarized proton project are therefore

- Production of a 20mA pulsed H^- beam.
- Polarimetry at various stages in the acceleration chain.
- Acceleration through the complete accelerator chain with little loss of polarization.
- Storage of a polarized beam at the top energy over many hours with little loss of polarization.

Today polarized proton beams can be produced either by a polarized atomic beam source (ABS) or in an optically pumped polarized ion source (OPPIS). Pulsed beams with polarization of up to 87% for 1mA H^- beam current [38, 39] and up to 60% for 5mA [40], respectively, have been achieved with these sources. Compared with the 60mA of DESY's current source this sounds rather limited. However experts claim that currents of up to 20mA could be possible in OPPIS sources [41, 40]. The maximal currents of 205mA in DESY III can already be achieved with such a source current. If DESY III were to become capable of handling more current, then the transfer efficiency of DESY's low energy beam transport (LEBT) and of the radio frequency quadrupole (RFQ) which is around 50% would have to be improved.

For polarization monitoring and optimization, polarimeters will have to be installed at several crucial places in the accelerator chain. The source would contain

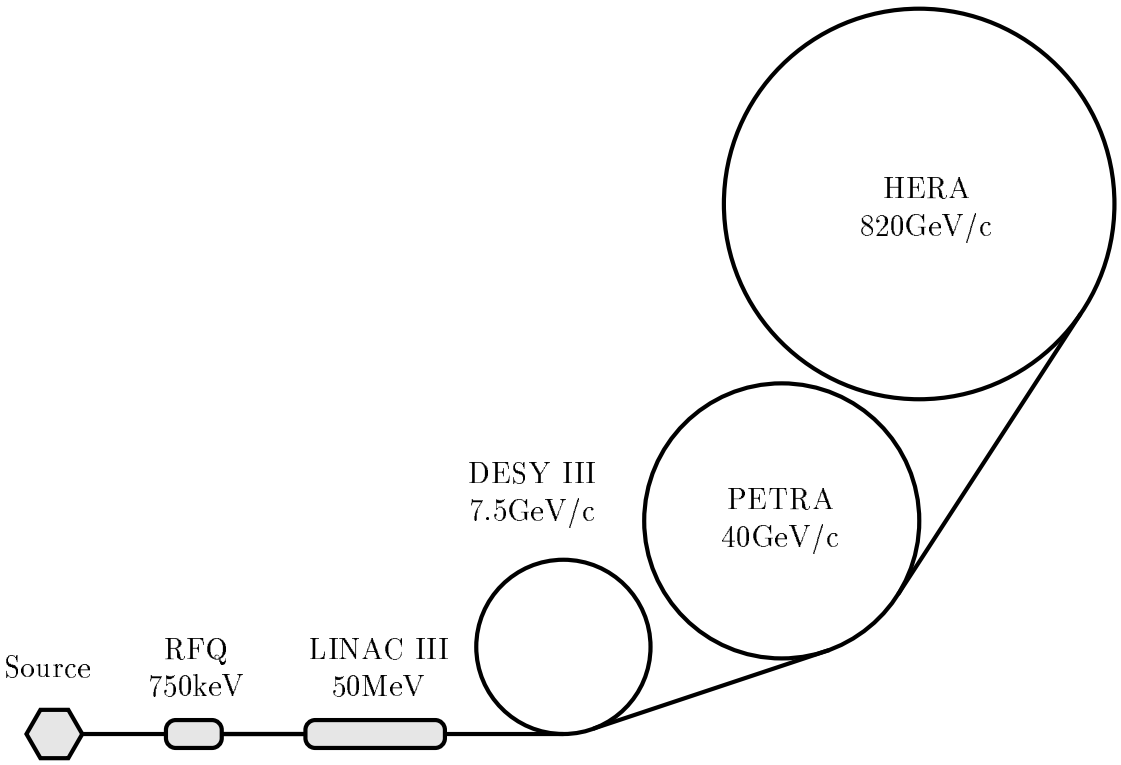

Figure 1.2: The accelerator chain for HERA–p.

a Lyman–α polarimeter. This does not disturb the beam [42]. Another polarimeter could be installed after the RFQ at 750keV [43]. This could not be operated continuously since it disturbs the beam. The transfer of polarized particles through LINAC III has to be optimized with the aid of yet another polarimeter which could be similar to that of the AGS LINAC [37]. Each of the other accelerator rings will need its own polarimeter. The polarimeter for DESY III could be similar to the AGS internal polarimeter.

Since polarization at the DESY III momentum of up to 7.5GeV/c has been achieved at several labs, the technology of all the polarimeters mentioned so far is well understood. It is different with the polarimeters required for PETRA and HERA–p energies; for these high energies there is no established polarimeter. Here one has to wait and see how the novel techniques envisioned and developed for RHIC [44, 45] will work.

The problems arising when accelerating polarized proton beams in DESY III and in PETRA will briefly be discussed, but since polarized beams at these energies have already been produced by other accelerators, the main emphasis of the work presented here will be on polarization dynamics in the high energy region which would be unique to HERA–p. After a polarized proton beam has been accelerated to the high energy of 920GeV, the polarization has to be stable for several hours in order to be useful for the experiments H1 and ZEUS. Furthermore the polarization

in all parts of the beam has to be nearly parallel during this storage time.

After a review in section 2.1 of the various ways of formulating spin motion which will be used in this report, it will be shown in section 2.2 that the concept of an invariant spin field is essential to our understanding of both acceleration and storage of polarized protons. The beam average of this field describes the maximum polarization available for particle physics experiments during the storage time of several hours. It will be shown that this maximum polarization depends on the particle energy and that it can be strongly reduced at critical energies. Furthermore this field allows to define an amplitude dependent spin tune which is in resonance with the orbital tunes at these critical energies, and that in turn allows higher–order resonances to be analyzed. Crossing these resonances while accelerating the beam can lead to a reduction of polarization. I will derive how the invariant spin field and the amplitude dependent spin tune can be used to compute the higher–order resonance strength and to describe this reduction of polarization.

An analysis of the ranges of applicability of linearized spin–orbit motion in section 3.1 will show, that higher–order effects have to be taken into account at HERA–p energies of up to 920GeV. Nevertheless this approximation is successfully used to find optimal schemes of Siberian Snakes for HERA–p.

Methods for computing the invariant spin field and the amplitude dependent spin tune non–perturbatively are introduced in chapter 4. They are used to show that the optimization of snake schemes is important for HERA–p but can not eliminate all destructive higher–order resonance effects. The phase space amplitudes of particles for which the polarization is not significantly reduced with the most optimized scheme of 8 Siberian Snakes leads to a limit for the proton emittance with which a polarized beam can be accelerated in HERA–p according to current knowledge and technology.

The novel methods for using the invariant spin field to analyze spin dynamics at high proton energies which will be emphasized in this report have become the basis of a very detailed analysis of the acceleration process in HERA–p [46] and are also becoming adopted by the RHIC group [47] for simulations of polarized beam in the AGS and of their planned 250GeV polarized proton beam, which is scheduled for 2002.

Chapter 2

Spin Dynamics

2.1 The Equation of Spin Motion

The expectation value of the vector operator representing the spin of a particle satisfies the equation of motion of a classical spin vector. Viewed in the particle's instantaneous rest frame, the direction of this expectation value will here be denoted by *the spin* $\vec{s}$ with $|\vec{s}| = 1$. This direction is $\frac{2}{\hbar}$ times the expectation value. The polarization P of a beam is defined as the absolute value of the spin average taken over all N particles of the beam,

$$P = |\frac{1}{N}\sum_{j=1}^{N}\vec{s}_j| = |<\vec{s}>_N| \ . \tag{2.1}$$

The expectation value $\vec{s}$ changes with the time t of the laboratory frame according to the Thomas–Bargmann–Michel–Telegdi (T-BMT) equation [48, 49, 50, 51]

$$\frac{d}{dt}\vec{s} = \vec{\Omega}_{BMT}(\vec{r},\vec{p}) \times \vec{s} \ . \tag{2.2}$$

The precession vector $\vec{\Omega}_{BMT}(\vec{r},\vec{p})$ depends on the particle's position $\vec{r}$ and its momentum $\vec{p}$. It can be expressed by the electric and magnetic fields $\vec{E}(\vec{r},t)$ and $\vec{B}(\vec{r},t)$, by the particle's charge q and its rest energy mc^2, the relativistic factor γ, and by the particle's anomalous gyro-magnetic g-factor $G = (g-2)/2$ in the following way:

$$\vec{\Omega}_{BMT}(\vec{r},\vec{p}) = -\frac{q}{m}[(\frac{1}{\gamma}+G)\vec{B} - \frac{G\vec{p}\cdot\vec{B}}{\gamma(\gamma+1)m^2c^2}\vec{p} - \frac{1}{mc^2\gamma}(G+\frac{1}{1+\gamma})\vec{p}\times\vec{E}] \ . \tag{2.3}$$

All frame dependent quantities are taken in the laboratory frame. The anomalous g-factor is about 1.793 for protons and about 0.00116 for electrons.

2.1.1 Spin motion in Flat Circular Accelerators

When introducing the components of the magnetic field $\vec{B}_\perp$ and $\vec{B}_{||}$ which are perpendicular and parallel to the particle's momentum, the Lorentz force equation and

the T-BMT equation in purely magnetic fields show some similarities,

$$\frac{d}{dt}\vec{p} = -\frac{q}{m\gamma}\{ \quad \vec{B}_\perp \quad \} \times \vec{p}\,, \tag{2.4}$$

$$\frac{d}{dt}\vec{s} = -\frac{q}{m\gamma}\{(G\gamma+1)\vec{B}_\perp + (1+G)\vec{B}_\parallel\} \times \vec{s}\,. \tag{2.5}$$

In a solenoid magnet, $\vec{B}_\parallel$ produces a spin rotation around the longitudinal direction. In transverse magnetic fields, where $\vec{B}_\parallel = 0$, several conclusions can immediately be drawn from these equations. This case is relevant, since a flat circular accelerator has only vertical magnetic fields in the center plane.

- In such a transverse magnetic field, the momentum $\vec{p}$ rotates in the plane perpendicular to the field. If $\vec{s}_p$ describes the spin in a coordinate system which rotates with the particle's momentum, the equation of spin motion relative to the particle motion becomes $\frac{d}{dt}\vec{s}_p = -\frac{q}{m}G\vec{B}_\perp \times \vec{s}_p$. The spin rotation relative to the orbit motion is therefore independent of energy, in contrast to the orbit deflection which varies like $1/\gamma$. For protons with velocity v close to the speed of light, a fixed field integral of $\int Bdl = \pi\frac{mcv}{qG} \approx 5.48$Tm leads to a spin rotation of π. Electrons require a field integral of 4.62Tm for a rotation angle of π. For fixed orbit deflections and thus fixed ratio of $\vec{B}_\perp/\gamma$, the spin precession rate, however, increases with energy.

- If the orbit is deflected by an angle ϕ in a transverse magnetic field, then the spin is rotated by an angle $G\gamma\phi$ relative to the orbit. A 1mrad orbit kick for a proton with 920GeV energy produces 100° of spin rotation. For electrons with 27.5GeV in HERA-e, such an orbit kick produces 3.6° of spin rotation.

- In a flat ring, the orbit deflection angle of 2π during one turn leads to $G\gamma$ full spin rotations around the vertical direction relative to the particle's direction. For 920GeV these are 1756 such rotations. This number of spin rotations performed during one turn along the closed orbit is called the closed-orbit spin tune ν_0 . A 27.5GeV electron beam in HERA-e has $\nu_0 = 62.5$.

- Whenever the energy of a proton is increased by 523MeV, the spin rotates once more per revolution around the ring. For an electron, this energy increase is 441MeV.

2.1.2 Spin Motion in the Curvilinear Coordinate System

The design trajectory of a particle accelerator is described by a space curve $\vec{R}(l)$ with $|d\vec{R}(l)| = dl$. A coordinate system is defined relative to this curve with the second unit vector tangential to the curve and the first and third unit vectors chosen to obtain a right handed orthonormal set of vectors called an orthonormal dreibein. The first and third unit vectors therefore lie in a plane perpendicular to the curve.

The orientation of the unit vectors in that plane is arbitrary and can change along the curve. The Frenet-Serret coordinate system is defined by

$$\vec{t}_2 = \frac{d}{dl}\vec{R}(l) \ , \quad \frac{1}{\rho} = |\frac{d}{dl}\vec{t}_2| \ , \quad \vec{t}_1 = -\rho\frac{d}{dl}\vec{t}_2 \ , \quad \vec{t}_3 = \vec{t}_1 \times \vec{t}_2 \ , \quad T = -\vec{t}_3 \cdot \frac{d}{dl}\vec{t}_1 \ , \quad (2.6)$$

where the torsion of the space curve $\vec{R}(l)$ is given by T . From these definitions and with $\frac{d}{dl}(\vec{t}_1 \cdot \vec{t}_2) = \vec{t}_2 \cdot \frac{d}{dl}\vec{t}_1 - \frac{1}{\rho} = 0$ it follows that

$$\frac{d}{dl}\vec{t}_1 = -T\vec{t}_3 + \frac{1}{\rho}\vec{t}_2 \ , \quad \frac{d}{dl}\vec{t}_3 = -\vec{t}_2 \times \frac{d}{dl}\vec{t}_1 = T\vec{t}_1 \ . \quad (2.7)$$

A space vector $\vec{r}$ is specified by l and by the two coordinates x and y via

$$\vec{r} = \vec{R}(l) + x\vec{t}_1(l) + y\vec{t}_3(l) \ . \quad (2.8)$$

A space curve is then specified by the two functions $x(l)$ and $y(l)$. The derivative with respect to l of such a space curve $\vec{r}(l)$ is given by

$$\frac{d}{dl}\vec{r}(l) = (\frac{d}{dl}x + Ty)\vec{t}_1 + (\frac{d}{dl}y - Tx)\vec{t}_3 + (1 + \frac{x}{\rho})\vec{t}_2 \ . \quad (2.9)$$

To remove the torsion T from the equation of motion, one introduces the unit coordinate vectors $\vec{e}_x$, $\vec{e}_l$, $\vec{e}_y$ by winding back the rotation which is due to the torsion,

$$\vartheta = \int_{l_0}^{l} T(\tilde{l})d\tilde{l} \ , \quad \vec{e}_x + i\vec{e}_y = e^{i\vartheta}(\vec{t}_1 - i\vec{t}_3) \quad \vec{e}_l = \vec{t}_2 \ . \quad (2.10)$$

The coordinate system with the unit vectors $\vec{e}_x$, $\vec{e}_l$, $\vec{e}_y$ is shown in figure 2.1 and is called the curvilinear coordinate system. It follows that

$$\frac{d}{dl}\vec{e}_x + i\frac{d}{dl}\vec{e}_y = e^{i\vartheta}\{-T\vec{t}_3 + \frac{1}{\rho}\vec{t}_2 - iT\vec{t}_1 + iT(\vec{t}_1 - i\vec{t}_3)\} = \frac{e^{i\vartheta}}{\rho}\vec{e}_l \ . \quad (2.11)$$

For the right handed orthonormal dreibein $[\vec{e}_x, \vec{e}_l, \vec{e}_y]$ of the curvilinear coordinate system [52, 53], one obtains

$$\begin{aligned}
\frac{d}{dl}\vec{R}(l) &= \vec{e}_l \ , \quad \vec{r} = \vec{R}(l) + x\vec{e}_x + y\vec{e}_y \ , & (2.12)\\
\frac{d}{dl}\vec{e}_x &= \frac{\cos\vartheta}{\rho}\vec{e}_l \ , \quad \frac{d}{dl}\vec{e}_y = \frac{\sin\vartheta}{\rho}\vec{e}_l \ , & (2.13)\\
\frac{d}{dl}\vec{e}_l &= -\frac{1}{\rho}\vec{t}_1 = -\frac{1}{\rho}(\cos\vartheta\vec{e}_x + \sin\vartheta\vec{e}_y) \ , & (2.14)\\
\frac{d}{dl}\vec{r} &= \vec{e}_x\frac{d}{dl}x + \vec{e}_y\frac{d}{dl}y + (1 + \frac{x\cos\vartheta + y\sin\vartheta}{\rho})\vec{e}_l \ . & (2.15)
\end{aligned}$$

For ease of notation, one can use $\vec{x} = (x, y)^T$, $\vec{\kappa} = (\cos\vartheta, \sin\vartheta)^T/\rho$, and $h = 1 + \vec{x}\cdot\vec{\kappa}$. Vectors like $\vec{p}$ which have a component in the $\vec{e}_3$ direction are described by

$$\begin{aligned}
\vec{p} &= p_x\vec{e}_x + p_y\vec{e}_y + p_l\vec{e}_l & (2.16)\\
\frac{d}{dl}\vec{p} &= (\frac{d}{dl}p_x - p_l\kappa_x)\vec{e}_x + (\frac{d}{dl}p_y - p_l\kappa_y)\vec{e}_y + (\frac{d}{dl}p_l + p_x\kappa_x + p_y\kappa_y)\vec{e}_l \ . & (2.17)
\end{aligned}$$

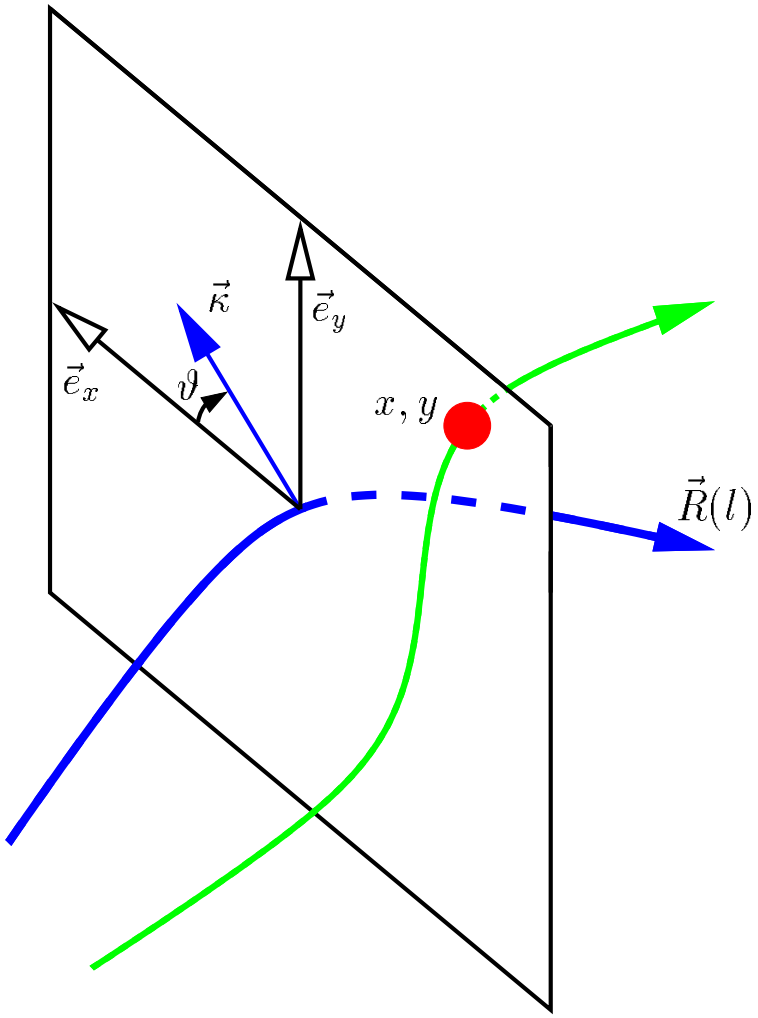

Figure 2.1: The unit vectors $\vec{e}_x$ and $\vec{e}_x$, the curvature vector $\vec{\kappa}$ of the design curve $\vec{R}(l)$ and the generalized coordinates x, y, and l of the curvilinear coordinate system. This system is rotated by θ with respect to the Frenet-Serret coordinate system.

To find the equations of particle motion in the curvilinear coordinate system, the independent coordinates in the equations of motion is changed from time t to arc length l by using

$$\frac{dt}{dl} = (\vec{e}_l \cdot \frac{d}{dl}\vec{r})/(\vec{e}_l \cdot \frac{d}{dt}\vec{r}) = \frac{h}{v}\frac{p}{p_l} \ , \tag{2.18}$$

where v is the velocity and $p = |\vec{p}|$ is the momentum. Properties of a reference particle moving on the design trajectory are We indicated by subscripts 0 and define the coordinates of all other particles relative to this reference particle through

$$x \ , \quad a = \frac{p_x}{p_0} \ , \quad y \ , \quad b = \frac{p_y}{p_0} \ , \quad \tau = (t_0 - t)\frac{K_0}{p_0} \ , \quad \delta = \frac{K - K_0}{K_0} \ . \tag{2.19}$$

where $K = mc^2(\gamma - 1)$ is the kinetic energy. These six phase space variables are denoted by the phase space vector $\vec{z}$. The coordinate pairs (x, a), (y, b), and (τ, δ)

are canonically conjugate [54, 55]. Since $\vec{R}(l)$ is the path of the reference particle, the particle transport is origin preserving, because a particle with $\vec{z} = 0$ will continue to travel along the design trajectory. The equation of motion for these phase space coordinates with l as independent variable [55, 53] is obtained by transforming the Lorentz force equation. Here I neglect the Stern–Gerlach forces since they are very small in comparison with the Lorentz force and since no practical schemes for using this force have been found so far [28, 29, 30, 31, 32].

To transform the equations of spin motion into the curvilinear coordinate system, $\frac{d}{dl}t = \frac{h}{v}\frac{p}{p_l}$ from equation (2.18) is used. The spin direction $\vec{s}$ is expressed by its components in the curvilinear coordinate system and the column vector of these components is written as $\vec{S}$. A potential torsion of the reference curve does not enter the equations of particle motion in this coordinate system and it also does not enter the equation of spin motion,

$$\begin{aligned} \vec{s} &= S_x\vec{e}_x + S_y\vec{e}_y + S_l\vec{e}_l \ , & (2.20)\\ \frac{d}{dl}\vec{s} &= (\frac{d}{dl}S_x - S_l\kappa_x)\vec{e}_x + (\frac{d}{dl}S_y - S_l\kappa_y)\vec{e}_y + (\frac{d}{dl}S_l + S_x\kappa_x + S_y\kappa_y)\vec{e}_l \\ &= \frac{h}{v}\frac{p}{p_l}\vec{\Omega}_{BMT}(\vec{r},\vec{p}) \times \vec{s} \ . & (2.21) \end{aligned}$$

For the column vector $\vec{S}$, the equation of motion is therefore given by

$$\frac{d}{dl}\vec{S} = \{\vec{\Omega}_{BMT}(\vec{r},\vec{p})\frac{hp}{vp_l} - \vec{\kappa} \times \vec{e}_l\} \times \vec{S} \ . \qquad (2.22)$$

The precession vector depends on the position and the momentum. This can be expressed as a dependence on l and on the 6 dimensional phase space variable $\vec{z}$.

2.1.3 Equation of Motion for Spins and Spin Fields

In a circular accelerator with circumference L, it is convenient to choose the azimuth $\theta = 2\pi l/L$ as independent variable, rather than the arc length l of the design trajectory. The coordinate vectors are not changed, with $\vec{e}_\theta = \vec{e}_l$. All fields are then 2π periodic in θ. The equation of particle motion is therefore 2π periodic,

$$\begin{aligned} \frac{d}{d\theta}\vec{z} &= \vec{v}(\vec{z},\theta) \ , \quad \vec{v}(\vec{z},\theta+2\pi) = \vec{v}(\vec{z},\theta) \ , & (2.23)\\ \frac{d}{d\theta}\vec{S} &= \vec{\Omega}(\vec{z},\theta) \times \vec{S} \ , \quad \vec{\Omega}(\vec{z},\theta+2\pi) = \vec{\Omega}(\vec{z},\theta) \ , & (2.24) \end{aligned}$$

where the precession vector is obtained from equation (2.22) as

$$\vec{\Omega}(\vec{z},\theta) = \frac{L}{2\pi}(\vec{\Omega}_{BMT}(\vec{r},\vec{p})\frac{hp}{vp_l} - \vec{\kappa} \times \vec{e}_l) \ . \qquad (2.25)$$

A particle starting with an initial phase space coordinate $\vec{z}_i$ and with an initial spin $\vec{S}_i$ propagates around an accelerator according to the equations of spin-orbit

motion (2.24). After it has traveled from azimuth θ_0 to θ, it will have the coordinates $\vec{z}(\theta) = \vec{M}(\vec{z}_i, \theta_0; \theta)$ and $\vec{S}(\theta) = \underline{R}(\vec{z}_i, \theta_0; \theta)\vec{S}_i$, where $\vec{M}(\vec{z}_i, \theta_0; \theta)$ is called the transport map and the orthogonal matrix $\underline{R}(\vec{z}_i, \theta_0; \theta)$ is called the spin transport matrix.

This rotation matrix can be computed by tracking three linearly independent spins along the phase space trajectory starting with $\vec{z}_i$ at azimuth θ_0. Transporting the nine real coefficients of these vectors is however not an efficient way of simulating spin motion, since a rotation can be described by three real numbers. Furthermore, the orthogonal structure of $\underline{R}$ does not change the angle between two spins which travel along the same trajectory and it does not change the length of a spin. These properties can be violated either by numerical errors or by computational approximations when individual spins are propagated. Therefore, more efficient methods will be introduced below.

A particle beam consists of particles at different phase space positions. Each particle can have a different spin direction. The function $\vec{f}(\vec{z}, \theta)$ describing the spin direction for a particle at phase space point $\vec{z}$ at azimuth θ is called a spin field. The equation of motion for a spin field is thus given by

$$\frac{d}{d\theta}\vec{f} = \partial_\theta \vec{f} + [\vec{v}(\vec{z}, \theta) \cdot \partial_{\vec{z}}]\vec{f} = \vec{\Omega}(\vec{z}, \theta) \times \vec{f} \; . \tag{2.26}$$

2.1.4 Equation of Motion for the Spin Transport Matrix

In the following sections I will investigate various methods for describing the propagation of spins and spin fields along particle trajectories. Inserting the relation $\vec{S}(\theta) = \underline{R}(\vec{z}_i, \theta_0; \theta)\vec{S}_i$ into the equation of motion (2.24) leads to the equation of motion for the spin transport matrix

$$\partial_\theta \underline{R}(\vec{z}_i, \theta_0; \theta) = \begin{pmatrix} 0 & -\Omega_3 & \Omega_2 \\ \Omega_3 & 0 & -\Omega_1 \\ -\Omega_2 & \Omega_1 & 0 \end{pmatrix} \underline{R}(\vec{z}_i, \theta_0; \theta) \; , \quad \underline{R}(\vec{z}_i, \theta_0; \theta_0) = \underline{1}_3 \; , \tag{2.27}$$

where $\underline{1}_3$ describes the 3×3 dimensional unit matrix. The spin rotation matrix for a particle trajectory which enters the nth particle optical element with $\vec{z}_{n-1}$ is computed by multiplying the spin transport matrices $\underline{R}_n(\vec{z}_{n-1})$ of the individual elements [56, 57]. This method has the same disadvantage as the transport of three individual spins. Nine real coefficients are transported, where three could already describe a rotation. Furthermore computational inaccuracies can again lead to violations of the orthogonal structure of the matrix, which therefore has to be orthogonalized whenever such violations become problematic.

Using the transport matrix, a spin is propagated by $\vec{S}(\theta) = \underline{R}(\vec{z}_i, \theta_0; \theta)\vec{S}_i$ and a spin field $\vec{f}(\vec{z}, \theta)$ can be propagated by

$$\vec{f}(\vec{z}, \theta) = \underline{R}(\vec{z}_i, \theta_0; \theta)\vec{f}(\vec{z}_i, \theta_0) \quad \text{with} \quad \vec{z}_i = \vec{M}(\vec{z}, \theta; \theta_0) \; . \tag{2.28}$$

Here the inverse transport map $\vec{M}(\vec{z}, \theta; \theta_0) = \vec{M}^{-1}(\vec{z}, \theta_0; \theta)$ describing the reverse motion from θ back to θ_0 has been used.

2.1.5 Equation of Motion for the Spin Transport Quaternion

As will now be demonstrated, it is more efficient to use an SU(2) representation rather than the SO(3) matrices when describing the rotations of spins. The matrix $\underline{R}$ of equation (2.27) describes the rotation of an initial spin $\vec{S}_i$ around a unit rotation vector $\vec{e}$ by an angle α. Splitting the spin into components parallel and perpendicular to $\vec{e}$, one obtains

$$\vec{S}(\theta) = \vec{e}(\vec{S}_i \cdot \vec{e}) + \cos\alpha[\vec{S} - \vec{e}(\vec{S}_i \cdot \vec{e})] + \sin\alpha\ \vec{e} \times \vec{S}_i\ . \tag{2.29}$$

With $a_0 = \cos\frac{\alpha}{2}$ and $\vec{a} = \sin\frac{\alpha}{2}\vec{e}$, the matrix $\underline{R}$ can therefore be written as [58, 59]

$$R_{ij} = (a_0^2 - \vec{a}^2)\delta_{ij} + 2a_i a_j - 2a_0\epsilon_{ijk}a_k\ , \tag{2.30}$$

where the vector product is expressed using the totally antisymmetric tensor ϵ_{ijk}. The SU(2) matrix representing a rotation around $\vec{e}$ by the angle α is given by the quaternion

$$A = \exp(-i\frac{\alpha}{2}\vec{e} \cdot \underline{\vec{\sigma}}) = a_0\underline{1}_2 - i\vec{a} \cdot \underline{\vec{\sigma}}\ . \tag{2.31}$$

Here the elements of the vector $\underline{\vec{\sigma}}$ are the three Pauli matrices. If a particle traverses an optical element which rotates the spin according to the quaternion A and then passes through an element which rotates the spin according to the quaternion B, the total rotation of the spin is given by

$$\begin{aligned} C &= c_0\underline{1}_2 - i\vec{c} \cdot \underline{\vec{\sigma}} = (b_0\underline{1}_2 - i\vec{b} \cdot \underline{\vec{\sigma}})(a_0\underline{1}_2 - i\vec{a} \cdot \underline{\vec{\sigma}}) \\ &= (b_0a_0 - \vec{b} \cdot \vec{a})\underline{1}_2 - i(b_0\vec{a} + \vec{b}a_0 + \vec{b} \times \vec{a}) \cdot \underline{\vec{\sigma}}\ . \end{aligned} \tag{2.32}$$

This concatenation of quaternions can be written in matrix form as

$$\vec{C} = \begin{pmatrix} c_0 \\ \vec{c} \end{pmatrix} = \underline{B}\begin{pmatrix} a_0 \\ \vec{a} \end{pmatrix}\ ,\quad \underline{B} = \begin{pmatrix} b_0 & -b_1 & -b_2 & -b_3 \\ b_1 & b_0 & -b_3 & b_2 \\ b_2 & b_3 & b_0 & -b_1 \\ b_3 & -b_2 & b_1 & b_0 \end{pmatrix}\ . \tag{2.33}$$

Sometimes it is useful to have the quaternions appear in reversed order, even though particles travel first through the optical element corresponding to A,

$$\vec{C} = \begin{pmatrix} c_0 \\ \vec{c} \end{pmatrix} = \underline{\tilde{A}}\begin{pmatrix} b_0 \\ \vec{b} \end{pmatrix}\ ,\quad \underline{\tilde{A}} = \begin{pmatrix} a_0 & -a_1 & -a_2 & -a_3 \\ a_1 & a_0 & a_3 & -a_2 \\ a_2 & -a_3 & a_0 & a_1 \\ a_3 & a_2 & -a_1 & a_0 \end{pmatrix}\ . \tag{2.34}$$

Since any quaternion vector has unit length, the matrices $\underline{B}$ and $\underline{\tilde{A}}$ are both orthogonal.

It has turned out to be useful to represent rotations in terms of a_0 and $\vec{a}$ for the following three reasons:

1. only 4 components are needed to describe and concatenate the rotation of spins,

2. even when numerical inaccuracies cause a small error in the computation of this representation, one can always normalize so that $a_0^2 + \vec{a}^2 = 1$, which then always leads to a an orthogonal spin transport matrix,

3. only 28 floating point operations are required to compute the combined spin transport quaternion of two particle optical elements from their individual quaternions. The multiplication of the spin transport matrices requires 45 floating point operations.

While particles are propagating along the design curve by a distance $d\theta$, spins are rotated by an angle $|\vec{\Omega}|d\theta$ around the vector $\vec{\Omega}$. After having been propagated to θ by the quaternion A, a spin gets propagated from θ to $\theta + d\theta$ by the quaternion B with $b_0 = 1$ and $\vec{b} = \frac{1}{2}\vec{\Omega}d\theta$. The resulting total rotation is given by $A + d\theta\frac{d}{d\theta}A$ and one obtains the differential equation

$$\frac{d}{d\theta}\begin{pmatrix} a_0 \\ \vec{a} \end{pmatrix} = \frac{1}{2}\begin{pmatrix} 0 & -\Omega_1 & -\Omega_2 & -\Omega_3 \\ \Omega_1 & 0 & -\Omega_3 & \Omega_2 \\ \Omega_2 & \Omega_3 & 0 & -\Omega_1 \\ \Omega_3 & -\Omega_2 & \Omega_1 & 0 \end{pmatrix}\begin{pmatrix} a_0 \\ \vec{a} \end{pmatrix} . \tag{2.35}$$

Writing the vector as $\vec{A}$ and the matrix as $\underline{\Omega}$, the spin-orbit equation of motion takes the form

$$\frac{d}{d\theta}\vec{z} = \vec{v}(\vec{z},\theta) \ , \quad \frac{d}{d\theta}\vec{A} = \frac{1}{2}\underline{\Omega}(\vec{z},\theta)\vec{A} \ . \tag{2.36}$$

The starting conditions at the initial azimuth θ_0 are $\vec{z} = \vec{z}_i$, $a_0 = 1$, and $\vec{a} = 0$. Sometimes, an equation of motion for the quaternion A itself is used rather than for the component vector $\vec{A}$,

$$\frac{d}{d\theta}A = -i\frac{1}{2}\vec{\Omega}\cdot\underline{\vec{\sigma}}A \ , \tag{2.37}$$

with the starting condition $A = \underline{1}_2$. When $\vec{A}(\vec{z}_i,\theta_0;\theta)$ is known, $\underline{R}(\vec{z}_i,\theta_0;\theta)$ can be constructed using equation (2.30) and one can again propagate an initial spin $\vec{S}_i$ and a spin field $\vec{f}(\vec{z}_i,\theta_0)$ by equation (2.28).

2.1.6 Equation of Motion for Spinors

In the SU(2) representation of rotations, a spin $\vec{S}$ is written in terms of the spinor $\Psi = (\psi_1,\psi_2)^T$ as $\vec{S} = \Psi^\dagger\underline{\vec{\sigma}}\Psi$ where ψ_1 and ψ_2 are two complex numbers [58]. To have $|\vec{S}| = 1$, it is required that $|\psi_1|^2 + |\psi_2|^2 = 1$. The spinor represents a spin direction in polar coordinates ϑ and ϕ, which is illustrated by the fact that the following spinor and the following vector describe the same spin:

$$\Psi = \begin{pmatrix} \psi_1 \\ \psi_2 \end{pmatrix} = \begin{pmatrix} \cos\frac{\vartheta}{2}e^{i\phi_1} \\ \sin\frac{\vartheta}{2}e^{i\phi_2} \end{pmatrix} \quad \Longrightarrow \quad \vec{S} = \begin{pmatrix} \sin\vartheta\cos(\phi_2-\phi_1) \\ \sin\vartheta\sin(\phi_2-\phi_1) \\ \cos\vartheta \end{pmatrix} . \tag{2.38}$$

The equation of motion for the spinor is given by

$$\frac{d}{d\theta}\Psi = -i\frac{1}{2}(\vec{\Omega}\cdot\vec{\underline{\sigma}})\Psi \ , \tag{2.39}$$

which leads back to the vector form of the differential equation of spin motion [13],

$$\begin{aligned}\frac{d}{d\theta}\vec{S} &= (\frac{d}{d\theta}\Psi^\dagger)\vec{\underline{\sigma}}\Psi + \Psi^\dagger\vec{\underline{\sigma}}(\frac{d}{d\theta}\Psi) \\ &= i\frac{1}{2}\Psi^\dagger[(\vec{\Omega}\cdot\vec{\underline{\sigma}})\vec{\underline{\sigma}} - \vec{\underline{\sigma}}(\vec{\Omega}\cdot\vec{\underline{\sigma}})]\Psi = \Psi^\dagger[\vec{\Omega}\times\vec{\underline{\sigma}}]\Psi = \vec{\Omega}\times\vec{S} \ .\end{aligned} \tag{2.40}$$

If a spin rotates by an angle α around a θ independent unit rotation vector $\vec{e}$ while the particle travels to θ, then equation (2.39) leads to the spinor propagation relation $\Psi(\theta) = \exp(-i\frac{\alpha}{2}\vec{e}\cdot\vec{\underline{\sigma}})\Psi_i$. A spinor is therefore propagated through an accelerator by the spin transport quaternion of equation (2.31),

$$\Psi(\theta) = (a_0\underline{1}_2 - i\vec{a}\cdot\vec{\underline{\sigma}})\Psi_i \ . \tag{2.41}$$

If a spin is parallel to the rotation vector $\vec{e}$, it is not changed during the rotation. The corresponding spinor Ψ_e however is changed by a phase factor. To show this, the polar coordinates ϑ and ϕ of the vector $\vec{e}$ are used and the free phase of the spinor is indicated by $e^{i\xi}$,

$$\Psi_e = e^{i\xi}\begin{pmatrix}\cos\frac{\vartheta}{2}\\ \sin\frac{\vartheta}{2}e^{i\phi}\end{pmatrix} \ , \tag{2.42}$$

$$\begin{aligned}\Psi(\theta) &= \exp(-i\frac{\alpha}{2}\vec{e}\cdot\vec{\underline{\sigma}})\Psi_i = (\cos\frac{\alpha}{2} - i\sin\frac{\alpha}{2}\vec{\underline{\sigma}}\cdot\vec{e})\Psi_i \\ &= \begin{pmatrix}\cos\frac{\alpha}{2} - i\sin\frac{\alpha}{2}\cos\vartheta & -ie^{-i\phi}\sin\frac{\alpha}{2}\sin\vartheta\\ -ie^{i\phi}\sin\frac{\alpha}{2}\sin\vartheta & \cos\frac{\alpha}{2} + i\sin\frac{\alpha}{2}\cos\vartheta\end{pmatrix}\begin{pmatrix}\cos\frac{\vartheta}{2}\\ \sin\frac{\vartheta}{2}e^{i\phi}\end{pmatrix}e^{i\xi} = e^{-i\frac{\alpha}{2}}\Psi_e\end{aligned} \tag{2.43}$$

In the spinor formalism, the phase change of the spinor which describes the rotation vector can therefore be used to determine the rotation angle α.

Once Ψ_i at θ_0 has been propagated to Ψ at θ, the spin of the particle can be computed as $\vec{S} = \Psi^\dagger\vec{\underline{\sigma}}\Psi$. Alternatively, one can propagate the spinor $\Psi_i = (1,0)^T$ to obtain $\Psi = (a_0 - ia_3, -ia_1 + a_2)^T$ from equation (2.41). From the real and imaginary parts one then obtains the spin transport quaternion, which makes this method equivalent to the transportation of quaternions in section 2.1.5.

A phase space function $\Psi_{\vec{f}}(\vec{z},\theta)$ with $|\psi_1|^2 + |\psi_2|^2 = 1$ can describe a spin field if it satisfies the equation of motion

$$\frac{d}{d\theta}\Psi_{\vec{f}}(\vec{z},\theta) = \partial_\theta\Psi_{\vec{f}}(\vec{z},\theta) + [\vec{v}(\vec{z},\theta)\cdot\partial_{\vec{z}}]\Psi(\vec{z},\theta) = -i\frac{1}{2}[\vec{\Omega}(\vec{z},\theta)\cdot\vec{\underline{\sigma}}]\Psi(\vec{z},\theta) \ . \tag{2.44}$$

In analogy to equation (2.28), such a spin field is transported by the spin transport quaternion $A(\vec{z}_i,\theta_0,\theta)$ from azimuth θ_0 to θ,

$$\Psi(\vec{z},\theta) = A(\vec{z}_i,\theta_0;\theta)\Psi(\vec{z}_i,\theta_0) \ \text{ with } \ \vec{z}_i = \vec{M}(\vec{z},\theta;\theta_0) \ . \tag{2.45}$$

A useful collection of equations for the description of spin motion can be found in [13].

2.2 Spin Motion in Circular Accelerators

2.2.1 Spin Motion on the Closed Orbit and Imperfection Resonances

Before I analyze spin motion on a general particle trajectory in a circular accelerator, I take a look at spin motion on the closed orbit. If no field errors, misaligned elements, or energy deviations are present, this orbit is the design trajectory of the accelerator. After a particle has traveled one turn along the closed orbit from azimuth θ_0 to azimuth $\theta_0 + 2\pi$ the spin has rotated around some unit rotation axis $\vec{n}_0(\theta_0)$ by a rotation angle $2\pi\nu_0$. The angle of rotation around $\vec{n}_0$ divided by 2π is called the closed orbit spin tune ν_0 and does not depend on the azimuth θ_0 at which $\vec{n}_0$ is determined. In the following discussion θ_0 is an arbitrary but fixed azimuth which will no longer be indicated. This spin rotation for the closed orbit $\vec{z} = 0$ is described by the spin transport matrix $\underline{R}(0, \theta_0; \theta_0 + 2\pi)$. In a flat accelerator without field errors and misaligned elements, the closed orbit is in the horizontal plane and passes only through vertical fields. Therefore $\vec{n}_0$ is vertical and $\nu_0 = G\gamma$. When ν_0 is close to an integer, a case which is referred to as an *imperfection resonance*, the rotation matrix is close to the identity and spin directions have hardly changed after one turn. Misalignments create horizontal field components on the design orbit of a flat ring, which produce spin precessions away from the vertical direction. For small misalignments, these rotations around the horizontal might be very small but they can still dominate spin motion when the main fields hardly produce any spin rotation during one turn, i.e. close to integer values of ν_0. Thus the rotation axis $\vec{n}_0$ for spins is vertical away from imperfection resonances but it can be nearly horizontal in their vicinity. At a fixed azimuth θ_0 , the rotation axis $\vec{n}_0$ changes smoothly with ν_0 in between these extremes.

When a particle's energy is accelerated such that ν_0 crosses an integer value, the rotation vector $\vec{n}_0$ can strongly change with energy. When the spin rotation is much faster than this change of the rotation vector, then a spin which is nearly parallel to $\vec{n}_0$ is dragged along with the changing $\vec{n}_0$. The projection of a spin on $\vec{n}_0$ hardly changes during this procedure and will be shown to be an adiabatic invariant. To illustrate this fact, one can imagine that $\vec{n}_0$ changes away from the spin sometimes and towards the spin at other times while the spin rotates around $\vec{n}_0$. Due to this rapid rotation, both cases happen in frequent change and the total effect averages out. This causes the spin to follow the slow change of $\vec{n}_0$.

Since it is inadvisable to let misalignments dominate spin motion, imperfection resonances ought to be avoided. However, since $\nu_0 = G\gamma$ in a flat ring, the closed–orbit spin tune changes during acceleration and the crossing of imperfection resonances is unavoidable. There are the following three possible regimes for resonance crossing [37]:

- If the effects of misalignments are very small, the resonance can be crossed so rapidly that the spins hardly react and the beam's polarization is hardly changed.

- When the effect of misalignments is very strong, the rotation axis $\vec{n}_0$ changes very slowly during acceleration since the precession around the horizontal fields of misaligned elements starts to dominate already far from an imperfection resonance. Then the spin can follow the slow change of $\vec{n}_0$. But while the average spin direction $< \vec{S} >_N$ changes, the change of the polarization $P = | < \vec{S} >_N |$ is very limited. The change of a spin's projection on $\vec{n}_0$ as $\vec{n}_0$ changes slowly will be discussed in the next section.

- When the effect of misalignments has an intermediate strength, the polarization will be reduced.

The following two strategies can therefore be used to limit the reduction of polarization when imperfection resonances are crossed:

- Careful correction of the closed orbit to limit horizontal field components [37].

- Increasing the horizontal field components, for example by introducing a solenoid magnet. Devices which are deliberately used to increase the effect of imperfection resonances are referred to as partial snakes [60, 61, 62]. A solenoid magnet has been installed in the AGS and very effectively avoids polarization loss at integer resonances of the closed–orbit spin tune. To avoid coupling between horizontal and vertical motion by the solenoid, a helical dipole partial snake is now being constructed for the AGS [17].

Since the closed orbit is not very well controlled in DESY III, a solenoid partial snake for overcoming the $\nu_0 = G\gamma = 8$ imperfection resonance at 4.08GeV/c can probably not be avoided. However, it would suffice to have it rotate spins by 14° around the longitudinal direction [22]. Figure 2.2(left) shows how the spin of a particle on the closed orbit would change while it is accelerated from $G\gamma = 7.97$ to $G\gamma = 8.03$ under the influence of a solenoid which rotates the spins by 0.8°. No misalignments are considered. A realistic acceleration rate of 5keV/turn was assumed. Figure 2.2 (right) shows that the product $s_3 = \vec{S} \cdot \vec{n}_0$ hardly changed during the slow acceleration. A small change close to $G\gamma = 8$ recovers after the resonance is crossed. This is not due to the adiabatic invariance but due to the symmetry of spin motion above and below the resonance. The adiabatic following of $\vec{n}_0$ shown in this figure illustrates how a reduction of polarization at imperfection resonances can be avoided.

For the acceleration process in a simple accelerator model, the change of $\vec{S} \cdot \vec{n}_0$ at a fixed azimuth θ_0 is described by the Froissart–Stora formula as will be seen in section 2.2.10. This formula allows a quantitative computation of the limited reduction of polarization when either crossing a weak resonance relatively quickly or when crossing a strong resonance relatively slowly.

2.2.2 The Adiabatic Spin Invariant on the Closed Orbit

It was conjectured above that spins which are nearly parallel to $\vec{n}_0$ will follow slow changes of this rotation vector at θ_0. In this section I will prove this property

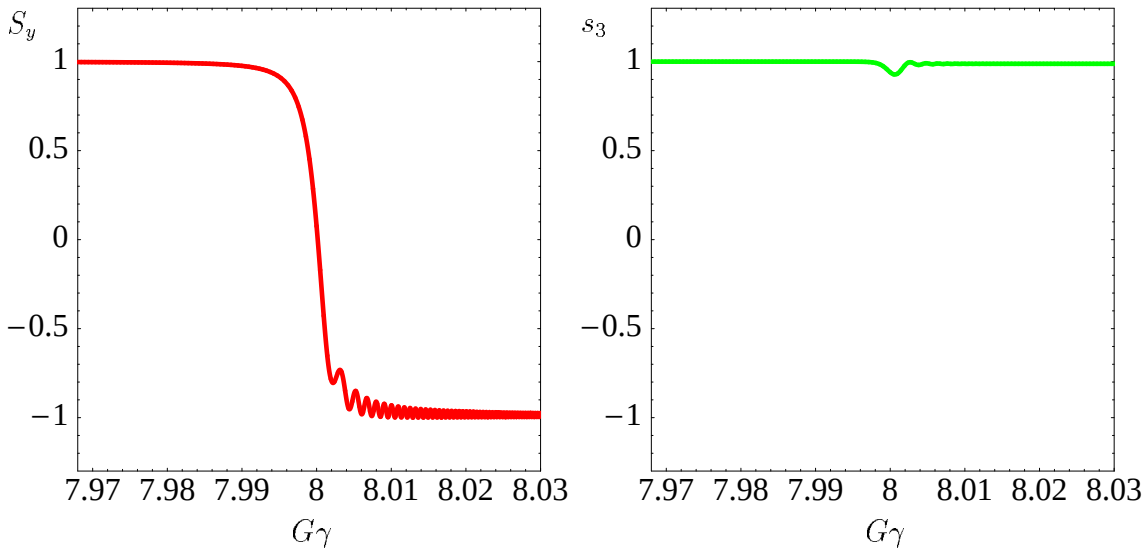

Figure 2.2: The change of $S_y = \vec{S} \cdot \vec{e}_y$ (left) and the change of $s_3 = \vec{S} \cdot \vec{n}_0$ (right) during the acceleration from $G\gamma = 7.97$ to $G\gamma = 8.03$ for particles on the closed orbit in DESY III in the presence of a 0.8° solenoid partial snake.

by showing that $\vec{S}(\theta) \cdot \vec{n}_0(\theta)$ is an adiabatic invariant of motion. For simplicity, a coordinate system is introduced which has $\vec{n}_0$ as one of its coordinate vectors and in which the spin motion on the closed orbit is as simple as possible.

The precession vector $\vec{\Omega}(\vec{z}, \theta)$ on the closed orbit $\vec{z} = 0$ is denoted by $\vec{\Omega}_0(\theta)$. The rotation axis $\vec{n}_0(\theta_0)$ of the one turn spin transport matrix is sometimes called the spin closed orbit [59]; it satisfies

$$\frac{d}{d\theta}\vec{n}_0(\theta) = \vec{\Omega}_0(\theta) \times \vec{n}_0(\theta) \ , \quad \vec{n}_0(\theta) = \vec{n}_0(\theta + 2\pi) \ . \tag{2.46}$$

Such a 2π periodic vector always exists on the closed orbit; it is the rotation axis of the spin rotation matrix $\underline{R}_0(\theta) = \underline{R}(0, \theta; \theta + 2\pi)$ which describes the rotation of initial spins $\vec{S}_i$ into final spins $\vec{S}_f = \underline{R}_0(\theta)\vec{S}_i$ during one turn around the closed orbit.

Two unit vectors $\vec{m}_0(\theta)$ and $\vec{l}_0(\theta)$ are now chosen which initially make up a right handed orthogonal dreibein $[\vec{m}_0(\theta_0), \vec{l}_0(\theta_0), \vec{n}_0(\theta_0)]$ and propagate around the ring according to the T–BMT equation on the closed orbit,

$$\frac{d}{d\theta}\vec{m}_0 = \vec{\Omega}_0(\theta) \times \vec{m}_0 \ , \quad \frac{d}{d\theta}\vec{l}_0 = \vec{\Omega}_0(\theta) \times \vec{l}_0 \ . \tag{2.47}$$

The three unit vectors will always constitute a right handed orthogonal dreibein, since all three get rotated by the same precession equation. Whereas $\vec{n}_0$ is periodic around the ring, the vectors $\vec{m}_0$ and $\vec{l}_0$ are rotated around $\vec{n}_0$ by the angle $2\pi\nu_0$ after one turn and the dreibein is therefore in general not 2π periodic in θ. Now a 2π periodic dreibein is defined by rotating $\vec{m}_0$ and $\vec{l}_0$ back uniformly by $2\pi\nu_0$ during one turn [63, 64],

$$\vec{m} + i\vec{l} = e^{i\nu_0\theta}(\vec{m}_0 + i\vec{l}_0) \ , \quad \frac{d}{d\theta}(\vec{m} + i\vec{l}) = (\vec{\Omega}_0 - \nu_0\vec{n}_0) \times (\vec{m} + i\vec{l}) \ . \tag{2.48}$$

In this coordinate system, a spin can be written as

$$\vec{S}(\theta) = s_1(\theta)\vec{m}(\theta) + s_2(\theta)\vec{l}(\theta) + s_3(\theta)\vec{n}_0(\theta) \ , \quad s_1^2 + s_2^2 + s_3^2 = 1 \ . \tag{2.49}$$

The equation of spin motion

$$\vec{\Omega}_0 \times \vec{S} = \frac{d}{d\theta}\vec{S} = \vec{m}\frac{d}{d\theta}s_1 + \vec{l}\frac{d}{d\theta}s_2 + \vec{n}_0\frac{d}{d\theta}s_3 + (\vec{\Omega}_0 - \nu_0\vec{n}_0) \times \vec{S} \tag{2.50}$$

can be decomposed into its components parallel to $\vec{m}$, $\vec{l}$, and $\vec{n}_0$, which leads to

$$\frac{d}{d\theta}(s_1 + is_2) = i\nu_0(s_1 + is_2) \ , \quad \frac{d}{d\theta}s_3 = 0 \tag{2.51}$$

and describes a uniform rotation around $\vec{n}_0$, which keeps s_3 invariant. It has been conjectured above that s_3 does not change much when parameters of the system are slowly varied. To show this, the definition of an adiabatic invariant given in [65, sec.8.1] is used.

Definition (Adiabatic invariant): *Consider an ordinary differential equation* $\frac{d}{d\theta}\vec{x} = \vec{g}(\vec{x}, \tau)$ *with* $\tau = \varepsilon\theta$ *and* $\vec{x} \in I\!R^n$ *for a small parameter* ε *so that* $\vec{g}$ *defines a slowly varying vector field. A function* $\vec{A}(\vec{x}, \tau)$ *is said to be an adiabatic invariant of this system if its variation on the interval* $\theta \in [0, 1/\varepsilon]$ *(which implies* $\tau \in [0, 1]$*) is small together with* ε*, except perhaps for a set of initial conditions whose measure goes to zero with* ε*; that is, for "most" initial conditions:*

$$\lim_{\varepsilon \to 0} \mathrm{Sup}_{\theta \in [0, 1/\varepsilon]} |\vec{A}(\vec{x}(\theta), \varepsilon\theta) - \vec{A}(\vec{x}(0), 0)| = 0 \ , \tag{2.52}$$

where the supremum Sup *over the interval* $[0, 1/\varepsilon]$ *is used.*

Sometimes a distinction is made between adiabatic invariants and almost adiabatic invariants. The first vary little for all initial conditions whereas the second allow for exceptional initial conditions from a set which has a measure that tends to 0 with ε [66, sec.4]; this distinction will not be made here.

To analyze whether $s_3 = \vec{S} \cdot \vec{n}_0$ is an adiabatic invariant, I consider a precession vector $\vec{\Omega}_0(\theta, \tau)$ which depends on a slowly changing parameter τ. For fixed τ, the rotation matrix for one turn has a unit rotation vector $\vec{n}_0(\theta, \tau)$ and one can again define the 2π periodic orthogonal dreibein using this vector together with the unit vectors $\vec{m}(\theta, \tau)$ and $\vec{l}(\theta, \tau)$. Since these vectors have unit length and constitute a right handed orthogonal dreibein for all values of τ, their variation with τ can only be a rotation around some vector $\vec{\eta}(\theta, \tau)$,

$$\partial_\tau \vec{n}_0 = \vec{\eta}(\theta, \tau) \times \vec{n}_0 \ , \quad \partial_\tau(\vec{m} + i\vec{l}) = \vec{\eta}(\theta, \tau) \times (\vec{m} + i\vec{l}) \ . \tag{2.53}$$

These equations can be rearranged to compute $\vec{\eta}$ by

$$\vec{\eta} = \frac{1}{2}(\vec{m} \times \partial_\tau \vec{m} + \vec{l} \times \partial_\tau \vec{l} + \vec{n}_0 \times \partial_\tau \vec{n}_0) \ . \tag{2.54}$$

Now using $\tau = \varepsilon\theta$, the spin of a particle which travels on the closed orbit while the parameter τ varies slowly is analyzed,

$$\begin{aligned} \vec{\Omega}_0(\theta,\tau)\times\vec{S} &= \frac{d}{d\theta}\vec{S} \qquad (2.55)\\ &= \vec{m}\frac{d}{d\theta}s_1 + \vec{l}\frac{d}{d\theta}s_2 + \vec{n}_0\frac{d}{d\theta}s_3 + (\vec{\Omega}_0 - \nu_0\vec{n}_0)\times\vec{S} + (\frac{d}{d\theta}\tau)\vec{\eta}\times\vec{S}\ . \end{aligned}$$

The term with $\frac{d}{d\theta}\tau = \varepsilon$ appears since the unit vectors' dependence on τ has been taken into account. For the spin coordinates, one obtains the following equation of motion:

$$\begin{aligned} \frac{d}{d\theta}\begin{pmatrix} s_1\\ s_2\\ s_3\end{pmatrix} &= \begin{pmatrix} \{[\nu_0(\tau)\vec{n}_0 - \varepsilon\vec{\eta}]\times\vec{S}\}\cdot\vec{m}\\ \{[\nu_0(\tau)\vec{n}_0 - \varepsilon\vec{\eta}]\times\vec{S}\}\cdot\vec{l}\\ \{\qquad\qquad -\varepsilon\vec{\eta}\ \times\vec{S}\}\cdot\vec{n}_0\end{pmatrix} \qquad (2.56)\\ &= \begin{pmatrix} \varepsilon(\eta_3 s_2 - \eta_2 s_3) - \nu_0(\tau)s_2\\ \varepsilon(\eta_1 s_3 - \eta_3 s_1) + \nu_0(\tau)s_1\\ \varepsilon(\eta_2 s_1 - \eta_1 s_2)\end{pmatrix}\ , \qquad (2.57) \end{aligned}$$

with $\tau = \varepsilon\theta$ and $\vec{\eta} = \eta_1\vec{m} + \eta_2\vec{l} + \eta_3\vec{n}_0$. For $1 - s_3^2 \geq \Delta$, $(\Delta \in I\!R^+)$, the angle ϕ is introduced with $s_1 = \sqrt{1-s_3^2}\cos\phi$ and $s_2 = \sqrt{1-s_3^2}\sin\phi$. Using $\sqrt{1-s_3^2}\frac{d}{d\theta}\phi = -\sin\phi\frac{d}{d\theta}s_1 + \cos\phi\frac{d}{d\theta}s_2$ one obtains

$$\frac{d}{d\theta}\begin{pmatrix} s_3\\ \phi\end{pmatrix} = \begin{pmatrix} \varepsilon\,(\eta_2\cos\phi - \eta_1\sin\phi)\sqrt{1-s_3^2}\\ \nu_0(\tau) + \quad \varepsilon[(\eta_2\sin\phi + \eta_1\cos\phi)\frac{s_3}{\sqrt{1-s_3^2}} - \eta_3]\end{pmatrix}\ . \qquad (2.58)$$

For small ε and when $|\nu_0|$ is larger than order ε, this system has the slowly varying coordinate s_3 and a quickly varying phase ϕ. It is therefore suitable for averaging methods. Bringing the equation into standard form for averaging theorems, where the frequency only depends on slowly changing variables, I make use of the slowly changing variable τ with $\frac{d}{d\theta}\tau = \varepsilon$. To obtain an autonomous differential equation as used in definition an adiabatic invariant, I use $\tilde{\theta} = \theta$ and add the equation $\frac{d}{d\theta}\tilde{\theta} = 1$, and define

$$\begin{aligned} f_3(s_3,\phi,\tau,\tilde{\theta}) &= [\eta_2(\tilde{\theta},\tau)\cos\phi - \eta_1(\tilde{\theta},\tau)\sin\phi]\sqrt{1-s_3^2}\ , \qquad (2.59)\\ f_\phi(s_3,\phi,\tau,\tilde{\theta}) &= [\eta_2(\tilde{\theta},\tau)\sin\phi + \eta_1(\tilde{\theta},\tau)\cos\phi]\frac{s_3}{\sqrt{1-s_3^2}} - \eta_3(\tilde{\theta},\tau)\ . \qquad (2.60) \end{aligned}$$

The equation of spin motion on the closed orbit is then

$$\frac{d}{d\theta}\begin{pmatrix} s_3\\ \tau\\ \phi\\ \tilde{\theta}\end{pmatrix} = \begin{pmatrix} 0\\ 0\\ \nu_0(\tau)\\ 1\end{pmatrix} + \varepsilon\begin{pmatrix} f_3(s_3,\phi,\tau,\tilde{\theta})\\ 1\\ f_\phi(s_3,\phi,\tau,\tilde{\theta})\\ 0\end{pmatrix}\ . \qquad (2.61)$$

It is apparent that this system of ordinary differential equations has two slowly changing and two quickly changing variables for small ε. It is written in the standard form of averaging theorems for two frequency systems [66, sec.1.8], [65, chapter 4].

To illustrate the basic idea of two–phase averaging and to show which resonances can appear, it is noted that $f_3(s_3,\phi,\tau,\tilde{\theta})$ is a 2π periodic function of $\tilde{\theta}$ and that it is linear in trigonometric functions of ϕ . One can obtain a simpler equation of motion by transforming to a coordinate $\bar{s}_3 = s_3 + \varepsilon u(s_3,\phi,\tau,\tilde{\theta})$ with a function u which should have the same periodicity properties as f_3 with respect to ϕ and $\tilde{\theta}$. These functions, f_3 and u, are now Fourier expanded,

$$f_3(s_3,\phi,\tau,\tilde{\theta}) = \sum_{k=-\infty}^{\infty} (f_k^+(s_3,\tau)e^{i(k\tilde{\theta}+\phi)} + f_k^-(s_3,\tau)e^{i(k\tilde{\theta}-\phi)} , \quad (2.62)$$

$$u(s_3,\phi,\tilde{\theta},\varepsilon) = \sum_{k=-\infty}^{\infty} (u_k^+(s_3,\tau)e^{i(k\tilde{\theta}+\phi)} + u_k^-(s_3,\tau)e^{i(k\tilde{\theta}-\phi)} , \quad (2.63)$$

which leads to

$$\frac{d}{d\theta}\bar{s}_3 = \varepsilon \sum_{k=-\infty}^{\infty} \{[f_k^+ + u_k^+ i(k+\frac{d}{d\theta}\phi)]e^{i(k\tilde{\theta}+\phi)} + [f_k^- + u_k^- i(k-\frac{d}{d\theta}\phi)]e^{i(k\tilde{\theta}-\phi)}\} \quad (2.64)$$

$$= \varepsilon \sum_{k=-\infty}^{\infty} \{[f_k^+ + u_k^+ i(k+\nu_0)]e^{i(k\tilde{\theta}+\phi)} + [f_k^- + u_k^- i(k-\nu_0)]e^{i(k\tilde{\theta}-\phi)}\} + O(\varepsilon^2) .$$

If there are no resonances where $\nu_0(\tau)$ is an integer, then one can choose $u_k^{\pm}(s_3,\tau) = if_k^{\pm}/(k\pm\nu_0(\tau))$ and all first–order terms are eliminated leaving $\frac{d}{d\theta}\bar{s}_3 = O(\varepsilon^2)$. In general such a transformation removes all terms which are first–order in ε except the zeroth Fourier coefficient $\frac{1}{(2\pi)^2}\int_0^{2\pi}\int_0^{2\pi} f_3(s_3,\phi,\tau,\tilde{\theta})d\phi d\tilde{\theta}$. Therefore the differential equation after the transformation is called the averaged system. For the case under consideration, the average of f_3 is zero; and for $\theta \in [0, 1/\varepsilon]$, changes of the variable $\bar{s}_3$ of the averaged system are of order ε. Changes of s_3 are of the same order, since the difference $\bar{s}_3 - s_3 = \varepsilon u$ is of order ε. This shows that $s_3 = \vec{S}\cdot\vec{n}_0$ is an adiabatic invariant as defined above. However, in this argument it was assumed that $\nu_0(\tau)$ never takes on integer values. Since the closed–orbit spin tune changes with energy ($\nu_0 = G\gamma$ in a flat ring), ν_0 can become an integer during the acceleration process. Resonance phenomena between the frequencies of the two quickly changing phases ϕ and $\tilde{\theta}$ can then occur.

I will therefore here state an averaging theorem for systems with two quickly changing phases which allows for the crossing of resonances and apply it to spin motion on the closed orbit. Various multi–phase averaging theorems could be used [65, chapters 4-6], [66]. Here theorem 3 of [65, sec.4.1] is used which is attributed to [67]. A remark is in order: The application of multi–phase averaging to the simple problem of spin motion on the closed orbit seems more complicated than necessary. However, I go through considerable detail here while dealing with the closed orbit, in order to set the stage for adiabatic invariants in the case of spin motion on a general trajectory.

Theorem (Averaging for two frequency systems): *Consider a system of the form*

$$\frac{d}{d\theta}\vec{I} = \varepsilon\vec{f}(\vec{I},\phi,\tilde{\theta},\varepsilon) , \quad (2.65)$$

$$\frac{d}{d\theta}\phi = \nu(\vec{I}) + \varepsilon g(\vec{I},\phi,\tilde{\theta},\varepsilon) \ , \tag{2.66}$$

$$\frac{d}{d\theta}\tilde{\theta} = 1 \ , \tag{2.67}$$

where $\vec{I}$ belongs to a regular compact subset of Euclidean $\mathbb{R}^m$. Each function on the right hand side is real, C^1 (first order differentials exist and are continuous) in $\vec{I}$ and ε, periodic with period 2π in ϕ and $\tilde{\theta}$, and each possesses an analytic extension for $\phi \in \mathbb{C}$, $\mathrm{Im}\{\phi\} < \sigma$ and $\tilde{\theta} \in \mathbb{C}$, $\mathrm{Im}\{\tilde{\theta}\} < \sigma$ with $\sigma > 0$. The associated averaged system is

$$\frac{d}{d\theta}\vec{\bar{I}} = \varepsilon\vec{\bar{f}}(\vec{\bar{I}}) \ , \quad \vec{\bar{f}}(\vec{\bar{I}}) = \frac{1}{(2\pi)^2}\int_0^{2\pi}\int_0^{2\pi}\vec{f}(\vec{\bar{I}},\phi,\tilde{\theta},0)d\phi d\tilde{\theta} \ , \tag{2.68}$$

with starting condition $\vec{\bar{I}}(0) = \vec{I}(0)$. Let every trajectory of the exact (not the averaged) system for which $\vec{I}$ stays in the range of definition for $\theta \in [0, 1/\varepsilon]$ have a strictly monotonic variation of $\nu(\vec{I})$ with θ, $|\frac{d}{d\theta}\nu| > c_1\varepsilon$ for some $c_1 \in R^+$. Then: On all these trajectories there exists $c \in R^+$ so that for sufficiently small ε

$$\mathrm{Sup}_{\theta\in[0,1/\varepsilon]}|\vec{I}(\theta) - \vec{\bar{I}}(\theta)| < c\sqrt{\varepsilon} \ . \tag{2.69}$$

In general the solution of the averaged system does not approximate the original system well if $\tilde{\theta}$ and ϕ are in resonance, which here means that the closed–orbit spin tune $\nu_0(\tau)$ is an integer m. A simple example is the system $\frac{d}{d\theta}s_3 = \varepsilon\cos(\phi - m\tilde{\theta})$ and $\frac{d}{d\theta}\phi = \nu_0$. The averaged system leads to $\bar{s}_3 = s_3(0)$ whereas the solution for an integer $\nu_0 = m$ is given by $s_3 = s_3(0) + \varepsilon\theta\cos[\phi(0)]$. The change in s_3 for $\theta \in [0, 1/\varepsilon]$ does not tend to zero for the limit $\varepsilon \to 0$ and s_3 is therefore not an adiabatic invariant.

This example illustrates that large changes of slowly changing variables can build up on resonances. The simplest way of avoiding this behavior at resonances is to consider only systems in which resonances are quickly passed and capture in resonances is avoided. This is the reason why the averaging theorem for two frequency systems requires $|\frac{d}{d\theta}\nu| > c_1\varepsilon$, which is often called condition A. This condition excludes systems where trajectories pass arbitrarily slowly through a resonance or cross the same resonance several times.

For spin motion on the closed orbit, the averaged system is $\frac{d}{d\theta}\bar{s}_3 = \bar{f}_3 = 0$ and leads to $\bar{s}_3 = s_3(0)$. If $|\frac{d}{d\theta}\nu_0(\varepsilon\theta)| > c_1\varepsilon$, then

$$\lim_{\varepsilon\to 0}\mathrm{Sup}_{\theta\in[0,1/\varepsilon]}|s_3(\theta) - s_3(0)| = 0 \ . \tag{2.70}$$

Cases where $\vec{S}$ is nearly parallel to $\vec{n}_0$ had to be excluded before equation (2.58) by the condition $1 - s_3^2 \geq \Delta$. For initial conditions with $1 - s_3(0)^2 \geq 2\Delta$, there is an ε^* so that $1 - s_3(\theta)^2 \geq \Delta$ for all $\varepsilon < \varepsilon^*$ according to equation (2.70). This is true for all $\Delta \in \mathbb{R}^+$. With the limit $\varepsilon^* \to 0$, the set of excluded initial conditions tends to $s_3 \in \{1, -1\}$ which has measure 0. The scalar product $s_3(\theta) = \vec{S}(\theta)\cdot\vec{n}_0(\theta)$ is therefore an adiabatic invariant as defined above.

The condition $|\partial_\tau \nu_0(\tau)| > c_1$ requires that the spin tune changes sufficiently during the adiabatic change of the parameter under consideration and therefore does not remain at an integer value for a long time while a parameter is slowly varied. When $\nu_0(\tau)$ has a finite distance to integers, s_3 is an adiabatic invariant even when $\partial_\tau \nu_0(\tau) = 0$, since then averaging theorems for non–resonant domains can be applied [66, sec.1.6].

2.2.3 Spin Motion for Phase Space Trajectories and Intrinsic Resonances

Assuming linearized phase space motion, the particles appear to perform harmonic oscillations around the closed orbit with the frequencies Q_x, Q_y, and Q_τ for horizontal, vertical, and longitudinal motion when viewed at a fixed azimuth θ_0 of the accelerator. These are called the orbital tunes. Some of the fields through which a particle propagates will therefore oscillate with the orbital tunes. Whenever the non–integer part of the spin precession frequency is in resonance with these oscillation frequencies of the particle's coordinates, a severe reduction of polarization can occur. The spin precession frequency of particles moving on the closed orbit is determined by the closed–orbit spin tune ν_0. In general the spin tune is denoted by ν and depends on the amplitude of a particle's oscillations around the closed orbit. Whenever ν is a linear combination of the frequencies of the particle's coordinates, the resulting coherent perturbation can reduce the beam's polarization,

$$\nu = j_0 P_s + j_1 Q_x + j_2 Q_y + j_3 Q_\tau \quad , \quad P_s, j_n, \in I\!N \ . \tag{2.71}$$

A super–periodicity P_s of a ring reduces the number of resonances. These resonances are called *intrinsic resonances* of order n for $n = |j_1| + |j_2| + |j_3|$. The depolarizing effect of these resonances has been experimentally verified in many low energy polarized proton accelerators [37, 14]. The first order intrinsic resonances are the dominant reason for a reduction of polarization after solenoids have been introduced to eliminate the effect of imperfection resonances. If the first–order resonances are avoided, however, higher–order resonances become dominant even for decoupled linear phase space motion, as will be shown for the case of HERA–p.

It has been explained in section 2.2.1 that the polarization can be reduced at imperfection resonances due the fact that field imperfections dominate the spin motion whenever the main guide fields produce an integer number of spin rotations, and therefore no apparent spin rotation after one completed turn. The depolarizing effect at intrinsic resonances can be understood in similar terms. For phase space trajectories which deviate little from the closed orbit, the spin motion is dominated by the main guide fields on the closed orbit except close to an intrinsic resonance, where the coherent perturbations described above can dominate over the main guide fields.

To illustrate for example the $\nu_0 = Q_y$ resonance, the spin directions are expressed in terms of a coordinate system which rotates by 2π around $\vec{n}_0$ during one betatron period of vertical motion. In this coordinate system the main guide fields produce a

rotation of the spins by $2\pi(\nu_0 - Q_y)$ during one turn. At $\nu_0 = Q_y$ the spin rotation due to the main guide fields vanishes and the remaining rotations are due to extra fields picked up by the oscillating trajectory some distance away from the closed orbit. At intrinsic resonances these spurious effects dominate over the effect of the accelerator's main guide fields. Since the dominant rotation at an intrinsic resonance is produced by the fields along a particle's phase space trajectory, it is different for different particles and the beam will therefore loose polarization under the influence of an intrinsic resonance.

With the averaging theorem for two frequency systems in section 2.2.2, I have proved that spins on the closed orbit follow any slow change of $\vec{n}_0$ as long as the system does not remain at a resonance for too long. Therefore, a severe reduction of polarization while accelerating through an imperfection resonances can be avoided by making the acceleration rate slow enough or by making the change of $\vec{n}_0$ slow enough by means of a partial snake as discussed in section 2.2.1.

At intrinsic resonances a reduction of polarization can be avoided by a similar mechanism. If a strong coherent perturbation is slowly switched on and off, an effect similar to adiabatically following $\vec{n}_0$ occurs and polarization is conserved. While an intrinsic resonance is crossed, perturbations influencing particles in the tails of a beam will slowly increase already before the resonance and an adiabatic conservation of polarization can occur. Polarization in the core of the beam will be only weakly influenced when crossing intrinsic resonances, but in intermediate parts of the beam, the polarization is reduced. Such a reduction of polarization can be overcome by slowly exciting the whole beam coherently at a frequency close to the orbital tune which causes the perturbation [68]. All spins then follow the adiabatic change of the polarization direction and the resonance can be crossed with little loss of polarization. The excitation amplitude is then reduced slowly so that the beam emittance does not change noticeably during the whole process. This mechanism has recently been tested successfully at the AGS [16, 17]. There, an RF dipole has been used to slowly excite all the particle amplitudes coherently. Then the dominant resonances $0 + Q_y$, $12 + Q_y$, $36 - Q_y$, and $36 + Q_y$ were crossed with little loss of polarization. Finally the RF dipole was slowly switched off. No noticeable increase of emittance has been observed. An older technique of avoiding the reduction of polarization at strong intrinsic resonances utilizes pulsed quadrupoles to move the orbital tune within a few microseconds just before a resonance so that the resonance is crossed so quickly that the spin motion is hardly disturbed [37].

For the case of a single resonance with frequency κ which is crossed by changing the closed–orbit spin tune according to $\nu_0 = \kappa + \alpha\theta$, the Froissart–Stora formula to be introduced in section 2.2.11 shows that polarization can be preserved when an intrinsic resonance is crossed either very quickly or very slowly.

A third method of avoiding loss of polarization at intrinsic resonances uses radial magnetic fields. The closed–orbit spin tune ν_0 is then no longer required to be $G\gamma$, in fact it can be made independent of energy and low order resonances can then be avoided during the acceleration process. It was mentioned below equation (2.5) that in a fixed transverse magnetic field the deflection angle of high energy particles depends on energy, whereas the spin rotation does not depend on energy. It is

therefore possible to devise a fixed field magnetic device which rotates spins by π whenever a high energy particle travels through it at the different energies of an acceleration cycle. Such field arrangements which rotate spins by π while perturbing the orbit only moderately are called Siberian Snakes [69, 70, 71, 72, 73]. Figure 2.3 illustrates how two Siberian Snakes make the spin tune ν_0 independent of energy and equal to $\frac{1}{2}$ in a flat ring. Starting at the far side of the ring, spins are rotated around the vertical (dashed line) by $\Psi = G\gamma\frac{\pi}{2}$ while the particles travel through one quadrant to the left side of the figure. The light arrow represents a spin which is rotated by Ψ whereas the dark arrow is only rotated by the Siberian Snakes and not by the fields in the arcs. The difference between the light and the dark arrow therefore indicates the rotation due to the fields of the quadrants. A radial Siberian Snake rotates all spins by π around the radial direction before the particles enter the second quadrant. Since the spins have now reversed their vertical orientation, the rotation due to the first quadrant is rewound during the second quadrant. The rotation of the third quadrant is rewound during the fourth, due to the longitudinal Siberian Snake between these quadrants. The rotations of different quadrants cancel for all energies. As indicated by the dark area, all spins have in total rotated by π around the vertical by the time they have returned to the far side of the ring. No net rotation due to the arcs remains and the dark arrow and the light arrow therefore coincide.

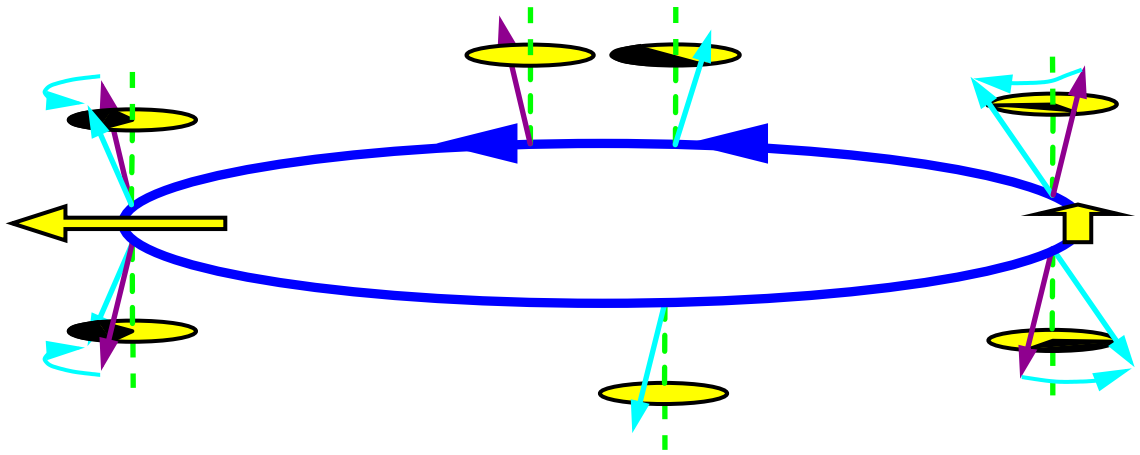

Figure 2.3: Schematic spin motion in a flat ring with a symmetrically arranged longitudinal and radial snake. The one turn spin motion has $\nu_0 = \frac{1}{2}$ and $\vec{n}_0$ vertical for all energies.

To be more general, one can consider N Siberian Snakes in a ring where a spin rotation angle Ψ_j around the vertical is produced between the $j$the and the $j+1$st Siberian Snake. These angles are in general energy dependent. The rotation axis of a snake is called the snake axis and the angle of this axis to the radial direction is referred to as the snake angle φ_j . The spin transport quaternion of one snake is

therefore $i[\cos(\varphi_j)\sigma_1 + \sin(\varphi_j)\sigma_2]$ and the total rotation during one turn is given by

$$A = \prod_{j=1}^{N} ie^{-i\frac{\Psi_j}{2}\sigma_3}[\cos(\varphi_j)\sigma_1 + \sin(\varphi_j)\sigma_2] \quad (2.72)$$

$$= i^N e^{-i\frac{\Delta\Psi}{2}\sigma_3} \prod_{j=1}^{N}[\cos(\varphi_j)\sigma_1 + \sin(\varphi_j)\sigma_2] \ . \quad (2.73)$$

Since σ_3 anti–commutes with the other two Pauli matrices, the exponent is given by $\Delta\Psi = \Psi_N - \Psi_{N-1} \pm \ldots \pm \Psi_1$. The total spin rotation is independent of energy when the snake locations are chosen to let $\Delta\Psi = 0$. A pair of snakes produces a rotation around a vertical axis of

$$\begin{aligned} & [\cos(\varphi_1)\sigma_1 + \sin(\varphi_1)\sigma_2] \cdot [\cos(\varphi_2)\sigma_1 + \sin(\varphi_2)\sigma_2] \cdot \\ = \ & \cos(\varphi_1 - \varphi_2) - i\sin(\varphi_1 - \varphi_2)\sigma_3 \ . \end{aligned} \quad (2.74)$$

An even number of Siberian Snakes therefore produces a vertical rotation vector $\vec{n}_0$. The polarization direction on the closed orbit is then vertical in the bending magnets of the ring and is not deflected in these magnets. For an odd number of Siberian Snakes, $\vec{n}_0$ is in the horizontal plane and rotates by an energy dependent angle in each bending magnet, even though the total rotation of one turn does not depend on energy. The number N is therefore required to be even. In this case the total rotation is given by

$$A = i^N e^{-i(\frac{\Delta\Psi}{2} + \Delta\varphi)\sigma_3} \ , \quad (2.75)$$

with $\Delta\varphi = \varphi_N - \varphi_{N-1} \pm \ldots - \varphi_1$. For N Siberian Snakes in a ring with otherwise spin rotations only around the vertical, the following three conditions are required:

- $\Delta\Psi = 0$, to make ν_0 independent of energy.
- N is even, to make $\vec{\nu}$ vertical in the arcs of the ring.
- $\Delta\varphi = \frac{\pi}{2}$, to make $\nu_0 = \frac{1}{2}$.

All imperfection resonances and, since the orbital tunes cannot be 1/2, also all first–order intrinsic resonances are avoided by the insertion of such Siberian Snakes [74], and polarized beam acceleration to very high energy could become possible. Siberian Snakes can only be used at sufficiently high energies since their fields are not changed during acceleration of the beam and they produce orbit distortions which are too big for energies below approximately 8GeV [75].

The orbit deviation in the Siberian Snakes built for RHIC is up to 3cm at injection momentum of about 25GeV/c as shown in figure 2.4 (left). The orbit motion outside the Siberian Snake, however, is hardly changed by the insertion of this device. One such snake is made of 4 helical dipole magnets of about 2.4m length [76]. Figure 2.4 (right) depicts the design orbit in a RHIC Siberian Snake in three dimensions. It is obvious why these devices, first suggested in Novosibirsk [69] received their name.

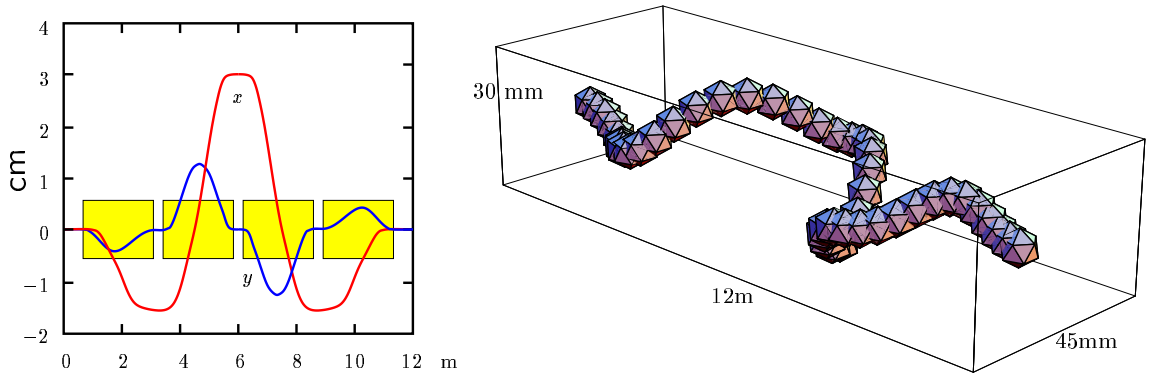

Figure 2.4: Orbit motion in a helical snake designed for RHIC.

Since DESY III, the first synchrotron in the HERA–p accelerator chain, has a super–periodicity 8, only 4 strong intrinsic first–order resonances have to be crossed. They are at momenta of 1.69GeV/c, 2.05GeV/c, 6.05GeV/c, and 6.37GeV/c where the closed–orbit spin tune $\nu_0 = G\gamma$ is $8-Q_y$, $0+Q_y$, $16-Q_y$, and $8+Q_y$ for $Q_y = 4.3$. The polarization can be conserved by jumping the tune with pulsed quadrupoles in a few microseconds or by excitation of a resonance with an RF dipole, whereas a solenoid partial snake would be used to cross the one strong imperfection resonance at $G\gamma = 8$ as mentioned in section 2.2.1. All these methods have been tested successfully at the AGS and it is likely that a highly polarized proton beam could be extracted from the DESY III synchrotron at 7.5GeV/c .

In PETRA it would be very cumbersome to cross all resonances by the aid of the tune jumping technique or by RF dipole excitation. Since Siberian Snakes can be constructed for the injection energy of PETRA [22, 75], the best choice will be to avoid all first–order resonances by means of two such devices. There is space for Siberian Snakes in the east and the west section of PETRA [21, 22].

2.2.4 Changes of the accelerator chain for HERA–p

HERA–p is a very complex accelerator and a brief look already indicates 4 reasons why producing a polarized beam in HERA–p is more difficult than in a conventional flat ring with some super–periodicity.

1. HERA–p has no exact super–periodicity and only an approximate mirror symmetry between the North and South halves of the ring. Therefore $P_s = 1$ in equation (2.71) and more resonances appear than in a ring with some higher super–periodicity. Furthermore, special schemes for canceling resonances in symmetric lattices [77] are not very effective in such a ring.

2. The proton ring of HERA–p is located above the electron ring in the arcs. The proton beam is bent down to the level of the electron ring on both sides of the three experiments H1, HERMES, and ZEUS in the North, East, and South straight sections. Figure 2.5 (left) schematically shows the dipole magnets

which bend the proton beam into the plane of the electron beam. On entering a vertical bend section from the arc, a beam first encounters a super–conducting magnet called BV which bends vertically downwards. This is followed by 4 identical magnets which are called BH in this report and which bend the beam towards the center. Finally, the beam is brought back to the horizontal by three identical vertical bend magnets called BU. The combined effect of the BV and BU magnets surrounding a straight section is only a local change in the vertical position of the beam pipe. Nevertheless, the spin motion is strongly affected as shown by the number of spin rotations performed in each magnet:

Magnet	bend	Bending direction	Spin rotations at 920GeV
BV	5.7mrad	vertically downwards	1.6
BU	1.9mrad	vertically upwards (3×)	0.5
BH	15.1mrad	horizontal	4.2

HERA–p is therefore not a flat ring and $\vec{n}_0$ is in general not vertical and will depend on the particles' energy, which can lead to a loss of polarization during the acceleration cycle and during the energy oscillation in every synchrotron period. This destructive effect of the vertical bends can, however, be eliminated by so–called flattening snakes [78, 79] which make $\vec{n}_0$ vertical outside the non–flat sections of HERA–p. These are radial Siberian Snakes, with a spin rotation characterized by $i\sigma_1$, which are inserted in the center between the BV and the BU magnets. When the BV magnet rotates spins by the angle Ψ_v and a pair of BH magnets produce the angle Ψ_h, then the total spin rotation of the non–flat region is given by the quaternion

$$e^{i\frac{\Psi_v}{2}\sigma_1}e^{-i\frac{\Psi_h}{2}\sigma_3}i\sigma_1 e^{-i\frac{\Psi_h}{2}\sigma_3}e^{-i\frac{\Psi_v}{2}\sigma_1} = e^{-i\frac{\Psi_v}{2}\sigma_1}i\sigma_1 e^{i\frac{\Psi_v}{2}\sigma_1} = i\sigma_1 \ ; \qquad (2.76)$$

which means that one non–flat region then rotates spins by π around the radial direction. Two non–flat regions, one to the right and one to the left of a collision point, compensate each other's spin rotation so that particles on the closed orbit leave these two non–flat regions with the same spin direction with which they entered. Since the rest of HERA–p has a horizontal flat design orbit, the flattening snakes create an effectively flat ring with vertical $\vec{n}_0$ and $\nu_0 = G\gamma - 6\Psi_h/\pi)$. The closed–orbit spin tune ν_0 is less than $G\gamma$ since the horizontal bends in the 6 non–flat regions in the North, East, and South do not contribute to the spin rotation during one turn.

3. There is space for spin rotators which make the polarization parallel to the beam direction inside the collider experiments while keeping it vertical in the arcs, and there is space for a flattening snake in the center of each non–flat region. There is also space for 4 Siberian Snakes. But installing more than 4 Siberian Snakes would involve a lot of costly construction work. Simulations have shown that 8 snakes would be desirable. However, it turned out to be critical to optimize the 8 snake angles since four–snake schemes can be better than eight–snake schemes when the snake angles are not properly chosen [80].

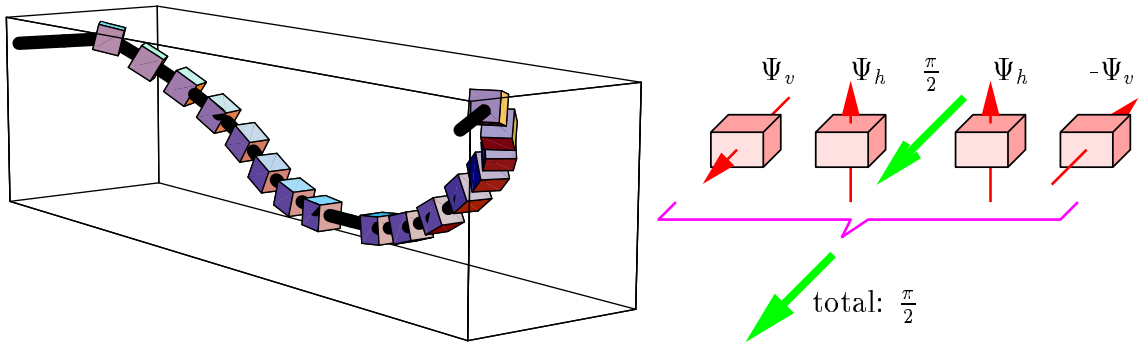

Figure 2.5: Left: Interleaved horizontal and vertical magnets in HERA–p which direct the proton beam into the plain of the electron beam. Right: The radial Siberian Snakes in between the vertical magnets are called flattening snakes. Every non–flat region with a flattening snake rotates spins by π around the radial direction.

4. The relevant energies, and thus the magnetic fields, are very high and therefore the spin rotates rapidly.

If HERA–p had been designed for polarized proton acceleration, several parts of the ring would probably have been constructed differently.

The changes required in the pre–accelerator chain and in HERA–p itself are summarized in figure 2.6. The polarized H^- source and the polarimeters mentioned in chapter 1 as well as the partial snake for DESY III and Siberian Snakes for PETRA are shown in this figure. In HERA–p, the flattening snakes and spin rotators, which make the spin longitudinal in the experiment, are indicated. Either 4 or 8 Siberian Snakes are indicated in HERA–p.

2.2.5 The Invariant Torus

The synchrotron radiation in proton synchrotrons which can be built today is so weak that particle motion can usually be described by a Hamiltonian. It is then often convenient to consider canonical phase space coordinates $\vec{z}$ in one Poincaré section [81] at azimuth θ_0 of the ring. I assume that action variables $J_j(\vec{z})$ and angle variables $\Phi_j(\vec{z})$ for each of the three degrees of freedom indicated by j can be introduced in a domain of the 6 dimensional phase space of equation (2.19). The actions have not changed after one turn around the ring and the angles advance by an action dependent phase advance $2\pi Q_j(\vec{J})$ during one 2π period in θ. In accelerator physics, the functions Q_j are the amplitude dependent tunes. A particle starting with an initial phase space coordinate $\vec{z}_i$ will arrive at the final coordinate $\vec{z}_f = \vec{M}(\vec{z}_i)$ after one turn around the ring; where $\vec{M}(\vec{z}) = \vec{M}(\vec{z}, \theta_0; \theta_0 + 2\pi)$ is the transport map for one turn starting at θ_0. In terms of action–angle variables, the motion after one turn is described by

$$\vec{J}(\vec{M}(\vec{z})) = \vec{J}(\vec{z}) \ , \quad \vec{\Phi}(\vec{M}(\vec{z})) = \vec{\Phi}(\vec{z}) + 2\pi\vec{Q}(\vec{J}(\vec{z})) \ . \tag{2.77}$$

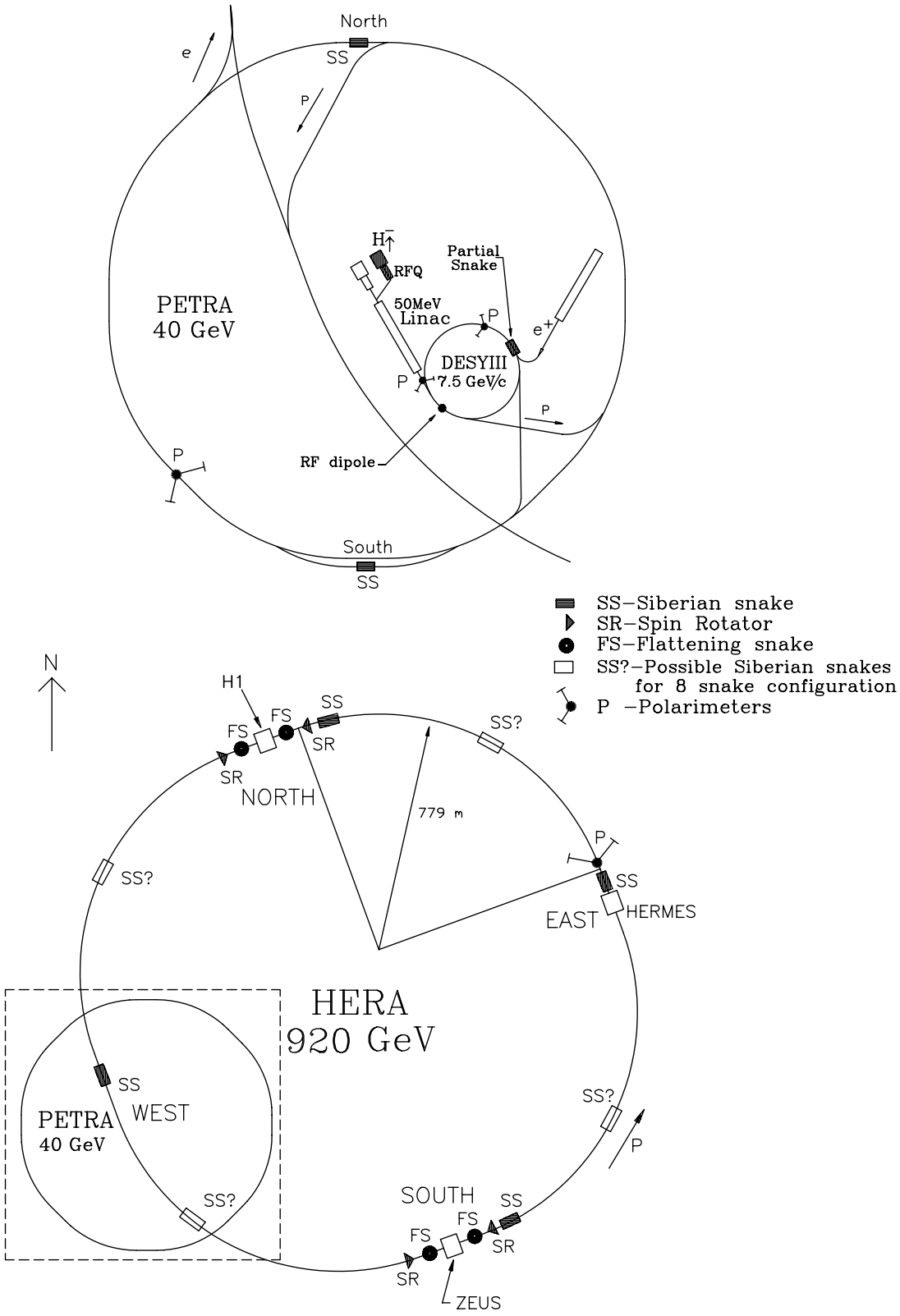

Figure 2.6: The required changes in the pre–accelerator chain and in HERA–p. (Drawing taken from [22, 26]).

Since it will be clear from the context which Poincaré section is under consideration, the dependence on θ_0 of the one turn transport map and of the transformation to action–angle variables is not indicated.

A particle with initial action variables $\vec{J}_i$ will travel on the invariant torus determined by $\vec{J}(\vec{z}) = \vec{J}_i$ at azimuth θ_0. If the three tunes and 1 are incommensurable so that there are no resonances $\vec{j} \cdot \vec{Q} = j_0$ for any integers j_n, the particle will come arbitrarily close to every phase space point of the invariant torus. One speaks of an invariant torus since the set of phase space points on the torus is mapped onto itself by the one turn transport map. This means that particles starting on an invariant torus get redistributed in phase space during one turn around the ring, but they stay on the same torus. Similarly one calls $I(\vec{z})$ an invariant function of motion if $I(\vec{M}(\vec{z})) = I(\vec{z})$.

For horizontal linear orbit motion, an example is the Courant Snyder invariants [54] $I_x(x, a, \theta) = \beta(\theta)a^2 + 2\alpha(\theta)ax + \gamma(\theta)x^2$. The invariant curve $I_x(x, a, \theta_0) = \epsilon_x$ encloses the area $\pi\epsilon_x$ in the Poincaré section at θ_0 . These rather well known concepts are mentioned here since there are much less known analogous concepts for spin motion.

2.2.6 The Invariant Spin Field

In order to maximize the number of collisions of particles inside the experimental detectors of a storage ring system, one tries to maximize the total number of particles in the bunches and tries to minimize the emittances so that the particle distribution across phase space is narrow and the phase space density is high. If the beam is spin polarized, one additionally requires that the polarization is high and that it does not change much with time.

When all particles of a beam are initially completely polarized parallel to each other, the polarization state of the beam is in general not 2π periodic and the average beam polarization can change from turn to turn. Spin fields are propagated by equation (2.28). A special spin field $\vec{n}(\vec{z}, \theta)$ which is 2π periodic in θ is called an invariant spin field,

$$\vec{n}(\vec{z}, \theta) = \underline{R}(\vec{z}_i, \theta_0; \theta)\vec{n}(\vec{z}_i, \theta_0) \ , \quad \vec{n}(\vec{z}, \theta + 2\pi) = \vec{n}(\vec{z}, \theta) \ . \tag{2.78}$$

If the spin of each particle in a beam is initially polarized parallel to $\vec{n}(\vec{z}, \theta_0)$, particles get redistributed in phase space during one turn, but they will stay polarized parallel to the invariant spin field. The beam is then in an equilibrium spin state. Particles change their location in phase space from some initial phase space coordinate $\vec{z}_i$ in the Poincaré section at azimuth θ_0 to some final coordinate after one turn $\vec{z}_f = \vec{M}(\vec{z}_i)$ according to the one turn map. After one turn, a spin has changed its direction according to the one turn spin transport matrix $\underline{R}(\vec{z}_i) = \underline{R}(\vec{z}_i, \theta_0; \theta_0 + 2\pi)$, but it is now parallel to the invariant spin field at the particle's new phase space coordinate $\vec{z}_f$, and equation (2.79) is therefore equivalent to the periodicity condition

$$\vec{n}(\vec{M}(\vec{z})) = \underline{R}(\vec{z})\vec{n}(\vec{z}) \ . \tag{2.79}$$

The invariant spin field was first introduced by Derbenev and Kondratenko [82] in the theory of radiative electron polarization and is often called the Derbenev–Kondratenko $\vec{n}$–axis. Note that $\vec{n}(\vec{z})$ is usually not an eigenvector of the spin transport matrix $\underline{R}(\vec{z})$ at some phase space point since the spin of a particle has changed after one turn around the ring, but the eigenvector does not change when it is transported by $\underline{R}(\vec{z})$.

The guide fields in storage rings are produced by dipole and quadrupole magnets. The dipole fields constrain the particles to almost circular orbits and the quadrupole fields focus the beam, thus ensuring that the particles do not drift too far away from the central orbit. In these fields, spins precess according to the T–BMT equation (2.22).

In horizontal dipoles, spins precess only around the vertical field direction. The quadrupoles have vertical and horizontal fields and additionally cause the spins to precess away from the vertical direction. The strength of the spin precession and the precession axis in machine magnets depends on the trajectory and the energy of the particle. Thus in one turn around the ring the effective precession axis can deviate from the vertical and can strongly depend on the initial position of the particle in 6 dimensional phase space of equation (2.19). From this it is clear that if an invariant spin field $\vec{n}(\vec{z})$ exists, it can vary strongly across the orbital phase space.

Once this field $\vec{n}(\vec{z})$ together with the phase space dependent polarization, its direction, and the phase space density function $\rho(\vec{z})$ of the beam are known, one has a complete specification of the polarization state of a beam of spin 1/2 particles. Maximizing the polarization of the ensemble implies two conditions: the polarization at each point in phase space should be high and the polarization vector $\vec{n}(\vec{z})$ at each point should be almost parallel to the average polarization vector of the particles.

At very high energy, as for example in the HERA proton ring [34, 21, 83], it can happen that $\vec{n}(\vec{z})$ for particles with realistic phase space amplitudes deviates by tens of degrees from the beam average $< \vec{n} >$ at azimuth θ_0. Thus even if each point in phase space were 100% polarized parallel to $\vec{n}(\vec{z})$, the beam average polarization could be much smaller than 100%. Clearly it is very important to have accurate and efficient methods for calculating $\vec{n}(\vec{z})$ and for ensuring that the spread of $\vec{n}(\vec{z})$ is as small as possible.

However, although it has been straightforward to define $\vec{n}(\vec{z},\theta)$, it is not easy to calculate this spin field in general and much effort has been expended on this topic [84, 85, 86, 87, 88, 89, 90, 91], but mainly for electrons at energies up to 46GeV. All methods developed before the polarized proton project at HERA–p were explicitly perturbative, and either do not go to high enough order [12, 63, 91] or have problems with convergence at high order and high proton energies [87, 92]. In chapter 4 several new methods for obtaining $\vec{n}(\vec{z},\theta)$ will be described and compared. But before that, some properties of the invariant spin field will have the be derived.

2.2.7 The Amplitude Dependent Spin Tune and the Uniqueness of $\vec{n}(\vec{z})$

The closed–orbit spin tune ν_0 has been introduced as the rotation angle of one turn spin motion for particles on the closed orbit. For particles which oscillate around the closed orbit, this rotation angle can depend on the amplitude of their oscillation. For the case that the orbit motion can be described in terms of action and angle variables $\vec{J}$ and $\vec{\Phi}$, as is always the case for stable linear motion, and the tunes Q_j are not in resonance on the invariant torus described by $\vec{J}$, it will now be shown how to define a spin rotation angle which is independent of $\vec{\Phi}$ on that torus. Assuming that an $\vec{n}$–axis exists, one can introduce two unit vectors $\vec{u}_1(\vec{z})$ and $\vec{u}_2(\vec{z})$ to create a right handed dreibein $[\vec{u}_1, \vec{u}_2, \vec{n}]$. The vectors $\vec{u}_1$ and $\vec{u}_2$ are therefore defined up to a rotation around the $\vec{n}$–axis by an arbitrary phase space dependent angle $\phi(\vec{z})$. The spin direction $\vec{S}$ is expressed in terms of this coordinate system by $\vec{S} = s_1\vec{u}_1 + s_2\vec{u}_2 + J_S\vec{n}$. The coefficient J_S is called the spin action and does not change during the particle motion around the ring since the particle transport matrix $\underline{R}(\vec{z})$ is orthogonal and ensures that $J_S = \vec{S}\cdot\vec{n}$ is invariant. The spin motion in this coordinate system is a rotation around the $\vec{n}$–axis by a phase space dependent angle $2\pi\tilde{\nu}(\vec{z})$.

$$\begin{pmatrix} s_{f1} \\ s_{f2} \\ J_S \end{pmatrix} = \begin{pmatrix} \cos(2\pi\tilde{\nu}(\vec{z})) & -\sin(2\pi\tilde{\nu}(\vec{z})) & 0 \\ \sin(2\pi\tilde{\nu}(\vec{z})) & \cos(2\pi\tilde{\nu}(\vec{z})) & 0 \\ 0 & 0 & 1 \end{pmatrix} \begin{pmatrix} s_{i1} \\ s_{i2} \\ J_S \end{pmatrix} . \tag{2.80}$$

If now the complex quantity $\hat{s} = e^{i\phi(\vec{z})}(s_1 + is_2)$ is introduced where $\phi(\vec{z})$ is the arbitrary angle of $\vec{u}_1$ and $\vec{u}_2$, the spin transport is described by

$$s_{f1} + is_{f2} = e^{i2\pi\tilde{\nu}(\vec{z})}(s_{i1} + is_{i2}) , \tag{2.81}$$

$$e^{-i\phi(\vec{M}(\vec{z}))}\hat{s}_f = e^{i[2\pi\tilde{\nu}(\vec{z}) - \phi(\vec{z})]}\hat{s}_i . \tag{2.82}$$

The one turn transport of phase space motion is described by $\vec{J}_f = \vec{J}_i$ and $\vec{\Phi}_f = \vec{\Phi}_i + 2\pi\vec{Q}$. Using the symbols $2\pi\tilde{\nu}_{\vec{J}}(\vec{\Phi})$ and $\phi_{\vec{J}}(\vec{\Phi})$ to indicate the spin rotation angle and the free phase of the coordinate system for motion on the invariant torus characterized by $\vec{J}$,

$$\hat{s}_f = e^{i(2\pi\tilde{\nu}_{\vec{J}}(\vec{\Phi}) - \phi_{\vec{J}}(\vec{\Phi}) + \phi_{\vec{J}}(\vec{\Phi}+2\pi\vec{Q}))}\hat{s}_i . \tag{2.83}$$

The goal of the subsequent manipulation is to chose $\phi_{\vec{J}}(\vec{\Phi})$ so that the spin motion characterized by the exponent is simplified to the extent that the rotation angle becomes independent of $\vec{\Phi}$. As with any function of phase space, the rotation $e^{i\phi_{\vec{J}}(\vec{\Phi})}$ is 2π periodic in all components Φ_j. Therefore, the rotation angle $\phi_{\vec{J}}(\vec{\Phi})$ can have a 2π periodic contribution $\phi_{\circ\vec{J}}(\vec{\Phi})$ and a linear contribution in the phases

$$\phi_{\vec{J}}(\vec{\Phi}) = \phi_{\circ\vec{J}}(\vec{\Phi}) + \vec{j}\cdot\vec{\Phi} \tag{2.84}$$

with some vector $\vec{j}$ that has integer components. The phase space dependent spin rotation $e^{i2\pi\tilde{\nu}_{\vec{J}}(\vec{\Phi})}$ is also a 2π periodic function of the angle variables. But since on

the closed orbit ($\vec{J}=0$) the spin motion does not depend on $\vec{\Phi}$, $\tilde{\nu}_{\vec{J}}(\vec{\Phi})$ only has a periodic component and no component linear in $\vec{\Phi}$.

If the orbit tunes $\vec{Q}$ are not in resonance, then $\phi_{\vec{J}}(\vec{\Phi})$ can be chosen to eliminate the phase dependence of the exponent in equation (2.83) completely. This can be seen by Fourier transformation of the periodic functions $\tilde{\nu}_{\vec{J}}(\vec{\Phi})$ and $\phi_{\circ\vec{J}}(\vec{\Phi})$ leading to the following exponent in equation (2.83):

$$2\pi\vec{j}\cdot\vec{Q}+\sum_{\vec{k}}[2\pi\breve{\nu}_{\vec{J}}(\vec{k})-\breve{\phi}_{\circ\vec{J}}(\vec{k})(1-e^{i2\pi\vec{k}\cdot\vec{Q}})]e^{i\vec{k}\cdot\vec{\Phi}}\ . \tag{2.85}$$

By choosing $\breve{\phi}_{\circ\vec{J}}(\vec{k})=2\pi\breve{\nu}_{\vec{J}}(\vec{k})/(1-e^{i2\pi\vec{k}\cdot\vec{Q}})$, one can eliminate all Fourier coefficients except for $\vec{k}=0$.

To guarantee the convergence of the Fourier series of $\phi(\vec{z})$, I require the orbit tunes and 1 to be strongly incommensurable [66, sec.1.5], which implies that they are strongly non–orbit–resonant, defined as follows using the distance to the nearest integer $[\ldots]_d$ and the 1 norm $|\vec{k}|_1=\sum_{n=1}^{3}|k_n|$:

Strongly non–orbit–resonant: *The particle motion is said to be strongly non–orbit–resonant if $C,r\in\mathbb{R}^+$ exist with $[\vec{k}\cdot\vec{Q}]_d\geq C|\vec{k}|_1^{-r}$.*

Strong incommensurability is a common requirement in perturbation theories and for $r>\dim(\vec{k})-1$ (here $\dim(\vec{k})$=3) the set of $\vec{Q}$ for which there is no C has measure 0 [93, 94], [65, appendix 4].

The denominator $1-e^{i2\pi\vec{k}\cdot\vec{Q}}$ then decreases with a power law, $|1-e^{i2\pi\vec{k}\cdot\vec{Q}}|=2|\sin(\pi\vec{k}\cdot\vec{Q})|\geq 4[\vec{k}\cdot\vec{Q}]_d\geq 4C|\vec{k}|_1^{-r}$. I further require that the spin rotation $\tilde{\nu}_{\vec{J}}(\vec{\Phi})$ has an analytic extension and therefore that its Fourier components fall off exponentially with $|\vec{k}|_1$ [65, appendix 1.1], which counterbalances the denominator and leads to a converging Fourier series. Alternatively one could have required sufficient differentiability of $\vec{\nu}_{\vec{J}}(\vec{\Phi})$, which would lead to a sufficiently strong power law fall off for the $\breve{\phi}_{\vec{J}}(\vec{k})$ [65, appendix 1.2].

The coordinate vectors $\vec{\breve{u}}_1$ and $\vec{\breve{u}}_2$ for this special choice of $\phi(\vec{z})$ are referred to as $\vec{u}_1$ and $\vec{u}_2$. The exponent reduces to $\nu(\vec{J})=\breve{\nu}_{\vec{J}}(0)+\vec{j}\cdot\vec{Q}$ and the spin rotation of equation (2.83) simplifies to

$$\hat{s}_f=e^{i2\pi\nu(\vec{J})}\hat{s}_i\ . \tag{2.86}$$

The goal of constructing a spin rotation depending only on orbital actions but not on the angle variables $\vec{\Phi}$ has now been achieved. The function $\nu(\vec{J})$ is called the amplitude dependent spin tune. It is not unique, since one can add an integer j_0 and a linear combination $\vec{j}\cdot\vec{Q}$ of the orbit tunes. It is interesting to note that for action variables $\vec{J}$ where the integer coefficients of $\vec{j}$ can be chosen so that

$$\nu(\vec{J})+\vec{j}\cdot\vec{Q}=0\ \mathrm{mod}\ 1\ , \tag{2.87}$$

one can eliminate the spin rotation completely. Here only the case when this resonance condition is not satisfied will be analyzed. Furthermore, when $-\vec{n}(\vec{z})$ is chosen

as the $\vec{n}$-axis to which the spin tune refers on a torus, the spin tune ν also changes sign and $-\nu + j_0 + \vec{j}\cdot\vec{Q}$ could alternatively be chosen as spin tune, which proves the following conclusion:

Existence of $\nu(\vec{J})$: *Given that an $\vec{n}$–axis exists, that the system is strongly non–orbit–resonant, and that the above mentioned analytic extension of the spin rotation $\tilde{\nu}$ exists, then a coordinate system $[\vec{u}_1, \vec{u}_2, \vec{n}]$ can be specified which defines an amplitude dependent spin tune $\nu(\vec{J})$. This choice is not unique, since $\pm\nu + j_0 + \vec{j}\cdot\vec{Q}$ can also be chosen as spin tune.*

Usually the integers are chosen to let the limit for small amplitudes be equal to the closed–orbit spin tune ν_0, which is $G\gamma$ for a flat ring.

To analyze the uniqueness of the $\vec{n}$–axis, the periodicity condition (2.79) is written in the coordinate system $[\vec{u}_1, \vec{u}_2, \vec{n}]$,

$$\vec{n}(\vec{M}(\vec{z})) = \begin{pmatrix} \cos(2\pi\nu) & -\sin(2\pi\nu) & 0 \\ \sin(2\pi\nu) & \cos(2\pi\nu) & 0 \\ 0 & 0 & 1 \end{pmatrix} \cdot \vec{n}(\vec{z}) \ , \tag{2.88}$$

with the obvious solution $\vec{n}(\vec{z}) = (0,0,1)^T$ for all $\vec{z}$. If another $\vec{n}$–axis $\vec{n}_2(\vec{z})$ exists, then $\vec{n}_2 - \vec{n}(\vec{n}\cdot\vec{n}_2)$ is non–zero at least at one phase space point and on all iterates of this point which can be reached during particle motion. This difference vector at these phase space points is normalized and written as $\cos(\alpha(\vec{z}))\vec{u}_1 + \sin(\alpha(\vec{z}))\vec{u}_2$ or as $e^{i\alpha(\vec{z})}$. In orbital action–angle variables, the function $\alpha_{\vec{J}}(\vec{\Phi}) = \alpha_{\circ\vec{J}}(\vec{\Phi}) + \vec{j}\cdot\vec{\Phi}$ has a 2π periodic contribution and a linear contribution; and in complex notation, the periodicity condition (2.88) reads

$$e^{i\alpha_{\vec{J}}(\vec{\Phi}+2\pi\vec{Q})} = e^{i[2\pi\nu(\vec{J})+\alpha_{\vec{J}}(\vec{\Phi})]} \ . \tag{2.89}$$

This requires that all Fourier coefficients of $\alpha_{\circ\vec{J}}(\vec{\Phi})$ vanish except $\breve{\alpha}_{\circ\vec{J}}(0)$. The resulting equation $\nu(\vec{J}) = \vec{j}\cdot\vec{Q}$ mod 1 shows that the periodicity condition (2.89) for $\vec{n}_2(\vec{z})$ can only be satisfied when a spin–orbit resonance occurs, otherwise the invariant spin field is unique. This is summarized as follows.

Uniqueness of $\vec{n}(\vec{z})$ - no spin–orbit resonance: *If an $\vec{n}$–axis and basis vectors $\vec{u}_1$, $\vec{u}_2$ exist and the spin rotation angle in one turn is not a linear combination of orbit phase advances modulo 2π, then the $\vec{n}$–axis is unique up to a sign.*

If the orbital tunes are rational, one can also formulate some statements about the uniqueness of the $\vec{n}$–axis. Given that the phase space motion can be described by action–angle variables and that the orbital tunes on an invariant torus in the Poincaré section at azimuth θ_0 are rational numbers, $Q_j = \frac{n_j}{m_j}$ where the smallest possible denominators are used, let N be the smallest common multiple of these denominators. Then $\vec{M}^N(\vec{z})$ is the identity map whereas $\vec{M}^n(\vec{z})$ is not the identity map for any $n < N$ and the following conclusions can be drawn:

Uniqueness of $\vec{n}(\vec{z})$ - rational tunes: *If for some $N \in \mathbb{N}$, the N turn spin transport matrix on an invariant torus is not the identity matrix but the N turn orbital transport map is the identity, then an $\vec{n}$–axis exists and is unique up to a sign on this invariant torus.*

To show this, the spin transport matrix $\underline{R}_N(\vec{z})$ for N turns around the ring starting at θ_0 is used. Since it is not the identity matrix, it describes a rotation around a vector $\vec{e}_N(\vec{z})$ which is unique up to a sign. After N turns, the phase space transport map is the identity map and the periodicity condition of equation (2.79) for an $\vec{n}$–axis $\vec{n}_N(\vec{z})$ of the N turn spin–orbit system becomes $\vec{n}_N(\vec{z}) = \underline{R}_N(\vec{z})\vec{n}_N(\vec{z})$. The rotation vector $\vec{e}_N(\vec{z})$ is therefore the $\vec{n}$–axis $\vec{n}_N(\vec{z})$, unique up to a sign. The rotation vector $\vec{e}_N(\vec{M}(\vec{z})$ of $\underline{R}_N(\vec{M}(\vec{z}))$ is given by $\pm\underline{R}(\vec{z})\vec{e}_N(\vec{z})$ due to

$$\underline{R}_N(\vec{M}(\vec{z}))\underline{R}(\vec{z})\vec{e}_N(\vec{z}) = \underline{R}(\vec{M}^N(\vec{z}))\underline{R}_N(\vec{z})\vec{e}_N(\vec{z}) = \underline{R}(\vec{z})\vec{e}_N(\vec{z}) \ . \tag{2.90}$$

Here the fact that $\vec{M}^N(\vec{z})$ is the identity map was used. The rotation vectors are unique up to a sign and $\vec{e}_N(\vec{z})$ satisfies the periodicity condition of an $\vec{n}$–axis up to a possible sign change,

$$\vec{e}_N(\vec{M}(\vec{z})) = \pm\underline{R}(\vec{z})\vec{e}_N(\vec{z}) \ . \tag{2.91}$$

Since $\vec{M}^N(\vec{z})$ is the identity map, a particle with initial phase space point $\vec{z}_i$ can only reach the N phase space points $Z(\vec{z}_i) = \{\vec{z}|\vec{M}^n(\vec{z}_i), n \in \{1, \ldots, N\}\}$ which will be called the trajectory to $\vec{z}_i$. Given that the sign for $\vec{e}_N(\vec{z}_i)$ has been chosen, then the sign of the rotation vectors on the trajectory to $\vec{z}_i$ is chosen so that the $+$ sign in equation (2.91) is obtained. This equation is then the periodicity condition of equation (2.79) for $\vec{e}_N(\vec{z})$ and shows that $\vec{n}(\vec{z}) = \vec{e}_N(\vec{z})$ is an invariant spin field which is unique up to a sign for each trajectory. Assuming sufficient smoothness of $\underline{R}_N(\vec{z})$, the rotation vector $\vec{e}_N(\vec{z})$ will also vary smoothly over phase space and the signs on each trajectory is chosen so that $\vec{n}(\vec{z}) = \vec{e}_N(\vec{z})$ is a smooth function on the invariant torus.

Non–uniqueness of $\vec{n}(\vec{z})$: *If for some $N \in \mathbb{N}$, the N turn spin transport matrix on the invariant torus and also the N turn transport map are the identity, then an $\vec{n}$–axis exists but it is not unique.*

To show this, $\vec{f}(\vec{z}_0)$ is chosen arbitrarily, where the angle variables corresponding to $\vec{z}_0$ are $\vec{\Phi}_0 = 0$. An additional choice for the spin field $\vec{f}$ is $\vec{f}(\vec{z}) = \underline{R}(\vec{z}_0)\vec{f}(\vec{z}_0)$ for $\Phi_j = \frac{2\pi}{m_j}$ with the smallest possible denominators m_j of the rational tunes Q_j . All other values of $\vec{f}(\vec{z})$ on the set with $\Phi_j \in [0, 2\pi/m_j]$, which covers the complete torus when iterated N times, are chosen arbitrarily but smooth. If $\vec{z}_i$ is a point on this set, then the values of $\vec{f}(\vec{M}^n(\vec{z}_i))$ for the other $N-1$ points $\vec{M}^n(\vec{z}_i)$ of the trajectory $Z(\vec{z}_i)$ are chosen according to $\vec{f}(\vec{M}(\vec{z})) = \underline{R}(\vec{z})\vec{f}(\vec{z})$ so that a spin will be transported from $\vec{f}(\vec{z}_i)$ by the T–BMT equation to $\vec{f}(\vec{z}_f)$ whenever it comes to azimuth θ_0. This function $\vec{f}(\vec{z})$ is therefore an invariant spin field and since it was chosen arbitrarily for a set of points on the torus, it is not unique.

2.2.8 Maximum Time Average Polarization

If two particles travel along the same trajectory, the angle between their spins does not change. Since $\vec{n}(\vec{z})$ is a spin field on the Poincaré section at θ_0 and is therefore propagated according to the T–BMT equation (2.28), a particle which is initially polarized with an angle ϑ with respect to $\vec{n}(\vec{z}_i)$ will have the angle ϑ with respect to $\vec{n}(\vec{z})$ every time it comes back to θ_0. This is due to the fact that the scalar product $J_S(\vec{z},\vec{S}) = \vec{S}\cdot\vec{n}(\vec{z})$ is an invariant of spin–orbit motion. When $(\vec{z}_i,\vec{S}_i)$ are the initial phase space point and the initial spin of a particle then the final coordinates after one turn around the ring give

$$\begin{aligned} J_S(\vec{z}_f,\vec{S}_f) &= J_S(\vec{M}(\vec{z}_i),\underline{R}(\vec{z}_i)\vec{S}_i) = [\underline{R}(\vec{z}_i)\vec{S}_i]\cdot\vec{n}(\vec{M}(\vec{z}_i)) \\ &= [\underline{R}(\vec{z}_i)\vec{S}_i]\cdot[\underline{R}(\vec{z}_i)\vec{n}(\vec{z}_i)] = \vec{S}_i\cdot\vec{n}(\vec{z}_i) = J_S(\vec{z}_i,\vec{S}_i)\ . \end{aligned} \tag{2.92}$$

Whenever the particle comes back to θ_0 with a phase space coordinate which is close to $\vec{z}_i$, the spin will again have the angle ϑ with respect to $\vec{n}(\vec{z}_i)$, assuming $\vec{n}(\vec{z})$ is sufficiently continuous. Since the components perpendicular to the $\vec{n}$–axis average to zero after many turns, the time averaged polarization at $\vec{z}_i$ will be parallel to $\vec{n}(\vec{z}_i)$, and it can only have the magnitude 1 if the spin was initially parallel to the invariant spin field. However, even if all particles are initially polarized parallel to $\vec{n}(\vec{z})$, the beam polarization is not 1 but $|<\vec{n}>|$ where $<\ldots>$ denotes the average over the beam. The maximum time average beam polarization that can be stored in an accelerator at a given fixed energy is therefore $P_{lim} = |<\vec{n}>|$. It was first pointed out in [95] for the Super–conducting Super Collider (SSC) and in [20] for HERA–p that this maximum polarization can be small at high energy.

To prove in a formal way that the time average polarization is parallel to $\vec{n}(\vec{z})$ if an invariant spin field exists and if the phase space coordinates stay on an invariant torus, I assume the beam to have initially the spin field on the Poincaré section at θ_0 and perform the time average in the coordinate system $[\vec{u}_1,\vec{u}_2,\vec{n}]$ introduced in section 2.2.7. Action–angle variables are used and the initial spin field in this coordinate system is written as $\vec{f}_0(\vec{\Phi})$. The action variables $\vec{J}$ are constant during a particle's motion and will not be indicated in the following derivation.

It is assumed that $\vec{f}_0(\vec{\Phi})$ possesses an analytic extension for $\Phi_j \in \mathbb{C}$, $\mathrm{Im}\{\Phi_j\} < \sigma$ with $\sigma > 0$, and it is assumed that the system is strongly non–orbit–resonant, implying $[\vec{j}\cdot\vec{Q}]_d \geq C|\vec{j}|_1^{-r}$ for some $C, r \in \mathbb{R}^+$. Like the requirement of an analytic extension and of strong incommensurability in section 2.2.7, these conditions will be needed to guarantee the convergence of a Fourier series with resonance denominators. Furthermore it is assumed that the motion is strongly non–spin–orbit–resonant in the following sense:

Strongly non–spin–orbit–resonant: *The particle motion is said to be strongly non–spin–orbit–resonant if $C, r \in \mathbb{R}^+$ exist with $[\nu + \vec{k}\cdot\vec{Q}]_d \geq C|\vec{k}|_1^{-r}$. Note that this is a weaker condition than strong incommensurability of the spin–orbit tunes and 1 since ν is not multiplied by an integer.*

As in section 2.2.7, the set of spin and orbit tunes for which there is no C, given that $r > 2$, has measure 0.

As described in equation 2.28, the spin field is transported once around the ring by the one turn spin transport matrix, which has an especially simple form in the chosen coordinate system,

$$\vec{f}_j(\vec{\Phi}) = \begin{pmatrix} \cos(2\pi\nu) & -\sin(2\pi\nu) & 0 \\ \sin(2\pi\nu) & \cos(2\pi\nu) & 0 \\ 0 & 0 & 1 \end{pmatrix} \vec{f}_{j-1}(\vec{\Phi} - 2\pi\vec{Q}) \ , \tag{2.93}$$

where $\vec{f}_j(\vec{\Phi})$ is the spin field on the Poincaré section at θ_0 after N turns around the ring. The average at θ_0 after N turns in this coordinate system is therefore

$$\{\vec{f}\}_N(\vec{\Phi}) = \frac{1}{N+1}\sum_{j=0}^{N} \begin{pmatrix} \cos(j2\pi\nu) & -\sin(j2\pi\nu) & 0 \\ \sin(j2\pi\nu) & \cos(j2\pi\nu) & 0 \\ 0 & 0 & 1 \end{pmatrix} \vec{f}_0(\vec{\Phi} - j2\pi\vec{Q}) \ . \tag{2.94}$$

The third component of $\{\vec{f}\}_N$ is $\sum_{j=0}^{N} f_{0,3}(\vec{\Phi} - j2\pi\vec{Q})/(N+1)$ and the first and second components in complex notation are

$$\{\hat{f}\}_N = \{f\}_{N,1} + i\{f\}_{N,2} = \frac{1}{N+1}\sum_{j=0}^{N} e^{ij2\pi\nu}\hat{f}_0(\vec{\Phi} - j2\pi\vec{Q}) \ , \tag{2.95}$$

where $\hat{f}_0(\vec{\Phi}) = f_{0,1}(\vec{\Phi}) + if_{0,2}(\vec{\Phi})$. In terms of the Fourier components $\breve{f}_0(\vec{k})$ of $\hat{f}_0(\vec{\Phi})$ one obtains the inequality

$$\begin{aligned} |\{\hat{f}\}_N| &= |\frac{1}{N+1}\sum_{\vec{k}}\sum_{j=0}^{N} e^{ij2\pi(\nu-\vec{k}\cdot\vec{Q})}\breve{f}_0(\vec{k})e^{i\vec{k}\cdot\vec{\Phi}}| \\ &= \frac{1}{N+1}|\sum_{\vec{k}}\frac{1-e^{i(N+1)2\pi(\nu-\vec{k}\cdot\vec{Q})}}{1-e^{i2\pi(\nu-\vec{k}\cdot\vec{Q})}}\breve{f}_0(\vec{k})e^{i\vec{k}\cdot\vec{\Phi}}| \\ &\leq \frac{1}{N+1}\sum_{\vec{k}}\frac{2}{|1-e^{i2\pi(\nu-\vec{k}\cdot\vec{Q})}|}|\breve{f}_0(\vec{k})| \ . \end{aligned} \tag{2.96}$$

The sum over $\vec{k}$ is finite, since $\vec{f}_0(\vec{\Phi})$ was assumed to have analytic extension so that its Fourier components fall off exponentially with $|\vec{k}|_1$. Moreover, the denominator only falls off with a power law in $\vec{k}$ since the motion is strongly non–spin–orbit–resonant. Therefore $|1-e^{i2\pi(\nu-\vec{k}\cdot\vec{Q})}| = 2|\sin(\pi(\nu-\vec{k}\cdot\vec{Q}))| \geq 4[\nu-\vec{k}\cdot\vec{Q}]_d \geq C|\vec{k}|_1^{-r}$. As an alternative to requiring an analytic extension of $\vec{f}_0(\vec{\Phi})$, one could have required sufficient differentiability which would lead to a sufficiently strong power law fall off for the $\breve{f}_0(\vec{k})$ [65, appendix 1].

Similarly one obtains for the third component of $\{\vec{f}\}_N$

$$\{f\}_{N,3} = \breve{f}_{0,3}(0) + \frac{1}{N+1}\sum_{\vec{k}\neq 0}\frac{1-e^{-i2\pi(N+1)\vec{k}\cdot\vec{Q}}}{1-e^{-i2\pi\vec{k}\cdot\vec{Q}}}\breve{f}_{0,3}(\vec{k})e^{i\vec{k}\cdot\vec{\Phi}} \ , \tag{2.97}$$

were the sum over $\vec{k}$ converges for the given strongly non–orbit–resonant motion. For large N, $\{\vec{f}\}_N$ therefore converges linearly with $1/N$ to $\breve{f}_{0,3}\vec{n}$. The time average

polarization $\{\vec{f}\}(\vec{z}) = \lim_{N\to\infty}\{\vec{f}\}_N(\vec{z})$ at a phase space point $\vec{z}_i$, which is parallel to $\vec{n}(\vec{z}_i)$, can only be one if the initial spin state was already parallel to this $\vec{n}$–axis at every phase space point from which a particle can travel to $\vec{z}_i$. If $\{\vec{f}\}(\vec{z})$ is zero, there is no time average polarization usable for the particle physics experiment. This proves the following conclusion:

Time averaged polarization: *If the motion is strongly non–orbit–resonant and strongly non–spin–orbit–resonant and an invariant spin field $\vec{n}(\vec{z})$ exists on an invariant torus, then any initial spin field (which satisfies some requirement about analytic extensibility given above) has a time average polarization at a phase space point $\vec{z}$ which is parallel to $\vec{n}(\vec{z})$. The maximum time average polarization of a particle beam is the beam average $P_{lim} = |<\vec{n}>|$ which is only realized when initially all particles are polarized parallel to $\vec{n}(\vec{z})$.*

2.2.9 The Adiabatic Spin Invariant on Phase Space Trajectories

As described in the previous section, the maximum time average polarization attainable in a storage ring at a fixed energy can be small when $\vec{n}(\vec{z})$ has a large divergence over the beam leading to a small beam average $|<\vec{n}>|$. It is however often possible, as will be seen for HERA–p in later sections, to choose an operation energy where the spread of the invariant spin field over the beam is acceptably small. But how can a polarized proton beam be transported with little loss of polarization from low energy through regions with small $P_{lim} = |<\vec{n}>|$, and therefore small beam polarization, to a suitable energy where P_{lim} is acceptable? Can the beam polarization recover to large values at this suitable energy after it was much smaller, at least as small as P_{lim}, at lower energies?

This is possible if the spins which are initially parallel to $\vec{n}(\vec{z})$ remains close to the invariant spin field along its trajectory even when parameters of particle motion, for example the energy, are slowly changed. The invariant spin field $\vec{n}(\vec{z},\tau)$ on the Poincaré section at θ_0 changes when a parameter τ varies. Of course it is assumed that an $\vec{n}$–axis exists for every value of the parameter. A beam which is polarized according to the invariant spin field and initially has the polarization $|<\vec{n}(\vec{z},0)>|$ will remain closely polarized parallel to $\vec{n}(\vec{z},\tau)$ at changed parameter τ, as long as the change is slow enough and no very strong resonance effects diminish the polarization. While the beam is accelerated slowly, the beam polarization can be low when $P_{lim} = |<\vec{n}>|$ is small, but when the spins follow the slow change of $\vec{n}(\vec{z},\tau)$ with the energy parameter τ, the beam can have high polarization later, when energies are reached where P_{lim} is reasonably large.

I will prove that spins follow slow changes of the invariant spin field by showing that the product $J_S = \vec{S}\cdot\vec{n}(\vec{z})$ is an adiabatic invariant. On the closed orbit, the invariant spin field $\vec{n}(\vec{z})$ is parallel to the one turn rotation vector $\vec{n}_0$. It was shown in section 2.2.1 that the angle between $\vec{n}_0(\theta)$ and the spin $\vec{S}(\theta)$ of a particle traveling on the closed orbit changes little when the system changes slowly, and

thereby $s_3(\theta) = \vec{S}(\theta) \cdot \vec{n}_0(\theta)$ was proved to be an adiabatic invariant. This proof will now be generalized to show that $J_S = \vec{S} \cdot \vec{n}(\vec{z}, \tau)$ changes little along a particle trajectory while the spin motion $\vec{S}$ and the phase space motion $\vec{z}$ are subject to equations of motion which change slowly with the parameter $\tau = \varepsilon\theta$,

$$\frac{d}{d\theta}\vec{z} = \vec{v}(\vec{z}, \theta, \tau) \ , \quad \frac{d}{d\theta}\vec{S} = \vec{\Omega}(\vec{z}, \theta, \tau) \times \vec{S} \ . \tag{2.98}$$

It is assumed that action–angle variables $\vec{J}$, $\vec{\Phi}$ and an invariant spin field $\vec{n}(\vec{z}, \tau)$ exist for all fixed parameters $\tau \in [0, 1]$. Furthermore it is assumed that a dreibein $[\vec{u}_1, \vec{u}_2, \vec{n}]$ exists for all fixed parameters $\tau \in [0, 1]$. This leads to an amplitude dependent spin tune $\nu(\vec{J}, \tau)$ which in general depends on τ. These are non–trivial assumptions, since during the analysis of the existence of $\nu(\vec{J})$ in section 2.2.7, the existence of $\vec{u}_1$ and $\vec{u}_2$ was only guarantees when the system is strongly non–orbit–resonant. It is also taken into account that the tunes $\vec{Q}(\vec{J}, \tau)$ of phase space motion depend on the action variables and on the parameter τ which slowly changes the system.

Using the phase space dependent 2π periodic dreibein, the spin of a particle with phase space coordinate $\vec{z}$ at azimuth θ is described by $\vec{S} = s_1\vec{u}_1 + s_2\vec{u}_2 + J_S\vec{n}$. The periodic unit vectors depend on τ and their variation with τ can only be a rotation around some vector $\vec{\eta}(\vec{z}, \theta, \tau)$ when τ is changed,

$$\partial_\tau \vec{n} = \vec{\eta}(\vec{z}, \theta, \tau) \times \vec{n} \ , \quad \partial_\tau(\vec{u}_1 + i\vec{u}_2) = \vec{\eta}(\vec{z}, \theta, \tau) \times (\vec{u}_1 + i\vec{u}_2) \ . \tag{2.99}$$

Similar to equation (2.54) $\vec{\eta}$ can be computed by

$$\vec{\eta} = \frac{1}{2}(\vec{u}_1 \times \partial_\tau \vec{u}_1 + \vec{u}_2 \times \partial_\tau \vec{u}_2 + \vec{n} \times \partial_\tau \vec{n}) \ . \tag{2.100}$$

When now the parameter $\tau = \varepsilon\theta$ changes slowly, the spin changes according to

$$\begin{aligned} \vec{\Omega}(\vec{z}, \theta, \tau) \times \vec{S} &= \frac{d}{d\theta}\vec{S} \qquad (2.101) \\ &= \vec{u}_1 \frac{d}{d\theta}s_1 + \vec{u}_2 \frac{d}{d\theta}s_2 + \vec{n}\frac{d}{d\theta}J_S + (\vec{\Omega} - \nu\vec{n}) \times \vec{S} + (\frac{d}{d\theta}\tau)\vec{\eta} \times \vec{S} \end{aligned}$$

For the spin coordinates, one obtains the following equation of motion:

$$\begin{aligned} \frac{d}{d\theta}\begin{pmatrix} s_1 \\ s_2 \\ J_S \end{pmatrix} &= \begin{pmatrix} \{[\nu(\vec{J}, \tau)\vec{n} - \varepsilon\vec{\eta}] \times \vec{S}\} \cdot \vec{u}_1 \\ \{[\nu(\vec{J}, \tau)\vec{n} - \varepsilon\vec{\eta}] \times \vec{S}\} \cdot \vec{u}_2 \\ \{ \qquad\qquad - \varepsilon\vec{\eta} \times \vec{S}\} \cdot \vec{n} \end{pmatrix} \qquad (2.102) \\ &= \begin{pmatrix} \varepsilon(\ \eta_3 s_2 \ - \ \eta_2 J_S \ ) - \nu(\vec{J}, \tau)s_2 \\ \varepsilon(\ \eta_1 J_S \ - \ \eta_3 s_1 \ ) + \nu(\vec{J}, \tau)s_1 \\ \varepsilon(\ \eta_2 s_1 \ - \ \eta_1 s_2 \ ) \end{pmatrix} \ , \end{aligned}$$

with $\vec{\eta} = \eta_1\vec{u}_1 + \eta_2\vec{u}_2 + \eta_3\vec{n}$ and $\tau = \varepsilon\theta$. This equation is obviously very similar to the equation (2.57) for particles on the closed orbit and again ϕ is introduced for

$1 - J_S^2 \geq \Delta \in I\!R^+$ with $s_1 = \sqrt{1-J_S^2}\cos\phi$ and $s_2 = \sqrt{1-J_S^2}\sin\phi$ and one obtains

$$\frac{d}{d\theta}\begin{pmatrix} J_S \\ \phi \end{pmatrix} = \begin{pmatrix} \varepsilon\,(\eta_2\cos\phi - \eta_1\sin\phi)\sqrt{1-J_S^2} \\ \nu(\vec{J},\tau)+ \quad \varepsilon[(\eta_2\sin\phi + \eta_1\cos\phi)\frac{J_S}{\sqrt{1-J_S^2}} - \eta_3] \end{pmatrix} . \tag{2.103}$$

A similar equation for the change of J_S with slowly changing particle energy has been derived in [95]. Since $\vec{\eta}$ depends on the orbit variables $\vec{J}$ and $\vec{\Phi}$, this system has the slowly varying coordinates $\vec{J}$ and J_S and the quickly varying phases $\vec{\Phi}$ and ϕ. It is therefore suitable for averaging methods. To bring it into standard form, where the frequency only depends on slowly changing variables and the right hand side is 2π periodic in all phases, the slowly changing variable τ with $\frac{d}{d\theta}\tau = \varepsilon$ is used and $\tilde{\theta}$ is introduced as a phase variable with $\frac{d}{d\theta}\tilde{\theta} = 1$. To simplify notations, $\vec{\eta}(\vec{J},\vec{\Phi},\tilde{\theta},\tau)$ is used to define

$$f_{J_S}(\vec{J},\vec{\Phi},J_S,\phi,\tau,\tilde{\theta}) = [\eta_2\cos\phi - \eta_1\sin\phi]\sqrt{1-J_S^2} , \tag{2.104}$$

$$f_{\phi}(\vec{J},\vec{\Phi},J_S,\phi,\tau,\tilde{\theta}) = [\eta_2\sin\phi + \eta_1\cos\phi]\frac{J_S}{\sqrt{1-J_S^2}} - \eta_3 , \tag{2.105}$$

with $\tau = \varepsilon\tilde{\theta}$. The equation of spin–orbit motion becomes

$$\frac{d}{d\theta}\begin{pmatrix} \vec{J} \\ J_S \\ \tau \\ \vec{\Phi} \\ \phi \\ \tilde{\theta} \end{pmatrix} = \begin{pmatrix} 0 \\ 0 \\ 0 \\ \vec{Q}(\vec{J},\tau) \\ \nu(\vec{J},\tau) \\ 1 \end{pmatrix} + \varepsilon \begin{pmatrix} p_J(\vec{J},\vec{\Phi},\tau,\tilde{\theta}) \\ f_{J_S}(\vec{J},\vec{\Phi},J_S,\phi,\tau,\tilde{\theta}) \\ 1 \\ p_{\Phi}(\vec{J},\vec{\Phi},\tau,\tilde{\theta}) \\ f_{\phi}(\vec{J},\vec{\Phi},J_S,\phi,\tau,\tilde{\theta}) \\ 0 \end{pmatrix} . \tag{2.106}$$

The small perturbations p_J and p_Φ to the motion of the action and angle variables are due to the variation of the equation of phase space motion (2.98) with the parameter τ . For accelerators, the 6 dimensional phase space of equation (2.19) is considered and therefore this system of ordinary differential equations has 5 slowly and 5 quickly changing variables for small ε. It is written in the standard form of multi–phase averaging theorems [66, sec.1.9], [65, chapter 6].

To illustrate which kind of resonances can disturb the coupled spin–orbit motion, I perform a coordinate transformation leading to the averaged system in first order of ε . This procedure is very similar to the averaging transformation for the two frequency system obtained for particles on the closed orbit in section 2.2.1. Here $f_{J_S}(\vec{J},\vec{\Phi},J_S,\tau,\phi,\tilde{\theta})$ is linear in trigonometric functions of ϕ and one can try to find a transformation $\bar{J}_S = J_S + \varepsilon u(\vec{J},\vec{\Phi},J_S,\phi,\tau,\tilde{\theta})$ which leads to a simpler equation of motion. These functions u and f_{J_S} are Fourier expanded,

$$f_{J_S} = \sum_{j_0,\vec{j}} (f_j^+(\vec{J},J_S,\tau)e^{i(\vec{j}\cdot\vec{\Phi}+j_0\tilde{\theta}+\phi)} + f_j^-(\vec{J},J_S,\tau)e^{i(\vec{j}\cdot\vec{\Phi}+j_0\tilde{\theta}-\phi)} , \tag{2.107}$$

$$u = \sum_{\vec{j},j_0} (u_j^+(\vec{J},J_S,\tau)e^{i(\vec{j}\cdot\vec{\Phi}+j_0\tilde{\theta}+\phi)} + u_j^-(\vec{J},J_S,\tau)e^{i(\vec{j}\cdot\vec{\Phi}+j_0\tilde{\theta}-\phi)} , \tag{2.108}$$

which leads to

$$\begin{aligned}
\frac{d}{d\theta}\bar{J}_S &= \varepsilon\sum_{\vec{j},j_0}\{[f_j^+ + u_j^+ i(\vec{j}\cdot\frac{d}{d\theta}\vec{\Phi} + j_0 + \frac{d}{d\theta}\phi)]e^{i(\vec{j}\cdot\vec{\Phi}+j_0\tilde{\theta}+\phi)} \\
&+ \quad [f_k^- + u_k^- i(\vec{j}\cdot\frac{d}{d\theta}\vec{\Phi} + j_0 - \frac{d}{d\theta}\phi)]e^{i(\vec{j}\cdot\vec{\Phi}+j_0\tilde{\theta}-\phi)}\} \\
&= \varepsilon\sum_{\vec{j},j_0}\{[f_j^+ + u_j^+ i(\vec{j}\cdot\vec{Q} + j_0 + \nu)]e^{i(\vec{j}\cdot\vec{\Phi}+j_0\tilde{\theta}+\phi)} \\
&+ \quad [f_j^- + u_j^- i(\vec{j}\cdot\vec{Q} + j_0 - \nu)]e^{i(\vec{j}\cdot\vec{\Phi}+j_0\tilde{\theta}-\phi)}\} + O(\varepsilon^2) \ .
\end{aligned}$$

If there is no spin–orbit resonance, then one can choose $u_j^\pm = if_j^\pm/(\vec{j}\cdot\vec{Q} + j_0 \pm \nu)$ and all first–order terms are eliminated except the zeroth Fourier coefficient, leaving the averaged system $\frac{d}{d\theta}\bar{J}_S = \frac{1}{(2\pi)^5}\int_0^{2\pi}\ldots\int_0^{2\pi} f_{J_S}(\vec{J},\vec{\Phi},J_S,\theta,\phi,\tilde{\theta})d\vec{\Phi}d\phi d\tilde{\theta} + O(\varepsilon^2)$. For the case under consideration, the average of f_{J_S} is zero; and for $\theta \in [0, 1/\varepsilon]$, changes of the variable $\bar{J}_S$ of the averaged system are of order ε. Changes of J_S are of the same order, since the difference $\bar{J}_S - J_S = \varepsilon u$ is of order ε, which makes $J_S = \vec{S}\cdot\vec{n}$ an adiabatic invariant as defined in section 2.2.2. However, for this argument it was assumed that $\vec{j}\cdot\vec{Q} + \nu$ does not become integer. Usually however, this cannot be avoided and resonance phenomena between the 5 frequencies of the 5 quickly changing phases can occur. In the following, a multi–phase averaging theorem which includes the crossing of resonances will be applied to the spin–orbit motion. Here I use theorem 2 of [65, sec.6.1] which is attributed to [96].

Theorem (Averaging for N frequency systems): *Consider a system of the form*

$$\frac{d}{d\theta}\vec{I} = \varepsilon\vec{f}(\vec{I},\vec{\phi},\varepsilon) \ , \tag{2.109}$$

$$\frac{d}{d\theta}\vec{\phi} = \vec{\nu}(\vec{I}) + \varepsilon g(\vec{I},\vec{\phi},\varepsilon) \ , \tag{2.110}$$

where $\vec{I}$ belongs to a regular compact subset of Euclidean $\mathbb{R}^m$ and $\vec{\phi} \in \mathbb{R}^n$. Each function on the right hand side is real, C^1 (first–order differentials exist and are continuous) in $\vec{I}$ and ε, periodic with period 2π in all ϕ_j, and each possesses an analytic extension for $\phi_j \in \mathbb{C}$, $\mathrm{Im}\{\phi_j\} < \sigma$ with $\sigma > 0$. The associated averaged system is

$$\frac{d}{d\theta}\bar{\vec{I}} = \varepsilon\bar{\vec{f}}(\bar{\vec{I}}) \ , \quad \bar{\vec{f}}(\bar{\vec{I}}) = \frac{1}{(2\pi)^n}\int_0^{2\pi}\vec{f}(\bar{\vec{I}},\vec{\phi},0)d\vec{\phi} \ , \tag{2.111}$$

with $\bar{\vec{I}}(0) = \vec{I}(0)$. Let the following non–degeneracy condition (called Arnold's condition) be satisfied: "Assuming the frequency $\nu_n(\vec{I}) \neq 0$ (with no loss of generality, since in every region at least one frequency will be non–zero), then the map $\vec{I} \to (\nu_1(\vec{I}),\ldots,\nu_{n-1}(\vec{I}))/\nu_n(\vec{I})$ has maximal rank, equal to $n-1$". Then: for every continuous function $\rho(\varepsilon)$ with $C_1\sqrt{\varepsilon} \leq \rho(\varepsilon) \leq C_2$, $C_1, C_2 \in \mathbb{R}^+$, the set of allowed

initial conditions V *is partitioned* $V = V'(\varepsilon,\rho(\varepsilon)) \bigcup V''(\varepsilon,\rho(\varepsilon))$ *for sufficiently small* ε *such that*

$$\mathrm{Sup}_{\theta\in[0,1/\varepsilon]}|\vec{I}(\theta) - \bar{\vec{I}}(\theta)| < \rho(\varepsilon) \tag{2.112}$$

for $(\vec{I}(0),\vec{\phi}(0)) \in V'$, *i.e. for initial conditions in* V', *the separation between the exact solution and the solution of the averaged system is less than* $\rho(\varepsilon)$. *Moreover, the measure of* $V''(\varepsilon,\rho(\varepsilon))$ *is smaller than* $C\sqrt{\varepsilon}/\rho(\varepsilon)$ *for some* $C \in \mathbb{R}^+$.

When the frequencies are in resonance, the slowly changing variables $\vec{I}$ can accumulate large changes and the solution of the averaged system does not approximate the original system well. In the above theorem, Arnold's condition ensures that no slowly changing variable I_j can change at a resonance without moving the system out of this resonance.

I now apply this averaging theorem for N frequency systems to equation (2.106) of spin–orbit motion. The frequency of the variable $\tilde{\theta}$ is 1 and can therefore be used as ν_n of Arnold's condition. The 4 frequencies $(\vec{Q}(\vec{J},\tau),\nu(\vec{J},\tau))$ depend on 4 of the 5 slowly changing variables and I assume that the rank is 4 so that the Jacobi matrix of the 4 frequencies has non–vanishing determinant, $\det[\partial_{(\vec{J},\tau)}(\vec{Q},\nu)] \neq 0$. A more detailed analysis of the requirement on the involved function is possible [97].

Choosing $\rho(\varepsilon) = \varepsilon^{1/4}$ one finds that the set of initial conditions for which $\mathrm{Sup}_{\theta\in[0,1/\varepsilon]}|\vec{J}(\theta) - \vec{J}(0)| \geq \varepsilon^{1/4}$ has a measure smaller than $C\varepsilon^{1/4}$. The variation of the action variables $\vec{J}$ for $\theta \in [0,1/\varepsilon]$ therefore tends to 0 with ε, except for initial conditions from a set with a measure that also tends to 0 with ε. The action variables are therefore adiabatic invariants as defined in section 2.2.2, which is a well known fact. Additionally it is found that the set of initial conditions for which $\mathrm{Sup}_{\theta\in[0,1/\varepsilon]}|J_S(\theta) - J_S(0)| \geq \varepsilon^{1/4}$ has a measure smaller than $C\varepsilon^{1/4}$. Furthermore the condition $1 - J_S^2 \geq \Delta$ above equation (2.103) excludes a set of initial conditions with a measure that tends to 0 with $\varepsilon \to 0$, as argued after equation (2.70); and therefore $J_S = \vec{S}\cdot\vec{n}(\vec{z})$ is an adiabatic invariant as defined in section 2.2.2.

2.2.10 The Single Resonance Model (SRM)

In the previous sections, $\vec{n}$, $\vec{u}_1$, $\vec{u}_2$, and ν have been introduced and the adiabatic invariance of J_S has been established for a very general class of systems. Now the introduced quantities will be computed for an analytically solvable model and the adiabatic invariance will be illustrated by examining changes of a parameter of this model.

The spin precession vector for particles which oscillate around the closed orbit can be decomposed in the closed orbit contribution $\vec{\Omega}_0$ and a part $\vec{\omega}$ due to the oscillation amplitude, $\vec{\Omega}(\vec{z},\theta) = \vec{\Omega}_0(\theta) + \vec{\omega}(\vec{z},\theta)$. The one turn rotation axis $\vec{n}_0$ precesses around $\vec{\Omega}_0$ and the 2π periodic dreibein $[\vec{m},\vec{l},\vec{n}_0]$ which was introduced in section 2.2.2 precesses according to equation (2.48), $\frac{d}{d\theta}(\vec{m} + i\vec{l}) = (\vec{\Omega}_0 - \nu_0\vec{n}_0)\times(\vec{m} + i\vec{l})$. In this coordinate system, the complex notation $\hat{s} = s_1 + is_2$ and $\omega = \omega_1 + i\omega_2$ is used, with

$$\vec{S} = s_1\vec{m} + s_2\vec{l} + s_3\vec{n}_0 \ , \quad \vec{\omega} = \omega_1\vec{m} + \omega_2\vec{l} + \omega_3\vec{n}_0 \ . \tag{2.113}$$

The equation of motion for $\hat{s}$ is obtained from

$$\vec{\Omega} \times \vec{S} = \vec{m}\frac{d}{d\theta}s_1 + \vec{l}\frac{d}{d\theta}s_2 + \vec{n}_0\frac{d}{d\theta}s_3 + (\vec{\Omega}_0 - \nu_0\vec{n}_0) \times \vec{S} \tag{2.114}$$

by multiplication with $\vec{m} + i\vec{l}$, and taking into account that $s_3 = \sqrt{1 - |\hat{s}|^2}$,

$$\frac{d}{d\theta}\hat{s} = i(\nu_0 + \omega_3)\hat{s} - i\omega\sqrt{1 - |\hat{s}|^2} \ . \tag{2.115}$$

When the motion in phase space can be transformed to action–angle variables, the spin precession vector $\vec{\omega}(\vec{J}, \vec{\Phi}, \theta)$ for particles which oscillate around the closed orbit is a 2π periodic function of $\vec{\Phi}$ and θ . With the possibly amplitude dependent orbit tunes $\vec{Q} = \frac{d}{d\theta}\vec{\Phi}$, the Fourier spectrum of ω has frequencies $j_0 + \vec{j}\cdot\vec{Q}$ with integers j_n . The integer contributions j_0 are due to the 2π periodicity of $\vec{\omega}$ with θ and the contributions of integer multiples of the obit tunes Q_k are due to the periodicity of $\vec{\omega}$ with Φ_k . When one of the Fourier frequencies is nearly in resonance with ν_0, it can be a good approximation to drop all other Fourier components. This is referred to as the single resonance approximation. However, this is not always a good approximation as will become apparent when HERA–p is analyzed in section 3.2.1; it can only be good when the influence of individual resonances is well separated. That model corresponds to the rotating field approximation often used to discuss spin resonance in solid state physics [98]. For a conventional flat ring, the first–order resonance due to vertical motion dominates and therefore most often the resonance $\kappa = j_0 \pm Q_y$ is considered.

The amplitude of the one remaining Fourier contribution is called the resonance strength ϵ_κ. For first–order resonances, where $\sum_{n=1}^{3} |j_n| = 1$, ϵ_κ is computed in section 3.2.1. A method for computing higher–order resonance strength, where $\sum_n = 1^3|j_n| > 1$, is presented for the first time in section 2.2.12.

The analytically solvable model which is now considered consists of $\vec{\Omega}_0 = \nu_0\vec{n}_0$ and of an $\vec{\omega}$ which only has one Fourier contribution, $\vec{\omega} = \epsilon_\kappa(\vec{m}\cos\Phi + \vec{l}\sin\Phi)$, with $\Phi = j_0\theta + \vec{j}\cdot\vec{\Phi} + \Phi_0$. Since $\frac{d}{d\theta}\vec{\Phi} = \vec{Q}$, the frequency is $\kappa = j_0 + \vec{j}\cdot\vec{Q}$. When the coordinates in the $[\vec{m}, \vec{l}, \vec{n}_0]$ system are arranged in column vectors [99, 100], one obtains

$$\frac{d}{d\theta}\Phi = \kappa \ , \quad \frac{d}{d\theta}\vec{s} = \vec{\Omega}(\Phi) \times \vec{s} \ , \quad \vec{\Omega} = \begin{pmatrix} \epsilon_\kappa \cos\Phi \\ \epsilon_\kappa \sin\Phi \\ \nu_0 \end{pmatrix} \ . \tag{2.116}$$

Initial coordinates $\vec{z}_i$ are taken into final coordinates $\vec{z}_f$ by $\vec{\Phi}_f = \vec{\Phi}_i + 2\pi\vec{Q}$ and therefore $\Phi_f = \Phi_i + 2\pi\kappa$. Now the orthogonal matrix $\underline{T}(\vec{e}, \varphi)$ is introduced to describe a rotation around a unit vector $\vec{e}$ by an angle φ. Transforming the spin components of $\vec{s}$ into a rotating frame by $\vec{s}_R = \underline{T}(\vec{e}_1, -\Phi)\cdot\vec{s}$, one obtains the simplified equation of spin motion

$$\frac{d}{d\theta}\vec{s}_R = \vec{\Omega}_R \times \vec{s}_R \ , \quad \vec{\Omega}_R = \begin{pmatrix} \epsilon_\kappa \\ 0 \\ \delta \end{pmatrix} \ , \quad \delta = \nu_0 - \kappa \ . \tag{2.117}$$

If a spin field is oriented parallel to $\vec{\Omega}_R$ in this frame, it does not change from turn to turn. Therefore $\vec{n}_R = \vec{\Omega}_R/|\vec{\Omega}_R|$ is an $\vec{n}$–axis. In the original frame, this $\vec{n}$–axis is

$$\vec{n}(\Phi) = \mathrm{sig}(\delta)\frac{1}{\Lambda}\begin{pmatrix} \epsilon_\kappa \cos\Phi \\ \epsilon_\kappa \sin\Phi \\ \delta \end{pmatrix} \ , \quad \Lambda = \sqrt{\delta^2 + \epsilon_\kappa^2} \ , \tag{2.118}$$

where the 'sign factor' $\mathrm{sig}(\delta)$ has been chosen so that on the closed orbit ($\epsilon_\kappa = 0$) the $\vec{n}$–axis $\vec{n}(\Phi)$ coincides with $\vec{n}_0 = \vec{e}_3$. As with any function of phase space, this $\vec{n}$–axis is a 2π periodic function of the angle variables $\vec{\Phi}$ and of θ . As required, $\vec{n}$ is a solution of the T–BMT equation (2.116), $\frac{d}{d\theta}\vec{n} = \mathrm{sig}(\delta)Q(\vec{e}_2\cos\Phi - \vec{e}_1\sin\Phi) = \vec{\Omega}\times\vec{n}$.

This analytically solvable model can also be used to illustrate the construction of a phase independent but amplitude dependent spin tune $\nu(\vec{J})$ which has been introduced in section 2.2.7. It will be seen that this spin rotation angle, and no other angle which might be alternatively proposed [13, 101], determines the location of resonances. Having got an $\vec{n}$–axis, one can transform the components of $\vec{s}$ into a coordinate system $[\vec{n}, \tilde{\vec{u}}_1, \tilde{\vec{u}}_2]$. With the simple choice

$$\tilde{\vec{u}}_2(\Phi) = \frac{\vec{e}_3\times\vec{n}}{|\vec{e}_3\times\vec{n}|} = \mathrm{sig}(\delta)\begin{pmatrix} -\sin\Phi \\ \cos\Phi \\ 0 \end{pmatrix} \ , \quad \tilde{\vec{u}}_1(\Phi) = \frac{1}{\Lambda}\begin{pmatrix} \delta\cos\Phi \\ \delta\sin\Phi \\ -\epsilon_\kappa \end{pmatrix} \ , \tag{2.119}$$

$\tilde{\vec{u}}_1$ is equal to $\tilde{\vec{u}}_2\times\vec{n}$ and the basis vectors are clearly 2π periodic in $\vec{\Phi}$ and in θ as required. Since the basis vectors $\tilde{\vec{u}}_1$ and $\tilde{\vec{u}}_2$ build an orthogonal dreibein with $\vec{n}$ for all θ, and since $\vec{n}$ precesses around $\vec{\Omega}$, one obtains $\frac{d}{d\theta}\tilde{\vec{u}}_2 = (\vec{\Omega} - \tilde{\nu}\vec{n})\times\tilde{\vec{u}}_2$ for some function $\tilde{\nu}$ of phase space. This definition of $\tilde{\nu}$ was already used in equation (2.80). It is computed by

$$\tilde{\nu} = (\frac{d}{d\theta}\tilde{\vec{u}}_2 - \vec{\Omega}\times\tilde{\vec{u}}_2)\cdot\tilde{\vec{u}}_1 = \mathrm{sig}(\delta)[\begin{pmatrix} -\kappa\cos\Phi + \nu_0\cos\Phi \\ -\kappa\sin\Phi + \nu_0\sin\Phi \\ -\epsilon_\kappa \end{pmatrix}]\cdot\tilde{\vec{u}}_1 = \mathrm{sig}(\delta)\Lambda \ . \tag{2.120}$$

In section 2.2.7, an additional rotation of $\tilde{\vec{u}}_1$ and $\tilde{\vec{u}}_2$ around $\vec{n}$ was used to make $\tilde{\nu}$ independent of the angle variables $\vec{\Phi}$ and to define the amplitude dependent spin tune. Here however, $\tilde{\nu}$ is already independent of $\vec{\Phi}$. In the SRM, $\epsilon_\kappa = |\vec{\omega}(\vec{z})|$, and therefore $\tilde{\nu}$ depends on the orbital amplitude. The amplitude dependent spin tune $\nu(\vec{J})$ can be changed by multiples of the orbit tune, as stated in section 2.2.7. This freedom can be used to obtain a ν which reduces to ν_0 on the design orbit ($\epsilon_\kappa = 0$). This choice is obtained by a rotation of $\tilde{\vec{u}}_1$ and $\tilde{\vec{u}}_2$ around $\vec{n}$ by $-\Phi$, which leads to the amplitude dependent spin tune

$$\nu = \mathrm{sig}(\delta)\Lambda + \kappa \ . \tag{2.121}$$

The corresponding uniformly rotating basis vectors $\vec{u}_1$ and $\vec{u}_2$ become

$$\vec{u}_1 = \tilde{\vec{u}}_1\cos\Phi - \tilde{\vec{u}}_2\sin\Phi \ , \quad \vec{u}_2 = \tilde{\vec{u}}_2\cos\Phi + \tilde{\vec{u}}_1\sin\Phi \ . \tag{2.122}$$

On the closed orbit, the coordinate system now reduces to

$$\vec{n} \to \vec{n}_0 \ , \quad \vec{u}_1 \to \mathrm{sig}(\delta)\vec{m} \ , \quad \vec{u}_2 \to \mathrm{sig}(\delta)\vec{l} \ , \quad \nu \to \nu_0 \ . \tag{2.123}$$

This model leads to the average polarization

$$P_{lim} = |<\vec{n}(\vec{z})>| = \frac{|\delta|}{\sqrt{\delta^2+\epsilon_\kappa^2}} = \sqrt{1-\left(\frac{\epsilon_\kappa}{\Delta}\right)^2} \ , \ \Delta = \nu - \kappa \ , \ \delta = \nu_0 - \kappa \tag{2.124}$$

which is plotted in figure 2.7 (top). The distance of the amplitude dependent spin tune ν from resonance has here been denoted by Δ, which is equivalent with $\tilde{\nu} = \mathrm{sig}(\delta)\Lambda$. In the bottom figure, the spin tune ν of equation (2.121) jumps by $2\epsilon_\kappa$ at the resonance where $\nu_0 = \kappa$. This jump of the spin tune could in general be transformed away since the sign of the spin tune is not uniquely determined, as described in section 2.2.7. This however requires a change of the sign of $\vec{n}$. Here the sign of $\vec{n}$ in equation (2.118) has been fixed by choosing $\vec{n}_0 \cdot \vec{n} > 0$; and the tune jump at resonance can therefore not be transformed away.

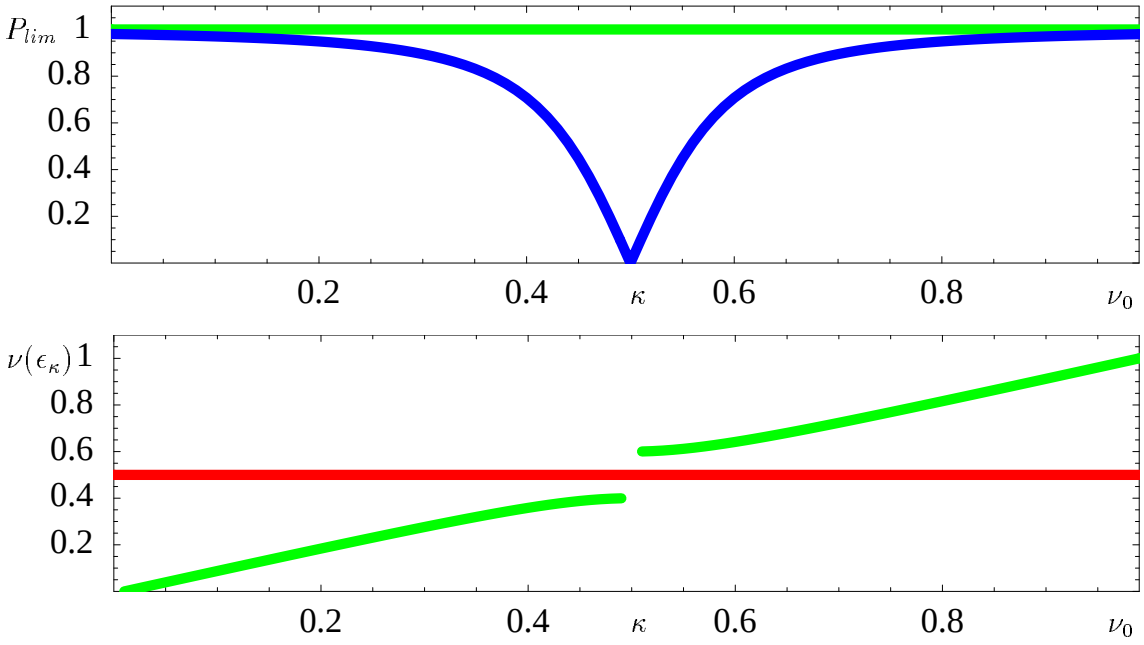

Figure 2.7: P_{lim} and the amplitude dependent spin tune $\nu(\epsilon_\kappa)$ for the SRM in the vicinity of $\nu_0 = \kappa$, for $\kappa = 0.5$ and $\epsilon_\kappa = 0.1$.

For the SRM, we will now go through the steps which were used in section 2.2.9 to describe spin motion when a parameter τ of the system is slowly being changed, i.e. $\frac{d}{d\theta}\tau = \varepsilon$. To avoid confusion with ϵ_κ and to use conventional notation for the SRM, we will subsequently use α instead of ε. To obtain the equation of motion in standard form of averaging theorems, the spin motion was described in the coordinate system $[\vec{u}_1, \vec{u}_2, \vec{n}]$. In order to take account for the change of the basis vectors with the parameter τ, the vector $\vec{\eta}$ was introduced in equation (2.100),

$$\vec{\eta} = \frac{1}{2}(\vec{u}_1 \times \partial_\tau \vec{u}_1 + \vec{u}_2 \times \partial_\tau \vec{u}_2 + \vec{n} \times \partial_\tau \vec{n}) \ . \tag{2.125}$$

Due to $\nu_0 = G\gamma$ in a flat ring, the acceleration process in the SRM is usually described by a slowly changing spin tune $\nu_0 = \kappa + \tau$ with $\tau = \alpha\theta$ while assuming that κ and ϵ_κ do not change with energy. This leads to the following expressions for the variation of the basis vectors and for $\vec{\eta}$:

$$\begin{aligned} \partial_\tau \vec{u}_1 &= \mathrm{sig}(\delta)\frac{\epsilon_\kappa}{\Lambda^2}\vec{n}\cos\Phi \ , \quad \partial_\tau \vec{u}_2 = \mathrm{sig}(\delta)\frac{\epsilon_\kappa}{\Lambda^2}\vec{n}\sin\Phi \ , \quad \partial_\tau \vec{n} = -\mathrm{sig}(\delta)\frac{\epsilon_\kappa}{\Lambda^2}\vec{\tilde{u}}_1 \ , \\ \vec{\eta} &= \mathrm{sig}(\delta)\frac{\epsilon_\kappa}{\Lambda^2}\frac{1}{2}(-\vec{\tilde{u}}_2 - \vec{u}_2\cos\Phi + \vec{u}_1\sin\Phi) = -\mathrm{sig}(\delta)\frac{\epsilon_\kappa}{\Lambda^2}\vec{\tilde{u}}_2 \ . \end{aligned} \tag{2.126}$$

In a general system, the equation of motion for the coefficients of $\vec{S} = \vec{u}_1 s_1 + \vec{u}_2 s_2 + \vec{n} J_S$ are described in equation (2.102) as

$$\frac{d}{d\theta}\begin{pmatrix} s_1 \\ s_2 \\ J_S \end{pmatrix} = \begin{pmatrix} \alpha(\ \eta_3 s_2 \ - \ \eta_2 J_S \ ) - \nu(\vec{J},\tau)s_2 \\ \alpha(\ \eta_1 J_S \ - \ \eta_3 s_1 \ ) + \nu(\vec{J},\tau)s_1 \\ \alpha(\ \eta_2 s_1 \ - \ \eta_1 s_2 \ ) \end{pmatrix} \ . \tag{2.127}$$

In complex notation with $\hat{s} = s_1 + i s_2$, $\eta = \eta_1 + i\eta_2$ and $J_S = \sqrt{1 - |\hat{s}|^2}$, one obtains

$$\frac{d}{d\theta}\hat{s} = i[\nu(\vec{J},\tau) - \alpha\eta_3]\hat{s} + i\alpha\eta\sqrt{1 - |\hat{s}|^2} \ . \tag{2.128}$$

For the SRM, the equations (2.126) and (2.122) lead to $\eta = -i\alpha\frac{\epsilon_\kappa}{\Lambda^2}e^{i\Phi}$, $\eta_3 = 0$, and

$$\frac{d}{d\theta}\hat{s} = i[\mathrm{sig}(\delta)\Lambda + \kappa]\hat{s} + \alpha\frac{\epsilon_\kappa}{\Lambda^2}e^{i\Phi}\sqrt{1 - |\hat{s}|^2} \ . \tag{2.129}$$

This equation of motion for the SRM in the coordinate system $[\vec{u}_1, \vec{u}_2, \vec{n}]$ describes how spins follow a slow change of $\vec{n}$ adiabatically, but it also describes how $J_S = \sqrt{1 - |\hat{s}|^2}$ is reduced when the resonance $\nu_0 = \kappa$ is crossed.

In this equation, the spin tune $\mathrm{sig}(\delta)\Lambda + \kappa$ jumps by $2\epsilon_\kappa$ at the resonance. Note that the dreibein $[\vec{u}_1, \vec{u}_2, \vec{n}]$ has a discontinuity at $\delta = 0$ where $\vec{n}$ and $\vec{\tilde{u}}_2$ change sign. When denoting the unit vectors just below the resonance by the index $-$ and just above the resonance by an index $+$, the discontinuity in the basis vectors is reflected in a discontinuity in $\hat{s}$ at $\delta = 0$,

$$\vec{S} = \vec{u}_{1-}s_{1-} + \vec{u}_{2-}s_{2-} + \vec{n}_- J_{S-} = \vec{u}_{1+}s_{1+} + \vec{u}_{2+}s_{2+} + \vec{n}_+ J_{S+} \ . \tag{2.130}$$

Due to the sign choice for the $\vec{n}$–axis, $J_{S+} = -J_{S-}$ and a particle with upwards spin far below resonance will have a flipped spin far above the resonance. When propagating a spin with initial condition $\hat{s}_i$ by equation (2.129), one has to solve the equation up to the resonance, where the spin coordinate is denoted by $\hat{s}_-$;. Equation (2.130) then leads to $\hat{s}_+$, which is then used as initial condition for a further propagation of the spin.

2.2.11 The Froissart–Stora Formula

The adiabatic spin invariant was established for general systems in section 2.2.9. For the analytically solvable SRM the change of this adiabatic invariant can be computed. When the closed–orbit spin tune ν_0 changes during the acceleration process,

intrinsic resonances and imperfection resonances have to be crossed. While the spin is under the strong influence of an approximately resonant Fourier contribution of ω, a reduction of polarization can occur which does not recover after the energy has increased and the resonance is crossed.

The reduction of polarization during resonance crossing is traditionally described in the framework of the SRM by the Froissart–Stora formula. To describe resonance crossing, a changing closed–orbit spin tune ν_0 has to be inserted in the equation of motion (2.116). For various functions $\nu_0(\theta)$, different approaches are possible [102, 103, 59, 104]. If the closed–orbit spin tune changes like $\nu_0 = \kappa + \alpha\theta$, the corresponding spinor equation of motion (2.39) can be solved in terms of confluent hypergeometric functions. The equations for arbitrary initial conditions are quite complicated but when at $\theta \to -\infty$ a vertical spin $s_3(-\infty) = 1$ is chosen as initial condition then the vertical component at $\theta \to +\infty$ is given by the Froissart–Stora formula

$$s_3(\infty) = 2e^{-\pi \frac{\epsilon_\kappa^2}{2\alpha}} - 1 \ . \tag{2.131}$$

In the case of a strong perturbation ϵ_κ, or when the acceleration is very slow, spins follow the change of $\vec{n}(\Phi)$. The $\vec{n}$–axis in equation (2.118) has a discontinuity from $\vec{n}_- = -\epsilon_\kappa(\vec{e}_1 \cos\Phi + \vec{e}_2 \sin\Phi)$ just below resonance to $\vec{n}_+ = -\vec{n}_-$ just above resonance. Spins do not follow this instantaneous change of sign, but they then follow $-\vec{n}$ adiabatically after the resonance has been crossed. Therefore $s_3(\infty)$ is close to -1 for a slow change of ν_0 . When the perturbation is weak or crossed very quickly, then spin motion is hardly affected and $s_3(\infty)$ is close to 1 in equation (2.131). In intermediate cases, the polarization is reduced.

2.2.12 Froissart–Stora Formula for Higher–Order Resonances

The Froissart–Stora formula is regularly used to describe the reduction of polarization during resonance crossing in accelerators where the closed–orbit spin tune ν_0 changes with energy, normally for flat rings and $\nu_0 = G\gamma$. Since Siberian Snakes are unavoidable for polarized beam acceleration in HERA–p, the closed–orbit spin tune is $\nu_0 = \frac{1}{2}$ in most systems which will be considered here and it does not change during acceleration. Since the orbital tunes are never chosen to be $\frac{1}{2}$, no first–order resonances $\nu_0 = j_0 + Q_k$ can occur. When only linear orbital motion is considered, $\vec{\omega}$ can however only have Fourier components to the first–order frequencies $j_0 \pm Q_k$. Higher–order resonances can nevertheless appear, which will be seen in the examples of this report which were all computed for linear phase space motion. To use the Froissart–Stora Formula when Siberian Snakes are in use, a method is required with which one can obtain the strength of the higher–order resonances. The discussion so far about the approximation of spin motion by a single Fourier component in ω which is approximately in resonance with ν_0 is therefore usually not useful when Siberian Snakes are present.

Even when the precession vector $\vec{\omega}$ is a linear function of phase space variables and first–order resonances are excluded by the use of Siberian Snakes, higher–order

resonances of the form $\nu_0 = \frac{1}{2} \approx j_0 + \vec{j} \cdot \vec{Q}$ can occur [105, 106, 59]. But when spin motion in a ring is approximated by a single resonance with $\kappa = j_0 \pm Q_y$ and then Siberian Snakes are included in the ring, it has often been noted that only odd order resonances with $\kappa = j_0 + j_y Q_y$ appear, i.e. j_y is odd. But this is only true for rings with mid–plane symmetric spin–orbit motion, otherwise also even order resonances can appear. It can be shown by nonlinear normal form theory that this is a feature of any ring with mid–plane symmetric spin–orbit motion and is not peculiar to rings with Siberian Snakes.

HERA–p has non–flat regions, and rings with closed orbit distortions in general do not have mid–plane–symmetric motion. Then, resonances with even j_y can also be destructive. In fact, the resonances with $j_y = 2$ are the most destructive spin–orbit resonances in HERA–p after Siberian Snakes are included.

As mentioned in section 2.2.4, HERA–p will require flattening snakes. Additionally at least 4 Siberian Snakes are required. The snake angle φ_j of these 4 snakes can be chosen quite arbitrarily, obeying only the restriction $\Delta\varphi = \varphi_4 - \varphi_3 + \varphi_2 - \varphi_1 = \frac{\pi}{2}$ derived in section 2.2.3. Since various choices of snake angles lead to different performance of HERA–p for polarized beam acceleration and storage, section 4.1.3 will be dedicated to finding an optimal choice for these snake angles. To illustrate the main concepts, two different example schemes having 1 snake in each of the 4 straight sections will be considered. In the following I will characterize snake schemes by their snake angles starting with the Siberian Snake in the South and going East around the ring. The two example schemes are denoted by $(\frac{\pi}{4}0\frac{\pi}{4}0)$ and $(\frac{3\pi}{4}\frac{3\pi}{8}\frac{3\pi}{8}\frac{\pi}{4})$ and are shown in figure 2.8. A pair of non–flat regions is located in the South, East, and North straight sections of HERA–p and therefore 6 flattening snakes are required. Nevertheless, it can be useful to symmetrize HERA–p by two additional flattening snakes in the West section. When referring to snake schemes, the number of flattening snakes will be referred to as *6fs* or *8fs* scheme. The two example schemes are:

1. Scheme $(\frac{\pi}{4}0\frac{\pi}{4}0)6fs$ with snake angles South: 45°, East: 0°, North: 45°, West: 0°. Such a scheme and similar symmetric schemes were originally considered advantageous by a popular opinion [107], mostly due to their symmetry.

2. Scheme $(\frac{3\pi}{4}\frac{3\pi}{8}\frac{3\pi}{8}\frac{\pi}{4})8fs$ with snake angles South: 135°, East: 67.5°, North: 67.5°, West: 45°. This scheme was found by the optimization described in section 4.1.3.

In figure 2.9 the amplitude dependent spin tune and P_{lim} are plotted for an amplitude of 70πmm mrad (green), which shows that many higher–order resonances can be observed in HERA–p for the luminosity upgrade optics for the year 2000. The ring was made effectively flat by flattening snakes and 4 Siberian Snakes were included with the snake arrangement $(\frac{\pi}{4}0\frac{\pi}{4}0)8fs$.

While the closed–orbit spin tune remains at $\frac{1}{2}$, the amplitude dependent spin tune $\nu(J_y)$ changes with energy and is in resonance with $2Q_y$ at the second line (red) and with $5Q_y - 1$ at the bottom line. In both cases a clearly marked change of P_{lim} can be observed. The drop of P_{lim} at 811.2GeV/c is due to the $2 - 5Q_y$ resonance, which

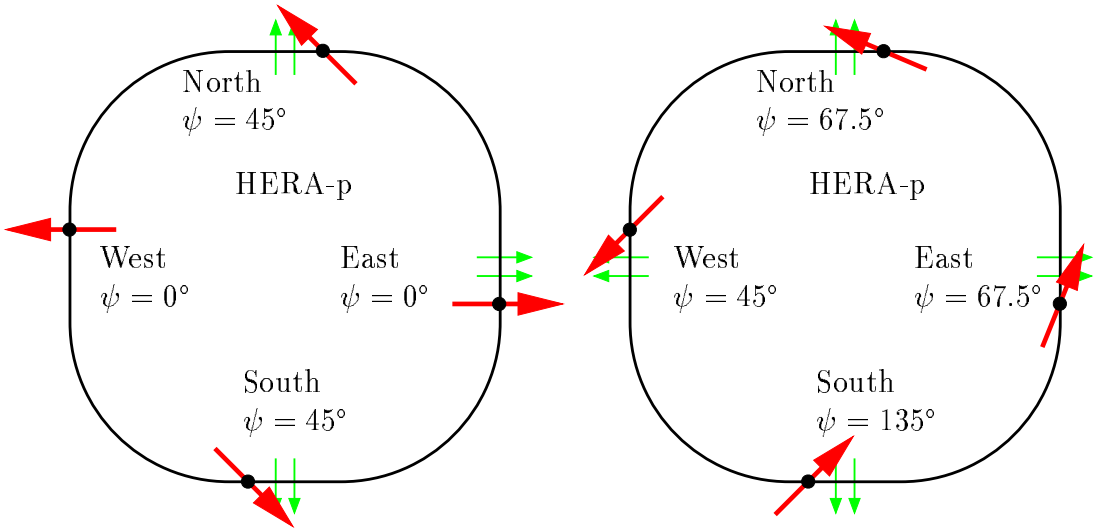

Figure 2.8: An originally suggested snake scheme (left) and a snake scheme after the optimizations described in section 4.1.3 (right). The flattening snakes (small arrows) and 4 Siberian Snakes (large arrows) are indicated with their snake angle.

lies a little below the $2Q_y$ line. At all other energies where this resonance is crossed, no influence on P_{lim} can be observed since the corresponding fifth–order resonance strength is very small. At some second–order resonances, P_{lim} increases resonantly. Presumably, two resonant effects are in constructive interference at these energies. Nonetheless, polarization can be reduced when these resonance positions are crossed since also a sudden increase of $< \vec{n} >$ might be due to a change of $\vec{n}(\vec{z})$ which is too sudden for the adiabatic invariance of $J_S = \vec{n}(\vec{z}) \cdot \vec{S}$ to be maintained. Additionally one can see in figure 2.9 that the spin tune $\nu(J_y)$ has discontinuities at some of the resonances.

In this more general setting where the amplitude dependent spin tune $\nu(\vec{J})$ crosses a resonance, the spin motion is described in the coordinate system $[\vec{u}_1, \vec{u}_2, \vec{n}]$ by equation (2.128),

$$\frac{d}{d\theta}\hat{s} = i(\nu(\vec{J}, \tau) - \alpha\eta_3)\hat{s} + i\alpha\eta\sqrt{1 - |\hat{s}|^2} \ , \quad \alpha = \frac{d}{d\theta}\tau \ . \tag{2.132}$$

This equation implicitly describes the change of $J_S = \sqrt{1 - |\hat{s}|^2}$ during acceleration when τ is taken to be the reference energy of the circular accelerator. When the average of J_S taken over all N particles of the beam is denoted by $< J_S >_N$, then even a very small polarization of the beam $P =< \vec{s} >_N$ can in principle always be recovered to a value close to $< J_S >_N$ by changing the invariant spin field sufficiently slowly so that it is nearly parallel over the phase space of the beam, which makes P_{lim} close to 1. A small average beam polarization during acceleration is therefore not destructive as long as J_S stays large for each particle. On the other hand, a reduction of $< J_S >_N$ describes a reduction of polarization which is not reversible by a slow change of the invariant spin field [108].

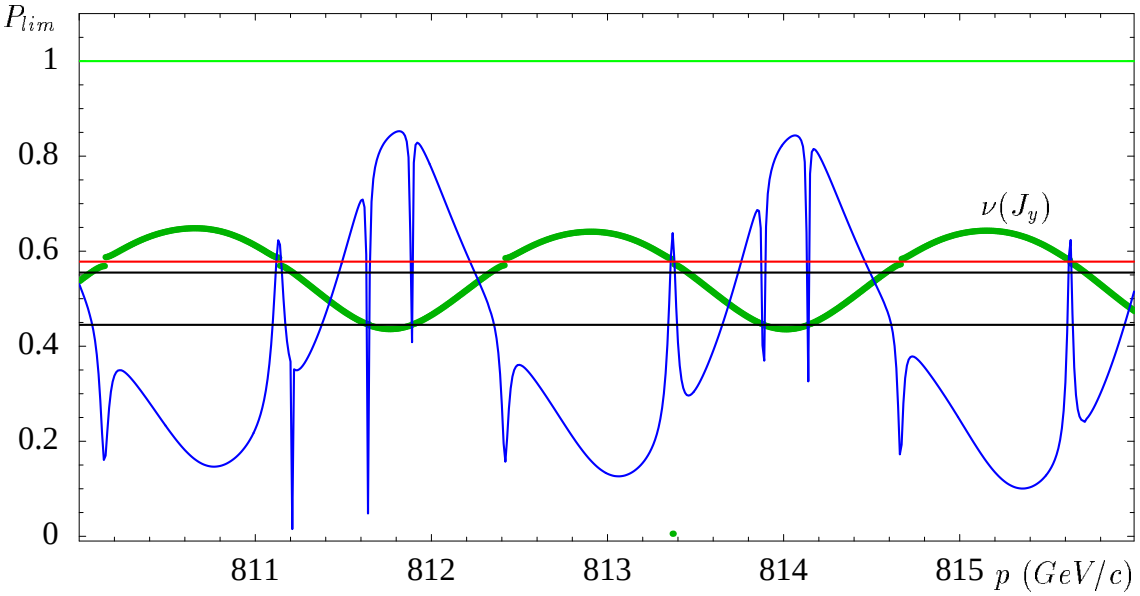

Figure 2.9: P_{lim} (blue) and $\nu(J_y)$ (green) for particles with a 4.2σ vertical amplitude of 70πmm mrad in HERA–p with the $(\frac{\pi}{4}0\frac{\pi}{4}0)8fs$ snake scheme and $Q_y = 0.289$. Three resonance lines cross ν and at the crossing P_{lim} drops and there are jumps in ν, bottom: $\nu = 5Q_y - 1$, middle: $\nu = 2 - 5Q_y$, and top $\nu = 2Q_y$.

In the following I will show that equation (2.132) can resemble characteristics of the equation of spin motion (2.129) of the SRM. If the spin tune ν has a discontinuity from ν_- to ν_+ at some energy, then I define a resonant frequency $\kappa = \frac{1}{2}(\nu_- + \nu_+)$ and a resonance strength as one half of the discontinuity, $\epsilon_\kappa = \frac{1}{2}|\nu_+ - \nu_-|$. I now define $\Lambda = |\nu - \kappa|$, which does not have a discontinuity and express the spin tune as $\nu = \mathrm{sig}(\nu - \kappa)\Lambda + \kappa$.

Since $\vec{\eta}$ is related to the basis vectors by equation (2.100), it is a 2π periodic functions of $\vec{\Phi}$ and θ, and equation (2.132) has a similar structure as the equation of motion in the coordinate system $[\vec{m}, \vec{l}, \vec{n}_0]$ in equation (2.115) to which the single resonance approximation was applied. Accordingly, one can analyze what happens when the Fourier component of η at a frequency κ with amplitude η_κ dominates the motion of $\hat{s}$. For that analysis, all other Fourier components of η are ignored. For spins which are initially close to parallel to the $\vec{n}$–axis, $\hat{s}$ is small and together with the small parameter α, $\alpha\eta_3\hat{s}$ can also be ignored. This leads to

$$\frac{d}{d\theta}\hat{s} = i(\mathrm{sig}(\nu - \kappa)\Lambda + \kappa)\hat{s} + i\alpha\eta_\kappa\sqrt{1 - |\hat{s}|^2} \ , \tag{2.133}$$

which is already quite similar to equation (2.132). If ν and η_κ are computed in the vicinity of the energy where the discontinuity occurs and $\eta_\kappa(\nu - \kappa)^2$ is observed to be approximately ϵ_κ, one is left with a relation which has exactly the structure of the equation of motion (2.129) for the SRM. Therefore, the Froissart–Stora formula can be applied to estimate how much polarization is lost when a polarized beam is accelerated through the energy region where the spin tune jumps by $2\epsilon_\kappa$. In

the following we will check for some higher–order resonances in HERA–p whether all assumptions leading to the approximative equation (2.133) are satisfied to the extent that the Froissart–Stora formula describes the reduction of polarization well. Checking whether the Froissart–Stora formula can be used to determine depolarization when a higher order resonance is crossed was largely inspired by a comment of A. Lehrach during a talk by M. Vogt [126].

The basis vectors $\vec{n}$, $\vec{u}_1$, and $\vec{u}_2$, and the amplitude dependent spin tune ν can in general only be computed by computationally intensive methods which will be described in later sections. The perturbing function η is then obtained from

$$\begin{aligned} \eta &= \vec{\eta} \cdot (\vec{u}_1 + i\vec{u}_2) = \vec{\eta} \cdot (-\vec{n} \times \vec{u}_2 + i\vec{n} \times \vec{u}_1) \\ &= (\vec{\eta} \times \vec{n}) \cdot (-\vec{u}_2 + i\vec{u}_1) = i(\vec{u}_1 + i\vec{u}_2) \cdot (\partial_\tau \vec{n}) \ . \end{aligned} \tag{2.134}$$

The required differentiation is often prone to numerical inaccuracies. When $\vec{n}$ is computed by perturbative normal form theory using differential algebra (DA) [92], the differentiation with respect to τ can be performed automatically. After η is computed, the Fourier integral over the complete ring would finally be required in order to compute ϵ_κ.

If equation (2.132) can be approximated well by a SRM, there is however a different and much less cumbersome method for determining the relevant resonance strength and the resonant frequency. Observation of the amplitude dependent spin tune $\nu(\vec{J})$ allows the determination of all parameters which are required to evaluate the Froissart–Stora formula for higher–order resonances whenever a SRM for η is applicable: The spin tune jumps by $2\epsilon_\kappa$, the center of the jump is located at frequency κ itself, and the rate of change of ν with changing energy is used to determine the parameter α for equation (2.131). This parameter is $\frac{\nu_0 - \kappa}{\theta}$ in the SRM. Here the corresponding frequency ν_0, which would be observed when no perturbation η were present, is not directly computed. But it can be inferred from the slope $\partial_\tau \nu$ at some distance from the resonance.

It is important to note that the discontinuity of the spin tune could in general be transformed away since its sign can be changed by choosing $-\vec{n}$ as the $\vec{n}$–axis to which the spin tune refers, which was derived in section 2.2.7. If the sign of $\vec{n}$ is fixed so that the $\vec{n}$–axis $\vec{n}_-$ shortly below and $\vec{n}_+$ shortly above the resonance have $\vec{n}_- \cdot \vec{n}_+ < 0$, then the discontinuity of ν at the resonance cannot be transformed away.

According to equation (2.124), $< \vec{n} >$ is given by $P_{lim}^{SRM} = \sqrt{1 - (\frac{\epsilon_\kappa}{\nu - \kappa})^2}$ in the SRM. To check whether the observed drop of P_{lim} indeed satisfies the characteristics of the SRM, the width of the resonance dip in P_{lim}^{SRM} was obtained from the amplitude dependent spin tune alone and then compared to the width of the dip in the actual P_{lim} of the system. This analysis was done for a resonance at approximately 812.5GeV/c. For vertical amplitudes of 70πmm mrad which is currently approximately the 4.2σ emittance, P_{lim} and ν in the vicinity of this resonance are shown in figure 2.10 (top left). It displays a momentum range of figure 2.9. The low P_{lim} shows that many perturbing effects interfere in this region. In units of πmm mrad, the vertical amplitude of the particles in the top left graph are 70, in the middle

graphs it is 40 and 60, and in the bottom graphs 80 and 100. The horizontal scale Δp is the distance in GeV/c from the momentum at the resonance.

In the 4 bottom graphs, P_{lim} and P_{lim}^{SRM} are plotted for different orbital amplitudes, and the different resonance strengths are obtained from the jump in $\nu(J_y)$. Only information about ν was used to compute P_{lim}^{SRM} . To allow better comparison, the rate of change of P_{lim}^{SRM} with momentum and the height of the dip were scaled to fit the actual P_{lim}. The width however was not changed. The distance between spin tune and resonance has been magnified by 10, $\nu^* = \kappa + 10 \cdot (\kappa - \nu)$ in these graphs. The tune jump is symmetric to the resonance line $\nu = 2Q_y$, which shows that a second–order resonance is excited.

The tune jump scales approximately linearly with the orbital action variable J_y as plotted in figure 2.10 (top right), which is constant with crossing a second–order resonance. This linear scaling is not exact for two reasons: (1) When the amplitude is so small that $\nu(J_y)$ does not cross the resonance line, no jump occurs. (2) When the amplitude is changed, the momentum at which the resonance occurs changes, and the resonance strength is in general different at different energies. Deviations from a linear dependence should therefore be expected. P_{lim} is already very low away from the resonance at $\nu = 2Q_y$, indicating that other strong perturbations distort the invariant spin field and can interfere with the resonance harmonic.

Thus I conclude that the resonance width computed by the tune jump $2\epsilon_\kappa$ agrees surprisingly well with the actual drop in P_{lim} .

Since higher–order resonances show the established and characteristic relation between tune jump and reduction of P_{lim}, it will now be tested whether the Froissart–Stora formula can be applied to such a case. This would be of great significance for analyzing the acceleration of polarized beams through such higher–order resonances.

In figure 2.11 (top) P_{lim} and ν are shown for the current HERA optics with 4 Siberian Snakes in the scheme $(\frac{\pi}{4}0\frac{\pi}{4}0)8fs$. P_{lim} is reduced at two resonances with $\nu = 2Q_y$. The vertical tune had been chosen as $Q_y = 0.2725$ so that these resonances are crossed already for the small 0.75σ vertical amplitude of 2.25πmm mrad. At this small amplitude P_{lim} is reasonably large.

The spins of a set of particles were set parallel to the invariant spin field at $\vec{n}(\vec{z})$ so that all had $J_S = 1$ at the momentum of 801GeV/c. The $\vec{n}$–axis had been computed by stroboscopic averaging to be described in section 4.2. Due to the rather large P_{lim} at that energy the initial polarization was approximately 97%. Starting with this spin configuration, the beam was accelerated to 804GeV/c at various rates. The average $< J_S >_N$ over the tracked particles is plotted versus acceleration rate in figure 2.11 (bottom) together with the prediction of the Froissart–Stora formula. As already explained, the average $< J_S >_N$ describes the degree of beam polarization which could be recovered due to the adiabatic invariance of J_S when moving into an energy regime where $\vec{n}(\vec{z})$ is close to parallel to the vertical.

The resonance strength ϵ_{2Q_y} has been determined from the tune jump. The parameter $\alpha = \frac{1}{2\pi}\frac{\Delta\nu}{\Delta E}d_E$ is determined by the tune slope $\frac{\Delta\nu}{\Delta E}$ in figure 2.11 (top right) and is proportional to the energy increase per turn d_E.

The polarization obtained by accelerating particles through the second order resonance agrees remarkably well with the Froissart–Stora Formula. For the slow

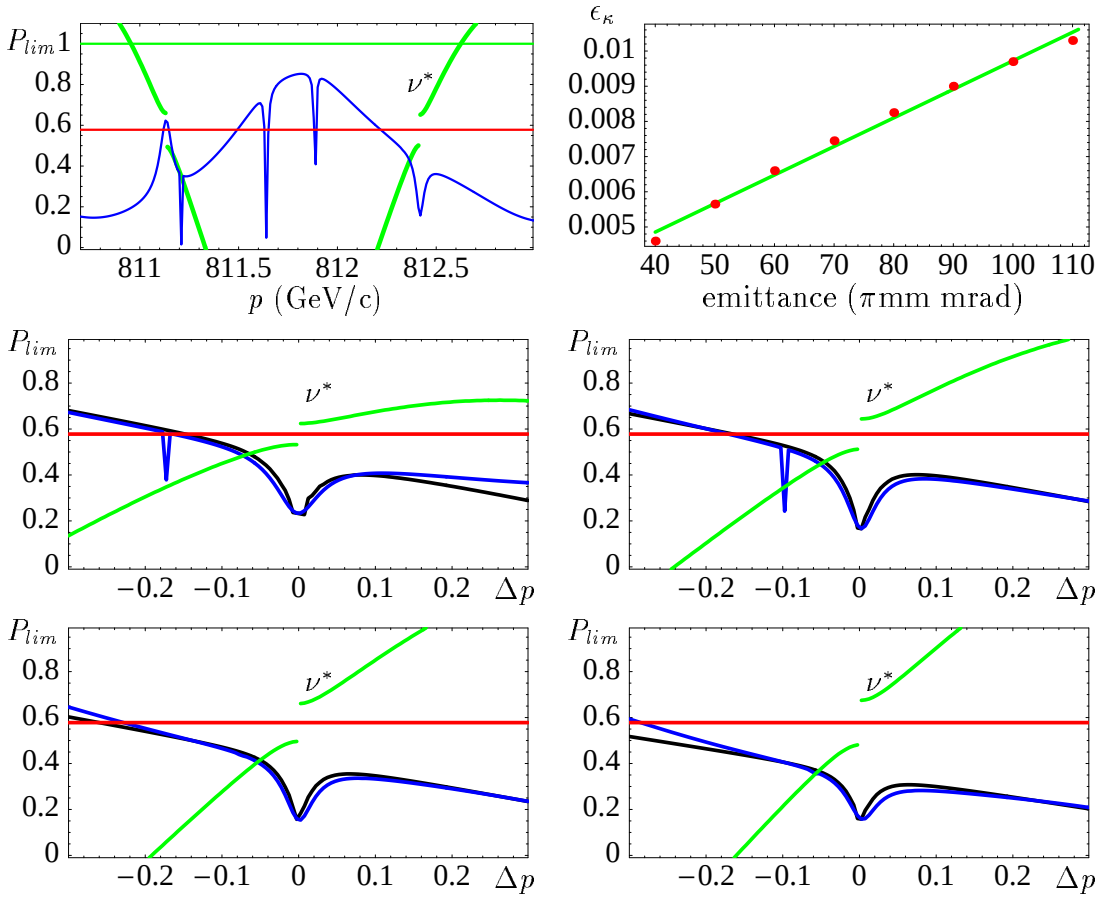

Figure 2.10: Top left: P_{lim} and ν in the vicinity of the resonance at approximately 812.5GeV/c. Top right: Proportionality between tune jump and orbital action J_y . Middle and bottom: Correlation between the width of the actual drop of P_{lim} and the predictions of the single resonance approximation using only the amplitude dependent spin tune. The distance between ν and resonance has been magnified by 10, $\nu^* = \kappa + 10 \cdot (\kappa - \nu)$. Vertical amplitude of particles in HERA–p with the $(\frac{\pi}{4}0\frac{\pi}{4}0)8fs$ snake scheme in units of πmm mrad from top left to bottom right: 70, 40, 60. 80, and 100. Δp: distance from the momentum at resonance.

acceleration of about $50keV$ per turn in HERA–p, the polarization would be completely reversed on the 0.75 sigma invariant torus. This would lead to a net reduction of beam polarization, since the spins in the center of the beam are not reversed.

This result on the applicability of equation (2.131) for the resonance strength and α obtained from the amplitude dependent spin tune is so important for detailed analysis of the acceleration process that it will be checked in more realistic cases. In the next example, the HERA–p luminosity upgrade lattice was used, the tune was adjusted to a realistic value of $Q_y = 0.289$ and a 2.5σ vertical amplitude of 70πmm mrad was chosen. At this large amplitude, the second and fifth–order resonances already shown in figure 2.9 are observed. Particles were then accelerated from 812.2GeV/c to 812.6GeV/c with different acceleration rates. Note that the

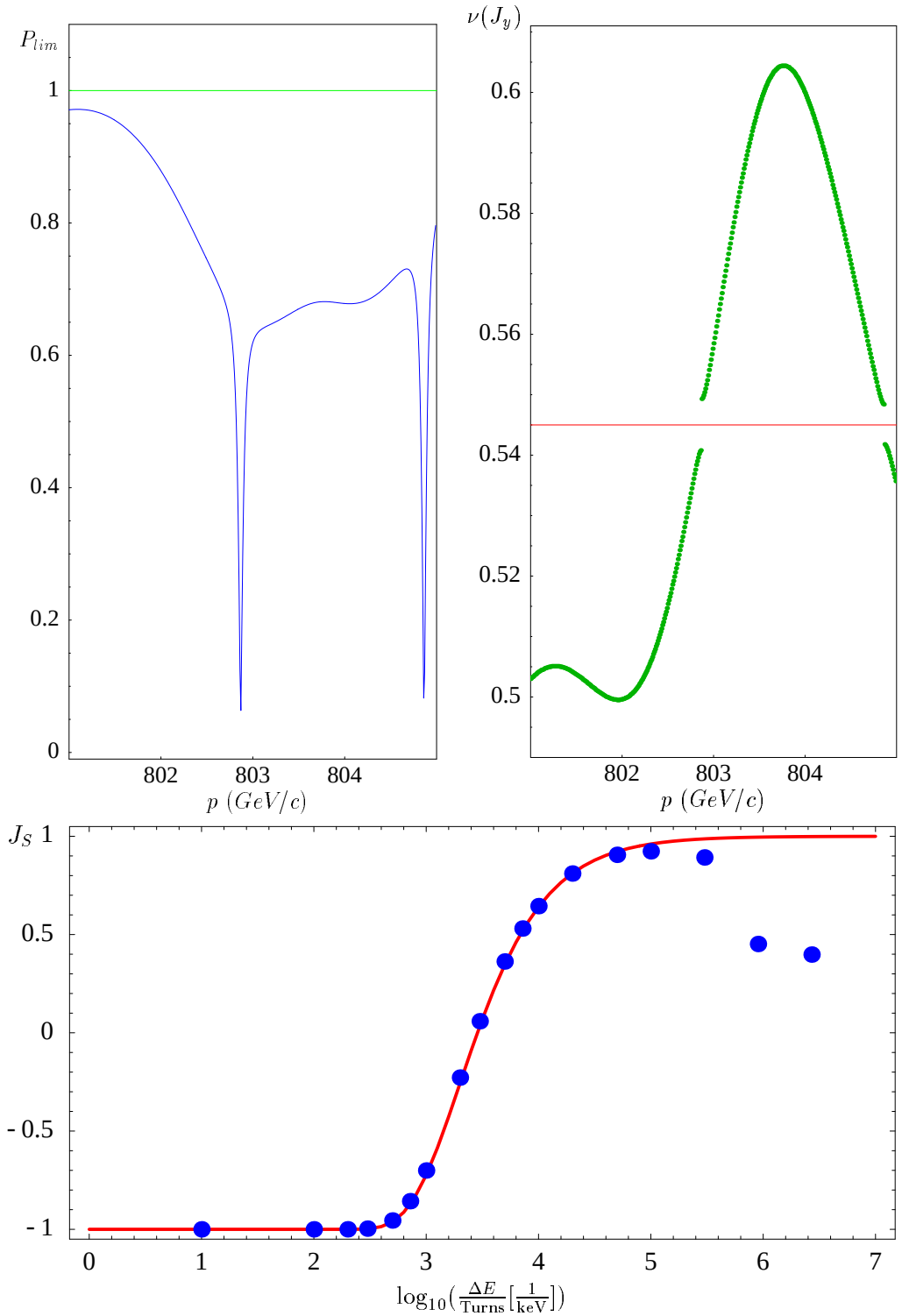

Figure 2.11: Top: P_{lim} and ν for a second–order resonance of the current HERA–p optics with a $(\frac{\pi}{4}0\frac{\pi}{4}0)6fs$ snake scheme for $Q_y = 0.2725$ and a 0.75σ vertical amplitudes of 2.25πmm mrad with the $(\frac{\pi}{4}0\frac{\pi}{4}0)6fs$ snake scheme. Bottom: J_S after acceleration from 801GeV/c to 804GeV/c with different acceleration rates (blue points) and the prediction of the Froissart–Stora formula (red curve) for parameters ϵ_{2Q_y} and α obtained from ν.

initial condition has a vertical polarization of only 60%. Nevertheless this state of polarization corresponds to a completely polarized beam, and 100% polarization can potentially recovered by changing the energy adiabatically into a region where $\vec{n}(\vec{z})$ is tightly bundled. Vertically polarized spins would rotated around $\vec{n}(\vec{z})$ and would lead to a fluctuating polarization, even without a resonance and it would not be possible to establish a Froissart–Stora formula for higher–order resonances.

As shown in figure 2.12, the polarization in this region is reduced down to 0.1 and obviously other strong effects beyond the second–order resonance are present and overlap with it. Therefore it is again important that the particles which should be accelerated through the resonance are initially polarized parallel to the invariant spin field. The bottom figure shows J_S after the acceleration; it is an impressive confirmation of J_S being again described very well by the Froissart–Stora formula (2.131).

Here the parameter τ was the slowly changing momentum. This generalized way of using the Froissart–Stora formula can however also be used when other system parameters change. An example can be found in section 4.3, where the particle amplitude is changed artificially slowly in order to compute the invariant spin field at various orbital amplitudes.

2.2.13 The Choice of Orbital Tunes

When the amplitude dependent spin tune $\nu(\vec{J})$ crosses a resonance, the beam polarization is usually reduced. When the acceleration is slow enough to allow for the adiabatic invariance of J_S, the spin on the torus given by $\vec{J}$ is reversed after the resonance, whereas it is unchanged at smaller phase space amplitudes. This can be either because the resonance is weaker at smaller amplitudes, or because the $\nu(J_y)$ does not cross the resonance for particles in the core of the beam. Often the polarization recovers, since ν usually fluctuates with energy as shown in figures 2.9, 2.11, and 2.12 so that $\nu(\vec{J})$ will cross the resonance for a second time and the polarization will be flipped back.

Nevertheless, there is some reduction of polarization involved, even after two successive resonance crossings. There are three reasons: Firstly, there are amplitudes where the spin tune only comes into the vicinity of a resonance and then moves away with energy before the resonance has been crossed completely; and secondly, the resonance strength is different for different energies. Even though the spin tune might cross the same resonance condition when returning back to $\frac{1}{2}$ at a higher energy, the strength of the two resonances is usually different. If the first resonance was sufficiently strong on the torus $\vec{J}$ to reverse the sign of spins, the second resonance might not be strong enough to reverse it again. Thirdly, there are amplitudes where the resonance has intermediate strength and polarization is neither reversed nor conserved, but reduced.

Due to these problems occurring at resonance crossings, it is important to find suitable orbital tunes so that low order spin–orbit resonances are far away from the operating point. In figure 2.13 (right), the plane of vertical orbit tune Q_y and spin tune ν is drawn. The resonance lines $\nu = j_0 + jQ_y$ are drawn up to order 10. While

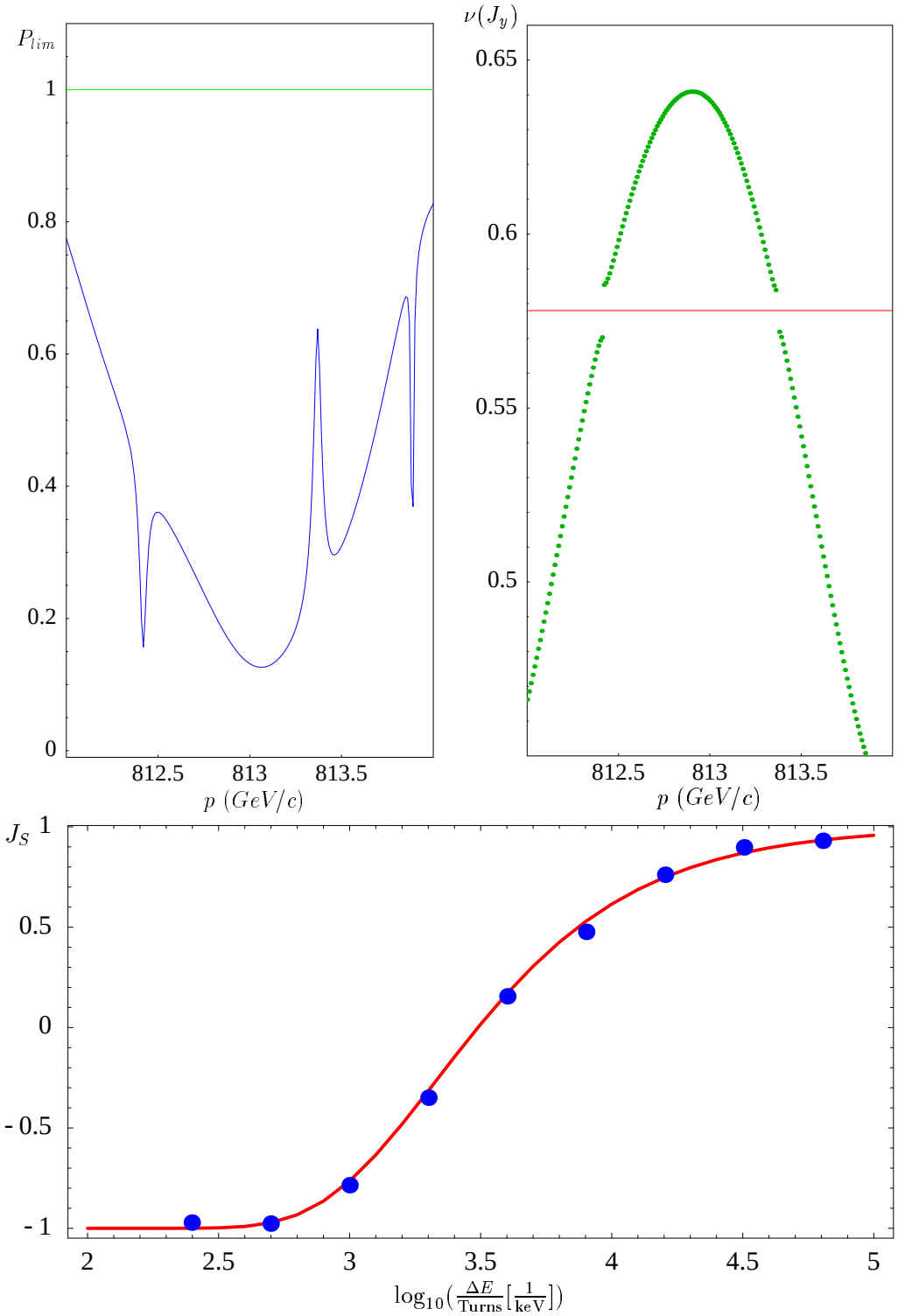

Figure 2.12: Top: P_{lim} and ν for a second–order resonance of the luminosity upgrade optics with realistic tune of $Q_y = 0.289$ and a large 4.2σ vertical amplitudes of 70πmm mrad with the $(\frac{\pi}{4}0\frac{\pi}{4}0)8fs$ snake scheme. Bottom: J_S after acceleration from 812.2GeV/c to 812.6GeV/ the with different acceleration rates (blue points) and the prediction of the Froissart–Stora formula (red curve) for parameters ϵ_{2Q_y} and α obtained from ν.

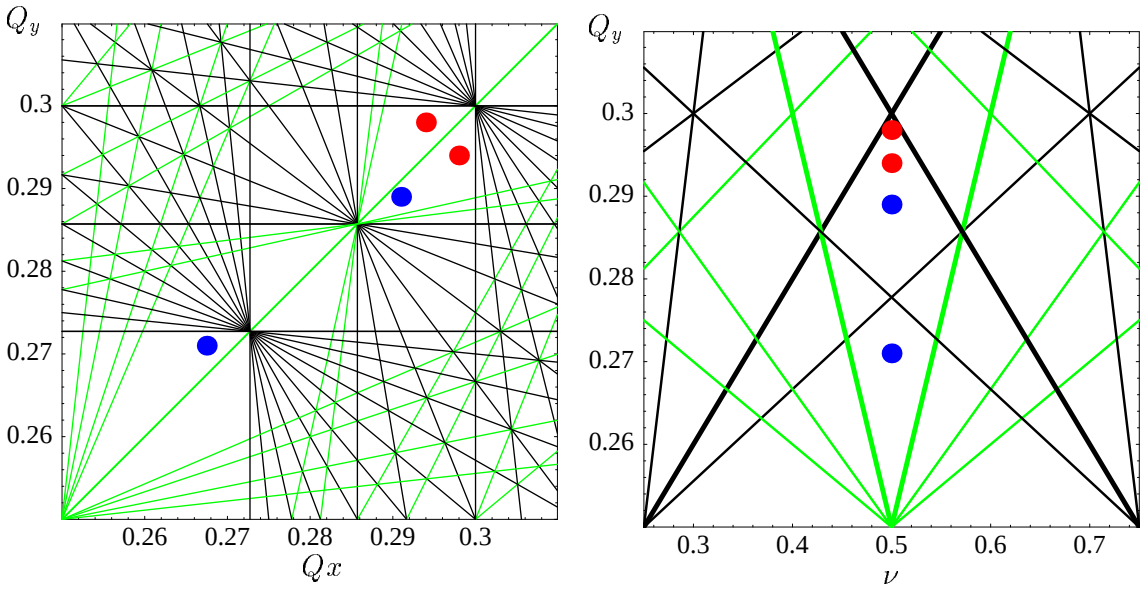

Figure 2.13: Left: the current orbit tunes ($Q_x = 0.294$,$Q_y = 0.298$) or ($Q_x = 0.298$,$Q_y = 0.294$) (red) and the new orbit tunes for polarized proton operation ($Q_x = 0.291$,$Q_y = 0.289$) or ($Q_x = 0.2675$, $Q_y = 0.271$) (blue) in the x–y resonance diagram. All resonances up to order 11 are shown, difference resonances are indicated in green. Right: The current vertical tunes (red) and the new vertical tunes (blue) in the spin–orbit resonance diagram. The odd snake resonances (black) and the even snake resonances (green) are shown up to order 10 in the vicinity of closed–orbit spin tune $\nu_0 = \frac{1}{2}$. For HERA–p, the resonances of second order (fat green) and of fifth order (fat black) are most destructive.

the spin tune on the closed orbit is fixed to $\nu_0 = \frac{1}{2}$ by Siberian Snakes the orbital tune can be chosen to avoid resonance lines. Additionally the dynamic aperture of proton motion should not be reduced and the tunes have to be far away from low order orbital resonances. Figure (2.13) (left) shows the Q_x–Q_y tune diagram with resonance lines up to order 11. The operating point has to stay away from these resonance lines.

The established tunes of the 1999 HERA–p operation $Q_x = 0.294$, $Q_y = 0.298$ or $Q_x = 0.298$, $Q_y = 0.294$ (red points) would be unfortunate choices due to their vicinity to the resonance $\nu = j_0 \pm 5Q_y$. For the IUCF cooler ring with only a partial snake, second–order resonances have been observed experimentally [109]. For HERA–p with Siberian Snakes, several simulations have shown that the resonances of second order and of fifth order are most destructive. This is supported by figure 2.9. Therefore two new tunes (blue points) are suggested which have an optimal distance from low order spin–orbit resonances. For the simulations of this report, the orbit tunes for polarized proton operation where chosen to be ($Q_x = 0.291$,$Q_y = 0.289$). The working point ($Q_x = 0.2675$,$Q_y = 0.271$) would also be a good choice.

To test whether HERA–p could currently operate with these tune, Q_y was slowly shifted from the current working point in the direction of the 7th order resonance to the first choice of polarization tunes. No increase in beam collimation rates or in

beam loss monitor rates were observed during this procedure.

Moreover, the second choice for polarization with somewhat lower tunes could be reached. Crossing the 7th order resonance at $Q_y \approx 0.286$ did not cause any problems. However, when crossing the 11th order resonance at $Q_y = 0.273$, the collimation rates increased from about 250Hz to up to 14kHz. After this resonance had been crossed, the rates fell to about 1.5kHz. Whereas the working point close to the 7th order resonance would seem unproblematic, more work would have to be invested in establishing good tunes in the vicinity of $\frac{3}{11}$.

2.2.14 Importance of the Invariant Spin Field for HERA–p

After having derived many properties and several applications of the invariant spin field in this chapter, I want to summarize why knowledge of the invariant spin field is essential when analyzing polarized proton beams in HERA–p.

Firstly, when the invariant spin field is known, a much clearer simulation of spin motion is possible than with simple spin–orbit tracking alone. Figure 2.14 shows the average vertical polarization of 100 particle which all have different angle variables of vertical motion but the same normalized amplitude of 4πmm mrad. These particles have been tracked through the current HERA–p lattice for 500 turns while the beam was initially polarized 100% parallel to $\vec{n}_0$. Similar kinds of tracking results have been presented in [110]. Since the spins of these particles are not parallel to the invariant spin field, the averaged polarization exhibits a strong beat. This figure also shows that when particles at a phase space coordinate $\vec{z}$ are initially parallel to $\vec{n}(\vec{z})$, the averaged polarization stays constant. Therefore, by starting simulations with spins parallel to the $\vec{n}$–axis one can perform a much cleaner analysis of beam polarization in accelerators.

After acceleration in HERA–p, the polarized beam has to be stored over several hours during which the polarization should be invariant and high. Therefore each particle should be polarized parallel to the invariant spin field $\vec{n}(\vec{z})$ at its phase space position $\vec{z}$. To have a high time average beam polarization, every phase space point must have a polarization direction $\vec{n}(\vec{z})$ which is almost parallel to the beam average $< \vec{n} >$. Figure 2.15 (top left) shows that the invariant spin field at different phase space points can be rather parallel (leading to high polarization $P_{lim} = | < \vec{n} > |$) and suddenly diverges at a critical energy (leading to diminished polarization), even though only first–order effects have been considered in this figure by using linearized spin–orbit motion described in section 3.1. The invariant spin field then becomes parallel again at higher energies.

When particles at different phase space points in the beam are polarized in significantly different directions, three problems occur:

1. The divergence of the polarization direction reduces the time average polarization available to the particle physics experiments since $P_{lim} = | < \vec{n} > |$ is the maximum time average polarization which can be stored in a ring [111].

2. The polarization involved in each collision analyzed in a detector is strongly dependent on the phase space position of the interacting particle.

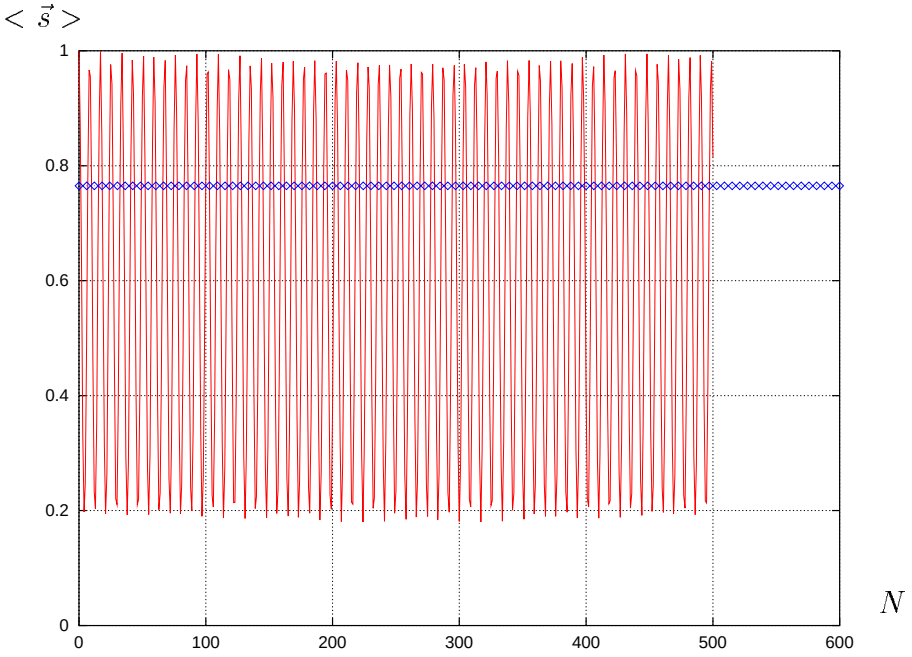

Figure 2.14: Propagation of a beam that is initially completely polarized parallel to $\vec{n}_0$ leads to a fluctuating average polarization (red). For another beam that is initially polarized parallel to the invariant spin field $\vec{n}$ the average polarization stays constant (blue), in this case equal to 0.765.

3. Polarimeters which measure the polarization of particles in the tails do not yield accurate values for the polarization of the beam.

It is clear from figure 2.15 (top left) that in HERA–p, acceptable polarization could be obtained only over a very restricted part of the energy range even if a completely polarized beam were delivered at high energy.

The invariant spin field is important during storage of polarized beams but also during the acceleration cycle. When a change of the invariant spin field $\vec{n}(\vec{z})$ during acceleration from an originally parallel to a divergent spin field and back to the original $\vec{n}(\vec{z})$ is fast enough, the spins do not react strongly. If it is slow enough, the adiabatic invariance of $J_S = \vec{S} \cdot \vec{n}(\vec{z})$ expresses that the spins follow the changing invariant spin field, keeping J_S nearly invariant. In both cases the beam will recover its polarization after the critical energy region is crossed. The beam polarization is only reduced in intermediate cases.

Strong divergence of the invariant spin field at critical energies can happen even when Siberian Snakes are present, as shown in figure 2.15 (top right), even though first–order resonances do not occur. In figure 2.15 (bottom), the energy dependences of P_{lim} with and without Siberian Snakes are overlayed, which shows that not all resonance effects are removed by Siberian Snakes, but resonance structures remain even with Siberian Snakes. This will be analyzed in detail in section 4.1. Siberian Snakes smooth the variation of $P_{lim} = | < \vec{n}(\vec{z}) > |$ with energy. As a result $\vec{n}(\vec{z})$ changes more slowly during acceleration when Siberian Snakes are inserted and the

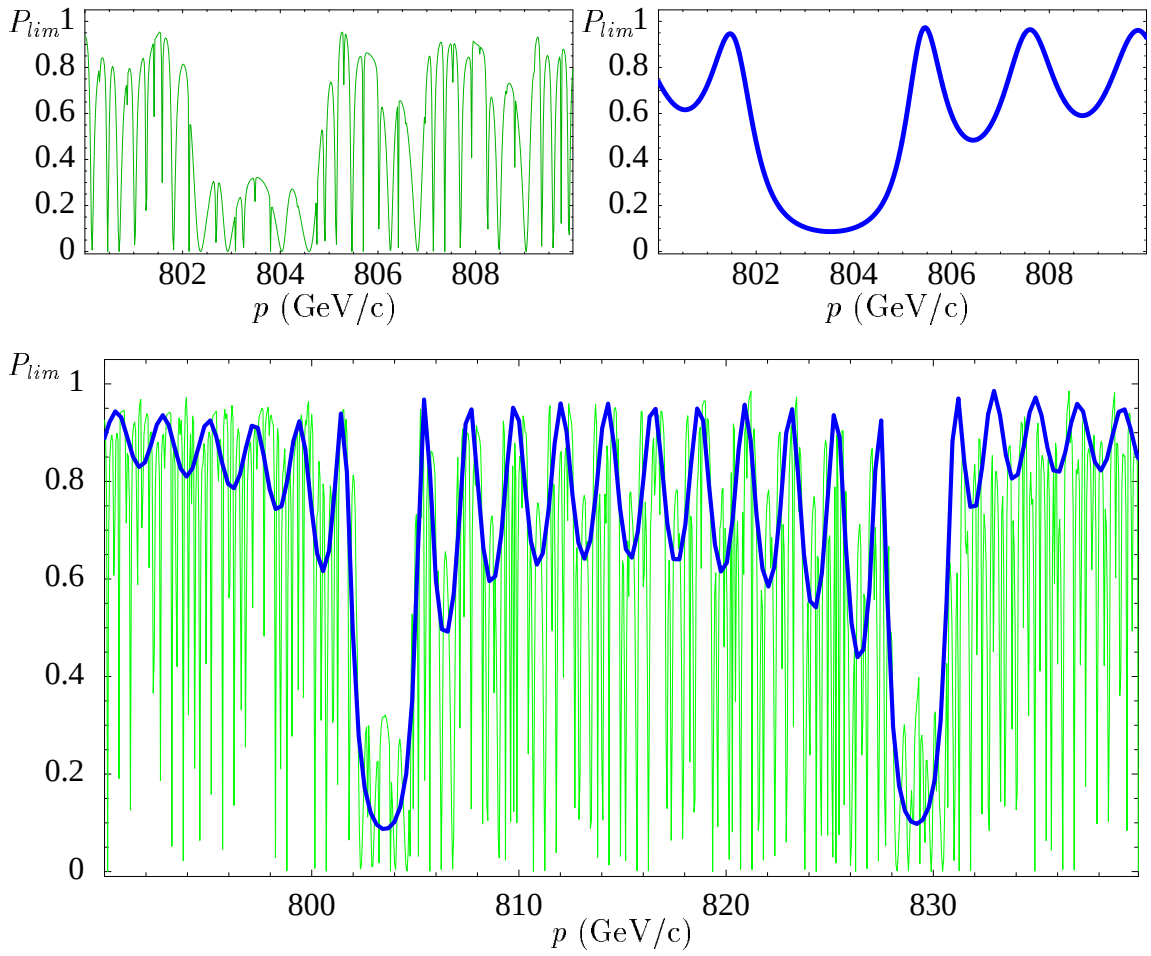

Figure 2.15: The dependence of the maximum time average polarization $P_{lim} = | < \vec{n} > |$ on momentum for a vertical amplitude of 25πmm mrad, which corresponds to 2.5σ of the beam size, after HERA–p is made effectively flat for spin motion by flattening snakes. Top left: At numerous intrinsic resonances, P_{lim} drops to small values. Top right: P_{lim} after the insertion of Siberian Snakes. Bottom: P_{lim} with and without Siberian Snakes in a wider region of energy. (Snake scheme $(\frac{\pi}{4}0\frac{\pi}{4}0)6fs$). In all three graphs, P_{lim} is shown for the South interaction region. Qualitatively similar curves are obtained at other positions in the ring.

spin can follow this change more easily, keeping changes of the adiabatic invariant J_S smaller.

A small polarization can occur due to the energy changes associated with synchrotron motion which can lead to a crossing of resonances. In HERA–p at 920GeV, a 1σ energy spread of $\frac{\Delta E}{E} = 1.1 \cdot 10^{-4}$ creates an associated spread of $G\Delta\gamma = 0.19$. The spin tune can therefore easily cross resonances during every synchrotron period when no snake is installed in the ring. The disruptive effect of this periodic crossing of resonances is shown in figure 2.16 (left) for a particle which moves on a phase space torus with 1σ longitudinal amplitude and $\frac{1}{2}\sigma$ vertical amplitude of 1πmm mrad. The vertical spin component of a particle with this amplitude changes sign twice every

synchrotron period, once for every crossing of the resonance $G\gamma = 1758 + Q_y$. When the spin tune's dependence on the energy deviation is eliminated, these resonance crossings are eliminated by Siberian Snakes which make the spin tune independent of the reference energy as well as independent of the energy oscillation within each synchrotron period. This is shown in figure 2.16 (right) which was computed with 4 Siberian Snakes.

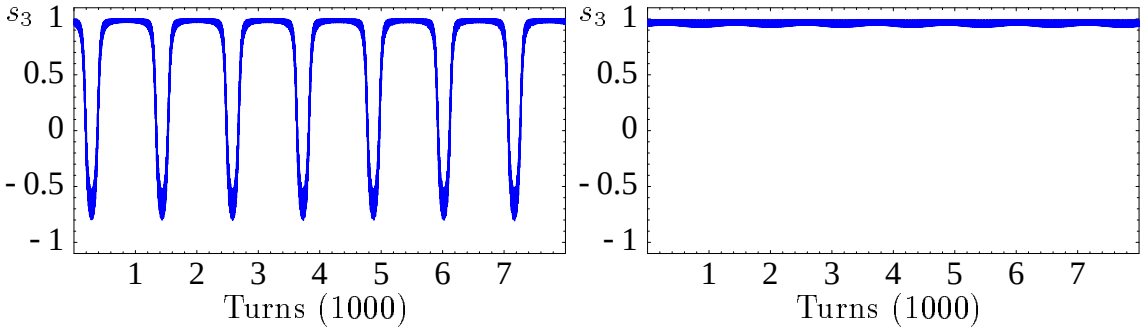

Figure 2.16: The vertical spin component of one particle during 7 synchrotron periods in HERA–p with 0.5σ vertical amplitude ($1\pi\mu$m) and 1σ longitudinal amplitude (18πmm). While energy of the particle oscillated due to the synchrotron motion, the reference energy of the ring remained constant. Left: without Siberian Snakes. Right: with 4 Siberian Snakes in the $(\frac{\pi}{4}0\frac{\pi}{4}0)6fs$ scheme.

An alternative view of the oscillating vertical spin component can be obtained when considering the invariant spin field $\vec{n}(\vec{z})$ on 6 dimensional phase space. In figure 2.16, the beam is not accelerated, therefore $J_S = \vec{S} \cdot \vec{n}(\vec{z})$ is invariant and should not even change adiabatically slowly. The changing sign of the vertical polarization reflects a change of $\vec{n}(\vec{z})$ at the particle's phase space position from nearly upwards to nearly downwards. This large spread over the phase space torus is reflected in a small $P_{lim} = | < \vec{n} > |$, where the average includes the longitudinal phase space. The installation of Siberian Snakes drastically reduces this spread, increasing P_{lim} drastically.

Siberian Snakes are therefore necessary for three reasons:

1. They increase P_{lim}, the maximum beam polarization usable at a fixed energy.

2. They smooth the dependence of the invariant spin field on the accelerators reference energy and therefore improve the possibility to accelerate a beam while keeping the adiabatic invariant $J_S = \vec{S} \cdot \vec{n}(\vec{z})$ nearly constant.

3. They reduce the dependence of spin transport on the energy oscillations of synchrotron motion.

Figure 2.15 was used to show that even with only first–order effects acceptable polarization could be obtained only over a restricted part of the energy range although 4 Siberian Snakes are used in the $(\frac{\pi}{4}0\frac{\pi}{4}0)6fs$ snake scheme. As a next step, I therefore tried to find better choices of snake positions and snake angles.

This search will be presented in section 4.1.3. Figure 2.17 shows the resulting improvements for $P_{lim} = | < \vec{n} > |$ and for the variations of ν obtained when going from the $(\frac{\pi}{4}0\frac{\pi}{4}0)8fs$ to the $(\frac{3\pi}{4}\frac{3\pi}{8}\frac{3\pi}{8}\frac{\pi}{4})8fs$ snake scheme of figure 2.8. Here a non–perturbative algorithm described in section 4.1.1 was used to include higher–order effects and to analyze improvements in the variation of the amplitude dependent spin tune.

In the following chapters, tools for reliable computation of the invariant spin field and for the selection of optimal snake schemes will be described. In section 3.3.2, light will be shed on the reasons which make certain snake schemes favorable. Since special snake schemes lead to comparatively large P_{lim} and small spin tune spread, it is expected that the reduction of polarization during the acceleration process is comparatively small for these schemes. In fact, tracking simulations will show that the snake schemes which I have found allow the acceleration of a beam with significantly larger emittance that standard snake schemes.

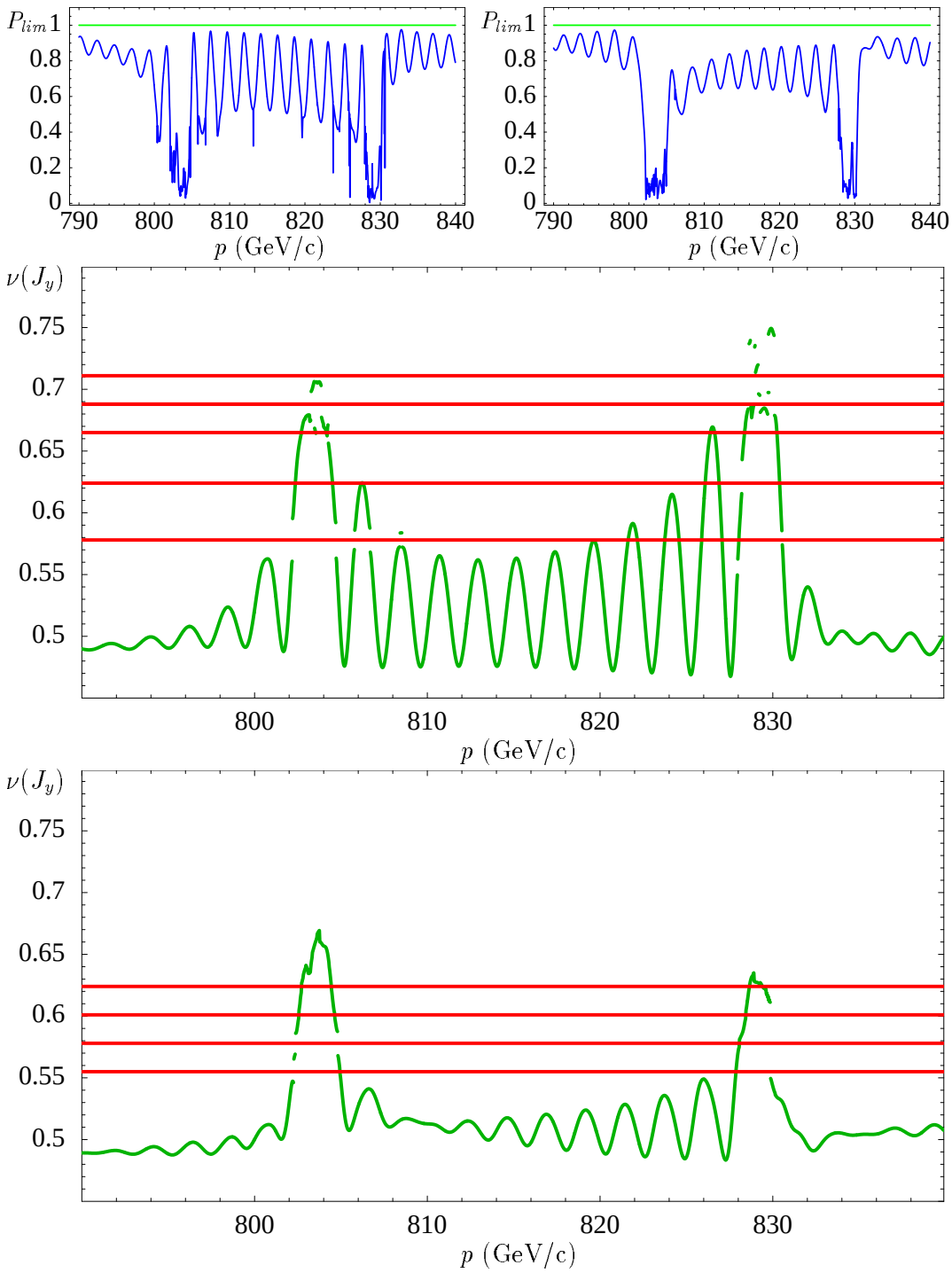

Figure 2.17: The maximum time average polarization P_{lim} for 2.5σ vertical motion (25πmm mrad) in HERA–p with a conventional snake scheme $(\frac{\pi}{4}0\frac{\pi}{4}0)8fs$ (left) and an optimized scheme $(\frac{3\pi}{4}\frac{3\pi}{8}\frac{3\pi}{8}\frac{\pi}{4})8fs$ (right). The amplitude dependent but orbital phase independent spin tune ν is shown for $(\frac{\pi}{4}0\frac{\pi}{4}0)8fs$ (middle) and for $(\frac{3\pi}{4}\frac{3\pi}{8}\frac{3\pi}{8}\frac{\pi}{4})8fs$ (bottom). From top to bottom, the following resonance lines are drawn, Middle: $1-Q_y$, $3-8Q_y$, $5-15Q_y$, $16Q_y-4$, $2Q_y$ and Bottom: $\nu=16Q_y-4$, $\nu=9Q_y-2$, $\nu=2-5Q_y$, $\nu=2Q_y$. From tune jumps at these higher–order resonances, their strength can be deduced.

Chapter 3

First–Order Spin Motion

3.1 Linearized Spin–Orbit Motion

At azimuth θ, a spin can be described by a complex coordinate α with

$$\vec{S} = \mathrm{Re}\{\alpha\}\vec{m}(\theta) + \mathrm{Im}\{\alpha\}\vec{l}(\theta) + \sqrt{1-|\alpha|^2}\vec{n}_0(\theta) \ , \tag{3.1}$$

where the right handed orthonormal dreibein $[\vec{m}, \vec{l}, \vec{n}_0]$ is used which was introduced in section 2.2.2 [63, 64]. The coordinate vectors $\vec{m}$ and $\vec{l}$ satisfy the equation of motion

$$\frac{d}{d\theta}(\vec{m} + i\vec{l}) = (\vec{\Omega}_0 - \nu_0\vec{n}_0) \times (\vec{m} + i\vec{l}) \ . \tag{3.2}$$

The spin of a particle which travels on the closed orbit precesses around $\vec{\Omega}_0$ and has rotated ν_0 times around $\vec{n}_0$ after one turn. According to equation (3.2), $\vec{m}$ and $\vec{l}$ also precess around $\vec{\Omega}_0$, but in addition a precession around $\vec{n}_0$ is subtracted, leaving no net rotation after one turn. Therefore, the dreibein $[\vec{m}, \vec{l}, \vec{n}_0]$ is 2π periodic in θ.

When the spin coordinate α and the phase space coordinates $\vec{z}$ are small so that the equation of spin–orbit motion can be linearized, then one approximates an initial spin of a particle at azimuth θ_0 by $\vec{S}_i \approx \mathrm{Re}\{\alpha_i\}\vec{m}(\theta_0) + \mathrm{Im}\{\alpha_i\}\vec{l}(\theta_0) + \vec{n}_0(\theta_0)$ and after the particle has traveled to azimuth θ, one has $\vec{S} = \mathrm{Re}\{\alpha\}\vec{m}(\theta) + \mathrm{Im}\{\alpha\}\vec{l}(\theta) + \vec{n}_0(\theta)$ where α is determined by the 7×7 spin–orbit transport matrix,

$$\begin{pmatrix} \vec{z} \\ \alpha \end{pmatrix} = \underline{M}_{77}(\theta_0;\theta) \begin{pmatrix} \vec{z}_i \\ \alpha_i \end{pmatrix} = \begin{pmatrix} \underline{M}(\theta_0;\theta) & \vec{0} \\ \vec{G}^T(\theta_0;\theta) & e^{i\nu_0(\theta-\theta_0)} \end{pmatrix} \begin{pmatrix} \vec{z}_i \\ \alpha_i \end{pmatrix} \ , \tag{3.3}$$

where $\underline{M}(\theta_0;\theta)$ is the 6×6 dimensional transport matrix for the phase space variables. For a particle on the closed orbit, the exponential describes the rotation of the spin component α around $\vec{n}_0$ with respect to $\vec{m}$ and $\vec{l}$. This rotation appears in equation (3.3) since spins precess around $\vec{\Omega}_0$ for $\vec{z} = 0$, while the coordinate vectors $\vec{m}$ and $\vec{l}$ rotate around $\vec{\Omega}_0 - \nu_0\vec{n}_0$. The complex row vector $\vec{G}^T(\theta_0;\theta)$ describes additional spin motion with respect to $\vec{m}$ and $\vec{l}$ due to off closed–orbit fields. The 6 dimensional zero vector $\vec{0}$ shows that the effect of Stern Gerlach forces on the orbit motion is not considered.

The linearized spin–orbit transport through two successive optical elements is described by the product of their 7×7 matrices. These matrices were derived long ago [12, 63, 5] for all standard optical elements and were initially used for the description of polarized electron beams.

Alternatively, the spin transport can be described by a spin transport quaternion as discussed in section 2.1.5. When linearizing with respect to phase space variables, indicated by $=_1$, a spin transport quaternion $\vec{C} =_1 \vec{C}^0 + \vec{C}^1(\vec{z})$ is separated into the quaternion for closed orbit motion $\vec{C}^0$ and a contribution $\vec{C}^1$ which is linear in the phase space variables. The spin–orbit transport through two successive optical elements is described by the action of first the quaternion $\vec{A}$ associated with the first element and then the quaternion $\vec{B}$ of the second element. The quaternion $\vec{C}$ describing the combined rotation is computed using the orthogonal 4×4 matrix $\underline{\tilde{A}}$ as described in equation (2.34),

$$\vec{C}^0 = \underline{\tilde{A}}^0 \vec{B}^0 \ , \quad \vec{C}^1 = \underline{\tilde{A}}^0 \vec{B}^1 + \underline{\tilde{A}}^1 \vec{B}^0 \ . \tag{3.4}$$

The spin transfer quaternion of an optical element does not depend on the basis vectors $[\vec{m}, \vec{l}, \vec{n}_0]$ and is therefore the same for two identical optical elements which are at different locations of the ring. The 7×7 matrix of individual optical elements does not have this advantage. Furthermore, a generalization to quaternions which depend nonlinearly on the phase space coordinates is straight forward (see section 4.1.4). Therefore, the quaternion method is used in the program SPRINT [112, 100] to describe spin transport.

The spin transport quaternion can be written as the concatenation of first the closed orbit spin transport described by $\vec{C}^0$ and then a purely phase space dependent spin transport which does not change the spin of particles on the closed orbit. With the quaternion $\vec{e}_1 = (1, 0, 0, 0)^T$ describing the identity transformation and with a quaternion $\vec{D}^1$ which vanishes for particles on the closed orbit, the purely phase space dependent spin transport is described by $\vec{e}_1 + \vec{D}^1$,

$$\vec{C} = \underline{\tilde{C}}^0 (\vec{e}_1 + \vec{D}^1) \ , \quad \vec{D}^1 = \underline{\tilde{C}}^{0T} \vec{C}^1 \ . \tag{3.5}$$

Advantage has here been taken of the fact that the 4×4 dimensional matrix $\underline{\tilde{C}}^0$ is orthogonal, as has been pointed out after equation (2.34), and thus inverted by transposition. The 3×3 spin rotation matrix on the closed orbit is written as $\underline{R}^0$ and the rotation matrix corresponding to the concatenated quaternion in equation (3.5) is the product $\underline{R}^D \underline{R}^0$. Equation (2.30) relates the quaternion $\vec{e}_1 + \vec{D}^1$ with $\vec{D}^1 = (d_0^1, \vec{d}^{\,1})^T$ with the rotation matrix $\underline{R}^D$, which to first order, becomes

$$R_{ij}^D = [(1 + d_0^1)^2 - (\vec{d}^{\,1})^2]\delta_{ij} + 2d_i^1 d_j^1 - 2(1 + d_0^1)\epsilon_{ijk} d_k^1 =_1 (1 + 2d_0^1)\delta_{ij} - 2\epsilon_{ijk} d_k^1 \ . \tag{3.6}$$

By the total spin rotation $\underline{R}^D \underline{R}^0$, the initial spin $\vec{S}_i = \vec{n}_0(\theta_0)$ is first transported to $\vec{n}_0(\theta) = \underline{R}^0 \vec{n}_0(\theta_0)$ and then to

$$\vec{S}_f = (1 + 2d_0^1)\vec{n}_0(\theta) + 2\vec{d}^{\,1} \times \vec{n}_0(\theta) \ . \tag{3.7}$$

When a spin with $\vec{S}_i = \vec{n}_0$ is transported by the 7×7 spin–orbit transport matrix, then $\alpha_f = \vec{S}_f \cdot [\vec{m}(\theta) + i\vec{l}(\theta)]$ is given by $\vec{G} \cdot \vec{z}$ which now equates to

$$\vec{G} \cdot \vec{z} = 2[\vec{d}^1 \times \vec{n}_0(\theta)] \cdot [\vec{m}(\theta) + i\vec{l}(\theta)] = -i2\vec{d}^1 \cdot [\vec{m}(\theta) + i\vec{l}(\theta)] \ . \tag{3.8}$$

This illustrates how the spin–orbit transport matrix $\underline{M}_{77}$ can easily be computed when its spin transfer quaternion is known.

3.1.1 The Invariant Spin Field for Linearized Spin–Orbit Motion

Although it is difficult to compute $\vec{n}$ in general, an approximation for $\vec{n}$ can easily be obtained [64, 87, 7] for linearized spin–orbit motion on a Poincaré section at azimuth θ_0. Its components perpendicular to $\vec{n}_0(\theta_0)$ are written as a complex function $n_\alpha(\vec{z})$ and use a 7 dimensional vector $\vec{n}_1$ to obtain the first–order expansion of $\vec{n}(\vec{z})$. Using the one turn matrix $\underline{M}_{7\times7} = M_{7\times7}(\theta_0; \theta_0 + 2\pi)$, the linearized periodicity condition (2.79) for the invariant spin field is

$$\vec{n}_1(\vec{z}) = \begin{pmatrix} \vec{z} \\ \alpha_n(\vec{z}) \end{pmatrix} \ , \quad \vec{n}_1(\underline{M}\vec{z}) = \underline{M}_{77}\vec{n}_1(\vec{z}) \ . \tag{3.9}$$

This equation can be solved for $\vec{n}_1$ after the matrices are diagonalized. Let $\underline{A}^{-1}$ be the column matrix of eigenvectors $\vec{v}_k^{\pm}$ of the one turn matrix $\underline{M}$. The eigenvalues are $e^{\pm i2\pi Q_k}$ with the orbital tunes Q_k. The matrix $\underline{\Lambda} = \underline{A}\ \underline{M}\ \underline{A}^{-1}$ is the diagonal matrix of these eigenvalues. Now the 7×6 dimensional matrix $\underline{T}$ is needed which is the column matrix of the first 6 eigenvectors of $\underline{M}_{77}$ and has the form

$$\underline{T} = \begin{pmatrix} \underline{A}^{-1} \\ \vec{B}^T \end{pmatrix} \ , \quad \underline{T}\,\underline{\Lambda} = \underline{M}_{77}\underline{T} \ , \tag{3.10}$$

where the 7th components of the eigenvectors form a vector $\vec{B}$. If a linear function $\vec{n}_1(\vec{z}) = \underline{K}\vec{z}$ of the phase space coordinates can be found which satisfies the periodicity condition (3.9), then an invariant spin field has been determined. Since the upper 6 components of $\vec{n}_1(\vec{z})$ are $\vec{z}$, the upper 6 rows of $\underline{K}$ form the identity matrix $\underline{1}_6$. Inserting $\vec{n}_1 = \underline{K}\vec{z}$ into equation (3.9) and multiplying the resulting condition $\underline{K}\ \underline{M} = \underline{M}_{77}\underline{K}$ by $\underline{A}^{-1}$ from the right leads to $\underline{K}\ \underline{A}^{-1}\underline{\Lambda} = \underline{M}_{77}\underline{K}\ \underline{A}^{-1}$. Therefore the columns of $\underline{K}\ \underline{A}^{-1}$ are eigenvectors of $\underline{M}_{7\times7}$ and are therefore proportional to the columns of $\underline{T}$. The upper 6 rows $\underline{1}_6\underline{A}^{-1}$ agree with those of $\underline{T}$; this requires the 6 proportionality constants to be 1. Therefore $\underline{K}\ \underline{A}^{-1} = \underline{T}$ and I conclude that there exists a unique linear invariant spin field given by

$$\vec{n}_1(\vec{z}) = \underline{T}\ \underline{A}\vec{z} \ , \quad \alpha_n = \vec{B} \cdot (\underline{A}\vec{z}) \ . \tag{3.11}$$

Now the steps which lead to the amplitude dependent spin tune for a general system in section 2.2.7 are repeated for linearized spin–orbit motion. Together

with $\vec{n}(\vec{z}) =_1 \mathrm{Re}\{\alpha_n\}\vec{m} + \mathrm{Im}\{\alpha_n\}\vec{l} + \vec{n}_0$, the following two basis vectors build an orthonormal dreibein in linear approximation at θ_0:

$$\vec{u}_1(\vec{z}) =_1 \vec{m} - \mathrm{Re}\{\alpha_n\}\vec{n}_0 \ , \quad \vec{u}_2(\vec{z}) =_1 \vec{l} - \mathrm{Im}\{\alpha_n\}\vec{n}_0 \ . \tag{3.12}$$

A spin $\vec{S}_i =_1 \mathrm{Re}\{\alpha_i\}\vec{m} + \mathrm{Im}\{\alpha_i\}\vec{l} + \vec{n}_0$ is transported to $\vec{S}_f =_1 \mathrm{Re}\{G + e^{i2\pi\nu_0}\alpha_i\}\vec{m} + \mathrm{Im}\{G + e^{i2\pi\nu_0}\alpha_i\}\vec{l} + \vec{n}_0$ after one turn, where

$$\vec{u}_1(\underline{M}\vec{z}) =_1 \vec{m} - \mathrm{Re}\{G + e^{i2\pi\nu_0}\alpha_n\}\vec{n}_0 \ , \quad \vec{u}_2(\underline{M}\vec{z}) =_1 \vec{l} - \mathrm{Im}\{G + e^{i2\pi\nu_0}\alpha_n\}\vec{n}_0 \ . \tag{3.13}$$

At the initial phase space point this leads to the projections $\vec{S}_i \cdot (\vec{u}_1(\vec{z}_i) + i\vec{u}_2(\vec{z}_i)) =_1 \alpha_i - \alpha_n$ and after one turn to $\vec{S}_f \cdot (\vec{u}_1(\vec{z}_f) + i\vec{u}_2(\vec{z}_f)) =_1 e^{i2\pi\nu_0}(\alpha_i - \alpha_n)$. The amplitude dependent spin tune ν in linearized spin–orbit motion is therefore simply given by ν_0 .

The eigenvector condition

$$\underline{M}_{77} \begin{pmatrix} \vec{v}_k^{\pm} \\ B_k^{\pm} \end{pmatrix} = e^{\pm i2\pi Q_k} \begin{pmatrix} \vec{v}_k^{\pm} \\ B_k^{\pm} \end{pmatrix} \tag{3.14}$$

leads to $\vec{G} \cdot \vec{v}_k^{\pm} + e^{i2\pi\nu_0} B_k^{\pm} = e^{\pm i2\pi Q_k} B_k^{\pm}$. Therefore α_n diverges at first–order intrinsic resonances where $\nu_0 = j_0 \pm Q_k$ due to

$$B_k^{\pm} = \vec{G} \cdot \vec{v}_k^{\pm} / (e^{\pm i2\pi Q_k} - e^{i2\pi\nu_0}) \ . \tag{3.15}$$

In the normal form space belonging to the diagonal matrix $\underline{\Lambda}$, the coordinates are given by the actions J_j and the angle variables Φ_j with

$$A\vec{z} = (\sqrt{J_1}e^{i\Phi_1}, \sqrt{J_1}e^{-i\Phi_1}, \sqrt{J_2}e^{i\Phi_2}, \sqrt{J_2}e^{-i\Phi_2}, \sqrt{J_3}e^{i\Phi_3}, \sqrt{J_3}e^{-i\Phi_3})^T \ . \tag{3.16}$$

The average over all angle variables on an invariant torus is described by $< \ldots >_{\vec{\Phi}}$. It leads to the average opening angle of

$$< \vartheta(\vec{n}, \vec{n}_0) >_{\vec{\Phi}} \approx \mathrm{atan}(\sqrt{< |\alpha_n|^2 >_{\vec{\Phi}}}) = \mathrm{atan}\left(\sqrt{\sum_{k=1}^{3}(|B_k^+|^2 + |B_k^-|^2)J_k}\right) \ , \tag{3.17}$$

where the $B_k^{\pm}$ are the 7th components of the eigenvectors in equation (3.10). The maximum time average polarization is approximately

$$P_{lim} =< \cos(\vartheta(\vec{n}, \vec{n}_0)) >_{\vec{\Phi}} \approx [1 + \sum_{k=1}^{3}(|B_k^+|^2 + |B_k^-|^2)J_k]^{-\frac{1}{2}} \ . \tag{3.18}$$

These approximations for $\vec{n}(\vec{z})$, $< \vartheta >$, and P_{lim} can only be accurate if $|\alpha_n|$ is small.

In a ring with midplane symmetry, the one turn spin–orbit matrix $\underline{M}_{7\times7}$ has a block structure with 2×2 matrix blocks and 2 dimensional zero and non–zero vectors,

$$\underline{M}_{7\times7} = \begin{pmatrix} \underline{*} & \underline{0} & \underline{*} & \vec{0} \\ \underline{0} & \underline{*} & \underline{0} & \vec{0} \\ \underline{*} & \underline{0} & \underline{*} & \vec{0} \\ \vec{0}^T & \vec{*}^T & \vec{0}^T & * \end{pmatrix} \ . \tag{3.19}$$

The 6×6 dimensional phase space transport matrix has a chequer–board structure, since there is no coupling between vertical motion and the other two degrees of freedom in a midplane–symmetric ring; and $\vec{G}$ has only contributions from vertical motion since a spin with $\vec{S}_i = \vec{n}_0$ ($\alpha_i = 0$) is not deflected out of the vertical unless the particle flies through horizontal magnetic field components, which only happens for particles with a vertical oscillation amplitude. The opening angle $< \vartheta >$ and P_{lim} then only depend on the vertical action J_y.

3.1.2 Spin–Orbit–Coupling Integrals

Instead of computing the one turn matrix $M_{7\times 7}$ as the product of spin–orbit transport matrices of individual elements or by concatenation of their spin transport quaternions, one can also solve the linearized equation of motion for α directly. To obtain simplified formulas, now the dreibein $[\vec{m}_0, \vec{l}_0, \vec{n}_0]$ is used which was introduced in section 2.2.2. The vectors $\vec{m}_0$ and $\vec{l}_0$ are perpendicular to $\vec{n}_0$, precess according to the T–BMT equation on the closed orbit, and are therefore related to $\vec{m}$ and $\vec{l}$ by a rotation around $\vec{n}_0$ with $\vec{m} + i\vec{l} = e^{i\nu_0(\theta-\theta_0)}(\vec{m}_0 + i\vec{l}_0)$, which was already derived in equation (2.48). Here it is assumed that the two dreibeins coincide at azimuth 0. Whereas the dreibein $[\vec{m}, \vec{l}, \vec{n}_0]$ constitutes a coordinate system which is 2π periodic in θ, $[\vec{m}_0, \vec{l}_0, \vec{n}_0]$ does not.

The precession vector for spins can be separated into a part for particles on the closed orbit and a part due to phase space amplitudes, $\vec{\Omega}(\vec{z}, \theta) = \vec{\Omega}_0(\theta) + \vec{\omega}(\vec{z}, \theta)$. The spin direction and the phase space dependent part $\vec{\omega}$ of the precession vector will be written in complex notation in the dreibein $[\vec{m}_0, \vec{l}_0, \vec{n}_0]$ as

$$\vec{S} = \mathrm{Re}\{\alpha_0\}\vec{m}_0 + \mathrm{Im}\{\alpha_0\}\vec{l}_0 + \vec{n}_0\sqrt{1+|\alpha_0|^2}\ , \tag{3.20}$$

$$\vec{\omega} = \mathrm{Re}\{\omega_0\}\vec{m}_0 + \mathrm{Im}\{\omega_0\}\vec{l}_0 + \vec{n}_0\omega_3\ . \tag{3.21}$$

The first equation differs from the equations (2.113) and (3.1) since α_0 refers to $\vec{m}_0$ and $\vec{l}_0$ whereas α referred to $\vec{m}$ and $\vec{l}$. Inserting this into the T–BMT equation (2.24), one obtains

$$\vec{\Omega} \times \vec{S} = \frac{d}{d\theta}\vec{S} = \mathrm{Re}\{\frac{d}{d\theta}\alpha_0\}\vec{m}_0 + \mathrm{Im}\{\frac{d}{d\theta}\alpha_0\}\vec{l}_0 + \vec{n}_0\frac{d}{d\theta}\sqrt{1-|\alpha_0|^2} + \vec{\Omega}_0 \times \vec{S}\ . \tag{3.22}$$

This leads to a differential equation for α_0,

$$\begin{aligned}\frac{d}{d\theta}\alpha_0 &= (\vec{\omega} \times \vec{S}) \cdot (\vec{m}_0 + i\vec{l}_0) = \vec{\omega} \cdot [\vec{S} \times (\vec{m}_0 + i\vec{l}_0)] \qquad (3.23)\\ &= \vec{\omega} \cdot [i\alpha_0\vec{n}_0 + \sqrt{1-|\alpha_0|^2}\ (\vec{l}_0 - i\vec{m}_0)] = -i\omega_0\sqrt{1-|\alpha_0|^2} + i\alpha_0\omega_3\ .\end{aligned}$$

Linearization with respect to $\vec{z}$ and α_0 leads to $\frac{d}{d\theta}\alpha_0 = -i\omega_0^1$, where the superscript signals the first–order expansion of $\omega(\vec{z}, \theta)$ with respect to $\vec{z}$. Since $\alpha = \alpha_0 e^{i\nu_0(\theta-\theta_0)}$, and since $\alpha_i = 0$ at azimuth θ_0 is transported to $\alpha_f = \vec{G} \cdot \vec{z}_i$ after one turn, one now obtains

$$\vec{G} \cdot \vec{z}_i = -ie^{i2\pi\nu_0}\int_{\theta_0}^{\theta_0+2\pi} \omega_0^1(\vec{z}(\theta), \theta)d\theta\ , \tag{3.24}$$

where the trajectory $\vec{z}(\theta)$ has started with $\vec{z}_i$ at azimuth θ_0.

In flat rings it is advantageous to use the comoving dreibein $[\vec{e}_x, \vec{e}_\theta, \vec{e}_y]$ introduced in section (2.1.2) with $\vec{e}_y$ vertical and with $\vec{e}_\theta$ parallel to the closed orbit. In such a ring, $\vec{n}_0$ and $\vec{\Omega}_0 = \Omega_0 \vec{e}_y$ are vertical, and for a particle on the closed orbit, a spin has rotated by the angle $\Psi = \int_{\theta_0}^{\theta} \Omega_0 d\theta$ between azimuth θ_0 and θ. Therefore $\vec{m}_0 + i\vec{l}_0 = e^{-i\Psi}(\vec{e}_x + i\vec{e}_y)$ and $\omega_0^1 = e^{-i\Psi}(\omega_x^1 + i\omega_\theta^1)$.

In a midplane–symmetric ring, there are no skew elements or solenoids and horizontal components of $\vec{\omega}$ only occur when a particle oscillates vertically around the closed orbit. When linearizing in $\vec{z}$, these components are produced by the quadrupole focussing strength k ($k > 0$ for a horizontally focussing effect). The spin rotations in these fields are $(G\gamma + 1)$ larger than the orbit deflections created by the quadrupoles, and one obtains $\omega_0^1 d\theta = (G\gamma + 1)e^{-i\Psi} y k dl$, where L is the circumference of the ring and $l = L\frac{\theta}{2\pi}$ is the path–length of the design trajectory. In terms of the vertical betatron function β_y and the betatron phase Φ_y, one has $y = \sqrt{2J_y\beta_y}\cos(\Phi_y + \Phi_{yi})$. This has lead to the definition of the one turn spin–orbit–coupling integrals [3, 4, 113]

$$I_y^{\pm} = -i(G\gamma + 1)\frac{1}{\sqrt{2}} \oint_{l_0}^{l_0+L} e^{i(-\Psi \pm \Phi_y)} \sqrt{\beta_y} k dl \ , \tag{3.25}$$

where $\Psi(\theta_0) = 0$ and the initial betatron phase is $\Phi_y(\theta_0) = 0$. When the initial phase space coordinate $\vec{z}_i$ has the vertical phase Φ_{yi} and the Courant–Snyder invariant [54] $2J_y$, equation (3.24) leads to

$$\vec{G} \cdot \vec{z}_i = e^{i2\pi\nu_0}(I_y^+ e^{i\Phi_{yi}} + I_y^- e^{-i\Phi_{yi}})\sqrt{J_y} \ . \tag{3.26}$$

With $\vec{z}_i = \sqrt{J_y}(\vec{v}_2^+ e^{i\Phi_{yi}} + \vec{v}_2^- e^{-i\Phi_{yi}})$ one obtains $\vec{G} \cdot \vec{v}_2^{\pm} = e^{i2\pi\nu_0} I_y^{\pm}$. Spin–orbit–coupling integrals are therefore useful for analyzing linear spin–orbit motion in the case of a midplane–symmetric ring. They will be used in section 3.3.2 for the optimization of Siberian Snake arrangements.

In a general setting, where $\vec{\omega}^{\,1}(\vec{z}(\theta), \theta)$ not only has radial components, generalized spin–orbit–coupling integrals at θ_0 are defined as $I_k^{\pm} = e^{-i2\pi\nu_0} \vec{G} \cdot \vec{v}_k^{\pm}$. This brings them into close relation with the components $B_k^{\pm}$ of the $\vec{n}$–axis, which can be written as

$$\alpha_n = \sum_{k=1}^{3} \sqrt{J_k}(B_k^+ e^{i\Phi_k} + B_k^- e^{-i\Phi_k}) \ , \quad B_k^{\pm} = \frac{I_k^{\pm}}{e^{i2\pi(\pm Q_k - \nu_0)} - 1} \ . \tag{3.27}$$

So far eigenvectors of the one turn matrix have only been used at the initial azimuth θ_0. Now the eigenvectors $\vec{v}_k^{\pm}(\theta)$ of the one turn matrix at θ are needed which lead to the trajectory $\vec{z}(\theta)$ for a particle which started with the initial phase variables Φ_{ki} at azimuth 0,

$$\vec{z}(\theta) = \sum_{k=1}^{3} \sqrt{J_k}[\vec{v}_k^+(\theta) e^{i(Q_k(\theta-\theta_0)+\Phi_{ki})} - \vec{v}_k^-(\theta) e^{-i(Q_k(\theta-\theta_0)+\Phi_{ki})}] \ , \tag{3.28}$$

By inserting this into equation (3.24) and taking advantage of the linearity of ω_0^1, one obtains

$$I_k^{\pm} = e^{-i2\pi\nu_0}\vec{G}\cdot\vec{v}_k^{\pm} = -i\int_{\theta_0}^{\theta_0+2\pi}\vec{\omega}^1(\vec{v}_k^{\pm}(\theta),\theta)\cdot(\vec{m}+i\vec{l})e^{i(\pm Q_k-\nu_0)(\theta-\theta_0)}d\theta\ . \qquad (3.29)$$

It has been suggested ad hoc in [78, 114] that $|I_2^+|^2 + |I_2^-|^2$ be used as a quality factor for polarized proton synchrotrons. Due to the central importance of the invariant spin field for the acceleration process and for storage of polarized beams, it now becomes clear that the quality factor should in general rather be $\sum_{k=1}^{3}[\frac{|I_k^+|^2}{\sin^2(\pi(Q_k-\nu_0))}+\frac{|I_k^{\pm}|^2}{\sin^2(\pi(-Q_k-\nu_0))}]$. Close to intrinsic resonances where $\pm Q_k-\nu_0$ is integer for some k, the opening angle of the $\vec{n}$–axis diverges in linearized spin–orbit motion.

3.1.3 Restrictions of Linearized Spin–Orbit Motion

The approximation of linearized spin–orbit motion is no longer justified when P_{lim} is not close to 1, which happens close to intrinsic resonances in the figures 3.1. Linearized spin–orbit motion can be applied even when the resonances are not well separated, but when computing the average polarization of a polarized beam, $|\alpha_n|$ must be small enough to justify the underlying approximation. If $|\alpha_n| \leq 0.5$ is accepted, the average polarization computed with linearized spin–orbit motion is only trustworthy as long as it is above about 87%.

Figure 3.1 shows for DESY III (top) and for PETRA (bottom), that at most energies spin dynamics can be described well by linearized spin–orbit motion.

For the luminosity upgrade optics of HERA–p with non–flat regions as they are today, figure 3.2 (top) shows that linearized spin–orbit motion leads to a P_{lim} which deviates strongly from 1 over a wide range of energies, so that linearization in α cannot be applied. When the flattening snakes are introduced as described in section 2.2.4, P_{lim} increases somewhat and a regular resonance structure can clearly be seen (bottom). Nevertheless, linearization cannot be accurate over a large range of energies.

The decreased P_{lim} at intrinsic resonances shows that Siberian Snakes have to be used to make the closed–orbit spin tune independent of energy, so that no first–order intrinsic resonances have to be crossed.

3.2 First–Order Resonance Spectrum

3.2.1 The Resonance Spectrum

The spin dynamics close to intrinsic resonances can be analyzed by Fourier expanding the field components $\vec{\omega}(\vec{z},\theta)$ which perturb the spin of a particle that oscillates around the closed orbit. For spins parallel to the rotation vector on the closed orbit $\vec{n}_0(\theta)$, only the components of $\vec{\omega}(\vec{z},\theta)$ which are perpendicular to $\vec{n}_0$ perturb the polarization.

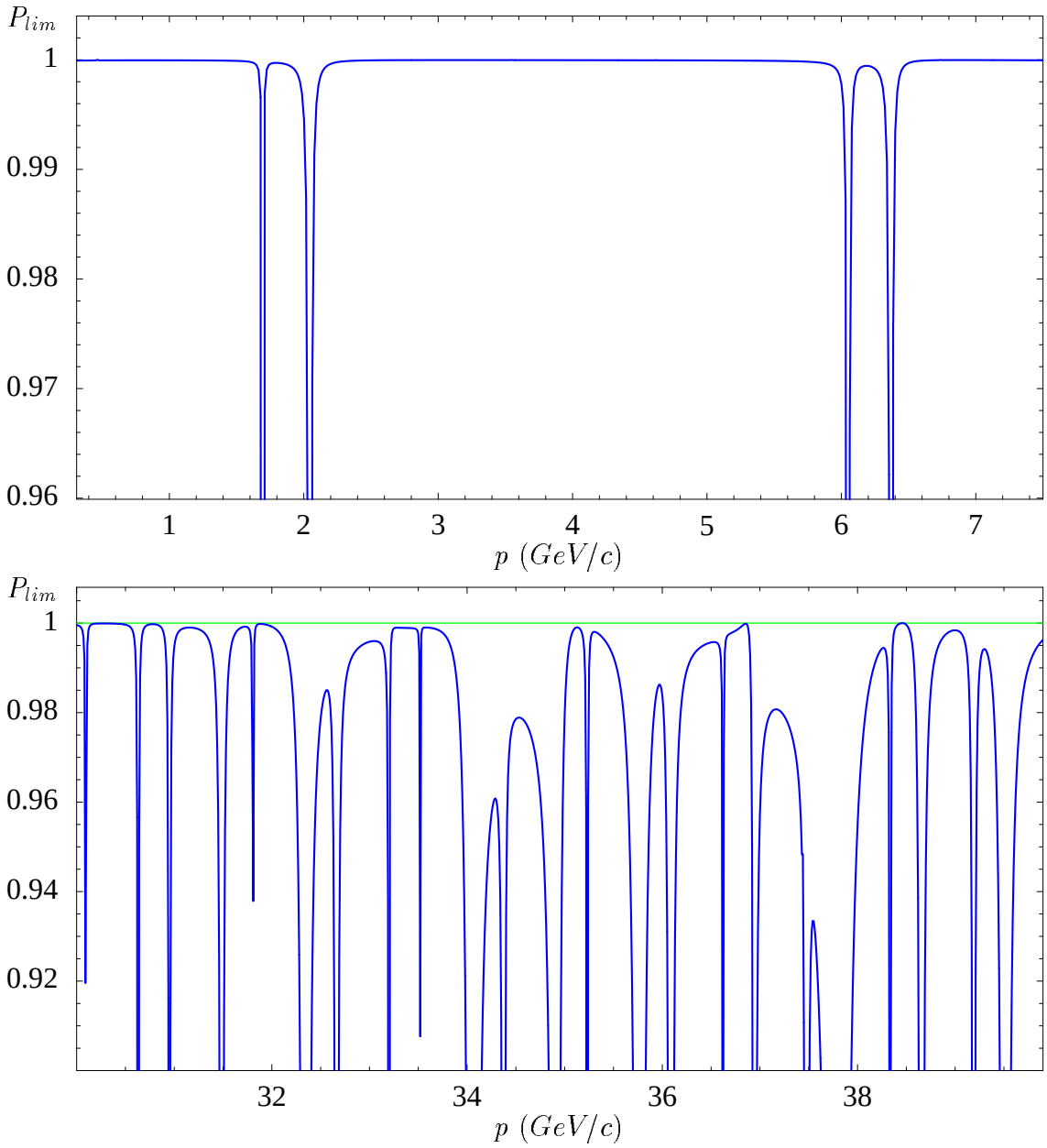

Figure 3.1: P_{lim} as approximated by linearized spin–orbit motion for DESY III (top) and for the high energy end of PETRA (bottom). The dips have been cut in order to magnify the interesting region where $|\alpha_n|$ is small.

As described in section 2.2.10, a depolarizing resonance occurs when a Fourier component of $\vec{\omega}(\vec{z}(\theta),\theta)$ rotates with the same frequency around $\vec{n}_0$ as the spins so that there is a strong perturbation. In the 2π periodic coordinate system constituted by $[\vec{m},\vec{l},\vec{n}_0]$, the Fourier component of $\omega = \vec{\omega}\cdot(\vec{m}+i\vec{l})$ for the frequency κ is computed by

$$\tilde{\epsilon}_\kappa = \lim_{N\to\infty} \frac{1}{2\pi N} \int_0^{2\pi N} \omega(\vec{z}(\theta),\theta) e^{-i\kappa\theta} d\theta \ . \tag{3.30}$$

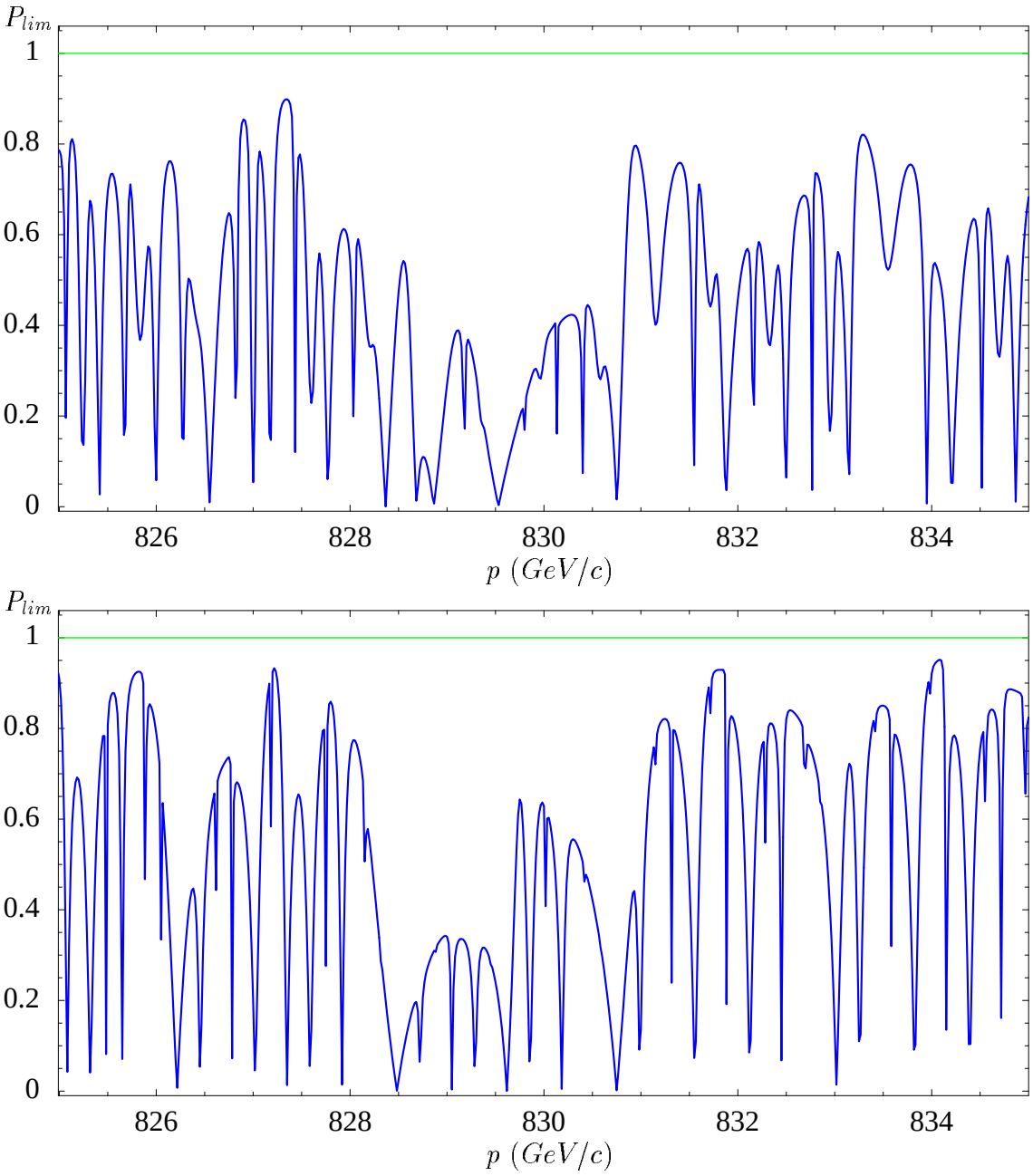

Figure 3.2: P_{lim} as approximated by linearized spin–orbit motion for high energies in HERA–p with non–flat regions as they are today (top) and after the installation of flattening snakes (bottom)

A warning is needed. The picture of perturbing effects suggests that the beam is slowly depolarized after it has been injected with 100% polarization. In fact the spins get deflected from their initial polarization direction $\vec{n}_0$ during one turn, only because the $\vec{n}$–axis $\vec{n}(\vec{z})$ is tilted away from the closed orbit spin direction $\vec{n}_0$. If an ensemble of the spins had started parallel to their invariant spin field, no net deflection due to the perturbing fields would have occurred and no reduction of

polarization would be noticed after one turn. However, since $\vec{n}(\vec{z})$ is tilted away from $\vec{n}_0$, the average polarization $P_{lim} = |<\vec{n}(\vec{z})>|$ for such an initial distribution is smaller than 1 to start with.

For each energy of the particle, there is in general a different Fourier spectrum of ω. Since at each energy the most important frequencies κ are those which are close to resonance with ν_0, it is customary to compute $\epsilon_{\nu_0(E)} = |\tilde{\epsilon}_{\nu_0(E)}|$, which is called the resonance strength, for all energies of the acceleration cycle. Obviously, $\epsilon_{\nu_0(E)}$ is zero, except when a Fourier frequency of $\omega(\vec{z}(\theta),\theta)$ at energy E is equal to $\nu_0(E)$. The resulting line spectrum of over E is called the depolarizing resonance spectrum of an accelerator.

For the three proton synchrotrons at DESY, these resonance strengths ϵ_{ν_0} are shown in the top figures 3.3, 3.4, and 3.5. They were all computed for an oscillation amplitude of $\vec{z}(\theta)$ corresponding to the 2.5σ vertical emittance of 25πmm mrad.

It is possible to recover the first–order isolated resonance strength from the one turn spin–orbit transport matrix. For a spin which was initially parallel to $\vec{n}_0$, equation (3.23) yields

$$\alpha_0(\theta) \approx -i \int_0^\theta \omega_0 d\theta \ , \quad \omega_0 = \vec{\omega}\cdot(\vec{m}_0 + i\vec{l}_0) = e^{-i\nu_0\theta}\vec{\omega}\cdot(\vec{m}+i\vec{l}) \ . \tag{3.31}$$

Comparing with equation (3.30), one can express the resonance strength by $\tilde{\epsilon}_{\nu_0} = i \lim_{N\to\infty} \frac{1}{2\pi N}\alpha_0(2\pi N)$. The resonance strength can therefore be computed from $\frac{1}{N}\underline{M}^N_{77}$ for large N. The computation becomes very efficient if one uses $\underline{M}^{2N}_{77} = (\underline{M}^N_{77})^2$ iteratively.

The coordinate vectors $\vec{m}_0(2\pi)$ and $\vec{l}_0(2\pi)$ to which $\alpha_0(2\pi)$ refers have rotated by $2\pi\nu_0$, whereas the final spin coordinate α_f computed by $\underline{M}_{77}$ refers to the coordinate vectors $\vec{m}_0(0)$ and $\vec{l}_0(0)$. Therefore $\alpha_0(2\pi N) = \alpha_f \exp(-i2\pi N\nu_0)$. The resonance strength ϵ_{ν_0} can most easily be computed when the powers of the one turn matrix are evaluated in diagonal form using the diagonal matrix $\underline{\Lambda}$ with the elements $e^{\pm i2\pi Q_k}$. For ease of notation, $\breve{Q}_k$ is used with $\breve{Q}_{2k-1} = Q_k$ and $\breve{Q}_{2k} = -Q_k$,

$$\begin{aligned}
\tilde{\epsilon}_{\nu_0} &= i \lim_{N\to\infty} \frac{1}{2\pi N}\alpha_0(2\pi N) = i \lim_{N\to\infty} \frac{1}{2\pi N}(0, e^{-iN2\pi\nu_0}) \begin{pmatrix} \underline{M} & \underline{0} \\ \vec{G}^T & e^{i2\pi\nu_0} \end{pmatrix}^N \begin{pmatrix} \vec{z} \\ 0 \end{pmatrix} \\
&= i \lim_{N\to\infty} e^{-iN2\pi\nu_0} \frac{1}{2\pi N} \sum_{j=0}^{N-1} [e^{i(N-j-1)2\pi\nu_0} \vec{G}^T \underline{A}^{-1} \underline{\Lambda}^j] \underline{A}\vec{z} \\
&= ie^{-i2\pi\nu_0} \sum_{k=1}^{6} G_l A^{-1}_{lk} A_{km} z_m \lim_{N\to\infty} \frac{1}{2\pi N} \sum_{j=0}^{N-1} e^{i2\pi j(\breve{Q}_k - \nu_0)}
\end{aligned} \tag{3.32}$$

where one has to sum over equal indices l, and m. This formula shows that the resonance strength is always zero, except at a resonance condition $\nu_0 = \kappa = j_0 \pm Q_k$. At such a closed–orbit spin tune, the resonance strength is given by

$$\begin{aligned}
2\pi\epsilon_{\nu_0} &= |\vec{G}^T \underline{A}^{-1} \underline{\mathrm{diag}}(0...1...0) \underline{A}\vec{z}| = |\vec{G}^T \underline{A}^{-1} (0...\sqrt{J_k} e^{\pm i\Phi_k}...0)^T| \\
&= |\vec{G}\cdot\vec{v}^{\pm}_k|\sqrt{J_k} = |I^{\pm}_k|\sqrt{J_k}
\end{aligned} \tag{3.33}$$

and $\tilde{\epsilon}_{\nu_0} = \epsilon_{\nu_0} e^{i2\pi(\pm\Phi_k - \nu_0)}$. The 1 in the diagonal matrix is in position $2k-1$ for $\nu_0 = j_0 + Q_k$ and at position $2k$ for $\nu_0 = j_0 - Q_k$. Here $\underline{A}^{-1}(0...\sqrt{J_k}e^{\pm i\Phi_k}...0)^T$ is the initial value for a phase space trajectory which has only Fourier components with frequencies $\pm Q_k$ plus integers and the eigenvector $\vec{v}_k^{\pm}$ of $\underline{M}$ has been used. The infinite Fourier integral in equation (3.30) has been reduced to the scalar product between the bottom row vector of $\underline{M}_{77}$ and an eigenvector of $\underline{M}$ which happens to equal the absolute value of the spin–orbit–coupling integral in equation (3.27). This very simple formula is used in the program SPRINT [112, 100].

After the first–order resonance strength for a frequency κ has been computed, one can investigate the influence of only the one corresponding Fourier contribution of ω to the spin motion. The resulting single resonance model (SRM) has been described in section 2.2.10.

3.2.2 Limitations of the SRM

Approximating the spin motion by the SRM is only accurate if the resonances are well separated so that one Fourier harmonic of ω dominates the dynamics. When a ring is not flat and has no exact super–periodicity, the first–order resonances appear when the spin tune comes close to $j_0 \pm Q_k$, where the tunes Q_k of all three degrees of motion can appear. HERA–p is not flat, but after the installation of flattening snakes, the first–order spin motion is very similar to that of a flat ring, where only resonances due to vertical motion appear. With a vertical orbit tune of approximately $\frac{1}{3}$ in HERA–p, the variation of ν_0 between resonances is $\frac{1}{3}$ or $\frac{2}{3}$. The resonance strength is related to the width of the resonance as shown in section 2.2.10; and to justify a single resonance approach, the resonance strength of two neighboring resonances should therefore be significantly less than $\frac{1}{3}$.

In linearized spin–orbit motion, the opening angle of the invariant spin field is approximately given by equation (3.17). In figure 3.3 the peaks in the resonance strength (top) are located exactly at the peaks of the big opening angles computed with the linearized approach (bottom); furthermore the widths of the peaks in opening angle are correlated with the resonance strengths. The resonances are well separated and in DESY III, first–order theories for analyzing polarization dynamics along with classical means of controlling depolarizing effects [22] are therefore applicable.

The corresponding figure for PETRA shows again that large opening angles of linearized spin–orbit motion are correlated with large resonance strength. However, the first–order resonances are getting so close at the high energy end of 39GeV that several pairs of resonances are close to overlapping. It has been observed experimentally [115] that Siberian Snakes can stabilize spin motion in the presence of overlapping resonances. The resonance strengths are still far away from PETRA's fractional vertical tune of about 0.2 and therefore also in this energy regime classical means of controlling depolarizing first–order resonances can be applied.

In HERA–p the situation changes even with flattening snakes as shown in figure 3.5. The first resonance which is stronger than $\frac{1}{3}$ for a normalized vertical amplitude of 25πmm mrad appears at about 150GeV/c and resonances start to overlap. Since

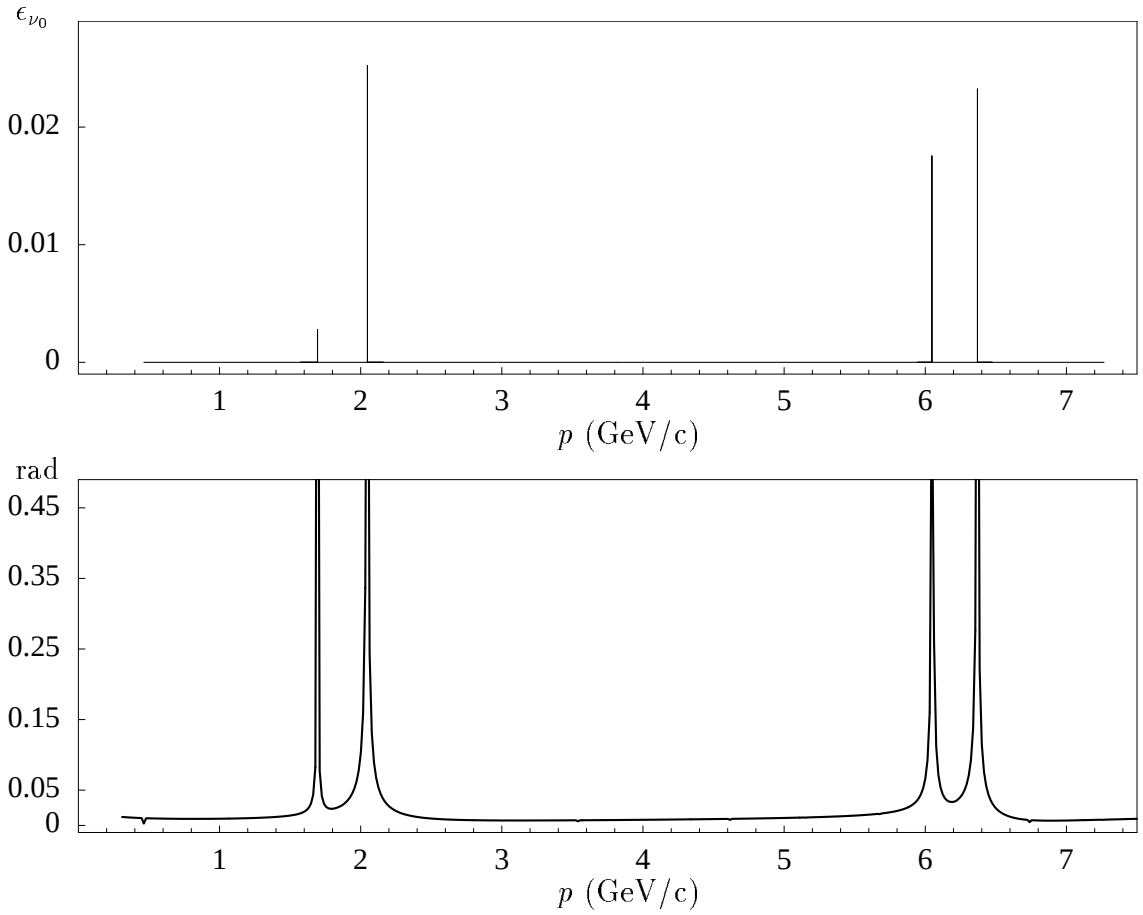

Figure 3.3: Resonance strength (top) and opening angles of linearized spin–orbit motion (bottom) for particles with a normalized vertical amplitude of 25πmm mrad in DESY III. The number of resonances is very low due to a super–periodicity 8.

there are over 3000 first–order resonances on the ramp of HERA–p from 39 to 920GeV/c, this effect can only be seen when looking at a smaller energy range as in figure 3.5. The resonances are strongly overlapping and the average opening angles of the invariant spin field are so big that linearized spin–orbit motion and the SRM for first–order resonances are not trustworthy anymore. Therefore methods which include higher–order spin effects have to be applied.

The average polarization computed with either of these two models, linearized spin–orbit motion or the single resonance model with first order resonances, is in any case only accurate if there are only effects which are dominated by first–order resonances. Effects which are not related to first–order resonances cannot be simulated by a first–order resonance strength or by linearized spin–orbit motion and therefore the first–order theories cannot be used to decide whether non–first–order effects are small or not. In general, therefore, a higher–order extension is needed to decide about the validity of the first–order theories.

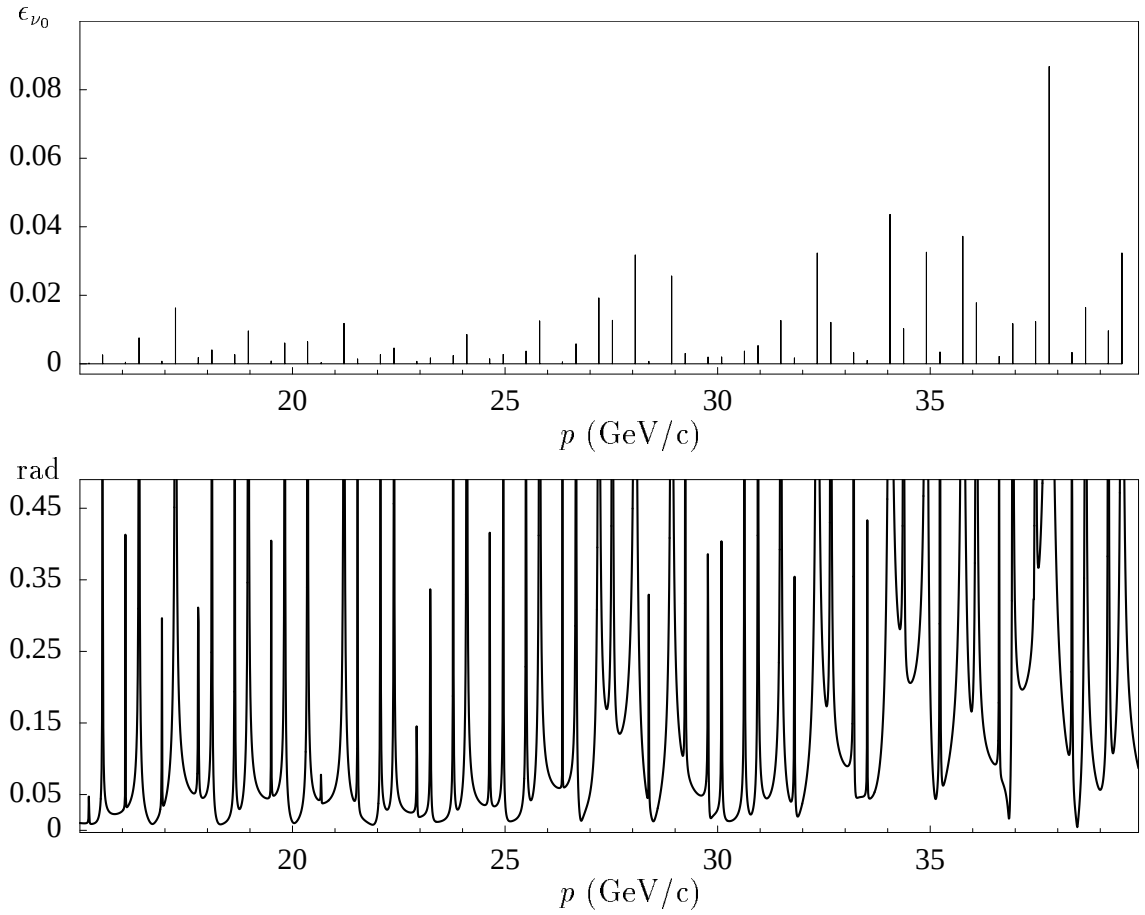

Figure 3.4: Resonance strength (top) and opening angles of linearized spin–orbit motion (bottom) for particles with normalized vertical amplitude of 25πmm mrad in PETRA.

3.2.3 First–Order Resonances in HERA–p

While the general approach described in section 3.2.1 can be applied to flat as well as to non–flat rings, but usually the single resonance model is used for midplane–symmetric rings, which have a vertical $\vec{n}_0$. There the resonance strength $\epsilon_{\nu_0} = \frac{\sqrt{J_k}}{2\pi}|\vec{G} \cdot \vec{v}_k^{\pm}|$ in equation (3.33) is only nonzero for the vertical degree of freedom due to the block structure described in equation (3.19). This reflects the fact that particles which stay in the midplane do not traverse horizontal fields and their spins are not deflected away from the vertical $\vec{n}_0$.

HERA–p is not midplane–symmetric. Its design trajectory does not even lie in a plane, due to the non–flat regions required to bend the proton beam to the level of the electron beam. This was already described in section 2.2.4, together with flattening snakes which are inserted at the center of each non–flat region to make the spin motion effectively that of a flat ring by forcing $\vec{n}_0$ to be vertical outside the non–flat regions. Nevertheless, $\vec{n}_0$ is non–vertical inside these regions and the spin–orbit–coupling integrals for horizontal and longitudinal motion are not identically zero so that more resonances occur in HERA–p than in other rings. Since

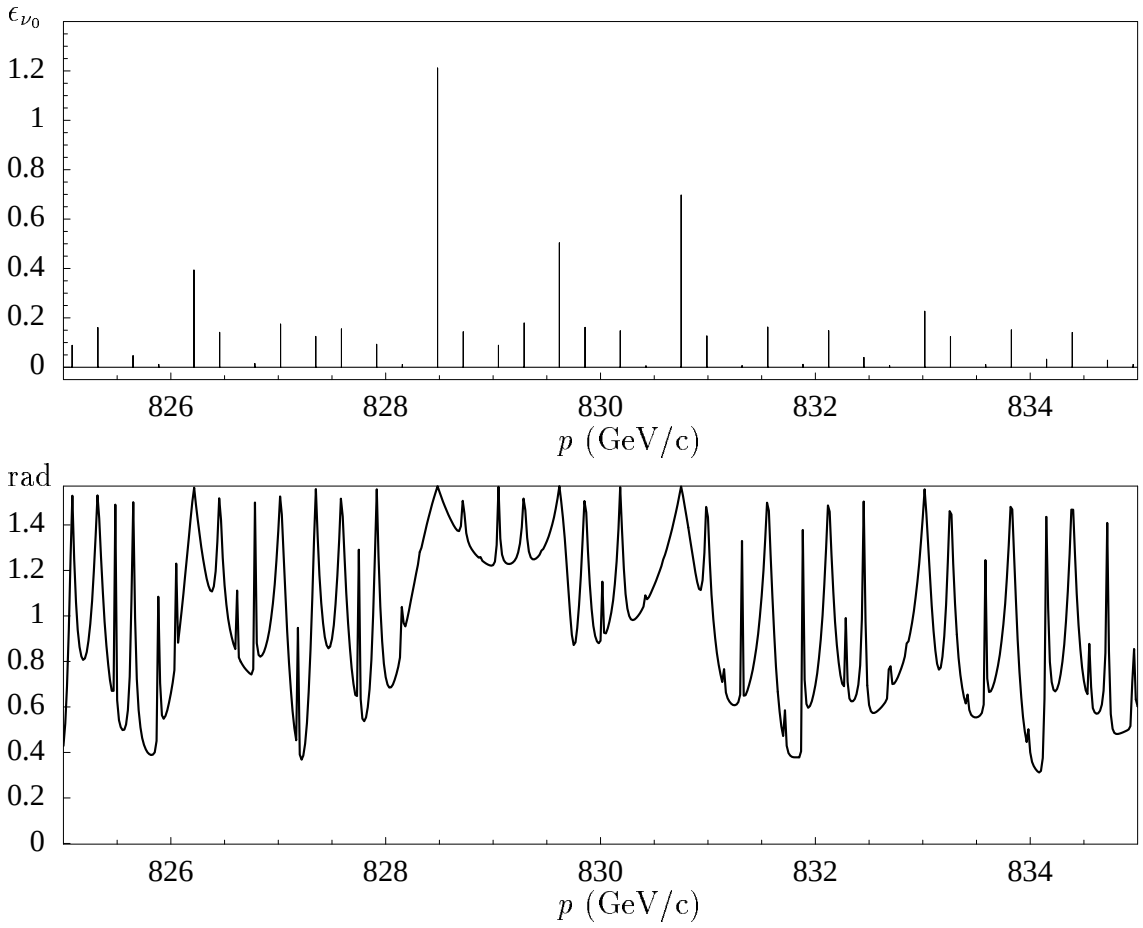

Figure 3.5: Resonance strength (top) and opening angles of linearized spin–orbit motion (bottom) for particles with normalized vertical amplitude of 25πmm mrad in HERA–p.

the vertical motion leads to the dominant perturbations of spin dynamics, first the resonances of this degree of freedom will be considered.

A flat circular accelerator with a super–periodicity P_s has a betatron phase advance (including the integer part) of $\frac{1}{P_s}\hat{Q}_k$ and a spin phase advance of $\frac{1}{P_s}G\gamma$ for each super–period. A resonance occurs whenever the non–integer part $\frac{1}{P_s}\hat{Q}_k - [\frac{1}{P_s}\hat{Q}_k]$ has a resonance condition with $\frac{1}{P_s}G\gamma$: $\frac{1}{P_s}G\gamma = j_0 \pm (\frac{1}{P_s}\hat{Q}_k - [\frac{1}{P_s}\hat{Q}_k])$, or $G\gamma = P_s n \pm \hat{Q}_k$ for some integers j_0 and n. The number of resonances is therefore reduced by a factor P_s.

HERA–p has no exact super–periodicity and therefore all resonance $G\gamma = n \pm Q_k$ can occur. There is only a very approximate super–periodicity 4, since the 4 arcs are identical. It is reasonable to make HERA–p as close to super–periodic as possible. Inserting flattening snakes in the non–flat regions South, East, and North is a step in this direction, since this makes the regions more similar to the flat West section. This lattice with 6 flattening snakes will be referred to as the *6fs* snake scheme.

In this scheme, however, the spin rotation across the West quadrant is larger than the rotation across the other quadrants. The non–flat regions produce two

spin rotation angles Ψ_h as shown in figure 2.5. The two non–flat regions around the interaction points, taken together, do not produce any net spin rotation, since they are compensated by the flattening snakes as derived in section 2.2.4. While spins rotate by $\frac{\pi}{2}G\gamma$ across the West quadrant, they only rotate by $\frac{\pi}{2}G\gamma - 4\Psi_h$ across the other three quadrants. This violation of periodicity can be compensated by using two more flattening snakes in appropriate regions around the West interaction point. These two flattening snakes do not compensate a vertical bend, they simply reduce the spin rotation. This choice of 8 flattening snakes is referred to as snake scheme *8fs*.

In figure 3.6 (top), the resonance strength ϵ_{ν_0} for $\nu = j_0 \pm Q_y$ are drawn for the *6fs* scheme. The middle figure describes the resonance strength of HERA–p from 40 to 1000GeV/c for the *8fs* scheme. While the strongest resonances are somewhat smaller in the *6fs* scheme, there are more of these very strong resonances clustering together around critical energies, leading to more overlapping strong resonances.

In a completely four–fold symmetric model of HERA–p, where the south quadrant has been repeated 4 times, such a clustering of resonances does not appear, as shown in figure 3.6 (bottom). Each of the very strong resonances consists of only one line. So there is no interference of several very strong resonance effects. The red points show the sum of the resonances in the *6fs* scheme which are very close to the critical energy. This sum is smaller in the *8fs* scheme (blue points) since there is some remnant periodicity recovered by the addition of the two Siberian Snakes in the West.

The very strong resonances which appear in all three figures at about 34 critical energies are most destructive for the acceleration of polarized proton beams. It is therefore important to understand how these very strong resonances are produced. To obtain a clearer picture of the structure of these resonances, the resonance spectrum is separated into two spectra in figure 3.7. Both, those corresponding to a frequency $\kappa = \nu_0 = j_0 + Q_y$ (left) and those to $\kappa = \nu_0 = j_0 - Q_y$ (right) have a regular structure of equally spaced very strong and medium strength resonances. In both graphs, the distance between two such resonances is 58.01GeV/c. A bend of 60.42mrad produces one complete extra spin rotation for every 58.01GeV/c increase in momentum. Since the bend angle of one of the HERA–p FODO cells is 60.42mrad, this indicates that the strong resonances are due to the constructive interference of spin perturbations in every FODO cell. Such an interference is seen in every circular accelerator built from identical elementary cells [59].

The mechanism leading to these very strong resonances is most easily derived from the spin–orbit–coupling integral, $I_y^{\pm} \propto \int \sqrt{\beta_y} e^{i(-\Psi \pm \Phi_y)} k dl$. The arc in HERA–p is a regular structure of identical FODO cells of alternating focusing and defocusing quadrupoles QX and QY. In between these quadrupoles there are bends $\phi_B =$ 30.21mrad with weak quadrupole windings for adjusting the tunes. The relative spin phase advance over one FODO cell is $G\gamma\Delta_c$ with $\Delta_c = \frac{2\phi_B}{2\pi}$ and the relative orbit phase advance (phase/2π) in a HERA–p FODO cell is about $\Delta = \frac{1}{4}$. Whenever the phase advance $-G\gamma\Delta_c \pm \Delta$ in the spin–orbit–coupling integrals $I_y^{\pm}$ in a FODO cell is an integer, the perturbation of spin motion in each FODO cell directly adds to that of the previous one.

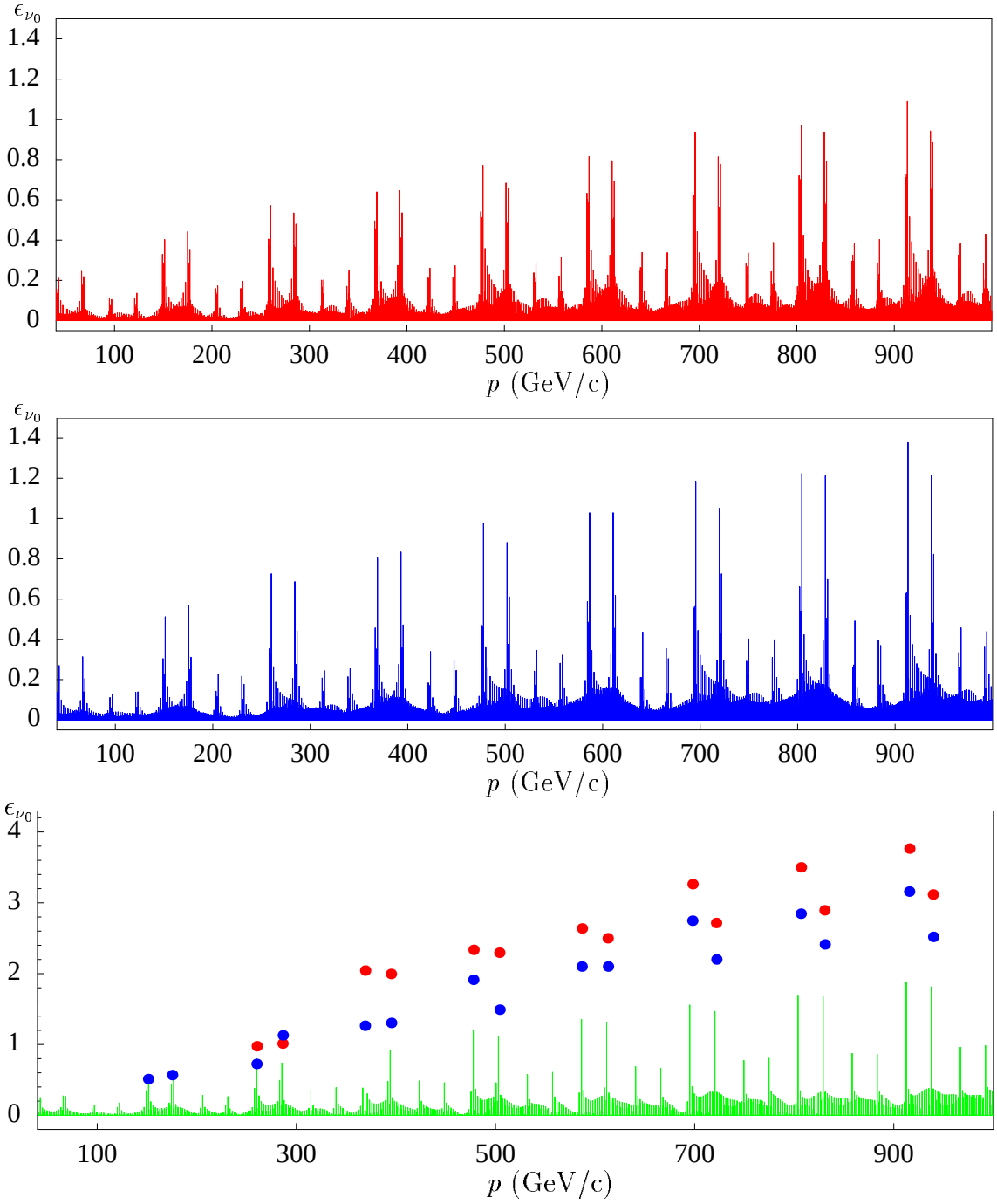

Figure 3.6: Top: The (red) line spectrum of resonances for HERA–p with 6 flattening snakes, one for each non–flat region. Middle: The (blue) line spectrum of resonances for HERA–p when symmetrized by 8 flattening snakes (*8fs* scheme). Bottom: A model of HERA–p with super–periodicity 4 has only well separated very strong resonances at critical energies, whereas for realistic models several overlapping strong resonances cluster at these energies. The points show the sum of the resonance strengths which are not well separated for two such models: This sum is larger (red) for the *6fs* scheme than for *8fs* (blue).

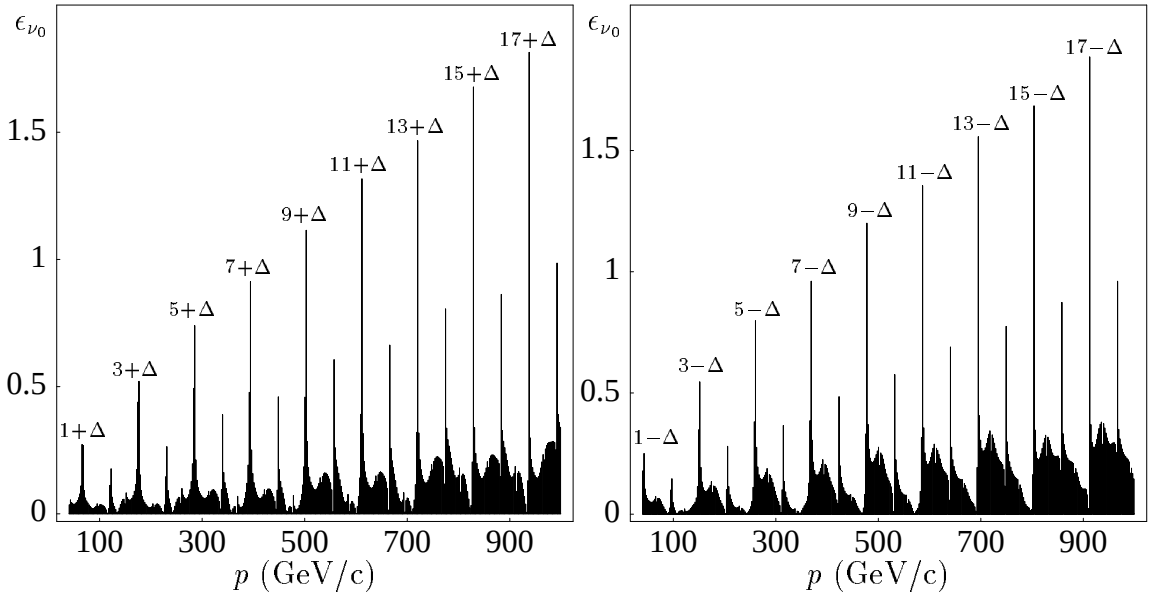

Figure 3.7: The resonance strength ϵ_{ν_0} for a HERA–p model with super–periodicity 4 for $\nu_0 = j_0 + Q_y$ (left) and for $\nu_0 = j_0 - Q_y$ (right). The numbers $N_{odd} + \Delta$ indicate the spin phase advance in one FODO cell which leads to a very strong resonance.

There are therefore strong resonances due to a large coupling integral I_y^+ around every energy with $\gamma = \frac{N+\Delta}{G\Delta_c}$ and due to a large coupling integral I_y^- around every energy with $\gamma = \frac{N-\Delta}{G\Delta_c}$. The FODO phase advance is not exactly $\frac{\pi}{2}$ for the current HERA–p lattice but a Δ of 0.243 produces exactly the position of the observed very strong and medium strength resonances.

This however does not explain why these resonances come in alternating pairs of stronger and weaker resonances. This effect is due to an alternation of constructive and destructive interference of spin perturbations in the focusing and the defocusing quadrupoles. Given a relative vertical phase advance of Δ_1 from QY to QX. The spin perturbation in the QY magnet is counteracted by that in the QX magnet when the phase advance $-\frac{1}{2}G\gamma\Delta_c \pm \Delta_1$ of the spin–orbit–coupling integral $I_y^\pm$ between these quadrupoles is an integer. This leads to a pair of weaker resonances. But at the other critical energies, where $-G\gamma\Delta_c \pm \Delta$ is approximately an odd integer, the spin perturbations of the QX and QY add to each other, leading to a pair of stronger resonances. When the FODO cell is symmetric, so that $\Delta = 2\Delta_1$, a cancelation occurs whenever $-G\gamma\Delta_c \pm \Delta = 2N$. However, the HERA–p FODO cell is not completely symmetric, due to a slight geometric asymmetry and due to two additional small quadrupoles of unequal strength for tune control. But the approximate symmetry is sufficient to cause the observed alternation between very strong and medium strength resonances. At each of the very strong resonances, the relative spin phase advance per FODO cell is therefore

$$-G\gamma\Delta_c = N_{odd} \pm \Delta \tag{3.34}$$

for odd integers N_{odd}. These values are indicated at each of the resonances associated

with I_y^+ (left) and I_y^- (right) in figure 3.7.

When operating HERA–p with polarized beams, one should choose an energy in between two medium strength resonances to limit the influence of the very strong resonances during the many hours of storage time. A good momentum in that respect would be 870GeV/c, where spins rotate 16 times in each FODO and the energy is just between the medium strength resonances at $G\gamma\Delta_c = 16 \pm \Delta$.

Resonances due to vertical motion can only occur at energies where $\nu_0 \pm Q_y$ is an integer. At these energies, the resonance condition for each FODO cell will in general not be satisfied exactly, but the resonances with $-G\gamma\Delta_c \pm \Delta \approx N_{odd}$ will be very strong. In the model with super–periodicity 4, the resonance strengths were shown as lines in figure 3.6 and only one resonance is very strong at each critical energy. Here the distance to the next resonance which is allowed by symmetry is 4 times larger than the distance in a ring without super–periodicity. This explains why several very strong and overlapping resonances cluster at critical energies in a realistic model of HERA–p.

As has been shown in figure 3.6, the number of these overlapping resonances can be reduced by adding two flattening snakes in the West. The advantage of symmetrizing HERA–p by these additional magnets is also apparent in the resonance effects which appear due to radial motion with the tune Q_x and due to longitudinal motion with the tune Q_τ .

Figure 3.8 displays a point for every resonance $\nu_0 = j_0 \pm Q_x$. The left figure for the *8fs* scheme shows a much clearer structure than the resonances for the *6fs* scheme. The average strength of the resonances are however similar.

The overall structure of these resonances can easily be explained. When the coordinate system $[\vec{m}_0, \vec{l}_0, \vec{n}_0]$ coincides with $[\vec{e}_x, \vec{e}_\theta, \vec{e}_y]$ just before the BV magnet, which bends the beam downwards by $\phi_{BV} = 5.74$mrad as shown in figure 2.5, then $\vec{m}_0 = \vec{e}_x$ and $\vec{l}_0 = \vec{e}_\theta \cos\Psi_v - \vec{e}_y \sin\Psi_v$ just behind the magnet, with $\Psi_v = G\gamma\phi_{BV}$. Subsequently these vectors rotate around the vertical in the horizontal bends of the non–flat region. These rotations leave $\vec{m}_0 \cdot \vec{e}_y = 0$ and $\vec{l}_0 \cdot \vec{e}_y = -\sin\Psi_v$ unchanged.

Particles which oscillate horizontally around the closed orbit experience a vertical spin precession vector $\vec{\omega}$ with $\vec{\omega}\cdot(\vec{m}_0 + i\vec{l}_0) = -i\omega_y \sin\Psi_v$. The horizontal spin–orbit–coupling integral over the non–flat regions is therefore $I_1^+ = -i\sin\Psi_v(\int_1 \omega_y(\vec{v}_1^+)d\theta - \int_2 \omega_y(\vec{v}_1^+)d\theta)$, where the first integral runs over the first half of the region, until the flattening snake rotates $\vec{l}_0$ and leads to a subtraction of the second integral. Using the eigenvector $\vec{v}_1^-(\theta)$ in this integral leads to I_1^- according to equation (3.29). Note that the spin phase advance Ψ_v is outside the integral here, and that therefore $I_1^- = (I_1^+)^*$ since $\vec{v}_1^- = (\vec{v}_1^+)^*$.

Note that the integral has a very simple energy dependence. The integrand ω_y is proportional to $\frac{G\gamma}{\sqrt{\gamma\frac{v}{c}}}$, where the numerator comes from the equivalent term in the BMT equation and the denominator reflects the adiabatic reduction of the emittance with energy. For high energies, one is therefore left with a contribution to the spin–orbit–coupling integrals which is proportional to $\sin(G\gamma\phi_{BV})\sqrt{\gamma}$. The absolute value of this function is plotted in figure 3.8 (red) and is exactly proportional to the curves of the resonance strength. This graph shows that all resonance strengths

ϵ_{ν_0} with $\nu_0 = j_0 \pm Q_x$ fall onto 4 curves which all have this variation with energy. This effect is due to 4 different ways in which the spin perturbations of the non–flat regions can add to each other as I now explain.

Let the contributions to the horizontal spin–orbit–coupling integrals I_1^+ over the South, East, and North be denoted by I_S^+, I_E^+, and I_N^+ . The resonance strength at $\nu_0 = j_0 + Q_x$ is then given by

$$\epsilon_{\nu_0} = \frac{\sqrt{J_x}}{2\pi}|I_1^+| \ , \quad I_1^+ = I_S^+ + e^{i\psi_{SE}} I_E^+ + e^{i(\psi_{SE}+\psi_{EN})} I_N^+ \tag{3.35}$$

with $\psi_{SE} = -\Psi_{SE} + \Phi_{xSE}$ and $\psi_{EN} = -\Psi_{EN} + \Phi_{xEN}$.

While the horizontal orbital phase advances Φ_{xSE} from the South to the East and Φ_{xEN} from the East to the North non–flat region do not depend on energy, the corresponding spin phase advances do have energy dependent values. In the non–symmetrized HERA–p ring with 6 flattening snakes (*6fs* scheme), the spin coupling integral is therefore the sum of the three contributions with quite arbitrary phase factors, leading to a spread of resonance strength in figure 3.8 (right).

When the *8fs* scheme is used to symmetrized HERA–p however, the phase factors are not arbitrary but the spin phase advances between the straight sections must be a quarter of the total spin phase advance, $\Psi_{SE} = \frac{\pi}{2}\nu_0 = \frac{\pi}{2}(j_0 + Q_x)$. With $\xi_1 = \Phi_{xSE} - \frac{\pi}{2}Q_x$ and $\xi_2 = \Phi_{xSE} + \Phi_{xEN} - \pi Q_x$, this leads to exactly 4 possible combinations of phases in equation (3.35) depending on the non–integer part of $\frac{j_0}{4}$:

	$j_0 = 4n$	$j_0 = 4n+1$	$j_0 = 4n+2$	$j_0 = 4n+3$
$e^{i\psi_{SE}}$	$e^{i\xi_1}$	$-ie^{i\xi_1}$	$-e^{i\xi_1}$	$ie^{i\xi_1}$
$e^{i(\psi_{SE}+\psi_{EN})}$	$e^{i\xi_2}$	$-e^{i\xi_2}$	$e^{i\xi_2}$	$-e^{i\xi_2}$

Correspondingly one finds 4 possibilities of phase factors for the integral I_1^- which are complex conjugated to the given factors. Therefore, the resonance strength for $\nu_0 = j_0 - Q_x$ are located on the same 4 curves as those for $\nu_0 = j_0 + Q_x$ in figure 3.8 (left) for the *8fs* scheme of HERA–p.

It becomes clear from figure 3.8 (top) that the spin motion is least disturbed by the synchrotron motion at magic energies where $\sin(G\gamma\phi_{BV}) = 0$. This is the case whenever $\vec{n}_0$ is vertical inside the non–flat region. In that respect, the most appropriate momentum would be 858GeV/c. Close to this momentum there is a medium strength resonance for vertical motion, but at the favored value of 870GeV/c, the factor $\sin(G\gamma\phi_{BV}) = 0.17$ is still small.

The resonances due to synchrotron motion at $\nu_0 = j_0 \pm Q_\tau$ shown in figure 3.8 (bottom) have high peaks around the energies where a pair of very strong resonances due to vertical motion is located. Therefore the number of spin rotations N within the bends of a FODO cell are some odd integer in the region of these high peaks. Additionally there are regions with medium strength resonances in each second gap between the strongly resonant regions. In these regions the number N is even, but not divisible by 4. In the rest of the gaps, where the number N of spin rotations within the bends of a FODO cell is divisible by 4, the very small resonance strengths ϵ_{ν_0} for $\nu_0 = j_0 \pm Q_\tau$ indicate that there are only very weak or no perturbations of spin motion due to longitudinal particle motion.

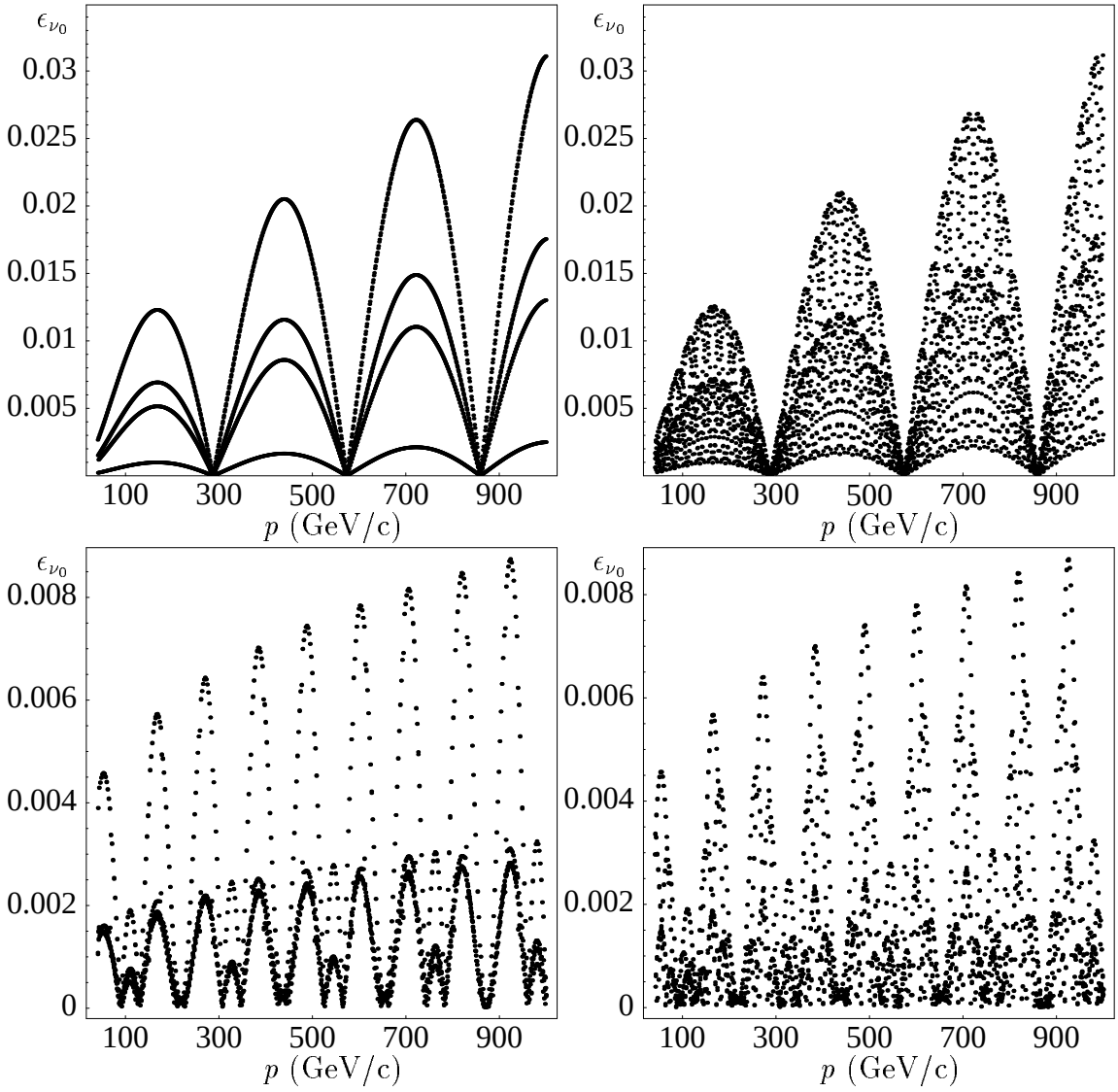

Figure 3.8: Top: The resonance strengths at $\nu_0 = j_0 \pm Q_x$ in HERA–p with the *8fs* scheme (left) and the *6fs* scheme (right). Bottom: The resonance strength at $\nu_0 = j_0 \pm Q_\tau$ in HERA–p with the two schemes *8fs* (left) and *6fs* (right).

Also this structure of the resonance spectrum can be explained by an investigation of the spin–orbit–coupling integrals. They describe the spin perturbation during one turn for a particle which has the initial spin $\vec{n}_0$ and an amplitude in longitudinal phase space. Here we choose the angle variable in longitudinal phase space to describe a particle with energy deviation δ. Since HERA–p has no vertical dispersion except in the non–flat regions, the particle travels in the horizontal plane through vertical magnetic fields and the spin is not deflected away from the vertical $\vec{n}_0$. Except in the non–flat region where $\vec{n}_0$ is not vertical and where the horizontal dispersion leads the particle through vertical fields in the quadrupoles which deflect the spin away from $\vec{n}_0$. However, the spin perturbations due to horizontal disper-

sion in the two non–flat regions, one right and one left of an interaction point, have opposite sign and cancel each other. This can be seen as follows: At the interaction point $\vec{n}_0 = \vec{e}_y$ is vertical, just before the BV magnet upstream of the interaction point $\vec{e}_y \cos\Psi_v + \vec{e}_\theta \sin\Psi_v$, and just after the BV magnet downstream the interaction point $\vec{n}_0 = \vec{e}_y \cos\Psi_v - \vec{e}_\theta \sin\Psi_v$. The horizontal component of $\vec{n}_0$ in the non–flat region to the right and to the left of the interaction point is therefore antisymmetric. Since the horizontal dispersion and the quadrupole strengths in these regions are both symmetric with respect to the interaction point, the deflections of a spin away from $\vec{n}_0$ in the two non–flat regions compensate each other. Spin perturbations for particles with energy deviation are therefore solely due to the vertical dispersion in the non–flat regions.

The structure of the vertical dispersion in a non–flat region is shown in figure 3.9 and will now be used to illustrate what gives rise to regions with very weak resonances in figure 3.8 (bottom). For that it is important to note that there are 4 horizontal bending magnets in each non–flat region which have been called BH in section 2.2.4, as has been shown in figure 2.5 (left). Each of these BH magnets bends by 15.11mrad, one quarter of the bending angle in a FODO cell. At energies where the number N of spin rotations within the bends of a FODO cell is divisible by 4, each BH leads to an integer number of rotations and therefore has no net effect on spin motion, so that the spin is only influenced by the quadrupoles. While a particle with energy deviation follows the dispersive trajectory with its vertical slope D'_y, the spin direction is then tilted by $(G\gamma+1)D'_y$ away from $\vec{n}_0$. Since D'_y is matched to zero at the end of the non–flat region as shown in figure 3.9, the total tilt after this region is zero and $\epsilon_{\nu_0} = 0$ at these special energies.

As with the resonance strength due to horizontal motion, also the resonance strength due to longitudinal motion have a clearer structure when the $8fs$ scheme of 8 flattening snakes is used, as shown in figure 3.8 (bottom–left). Similar to equation (3.35), the resonance strength for $\nu_0 = j_0 \pm Q_\tau$ is given by

$$\epsilon_{\nu_0} = \frac{\sqrt{J_\tau}}{2\pi} |I_3^+| \ , \quad I_3^+ = I_S^+ + e^{i\psi_{SE}} I_E^+ + e^{i(\psi_{SE}+\psi_{EN})} I_N^+ \tag{3.36}$$

with $\psi_{SE} = -\Psi_{SE} + \Phi_{\tau SE}$ and $\psi_{EN} = -\Psi_{EN} + \Phi_{\tau EN}$. Due to the low synchrotron tune of approximately $7 \cdot 10^{-3}$, the phase advances Φ_τ are nearly zero and $\nu_0 \approx j_0$. Depending on the non–integer part of $\frac{j_0}{4}$, the phase factors $e^{\psi_{SE}} \approx e^{\psi_{EN}}$ are $\pm i$ or ± 1 . Since the spin–orbit–coupling integrals I_S, I_E, and I_N have nearly the same magnitude, the total spin–orbit–coupling integral $I_3^\pm$ is close to either I_S of $3I_S$, and these two curves are seen in figure 3.8 (bottom–left).

The shape of these curves can be obtained by computing the dreibein $[\vec{m}_0, \vec{l}_0, \vec{n}_0]$ for the non–flat region to the right an to the left of an interaction point by rotating it in the vertical bends by Ψ_v and in the horizontal bends by Ψ_h . When the change of D'_y produced by the four regions with quadrupoles is denoted by $\Delta D'_j$, then the spin–orbit–coupling integral is found to be proportional to $\frac{G\gamma+1}{\gamma^{3/4}}[\Delta D'_1 + (\Delta D'_2 + \Delta D'_3)\cos\Psi_h + \Delta D'_3 \cos(2\Psi_h)]$, where the denominator takes account of the fact that the energy deviation δ decreases with $\gamma^{-3/4}$ during the acceleration process.

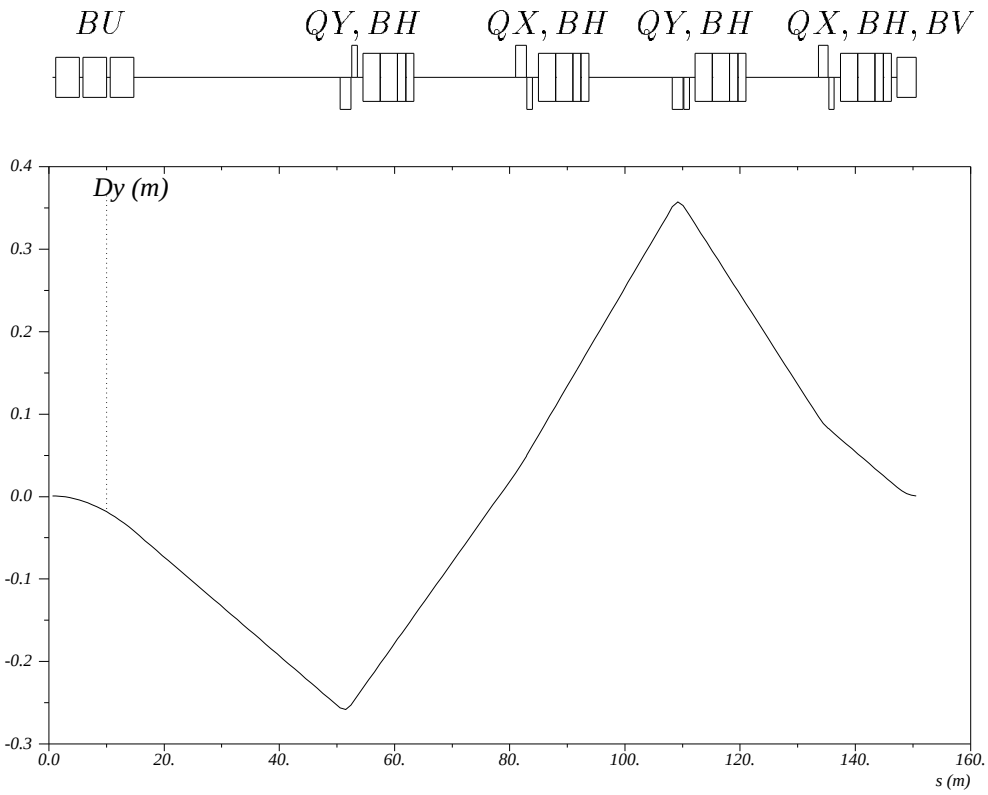

Figure 3.9: Vertical dipole magnets BV, BU, horizontal dipole magnets BH, and vertically focusing and defocusing quadrupole magnets QY and QX in the non–flat regions of HERA–p. The vertical dispersion and its slope at the end of this region is matched to zero.

One feature should be noted here: The influence of synchrotron motion on spin dynamics is zero in first–order approximation at a magic momentum of 870GeV/c, where the spins make complete turns around the vertical in the horizontal magnets of the non–flat region, which are called BH in this report. It is not just a lucky coincidence that the preferred momentum for small vertical perturbations and the preferred momentum for small longitudinal perturbations are equivalent. As described above, the perturbation of spin motion due to vertical particle oscillations is small when spins rotate 16 times around the vertical in a FODO cell at 870GeV/c. Then at this energy, spins precess 4 times in a BH magnet so that the spin perturbations for particles with an energy deviation are canceled within each non–flat region.

Considering all resonance strengths, it seems best to operate HERA–p around 870GeV/c. In addition to avoiding the influence of very strong resonances while storing polarized beams, this choice of a somewhat reduced momentum avoids the need of accelerating through the region of 913GeV/c, where a very strong resonance due to vertical motion is excited. In any case, keeping the current momentum of 920GeV/c is not advisable at all, since this energy is just between two very strong resonances.

3.3 Optimal Choices of Siberian Snakes

It has been pointed out several times that Siberian Snakes are indispensable if polarized proton beams are to be accelerated in a high energy synchrotron such as HERA–p. There were several reasons for this statement:

1. Siberian Snakes fix the closed–orbit spin tune to $\frac{1}{2}$ during the acceleration cycle so that no first–order resonances have to be crossed. Crossing first–order resonances can lead to a severe reduction of polarization by an amount described by the Froissart–Stora formula in section 2.2.11.

2. Siberian Snakes severely reduce the influence of energy variations on spin dynamics within a synchrotron period as has been illustrated in figure 2.16.

3. Siberian Snakes reduce the variation of $\vec{n}(\vec{z})$ for particles which oscillate vertically and therefore pass through horizontal fields which perturb the polarization. An example of this reduction and the associated increase in P_{lim} was shown in figure 2.15.

4. When $\vec{n}$ changes rapidly during acceleration, the adiabatic invariance of $J_S = \vec{n}(\vec{z}) \cdot \vec{S}$ might be violated and polarization would be reduced. It is therefore important that Siberian Snakes smoothen the rapid changes of $\vec{n}$ during the acceleration cycle as shown in figure 2.15.

5. Siberian Snakes can also compensate perturbing effects of misaligned optical elements [69, 110, 59] but this report will not cover the effect of misalignments.

There will be little reduction of polarization during the acceleration process and all particles will be polarized in nearly the same direction at high energy if the accelerator has an invariant spin field $\vec{n}(\vec{z})$ which changes slowly during the acceleration process and which is nearly parallel for all relevant phase space points. Achieving this is one of the non–trivial tasks of Siberian Snakes. However, there is so far no reliable formula for determining the number of Siberian Snakes required for an accelerator [116, 117]. To make things worse, for any given number of Siberian Snakes there are very many different possible combinations of the snake angles which lead to an energy independent closed–orbit spin tune of $\frac{1}{2}$ and to a vertical $\vec{n}_0$ in the accelerator's arcs. And so far there is also no reliable formula for determining which of these snake schemes leads to the highest polarization.

There used to be a popular opinion that, owing to their symmetry, 5 standard choices of the snake angles for 4 Siberian Snakes are advantageous for HERA–p. These choices are not optimal, as will be shown. For reasons why these standard schemes were considered useful see for example [107]. RHIC with its two snakes, will be operated with a similar standard scheme [118]. The energy dependence of P_{lim} in HERA–p produced by these 5 snake schemes is shown in figure 3.10. They seem to produce rather similar but very low maximum time average polarization P_{lim} in the critical energy regions where very strong resonances are excited. The observation of such rather small differences in the $\vec{n}$–axis lead to the investigation of the influence

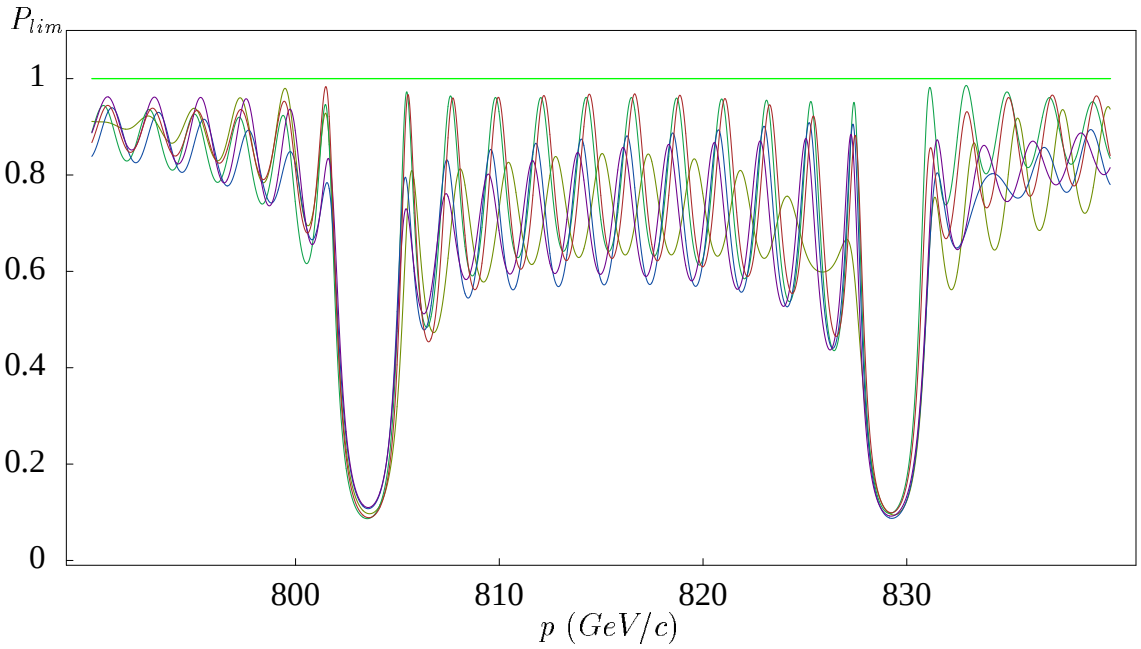

Figure 3.10: P_{lim} of linearized spin–orbit motion for 5 standard choices of 4 Siberian Snakes in HERA–p. A flattening snake was inserted in each non–flat region of the luminosity upgrade lattice. The right column shows an obvious notation to describe the snake angles in a snake scheme:

Scheme	South	East	North	West
$(0\frac{\pi}{2}00)$	$0°$	$90°$	$0°$	$0°$
$(\frac{\pi}{4}0\frac{\pi}{4}0)$	$45°$	$0°$	$45°$	$0°$
$(\frac{3\pi}{4}0\frac{3\pi}{4}0)$	$-45°$	$0°$	$-45°$	$0°$
$(\frac{5\pi}{8}\frac{\pi}{8}\frac{5\pi}{8}\frac{\pi}{8})$	$-22.5°$	$22.5°$	$-22.5°$	$22.5°$
$(\frac{\pi}{8}\frac{5\pi}{8}\frac{\pi}{8}\frac{5\pi}{8})$	$22.5°$	$-22.5°$	$22.5°$	$-22.5°$

of snake schemes on P_{lim}. Figure 3.11 (left) shows P_{lim} as computed for linearized spin–orbit motion by equation (3.27) for 4 other choices of schemes with 4 Siberian Snakes which were chosen to demonstrate that very different values of P_{lim} can be obtained depending on the snake scheme. In the following, I will try to improve P_{lim} by investigating methods of determining the optimal snake arrangement for an accelerator. Initially the approximation of linearized spin–orbit motion will be used and then higher–order effects with various snake schemes will be analyzed.

It turned out that large increases in P_{lim} can result from the choice of a suitable snake scheme. This is shown in figure 3.11 (right) where P_{lim} curves for the vertical motion with two different Siberian Snake arrangements in HERA–p are superimposed. For this figure, the betatron phase advances in the vertical optics had been specially tuned in a way to be described in section 3.3.2. For this special optics, the snake scheme $(0\frac{\pi}{2}\frac{\pi}{2}\frac{\pi}{2})8fs$ leads to an especially favorable maximum time average polarization even at critical energies as shown by the blue curve. Another snake scheme which is not suitable will produce a reduction of P_{lim} at all critical energies during the ramp, as shown by the red curve. This example, given here mostly for

motivational purposes, is somewhat extreme since the vertical optics was custom designed for the $(0\frac{\pi}{2}\frac{\pi}{2}\frac{\pi}{2})8fs$ snake scheme, but nevertheless it demonstrates how great the differences of P_{lim} for snake schemes can be.

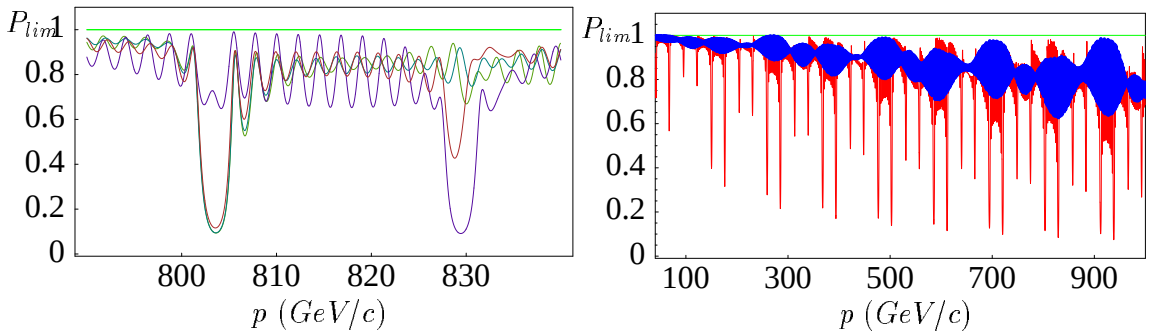

Figure 3.11: Left: P_{lim} for 4 different snake schemes which lead to an extremely different maximum time average polarization for the standard HERA–p lattice. Right: P_{lim} for the standard scheme $(\frac{\pi}{4}0\frac{\pi}{4}0)6fs$ (red) and for the $(0\frac{\pi}{2}\frac{\pi}{2}\frac{\pi}{2})8fs$ scheme (blue) after the vertical optics in HERA–p has been changed so that the contribution of the arcs to the spin–orbit–coupling integrals cancel when the latter scheme is used.

Comparing these figures with the resonance strengths of HERA–p shown in figure 3.6, the residual resonance structure after the installation of Siberian Snakes, which was already mentioned in section 2.2.14, can clearly be seen. Special snake schemes, however, are able to eliminate the influence even of the strongest resonances when only linearized spin–orbit motion is considered. In the following the reason for these large differences between different snake schemes will be analyzed and optimal snake schemes for HERA–p will be investigated.

3.3.1 Spin–Orbit–Coupling Integrals with Siberian Snakes

For the introduction of spin–orbit–coupling integrals in flat rings in section 3.1.2, $\vec{n}_0$ was initially assumed to point vertically upwards, and the coordinate system $[\vec{e}_x, \vec{e}_\theta, \vec{e}_y]$ was used. Now Siberian Snakes will be considered, which rotate all spins (and also $\vec{n}_0$) by π around some axis in the horizontal plane. Then it is convenient to use the coordinate system $[\vec{e}_x, \vec{n}_0 \times \vec{e}_x, \vec{n}_0]$. The second vector $\vec{e}_2$ corresponds to $\vec{e}_\theta$ when $\vec{n}_0$ is vertical upwards and to $-\vec{e}_\theta$ after a Siberian Snake has rotated $\vec{n}_0$ downwards. In this new coordinate system, I again use the complex notation $\hat{s} = s_1 + is_2$. When a particle with spin parallel to $\vec{n}_0$ travels along the trajectory $y = \sqrt{2J_y\beta_y}\cos\Phi_y$ through a quadrupole of focusing strength k with a vertical beta function β_y and betatron phase Φ_y, then its spin direction is deflected from $\vec{n}_0$ by the angle $(G\gamma + 1)\int_{\text{Quad}} ykdl$, leaving a change $\Delta\hat{s}$ in the spin coordinates of

$$\Delta\hat{s} = -i(G\gamma + 1)\int_{\text{Quad}} \sqrt{2J_y\beta_y}\cos\Phi_y k dl \tag{3.37}$$

where positive values of k describe vertically defocusing quadrupoles. When $\vec{n}_0$ points vertically upwards and a spin is initially parallel to $\vec{n}_0$, then a vertically

defocusing quadrupole rotates the spin in the direction of $-\vec{e}_\theta = -\vec{e}_2$. When $\vec{n}_0$ points vertically downwards, the spin rotates in the direction of $\vec{e}_\theta = -\vec{e}_2$ leaving equation (3.37) correct for both cases.

After the spin component $\hat{s}$ has been created by the deflection of a spin which was parallel to $\vec{n}_0$ when the particle entered a quadrupole, it subsequently rotates by $\Psi(\theta) = \int_{\theta_0}^{\theta} \Omega_{0y}(\tilde{\theta}) d\tilde{\theta}$. This describes spin precession around the vertically upward direction, independently of the fact that $\vec{n}_0$ might be pointing downwards. When $\vec{n}_0$ is pointing upwards, the disturbed spin rotates to $\hat{s}e^{i\Psi}$, whereas it subsequently rotates to $\hat{s}e^{-i\Psi}$ when $\vec{n}_0$ is pointing downwards.

The change of the spin away from $\vec{n}_0$ accumulated after a section of the ring from θ_0 to θ_1 in which there is no Siberian Snake is given by

$$\hat{s} = Ce^{i\Psi(\theta_1)} \int_{\theta_0}^{\theta_1} k2\sqrt{J_y\beta_y} \cos\Phi_y e^{-i\Psi(\theta)} d\theta \tag{3.38}$$

with $C = -i(G\gamma + 1)\frac{1}{\sqrt{2}}\frac{L}{2\pi}$, when $\vec{n}_0$ points upwards. When $\vec{n}_0$ points downwards, it is given by

$$\hat{s} = Ce^{-i\Psi(\theta_1)} \int_{\theta_0}^{\theta_1} k2\sqrt{J_y\beta_y} \cos\Phi_y e^{i\Psi(\theta)} d\theta \ . \tag{3.39}$$

To compute the spin change that accumulates over the whole ring, $\vec{n}_0$ is initially taken to be upwards.

In section 3.1.2, the spin–orbit–coupling integrals of the complete ring were defined. Here spin–orbit–coupling integrals of a subsection of the ring which does not contain a Siberian Snake is defined accordingly as

$$I_y^{\pm} = C \int_{\theta_0}^{\theta_1} k\sqrt{\beta_y} e^{i(-\Psi \pm \Phi_y)} d\theta \ , \tag{3.40}$$

where the initial phases are chosen to be $\Psi(\theta_0) = 0$ and $\Phi_y(\theta_0) = 0$.

It is now assumed that there are n Siberian Snakes in the ring and that n is even, to make $\vec{n}_0$ vertical in the arcs of the ring. The azimuth at the position of these snakes are denoted by θ_j and the spin phase advance around the vertically upward direction between snake j and $j+1$ is denoted by Ψ_j. The spin phase advance after the jth Siberian Snake is $\Psi_j(\theta)$ with $\Psi_j(\theta_j) = 0$. The deviation of the spin accumulated between just after the jth snake to just before the $(j+1)$st snake is denoted by $\hat{s}_j$.

For simplicity $\theta_0 = 0$, $\theta_{n+1} = 2\pi$ is used, and denote is the spin phase advance from azimuth θ_0 to the first Siberian Snake by Ψ_0 . Since the vector $\vec{n}_0$ initially points vertically upwards, one obtains

$$\hat{s}_0 = Ce^{i\Psi_0} \int_{\theta_0}^{\theta_1} k\sqrt{\beta_y} \cos\Phi_y e^{-i\Psi_0(\theta)} d\theta \ . \tag{3.41}$$

By considering the direction of $\vec{n}_0$ after the jth snake, one obtains

$$\hat{s}_j = Ce^{i(-)^j\Psi_j} \int_{\theta_j}^{\theta_{j+1}} k\sqrt{\beta_y} \cos\Phi_y e^{-i(-)^j\Psi_j(\theta)} d\theta \ . \tag{3.42}$$

Subsequently, a Siberian Snake with a snake axis which is in the horizontal plane will be referred to as horizontal Siberian Snake. And for historical reasons a snake which rotates spins around the vertical by some rotation angle will be referred to as type III snake. A horizontal Siberian Snake with a snake angle φ, is equivalent to a radial Siberian Snake followed by a type III snake with rotation angle $\alpha = 2\varphi$ since

$$-i(\sigma_1 \cos\varphi + \sigma_2 \sin\varphi) = (\cos\varphi - i\sigma_3 \cos\varphi)(-i\sigma_1) = e^{-i\frac{\alpha}{2}\sigma_3}(-i\sigma_1) \ . \qquad (3.43)$$

The radial Siberian Snake does not change $\hat{s}$, since it changes the axis $\vec{e}_2 = \vec{n}_0 \times \vec{e}_x$ along with the longitudinal component of the spin. The subsequent rotation around the vertical takes the spin from $\hat{s}$ to $\hat{s}e^{-i\alpha}$ for downward $\vec{n}_0$ after the snake and to $\hat{s}e^{i\alpha}$ for upward $\vec{n}_0$ after the snake.

The angle of the jth Siberian Snake is $\varphi_j = \frac{\alpha_j}{2}$ and the horizontal spin component accumulating over a complete turn from 0 to 2π is

$$\begin{aligned}
\hat{s} &= \hat{s}_n + \hat{s}_{n-1}e^{i(\alpha_n+\Psi_n)} + \hat{s}_{n-2}e^{i(-\alpha_{n-1}-\Psi_{n-1}+\alpha_n+\Psi_n)} \\
&+ \ \ldots + \hat{s}_1 e^{i(\alpha_2+\Psi_2-\alpha_3-\Psi_3\pm\ldots)} + \hat{s}_0 e^{i(-\alpha_1-\Psi_1+\alpha_2+\Psi_2-\alpha_3-\Psi_3\pm\ldots)} \\
&= \sum_{j=0}^{n} \hat{s}_j e^{i\sum_{k=j+1}^{n}(-)^k(\alpha_k+\Psi_k)} \\
&= C\sum_{j=0}^{n} e^{i(-)^j\Psi_j} \int_{\theta_j}^{\theta_{j+1}} k\sqrt{\beta_y}\cos\Phi_y e^{-i(-)^j\Psi_j(\theta)} d\theta e^{i\sum_{k=j+1}^{n}(-)^k(\alpha_k+\Psi_k)}
\end{aligned}$$

with $\sum_{k=n+1}^{n} \ldots = 0$.

As shown in section 2.2.3, the spin phase advances between snakes must satisfy $\sum_{k=0}^{n}(-)^k\Psi_k = 0$ to make the closed–orbit spin tune independent of energy and the snake angles must satisfy $\sum_{k=1}^{n}(-)^k\varphi_k = \frac{\pi}{2}$ to make the closed–orbit spin tune ν_0 equal to $\frac{1}{2}$.

For simplicity $\alpha_0 = 0$ is used, although there is no Siberian Snake at θ_0. This leads to

$$\begin{aligned}
\hat{s} &= C\sum_{j=0}^{n} e^{i(\pi-\sum_{k=0}^{j}(-)^k(\alpha_k+\Psi_k))} e^{i(-)^j\Psi_j} \int_{\theta_j}^{\theta_{j+1}} k\sqrt{\beta_y}\cos\Phi_y e^{-i(-)^j\Psi_j(\theta)} d\theta \\
&= -C\sum_{j=0}^{n} e^{-i\sum_{k=0}^{j-1}(-)^k(\alpha_k+\Psi_k)} \int_{\theta_j}^{\theta_{j+1}} k\sqrt{\beta_y}\cos\Phi_y e^{-i(-)^j(\Psi_j(\theta)+\alpha_j)} d\theta \ . \qquad (3.44)
\end{aligned}$$

The spin–orbit–coupling integrals for a ring with horizontal Siberian Snakes are therefore defined as

$$I_y^{\pm} = -C\sum_{j=0}^{n} e^{-i\sum_{k=0}^{j-1}(-)^k(\alpha_k+\Psi_k)} \int_{\theta_j}^{\theta_{j+1}} k\sqrt{\beta_y} e^{i[-(-)^j(\Psi_j(\theta)+\alpha_j)\pm\Phi_y]} dl \ . \qquad (3.45)$$

In terms of the orbital phase advance Φ_{yj} between snake j and $j+1$, one obtains

$$I_y^{\pm} = -C\sum_{j=0}^{n} e^{i\sum_{k=0}^{j-1}[-(-)^k(\alpha_k+\Psi_k)\pm\Phi_{yk}]} \int_{\theta_j}^{\theta_{j+1}} k\sqrt{\beta_y} e^{i[-(-)^j(\Psi_j(\theta)+\alpha_j)\pm\Phi_{yj}(\theta)]} d\theta \ . \qquad (3.46)$$

A corresponding formula has been used in [78] to introduce so–called strong spin matching, where Siberian Snakes are used to produce a cancelation of spin perturbations in different FODO cells. It is expected that the spin motion on vertical betatron orbits is relatively stable when a spin which is initially parallel to $\vec{n}_0$ comes back to that direction after one turn, this means $\hat{s}(2\pi) = 0$. This is achieved in linear approximation for all trajectories when both spin–orbit–coupling integrals vanish. The ring is then said to be spin matched or spin transparent.

3.3.2 Snake Matching in Rings with Super–Periodicity

The spin perturbations in different parts of the ring can compensate each other when these parts have similar spin–orbit–coupling integrals. In the following, the process of finding a snake scheme for which such a compensation occurs will be referred to as *snake matching*. It will be demonstrated how Siberian Snakes can be used to adjust the spin phase advances in such a way that spin–orbit–coupling integrals of symmetric parts of a ring cancel each other. After demonstrating the idea for type III snakes, which simply rotate spins around the vertical by some fixed angle with little influence on the orbit motion, I will demonstrate two quite general results:

1. A ring with super–periodicity 4 can be completely snake matched using 8 Siberian Snakes, i.e. a snake scheme can be found for which the spin–orbit–coupling integrals are zero due to a complete cancelation of spin perturbations in different parts of the ring. There are exactly two such possibilities which lead to energy independent snake angles.

2. Such a ring can also be snake matched using 4 Siberian Snakes. Then, however, the snake axes must depend on energy and have to be changed during the acceleration process. Such Siberian Snakes with variable snake axes can be constructed [119].

Snake Matching with Type III Snakes for Super–Periodicity 4

For a flat ring without horizontal Siberian Snakes the spin–orbit coupling integral for vertical motion was defined as

$$I^{\pm} = \int_0^L k\sqrt{\beta_y} e^{i(-\Psi \pm \Phi_y)} dl \ . \tag{3.47}$$

For ease of notation the constant C in equation (3.40) is now dropped and the arc–length $l = L\frac{\theta}{2\pi}$ is used rather than the azimuth θ, where L is the length of the ring. Furthermore, the index y on the spin–orbit–coupling integral and on the vertical tune will no longer be indicated, to simplify the following equations. In any case, the methods for canceling spin–orbit–coupling integrals by a special choice of snake angles which will now be derived can also be used for transverse and longitudinal motion. For a ring with super–periodicity 4, $I^{\pm}$ can be computed from

$$I^{\pm}_{\frac{1}{4}} = \int_0^{L/4} k\sqrt{\beta_y} e^{i(-\Psi \pm \Phi_y)} dl \ , \tag{3.48}$$

$$I^{\pm} \;=\; I^{\pm}_{\frac{1}{4}}[1 + e^{i(-\nu_0 \pm Q)/4} + e^{i2(-\nu_0 \pm Q)/4} + e^{i3(-\nu_0 \pm Q)/4}] \qquad (3.49)$$

where $\nu_0 = \Psi(2\pi)$ is the spin rotation angle during one turn and Q is the orbital phase advance during one turn. These are 2π times the closed–orbit spin tune and 2π times the vertical orbit tune, used in this section to simplify formulas. Spin transparency requires that I^+ as well as I^- vanish. Thus the bracket in equation (3.49) must vanish. This is only possible when $e^{i(-\nu_0 \pm Q)/4}$ is either -1 or i. Choosing the first possibility to eliminate I^+ and the second to eliminate I^-, one obtains

$$e^{i(-\nu_0 + Q)/4} = -1 \;, \quad e^{i(-\nu_0 - Q)/4} = i \;. \qquad (3.50)$$

This leads to $e^{iQ/2} = i$ and cannot be satisfied in a realistic ring. Therefore, a four–fold repetitive symmetry cannot lead to spin transparency at any energy.

The reason for this is that, except at very special orbital tunes, there is no energy where the spin disturbance of one quadrant of the ring cancels the spin disturbance of another quadrant in I^+ as well as in I^-. However, either one of these integrals of one quadrant can cancel against that of another quadrant whenever the spin phase advance between these quadrants is appropriate.

The situation changes if type III snakes are installed. It was first found in [21] that type III snakes can improve the spin dynamics in HERA–p by increasing $P_{lim} = | < \vec{n} > |$. They can be used to manipulate the spin phase advance to make the spin–orbit–coupling integrals of different parts of the ring cancel. To demonstrate this, 4 type III snakes are installed regularly spaced around the ring.

There are three possibilities for canceling the spin disturbances between quadrants of the ring. The quadrants whose destructive effects cancel are connected by arrows in figure 3.12.

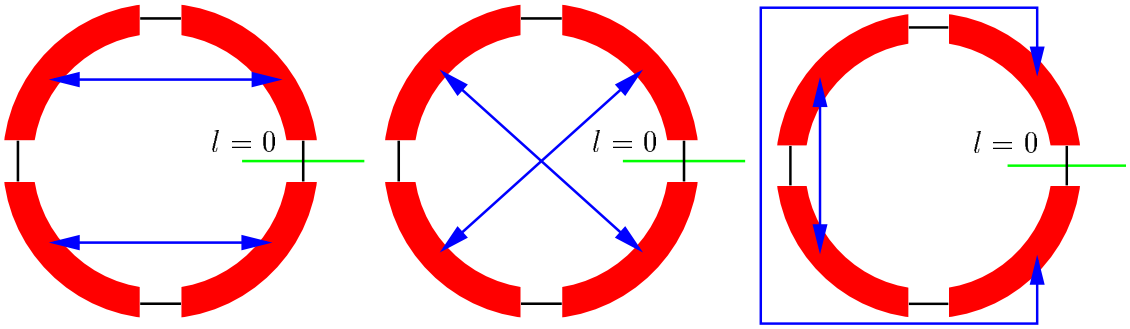

Figure 3.12: The three possibilities for canceling the depolarizing effects of quadrants of a ring with super–periodicity 4. The arrows indicate which quadrants cancel.

When the type III snake at $l = j\frac{L}{4}$ has the rotation angle ψ_j, then the spin–orbit–coupling integrals are

$$I^{\pm} = I^{\pm}_{\frac{1}{4}}(1 + e^{i(-\nu_0 \pm Q)/4 - \psi_1} + e^{i2(-\nu_0 \pm Q)/4 - \psi_1 - \psi_2} + e^{i3(-\nu_0 \pm Q)/4 - \psi_1 - \psi_2 - \psi_3}) \;. \qquad (3.51)$$

To snake match the ring, I^+ as well as I^- must vanish. Therefore the bracket on the right hand side has to vanish in both cases. A sum of 4 complex numbers with

unit modulus can only vanish when it consist of two pairs of numbers which cancel each other. This is shown in figure 3.13.

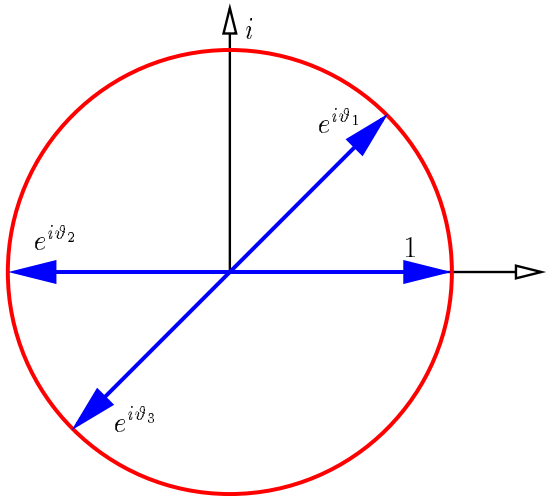

Figure 3.13: Four complex numbers with modulus one can only add up to zero when they consist of two pairs which individually add up to zero.

The three possibilities of cancelation demonstrated in figure 3.12 are given by the following three sets of equations:

1. $(-\nu_0 \pm Q)/4 - \psi_1 \stackrel{\circ}{=} \pi$ and $(-\nu_0 \pm Q)/4 - \psi_3 \stackrel{\circ}{=} \pi$,

2. $2(-\nu_0 \pm Q)/4 - \psi_1 - \psi_2 \stackrel{\circ}{=} \pi$ and $\psi_3 \stackrel{\circ}{=} \psi_1$,

3. $3(-\nu_0 \pm Q)/4 - \psi_1 - \psi_2 - \psi_3 \stackrel{\circ}{=} \pi$ and $(-\nu_0 \pm Q)/4 - \psi_2 \stackrel{\circ}{=} \pi$.

The symbol $\stackrel{\circ}{=}$ indicates equivalence modulo 2π. To snake match, one of these three conditions has to hold for $(-\nu_0 + Q)$, which causes I^+ to vanish and another of the conditions has to hold for $(-\nu_0 - Q)$, which causes I^- to vanish. I^+ and I^- cannot vanish due to the same condition if restrictions on the allowed orbital phase advance Q are to be avoided. There are therefore three possibilities:

1. $I^+ = 0$ due to condition 2 and $I^- = 0$ due to condition 3 requires

$$\psi_2 \stackrel{\circ}{=} \pi + 2(-\nu_0 + Q)/4 - \psi_1 \ , \quad \psi_3 \stackrel{\circ}{=} \psi_1 \ , \tag{3.52}$$

$$\psi_2 \stackrel{\circ}{=} \pi + (-\nu_0 - Q)/4 \ , \quad \psi_3 \stackrel{\circ}{=} 2(-\nu_0 - Q)/4 - \psi_1 \ . \tag{3.53}$$

The first and the third of these equations requires that $\psi_1 \stackrel{\circ}{=} (-\nu_0 + 3Q)/4$ whereas the second and the fourth equation requires that $\psi_1 \stackrel{\circ}{=} (-\nu_0 - Q)/4$. These two requirements are in general not compatible and the ring cannot be made spin transparent in this way.

2. $I^+ = 0$ due to condition 1 and $I^- = 0$ due to condition 3 requires

$$\psi_1 \stackrel{\circ}{=} \pi + (-\nu_0 + Q)/4 \ , \quad \psi_3 \stackrel{\circ}{=} \psi_1 \ , \tag{3.54}$$
$$\psi_2 \stackrel{\circ}{=} \pi + (-\nu_0 - Q)/4 \ , \quad \psi_3 \stackrel{\circ}{=} 2(-\nu_0 - Q)/4 - \psi_1 \ . \tag{3.55}$$

The first and the last of these equations together require $\psi_3 \stackrel{\circ}{=} \pi - (3Q - \nu_0)/4$. This is in conflict with the second equation. Thus this way also cannot lead to a spin transparent ring.

3. $I^+ = 0$ due to condition 1 and $I^- = 0$ due to condition 2 requires

$$\psi_1 \stackrel{\circ}{=} \pi + (-\nu_0 + Q)/4 \ , \quad \psi_3 \stackrel{\circ}{=} \psi_1 \ , \tag{3.56}$$
$$\psi_2 \stackrel{\circ}{=} \pi + 2(-\nu_0 - Q)/4 - \psi_1 \ , \quad \psi_3 \stackrel{\circ}{=} \psi_1 \ . \tag{3.57}$$

These 4 equations are compatible and lead to $\psi_1 \stackrel{\circ}{=} \psi_3 \stackrel{\circ}{=} \pi + (-\nu_0 + Q)/4$ and $\psi_2 \stackrel{\circ}{=} (-\nu_0 - 3Q)/4$.

The type III snake at $l = 0$ has the rotation angle ψ_4 which is chosen in such a way that the closed–orbit spin tune of the ring does not change due to the snakes, $\psi_1 + \psi_2 + \psi_3 + \psi_4 \stackrel{\circ}{=} 0$. The required rotation angles are

$$\psi_1 \stackrel{\circ}{=} \psi_3 \stackrel{\circ}{=} \pi + (-\nu_0 + Q)/4 \ , \quad \psi_2 \stackrel{\circ}{=} (-\nu_0 - 3Q)/4 \ , \quad \psi_4 \stackrel{\circ}{=} (Q - 3 - \nu_0)/4 \ . \tag{3.58}$$

Obviously a change in sign of Q leads to $I^+ = 0$ due to condition 2 and to $I^- = 0$ due to condition 1. There are therefore exactly two possibilities for making a ring with super–periodicity 4 spin transparent by means of 4 type III snakes. These possibilities are shown in figure 3.14. However, the scheme of 4 type III snakes presented here cannot be a practical snake scheme, since it does not make the closed–orbit spin tune independent of energy. But it was described here to illustrate how type III snakes can be used at fixed energy to make spin perturbations from different parts of the ring cancel each other. This feature can be used in combination with Siberian Snakes which have been installed to make the closed–orbit spin tune independent of energy.

Snake Matching with Type III Snakes for Super–Periodicity 4 and Mirror Symmetry

In particle optical systems, mirror symmetries are often used to cancel perturbative effects [52, 120, 121, 122]. Therefore it is interesting to see whether mirror symmetry can lead to the compensation of a spin–orbit–coupling integral when 4 Siberian Snakes are installed at the symmetry points of the ring. If one super–period is mirror symmetric, then

$$I^{\pm}_{\frac{1}{8}} = \int_0^{L/8} k\sqrt{\beta_y} e^{i(-\Psi \pm \Phi_y)} dl \ , \tag{3.59}$$
$$I^{\pm}_{\frac{1}{4}} = \int_0^{L/8} k(l)\sqrt{\beta_y(l)} e^{i(-\Psi(l) \pm \Phi_y(l))} dl + \int_{L/8}^{L/4} k(l)\sqrt{\beta_y(l)} e^{i(-\Psi(l) \pm \Phi_y(l))} dl$$

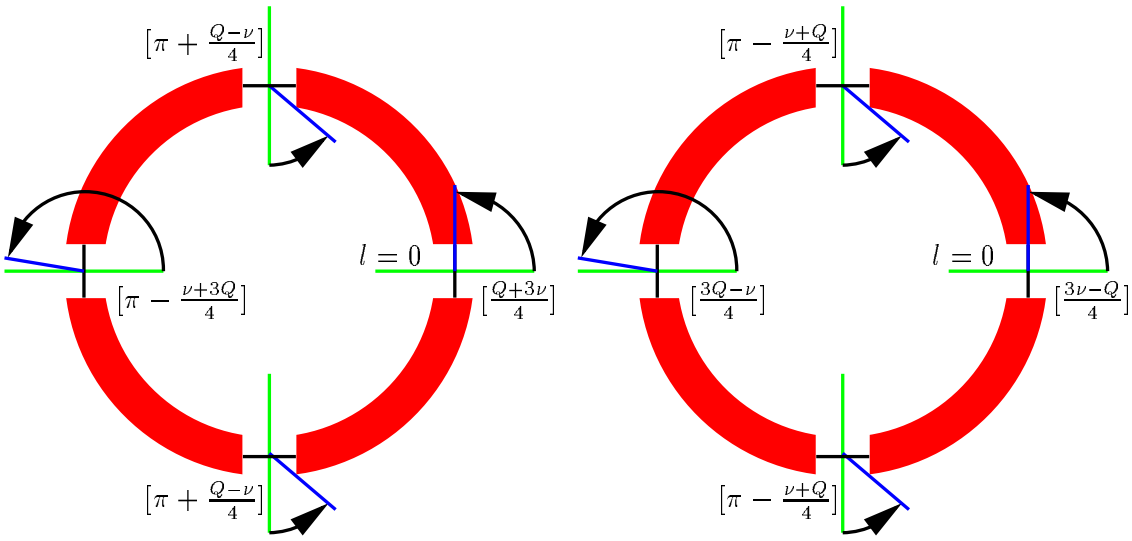

Figure 3.14: The two only ways to snake match a ring with super–periodicity 4 by 4 type III snakes. The number between 0 and 2π which equals x modulo 2π is written as $[x]$. The vertical tune times 2π is denoted by Q and $\nu_0 = G\gamma 2\pi$.

$$
\begin{aligned}
&= \int_0^{L/8} k(l)\sqrt{\beta_y(l)}e^{i(-\Psi(l)\pm\Phi_y(l))}dl \\
&+ \int_0^{L/8} k(\frac{L}{4}-l)\sqrt{\beta_y(\frac{L}{4}-l)}e^{i(-\Psi(\frac{L}{4}-l)\pm\Phi_y(\frac{L}{4}-l))}dl \qquad (3.60)\\
&= I^{\pm}_{\frac{1}{8}} + \int_0^{L/8} k(l)\sqrt{\beta_y(l)}e^{i(-(\Psi(\frac{L}{4})-\Psi(l))\pm(Q/4-\Phi_y(l)))}dl \qquad (3.61)\\
&= I^{\pm}_{\frac{1}{8}} + (I^{\pm}_{\frac{1}{8}})^* e^{i(-\nu_0\pm Q)/4} \; . \qquad (3.62)
\end{aligned}
$$

With $\Sigma^{\pm} = (-\nu_0 \pm Q)/4$ one obtains for the complete ring

$$I^{\pm} = (I^{\pm}_{\frac{1}{8}} + (I^{\pm}_{\frac{1}{8}})^* e^{i\Sigma^{\pm}}) \cdot (1 + e^{i\Sigma^{\pm}} + e^{i2\Sigma^{\pm}} + e^{i3\Sigma^{\pm}}) \; . \qquad (3.63)$$

Thus snake matching the ring with super–periodicity 4 is not influenced by the fact that the ring might have a mirror symmetry since the bracket in equation (3.63) is equivalent to the corresponding bracket in equation (3.49) for rings without mirror symmetry.

In this report, type III snakes will not be considered further, since a horizontal Siberian Snake with snake angle φ can be decomposed into a radial Siberian Snake and a type III snake with rotation angle 2φ, as pointed out in equation (3.43). A type III changes the difference between orbital phase Φ_y and spin phase, and that in turn changes the phase in the spin–orbit–coupling integral. This phase can be used to cancel the perturbation in one part of the accelerator against the perturbation in another part, but this can be achieved just as well and with less expense by a slight change of betatron phase advance Φ_y in the vertical optics of the ring. This technique will be used in section 3.3.3.

Snake Matching with Fixed Axes of Siberian Snakes at All Energies for Super–Periodicity 4

The snake matching technique with type III snakes has the great disadvantage that these snakes have to be ramped with the rest of the ring in order to snake match at each energy. Also horizontal Siberian Snakes can be used to manipulate the spin phase advance between parts of the ring and it will now be investigated how such Snakes can be used for snake matching.

Schemes with 4 Snakes: For 4 horizontal Siberian Snakes the spin–orbit–coupling integral in equation (3.46) is

$$\begin{aligned} I^{\pm} &= \int_0^{\theta_1} k\sqrt{\beta_y} e^{i(-\Psi_0 \pm \Phi_{y0})} dl \qquad (3.64)\\ &+ e^{i(-\Psi_0 \pm \Phi_{y0})} \int_{\theta_1}^{\theta_2} k\sqrt{\beta_y} e^{i(\Psi_1 + \alpha_1 \pm \Phi_{y1})} dl \\ &+ e^{i(-\Psi_0 + \alpha_1 + \Psi_1 \pm (\Phi_{y0} + \Phi_{y1}))} \int_{\theta_2}^{\theta_3} k\sqrt{\beta_y} e^{i(-\Psi_2 - \alpha_2 \pm \Phi_{y2})} dl \\ &+ e^{i(-\Psi_0 + \alpha_1 + \Psi_1 - \alpha_2 - \Psi_2 \pm (\Phi_{y0} + \Phi_{y1} + \Phi_{y2}))} \int_{\theta_3}^{L} k\sqrt{\beta_y} e^{i(\Psi_3 + \alpha_3 \pm \Phi_{y3})} dl \ . \end{aligned}$$

For a ring with super–periodicity 4 and with 4 equally spaced horizontal Siberian Snakes one obtains with $\nu_0 = \Psi(l)$, $\Psi_j = \Psi(l)/4$, and $\Phi_{yj} = Q/4$ the relation

$$I^{\pm}_{\frac{1}{4}} = \int_0^{\frac{L}{4}} k\sqrt{\beta_y} e^{i(-\Psi \pm \Phi_y)} dl \ , \qquad (3.65)$$

$$\begin{aligned} I^{\pm} &= I^{\pm}_{\frac{1}{4}} (1 + e^{i(-\Psi_0 + \alpha_1 + \Psi_1 - \alpha_2 \pm (\Phi_{y0} + \Phi_{y1}))}) \qquad (3.66)\\ &+ (I^{\mp}_{\frac{1}{4}})^* e^{i(-\Psi_0 + \alpha_1 \pm \Phi_{y0})} (1 + e^{i(\Psi_1 - \alpha_2 - \Psi_2 + \alpha_3 \pm (\Phi_{y1} + \Phi_{y2}))}) \\ &= I^{\pm}_{\frac{1}{4}} (1 + e^{i(\alpha_1 - \alpha_2 \pm 2Q/4)}) + (I^{\mp}_{\frac{1}{4}})^* e^{i((-\nu_0 \pm Q)/4 + \alpha_1)} (1 + e^{i(-\alpha_2 + \alpha_3 \pm 2Q/4)}) \ . \end{aligned}$$

Spin transparency of the ring is therefore obtained when

$$\alpha_1 - \alpha_2 \pm 2Q/4 \stackrel{\circ}{=} \pi \text{ and } -\alpha_2 + \alpha_3 \pm 2Q/4 \stackrel{\circ}{=} \pi \ . \qquad (3.67)$$

This cannot be satisfied in general since $\alpha_1 - \alpha_2 + 2Q/4 \stackrel{\circ}{=} \pi$ and $\alpha_1 - \alpha_2 - 2Q/4 \stackrel{\circ}{=} \pi$ have to be true simultaneously, which implies $Q \stackrel{\circ}{=} 0$.

In the case of mirror symmetry in the ring it was shown that $I^{+}_{\frac{1}{4}}$ and $I^{-}_{\frac{1}{4}}$ are related by equation (3.62) as

$$I^{\pm}_{\frac{1}{4}} = I^{\pm}_{\frac{1}{8}} + (I^{\pm}_{\frac{1}{8}})^* e^{i(-\nu_0 \pm Q)/4} \ , \qquad (3.68)$$

$$\begin{aligned} (I^{\mp}_{\frac{1}{4}})^* &= (I^{\mp}_{\frac{1}{8}})^* + I^{\mp}_{\frac{1}{8}} e^{-i(-\nu_0 \mp Q)/4} = ((I^{\mp}_{\frac{1}{8}})^* e^{i(-\nu_0 \mp Q)/4} + I^{\mp}_{\frac{1}{8}}) e^{-i(-\nu_0 \mp Q)/4} \\ &= I^{\mp}_{\frac{1}{4}} e^{-i(-\nu_0 \mp Q)/4} \ . \qquad (3.69) \end{aligned}$$

With a mirror symmetric quadrant the spin–orbit–coupling integral then simplifies to

$$I^{\pm} = I^{\pm}_{\frac{1}{4}} (1 + e^{i(\alpha_1 - \alpha_2 \pm 2Q/4)}) + I^{\mp}_{\frac{1}{4}} (1 + e^{i(-\alpha_2 + \alpha_3 \pm 2Q/4)}) e^{i(\alpha_1 \pm 2Q/4)} \qquad (3.70)$$

and again this additional symmetry does not simplify the compensation of the spin–orbit integrals.

Schemes with 8 Snakes: The same procedure can now be repeated with 8 snakes. For that purpose 4 more horizontal Siberian Snakes are placed at the locations $jL/4 + \Delta l$, $j \in \{0,1,2,3\}$. From

$$I^{\pm} = \sum_{j=0}^{n} e^{i\sum_{k=0}^{j-1}[-(-)^k(\alpha_k+\Psi_k)\pm\Phi_{yk}]} \int_{\theta_j}^{\theta_{j+1}} k\sqrt{\beta_y} e^{i[-(-)^j(\Psi_j(l)+\alpha_j)\pm\Phi_{yj}(l)]} dl \tag{3.71}$$

the spin–orbit–coupling integrals are obtained

$$I_0^{\pm} = \int_0^{\Delta l} k\sqrt{\beta_y} e^{i(-\Psi\pm\Phi_y)} dl \ , \quad I_1^{\pm} = \int_{\Delta l}^{\frac{L}{4}} k\sqrt{\beta_y} e^{i(\Psi\pm\Phi_y)} dl \ , \tag{3.72}$$

$$\begin{aligned} I^{\pm} &= I_0^{\pm}(1 + e^{i(-\Psi_0+\alpha_1+\Psi_1-\alpha_2\pm(\Phi_{y0}+\Phi_{y1}))} + \ldots & (3.73)\\ &+ e^{i(-\Psi_0+\alpha_1+\Psi_1-\alpha_2\mp\ldots-\alpha_{n-2}\pm(\Phi_{y0}+\ldots+\Phi_{yn-3}))}) \\ &+ I_1^{\pm} e^{i(-\Psi_0+\alpha_1\pm\Phi_{y0})}(1 + e^{i(\Psi_1-\alpha_2-\Psi_2+\alpha_3\pm(\Phi_{y1}+\Phi_{y2}))} + \ldots & (3.74)\\ &+ e^{i(\Psi_1-\alpha_2-\Psi_2+\alpha_3\pm\ldots+\alpha_{n-1}\pm(\Phi_{y1}+\ldots+\Phi_{yn-2}))}) \ . \end{aligned}$$

If there is an additional mirror symmetry and the snakes are all placed in the symmetry points, equation (3.62) implies $I_1^{\pm} = (I_0^{\pm})^* e^{i(-\nu_0\pm Q)/4}$, which again does not lead to simplifications. The complete spin phase advance of the ring is $\sum_{j=0}^{n}(-)^j(\Psi_j + \alpha_j) = \pi$. Since this phase advance is required to be independent of energy, $\sum_{j=0}^{n}(-)^j\Psi_j$ has to vanish. Because of the super–periodicity this requires $\Psi_0 = \Psi_1$, and all the spin phases Ψ_j in the equations (3.74) cancel. With the difference angles $\Delta_{jk} = \alpha_j - \alpha_k$ spin matching the ring therefore requires

$$1 + e^{i(\pm Q/4+\Delta_{12})} + e^{i(\pm 2Q/4+\Delta_{12}+\Delta_{34})} + e^{i(\pm 3Q/4+\Delta_{12}+\Delta_{34}+\Delta_{56})} = 0 \ , \tag{3.75}$$

$$1 + e^{i(\pm Q/4-\Delta_{23})} + e^{i(\pm 2Q/4-\Delta_{23}-\Delta_{45})} + e^{i(\pm 3Q/4-\Delta_{23}-\Delta_{45}-\Delta_{67})} = 0 \ . \tag{3.76}$$

Again these 4 complex numbers with modulus 1 can only add up to zero by the three schemes shown in figure 3.12. The equations (3.75) and (3.75) have the same structure as the matching conditions of equations (3.51) and the relations (3.58) can therefore be used to obtain the following two possibilities to satisfy equation (3.75):

$$\Delta_{12} \stackrel{\circ}{=} \Delta_{56} \stackrel{\circ}{=} \pi - Q/4 \ , \quad \Delta_{34} \stackrel{\circ}{=} 3Q/4 \ , \tag{3.77}$$

$$\Delta_{12} \stackrel{\circ}{=} \Delta_{56} \stackrel{\circ}{=} \pi + Q/4 \ , \quad \Delta_{34} \stackrel{\circ}{=} -3Q/4 \ . \tag{3.78}$$

Here equation (3.78) resulted from reversing the sign of Q in equation (3.77). There are also exactly two possibilities for solving equation (3.76),

$$\Delta_{23} \stackrel{\circ}{=} \Delta_{67} \stackrel{\circ}{=} \pi + Q/4 \ , \quad \Delta_{45} \stackrel{\circ}{=} -3Q/4 \ , \tag{3.79}$$

$$\Delta_{23} \stackrel{\circ}{=} \Delta_{67} \stackrel{\circ}{=} \pi - Q/4 \ , \quad \Delta_{45} \stackrel{\circ}{=} 3Q/4 \ . \tag{3.80}$$

There are now 4 possibilities to snake match the ring; these are obtained by combining the equations (3.77)&(3.79), (3.77)&(3.80), (3.78)&(3.79), or (3.78)&(3.80),

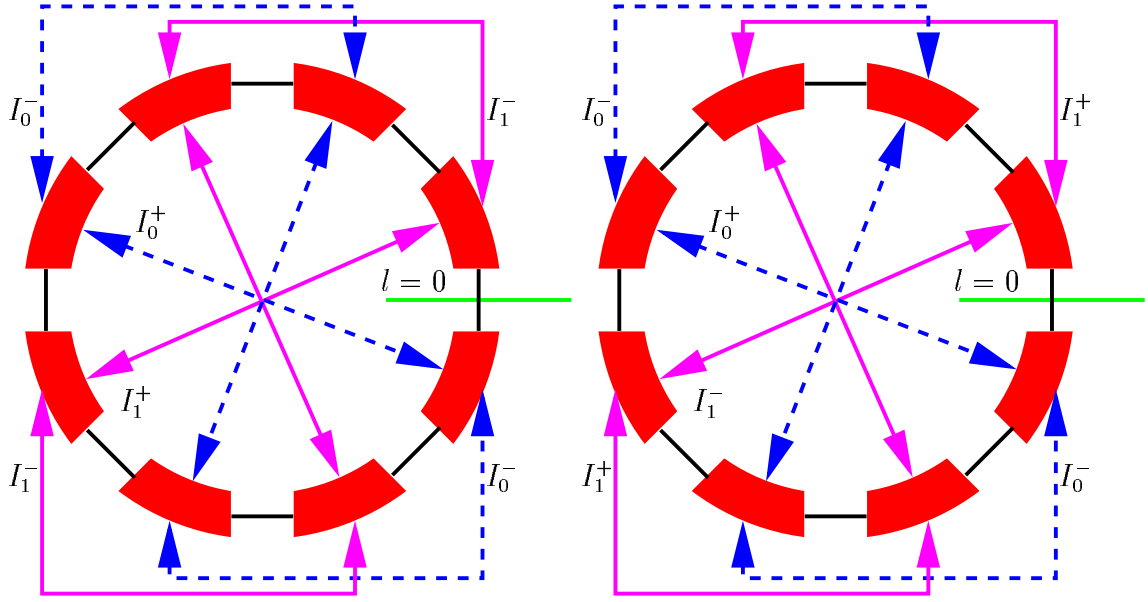

Figure 3.15: The two possibilities by which the individual parts of the ring cancel the spin–orbit–coupling integrals. Changing the sign of Q leads to two corresponding snake schemes. The symbols I_0^+, I_0^-, I_1^+, and I_1^- indicate which part of the spin–orbit–coupling integrals are canceled.

where the last two possibilities result from the first two by reversing the sign of Q. Figure 3.15 shows how parts of the ring cancel the depolarizing effects of other parts in these snake matching schemes.

Since only differences in the snake angles appear, one of the angles can be chosen arbitrarily. This then fixes all other snake angles. For simplicity I choose $\alpha_1 = 0$. This leads to the following possibilities:

Combination of the equations (3.77) and (3.79):

$$\alpha_1 \stackrel{\circ}{=} 0\,, \quad \alpha_2 \stackrel{\circ}{=} \pi + Q/4\,, \quad \alpha_3 \stackrel{\circ}{=} 0\,, \quad \alpha_4 \stackrel{\circ}{=} -3Q/4\,, \tag{3.81}$$

$$\alpha_5 \stackrel{\circ}{=} 0\,, \quad \alpha_6 \stackrel{\circ}{=} \pi + Q/4\,, \quad \alpha_7 \stackrel{\circ}{=} 0\,, \quad \alpha_8 \stackrel{\circ}{=} \pi + Q/4\,, \tag{3.82}$$

Combination of the equations (3.77) and (3.80):

$$\alpha_1 \stackrel{\circ}{=} 0\,, \quad \alpha_2 \stackrel{\circ}{=} \pi + Q/4\,, \quad \alpha_3 \stackrel{\circ}{=} 2Q/4\,, \quad \alpha_4 \stackrel{\circ}{=} -Q/4\,, \tag{3.83}$$

$$\alpha_5 \stackrel{\circ}{=} -4Q/4\,, \quad \alpha_6 \stackrel{\circ}{=} \pi - 3Q/4\,, \quad \alpha_7 \stackrel{\circ}{=} -2Q/4\,, \quad \alpha_8 \stackrel{\circ}{=} \pi - Q/4\,. \tag{3.84}$$

The values for α_8 were obtained from $\alpha_8 - \alpha_7 + \alpha_6 - \alpha_5 + \alpha_4 - \alpha_3 + \alpha_2 - \alpha_1 \stackrel{\circ}{=} \pi$. The last snake scheme can be simplified by decreasing all snake angles by $2Q/4$, leading to

$$\alpha_1 \stackrel{\circ}{=} Q/4\,, \quad \alpha_2 \stackrel{\circ}{=} \pi + 2Q/4\,, \quad \alpha_3 \stackrel{\circ}{=} 3Q/4\,, \quad \alpha_4 \stackrel{\circ}{=} 0\,, \tag{3.85}$$

$$\alpha_5 \stackrel{\circ}{=} -3Q/4\,, \quad \alpha_6 \stackrel{\circ}{=} \pi - 2Q/4\,, \quad \alpha_7 \stackrel{\circ}{=} -Q/4\,, \quad \alpha_8 \stackrel{\circ}{=} \pi\,. \tag{3.86}$$

These snake schemes are shown in figure 3.16. There account has been taken of the fact that the actual angle between the snake's rotation axis and the radial direction

is $\alpha/2$. Furthermore advantage has been taken of the fact that the angle $\alpha/2$ only needs to be known modulo π.

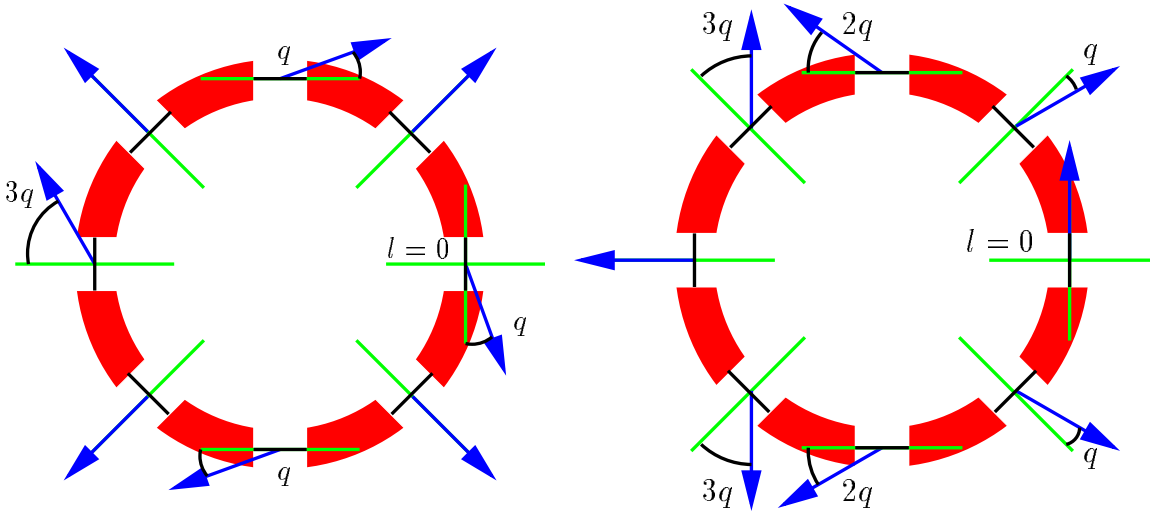

Figure 3.16: Two of the 4 ways to snake match a ring with super–periodicity 4 using 8 horizontal Siberian Snakes. The number between 0 and π which equals $Q/8$ modulo π is denoted by q. The vertical tune times 2π is denoted by Q and $\nu = G\gamma 2\pi$. The other two possible snake schemes are obtained by reversing the sign of Q. When all snake angles are increased by the same amount, then the ring remains spin transparent. Note that the snake angle is independent of ν and thus of energy.

Here it is very important to note that the snake angles are independent of $\nu = G\gamma$ and therefore that a snake match has been achieved for all energies. With 4 Siberian Snakes such an energy independent spin match is not possible.

One can now try to repeat the same procedure for a layout with 6 horizontal Siberian Snakes or with combinations of, for example, 6 horizontal Siberian Snakes and two type III snakes. These can be investigated using the methods already presented.

3.3.3 Snake Matching HERA–p

When the spin–orbit–coupling integrals starting at an azimuth θ_0 are minimized, then the opening angle of the invariant spin field at θ_0 in the approximation of linear spin–orbit motion is also minimized since

$$P_{lim} = [1 + \sum_{k=1}^{3}(|B_{2k-1}|^2 + |B_{2k}|^2)J_k]^{-\frac{1}{2}} \quad , \quad B_k = \frac{I_k}{e^{i2\pi(Q_k - \nu_0)} - 1} \; . \tag{3.87}$$

according to equation (3.27).

When snake matching a ring with super–periodicity according to the previously described technique, then all spin–orbit–coupling integrals are zero at one azimuth of

the ring and in linearized spin–orbit motion, the invariant spin field is then parallel to $\vec{n}_0$ at θ_0 for all particles. It has been seen from the example of a ring with super–periodicity 4 that 8 Siberian Snakes can be used to snake match the spin–orbit–coupling integrals to zero at one azimuth of the ring for all energies. This could be achieved since the snake angles were used to adjust the spin phase advances in such a way that perturbations in one part of the ring are compensated by identical perturbations in one of the identical super–periods of the ring.

Since HERA–p does not poses such a symmetry, it is in general not possible to find snake angles which completely compensate all spin–orbit–coupling integrals. However, in section 3.2.3 it was demonstrated that the 4 identical arc sections of HERA dominate the resonance strength of vertical motion; and the perturbing effect of these identical arcs can cancel each other.

The spin–orbit–coupling integrals from the first regular FODO cell to the last FODO cell of a regular arc in HERA–p are denoted as $\hat{I}_y^+$ and $\hat{I}_y^-$ and the azimuth of the beginnings of the 4 regular arcs as θ_1, θ_2, θ_3, and θ_4. The central points of the East, North, and West straight sections are denoted by E, N, and W. To compensate the spin phase advance between the arcs, the snake angles φ_E, φ_N, and φ_W are used. The spin phase advance between θ_i and θ_j is denoted by Ψ_{ij}. These notations are indicated in figure 3.17.

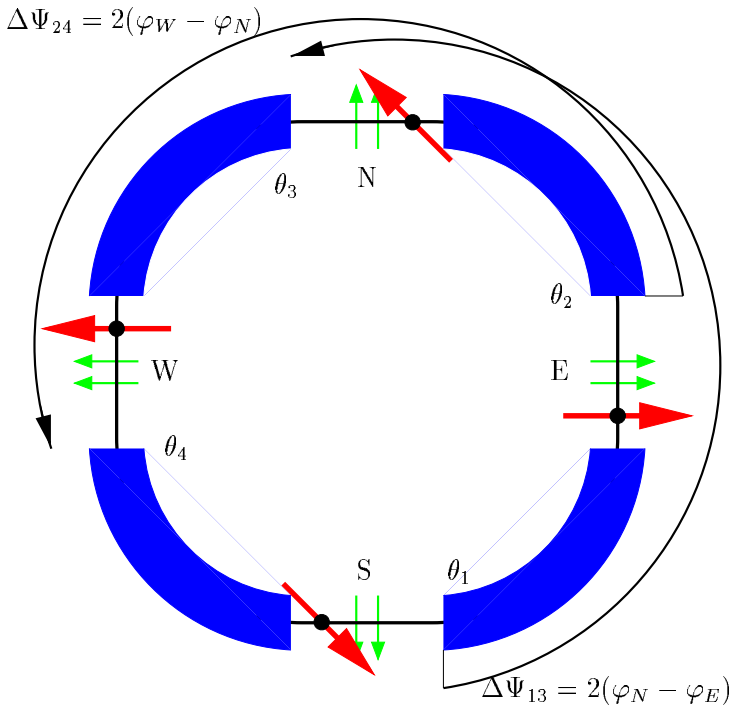

Figure 3.17: The spin phase advance from the beginning of one regular arc to the beginning of the regular arc on the opposite side of the ring.

With Siberian Snakes in each of the straight sections, the spin phase advance from θ_1 to θ_3 is given by $\Psi_{13} = \Psi_{1E} - 2\varphi_E - \Psi_{EN} + 2\varphi_N + \Psi_{N3}$. In the $8fs$ schemes,

the spin phase advance is identical in all quadrants of the ring and the total spin advance is solely determined by the snake angles and is therefore independent of energy: $\Psi_{13} = 2(\varphi_N - \varphi_E)$ and $\Psi_{24} = 2(\varphi_W - \varphi_N)$. The orbital phase advance $\Phi_y(\theta_3) - \Phi_y(\theta_1)$ also does not depend on energy. For simplicity, $\Phi_y(\theta_j) - \Phi_y(\theta_i)$ will now be denoted as Φ_{ij} .

The spin–orbit–coupling integrals at the South interaction point therefore contains the following contributions from the 4 regular arcs:

$$\begin{aligned} I^+_{\text{arcs}} &= \hat{I}^+ e^{i(-\Psi_{S1}+\Phi_{S1})}(1 + e^{i[2(\varphi_E-\varphi_N)+\Phi_{13}]}) \qquad (3.88)\\ &+ (\hat{I}^-)^* e^{i(2\varphi_E-\Psi_{SE}+\Psi_{E2}+\Phi_{S2})}(1 + e^{i[2(\varphi_W-\varphi_N)+\Phi_{24}]}) \\ I^-_{\text{arcs}} &= \hat{I}^- e^{i(-\Psi_{S1}-\Phi_{S1})}(1 + e^{i[2(\varphi_E-\varphi_N)-\Phi_{13}]}) \qquad (3.89)\\ &+ (\hat{I}^+)^* e^{i(2\varphi_E-\Psi_{SE}+\Psi_{E2}-\Phi_{S2})}(1 + e^{i[2(\varphi_W-\varphi_N)-\Phi_{24}]}) \end{aligned}$$

This shows that it is always possible to cancel one of the spin–orbit coupling integrals by a suitable choice of Siberian Snakes. The spin perturbation produced in one of the arcs is then canceled by the arc on the opposite side of the ring. Since $|I^+|$ and $|I^-|$ are different, neighboring arcs can in general not compensate each other.

It is however possible to use the eight–snake scheme found for symmetric lattices. The two special 8 Siberian Snake schemes which lead to an energy independent snake match in a ring with super–periodicity 4 will not spin-match HERA–p completely, but the spin perturbation from the arcs, which has been shown to be the dominant perturbation in section 3.2.3, will be compensated exactly. This possibility of having a set of Siberian Snake angles which do not have to be changed with energy and which lead to a tightly bundled invariant spin field is on the one hand very attractive; on the other hand it requires 8 Siberian Snakes; 4 of them would have to be installed at the centers of the HERA–p arcs, where technical requirements of moving cryogenic feed-throughs and super–conducting magnets would be very costly. If possible, a four–snake scheme should therefore be found.

Whereas it was shown below equation (3.67) that a four–snake scheme cannot cancel both spin–orbit–coupling integrals in a ring with super–periodicity, a corresponding cancelation of the spin perturbation due to the arcs in HERA–p can nevertheless be achieved. This is possible since the orbital phase advance between the arcs can be manipulated individually, while these four phase advances are equal for a lattice with super–periodicity 4.

To cancel both spin–orbit integrals in equation (3.90), 4 phase factors have to be -1, which requires

$$\begin{aligned} 2(\varphi_E - \varphi_N) + \Phi_{13} &= \pi \ , \qquad (3.90)\\ 2(\varphi_E - \varphi_N) - \Phi_{13} &= \pi \ , \qquad (3.91)\\ 2(\varphi_W - \varphi_N) + \Phi_{42} &= \pi \ , \qquad (3.92)\\ 2(\varphi_W - \varphi_N) - \Phi_{42} &= \pi \ . \qquad (3.93) \end{aligned}$$

For arbitrary betatron phase advances, this equation cannot be solved by a choice of Siberian Snakes, since there are only two free parameters which contain the snake angles. However, the betatron phase advances can be changed appropriately to

obtain a complete spin match of the arcs in HERA–p. Subtraction of the first two equations leads to the requirement that the betatron phase advance from θ_1 half way around the ring to θ_3 is an odd or even multiple of π. The same is true for the phase advance from θ_2 to θ_4. Correspondingly, the spin phase advance over these regions has to be a an odd multiple of π when the orbit phase advance is an even multiple and vice versa. With a rather benign change of the vertical optics in HERA–p which does not change the vertical tune, even in a four–snake scheme, the contribution of the regular arcs to both spin–orbit–coupling integrals is canceled.

A snake scheme $(0\frac{\pi}{2}\frac{\pi}{2}\frac{\pi}{2})8fs$ leads to $\Psi_{13} = 0$ and $\Psi_{24} = 0$. For this snake scheme, the betatron phase advances from θ_1 to θ_3 and from θ_2 to θ_4 were adjusted to be odd multiples of π. The maximum time average polarization P_{lim} is plotted (blue) in figure 3.18 for the complete range of HERA–p momenta and for the critical momentum regions above $800GeV/c$.

As a comparison, these curves are displayed together with P_{lim} for a standard snake scheme $(\frac{\pi}{4}0\frac{\pi}{4}0)$ (red). The complete snake match of the arcs in HERA–p in deed eliminates all strong reductions of P_{lim} over the complete momentum range. Nonlinear effects will be analyzed later, but as far as the linear effects are concerned, this snake matched lattice of HERA–p would be a rather promising choice for the acceleration of polarized proton beams.

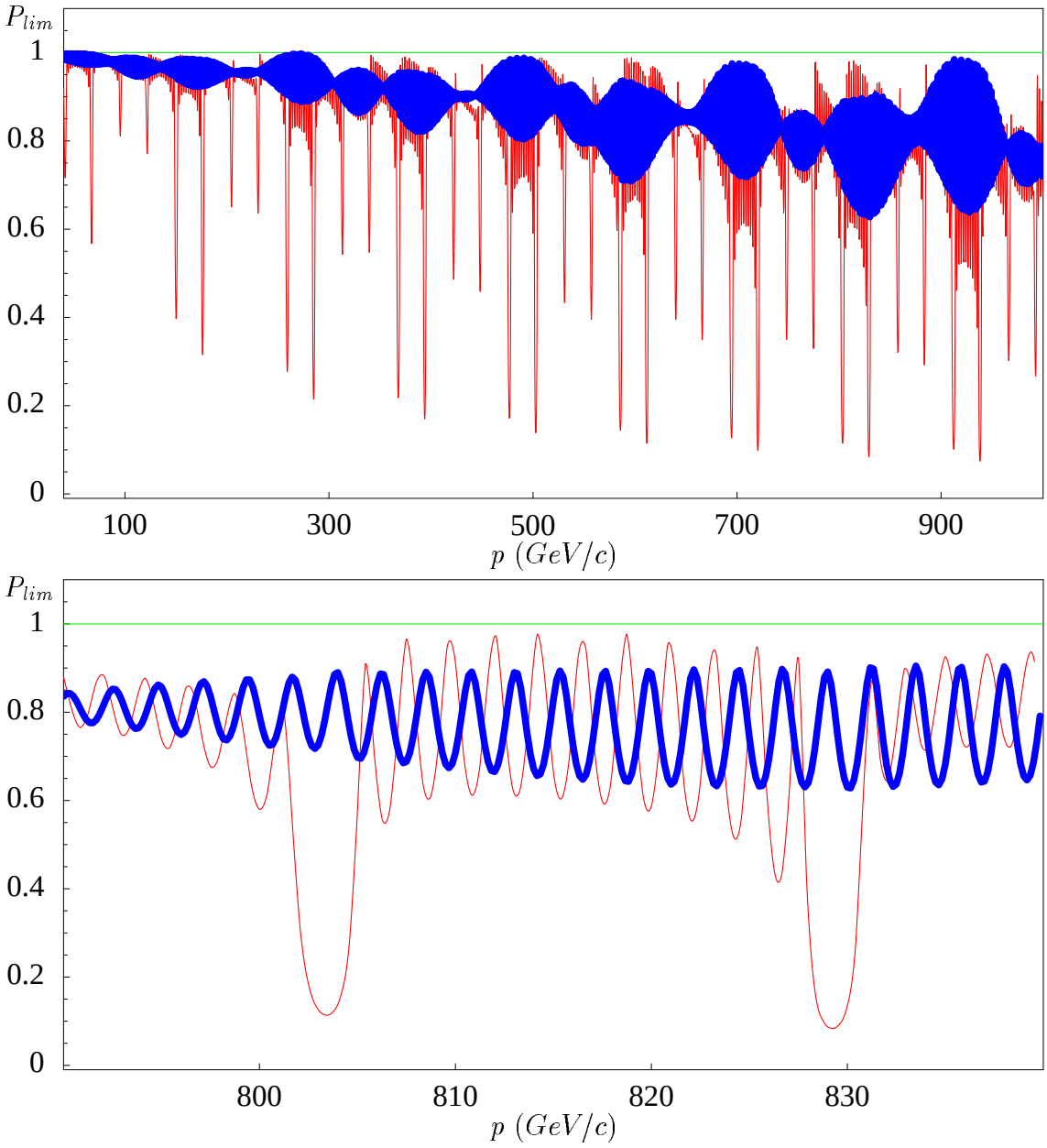

Figure 3.18: Improvement of P_{lim} by matching snake angles and the orbital phases. The snake arrangement is $(0\frac{\pi}{2}\frac{\pi}{2}\frac{\pi}{2})8fs$ (blue). As a comparison P_{lim} from linearized spin–orbit motion is shown for the same HERA–p optics with a $(\frac{\pi}{4}0\frac{\pi}{4}0)8fs$ snake scheme (red).

Chapter 4

Higher–Order Spin Motion

4.1 Higher–Order Resonances and Snake Schemes

At the critical energies, where the maximum time average polarization is low during the acceleration process, linearized spin–orbit motion and the SRM do not describe spin dynamics well and simulation results obtained with the computationally quick linearization of spin motion should always be checked with more time consuming non–perturbative methods if possible. This is also true for the snake–matched lattice of HERA–p with low P_{lim} described in section 3.3.3, even though it avoids large variations of the invariant spin field $\vec{n}(\vec{z})$ over the phase space of the beam in linearized spin–orbit motion. When first–order effects are canceled, the higher–order effects become dominant and the quality of the snake–matched lattice of HERA–p can only be evaluated with higher–order theories.

Until 1996, when stroboscopic averaging [100] was introduced, there was no non–perturbative method of computing the $\vec{n}$–axis at high energy in proton storage rings, where perturbative methods are usually not sufficient [123]. In addition, the method of anti–damping was derived, which also computes $\vec{n}(\vec{z})$ non–perturbatively and which can be faster when the $\vec{n}$–axis is required for a range of phase space amplitudes. Both methods of computing the invariant spin field are implemented in the spin–orbit dynamics code SPRINT, by which also the amplitude dependent spin tune $\nu(\vec{J})$ can be computed once $\vec{n}(\vec{z})$ is known. Since stroboscopic averaging and anti–damping are based on multi-turn tracking data, they are applicable to all kinds of circular accelerators and they are especially efficient for small rings and for simple model accelerators.

Recently a non–perturbative algorithm for computing $\vec{n}(\vec{z})$ and $\nu(\vec{J})$ has been derived [124]. It is called SODOM–2 since it was inspired by the earlier perturbative algorithm SODOM [86]. With some routines provided by K. Yokoya, SODOM–2 was incorporated into the program SPRINT [112, 100, 125] and leads to results which agree very well with those of stroboscopic averaging. For motion in one degree of freedom, SODOM–2 is often faster than stroboscopic averaging, especially for large rings like HERA–p where particle tracking is relatively time consuming. But for orbit motion in more than one degree of freedom or in the vicinity of spin–orbit resonances, SODOM–2 becomes exceedingly slow and then stroboscopic averaging

and anti–damping are needed and will be introduced later.

4.1.1 Computing $\vec{n}$ and $\nu(\vec{J})$ by SODOM–2

For phase space motion on an invariant torus, the final angle variables are $\vec{\Phi}_f = \vec{\Phi}_i + 2\pi\vec{Q}$ where the tunes $\vec{Q}$ can depend on $\vec{J}$. A spin field $\vec{f}(\vec{\Phi},\theta)$ can be described for action–angle in terms of a spinor $\Psi(\vec{\Phi},\theta)$ as $\vec{f}(\vec{\Phi},\theta) = \Psi^\dagger\vec{\underline{\sigma}}\Psi$. Since the action variables $\vec{J}$ are constants of motion, they are not indicated here. A multiplication of Ψ with an arbitrary phase factor does not change the corresponding spin field. According to equation (2.45) the spin field after one turn can be described by

$$\Psi(\vec{\Phi} + 2\pi\vec{Q}, \theta_0 + 2\pi) = A(\vec{\Phi})\Psi(\vec{\Phi},\theta_0) \ , \tag{4.1}$$

where $A(\vec{\Phi})$ is the phase space dependent spin transport quaternion for one turn around the ring starting at azimuth θ_0.

Let an invariant spin field on the Poincaré section at θ_0 be described by the spinor $\psi_n(\vec{\Phi})$. If the initial spin $\vec{S}_i$ of a particle is parallel to $\vec{n}(\vec{\Phi}_i)$, it is described by $\psi_n(\vec{\Phi}_i)$. After one turn $\vec{S}_f$ is then parallel to $\vec{n}(\vec{\Phi}_i + 2\pi\vec{Q})$ and can be described by $A(\vec{\Phi}_i)\psi_n(\vec{\Phi}_i)$ as well as by $\psi_n(\vec{\Phi}_i + 2\pi\vec{Q})$. These two spinors therefore have to agree up to an arbitrary phase,

$$A(\vec{\Phi})\psi_n(\vec{\Phi}) = e^{-i\pi\tilde{\nu}_{\vec{f}}(\vec{\Phi})}\psi_n(\vec{\Phi} + 2\pi\vec{Q}) \ . \tag{4.2}$$

By choosing an appropriate function $\phi_{\vec{f}}(\vec{\Phi})$, new spinor $\Psi_n(\vec{\Phi}) = e^{i\frac{1}{2}\phi_{\vec{f}}(\vec{\Phi})}\psi_n(\vec{\Phi})$ can now be found for which the phase factor in the periodicity condition (4.2) does not depend on the angle variables $\vec{\Phi}$. Thus $\phi_{\vec{f}}(\vec{\Phi})$ needs to make $\nu(\vec{J}) = 2\pi\tilde{\nu}_{\vec{f}}(\vec{\Phi}) - \phi_{\vec{f}}(\vec{\Phi}) + \phi_{\vec{f}}(\vec{\Phi} + 2\pi\vec{Q})$ independent of $\vec{\Phi}$. Such a function $\phi_{\vec{f}}(\vec{\Phi})$ was already required in equation (2.83) to find the amplitude dependent spin tune and it was shown that $2\pi\nu$ is the zeroth Fourier component of $\tilde{\nu}_{\vec{f}}(\vec{\Phi})$. This new spinor of the invariant spin field then satisfies the periodicity condition

$$A(\vec{\Phi})\Psi_n(\vec{\Phi}) = e^{-i\pi\nu}\Psi_n(\vec{\Phi} + 2\pi\vec{Q}) \ . \tag{4.3}$$

The one turn spin transport quaternion $A(\vec{\Phi})$ can be determined numerically by transporting particles with spin around a model of the circular accelerator. It is then a 2π periodic function of $\vec{\Phi}$ and can be written as a Fourier series. The spinor Ψ_n of the invariant spin field will also be written as a Fourier expansion,

$$A(\vec{\Phi}) = \sum_{\vec{j}} A_{\vec{j}} e^{i\vec{j}\cdot\vec{\Phi}} \ , \quad \Psi_n(\vec{\Phi}) = \sum_{\vec{j}} \Psi_{n,\vec{j}} e^{i\vec{j}\cdot\vec{\Phi}} \ . \tag{4.4}$$

The periodicity condition then reads as

$$e^{-i2\pi\vec{j}\cdot\vec{Q}} \sum_{\vec{k}} A_{\vec{j}-\vec{k}}\Psi_{n,\vec{k}} = e^{-i\pi\nu}\Psi_{n,\vec{j}} \ . \tag{4.5}$$

This is an eigenvector equation for the infinite dimensional matrix with coefficients $e^{-i2\pi\vec{j}\cdot\vec{Q}}A_{\vec{j}-\vec{k}}$. When an eigenvector with coefficients $\Psi_{n,\vec{j}}$ for the eigenvalue $e^{-i\pi\nu}$ is

found, then the spin tune ν and the spinor $\Psi_n(\vec{\Phi}) = \sum_{\vec{j}} \Psi_{n,\vec{j}} e^{i\vec{j}\cdot\vec{\Phi}}$ can be computed, which in turn leads to the $\vec{n}$–axis.

For some vector of integers $\vec{l}$, the vector with coefficients $\Psi'_{n,\vec{j}} = \Psi_{n,\vec{j}-\vec{l}}$ is also an eigenvector corresponding to the eigenvalue $e^{-i\pi(\nu-2\vec{l}\cdot\vec{Q})}$ since

$$e^{-i2\pi\vec{j}\cdot\vec{Q}} \sum_{\vec{k}} A_{\vec{j}-\vec{k}} \Psi'_{n,\vec{k}} = e^{-i\pi(\nu-2\vec{l}\cdot\vec{Q})} \Psi'_{n,\vec{j}} \; . \tag{4.6}$$

This leads to the spin tune $\nu - 2\vec{l}\cdot\vec{Q}$ and to the spinor $\Psi'_n(\vec{\Phi}) = e^{i\vec{l}\cdot\vec{\Phi}}\Psi_n(\vec{\Phi})$, which also represents $\vec{n}(\vec{z})$.

The spinor $\Psi''_n = i\underline{\sigma}_2 \Psi^*_n$ represents $\vec{n}'' = -\vec{n}(\vec{z})$, since

$$\vec{n}'' = \vec{n}''^* = (\Psi''^{\dagger}_n \underline{\vec{\sigma}} \Psi''_n)^* = \Psi^{\dagger}_n \underline{\sigma}_2^{\dagger} \underline{\vec{\sigma}}^* \, \underline{\sigma}_2 \Psi_n = -\Psi^{\dagger}_n \underline{\vec{\sigma}} \Psi_n = -\vec{n} \; , \tag{4.7}$$

where use was made of the relations $\sigma_2^{\dagger} = \sigma_2$ and $\sigma_2^* = -\sigma_2$. This spinor has the Fourier coefficients $\Psi''_{n,\vec{j}} = i\underline{\sigma}_2 (\Psi_{n-\vec{j}})^*$. Similarly, the Fourier coefficients of A^* are $(A^*)_{\vec{j}} = (A_{-\vec{j}})^*$. Thus when $\Psi^*_n = -i\underline{\sigma}_2 \Psi''_n$ is inserted into the complex conjugation of equation (4.5), one obtains

$$e^{i2\pi\vec{j}\cdot\vec{Q}} \sum_{\vec{k}} (A_{\vec{j}-\vec{k}})^* \underline{\sigma}_2 \Psi''_{n-\vec{k}} = e^{i\pi\nu} \underline{\sigma}_2 \Psi''_{n-\vec{j}} \; . \tag{4.8}$$

Now, with $\underline{\sigma}_2 A^* \underline{\sigma}_2 = \underline{\sigma}_2 (a_0 + i\vec{a}\cdot\underline{\vec{\sigma}^*})\underline{\sigma}_2 = a_0 - i\vec{a}\cdot\underline{\vec{\sigma}} = A$ and after reversing the sign of $\vec{j}$ and $\vec{k}$, one finds

$$e^{-i2\pi\vec{j}\cdot\vec{Q}} \sum_{\vec{k}} A_{\vec{j}-\vec{k}} \Psi''_{n,\vec{k}} = e^{i\pi\nu} \Psi''_{n,\vec{j}} \; . \tag{4.9}$$

The vector with coefficients $\Psi''_{n,\vec{k}}$ is therefore an eigenvector to the eigenvalue $e^{i\pi\nu}$, which leads to the spin tune $-\nu$.

When all Fourier harmonics above a given order N are neglected in equation (4.5), this is an eigenvector problem for a square matrix with coefficients $e^{-i2\pi\vec{j}\cdot\vec{Q}} A_{\vec{j}-\vec{k}}$. Since the square matrix can have several eigenvectors and eigenvalues, the result is not unique.

So far there are no rigorous arguments or proofs about properties of the eigenvalue spectrum of the matrix in equation (4.5) for a given N. If the number of considered Fourier coefficients is large, one would expect, even though no proof has been given so far, that each eigenvalue of the matrix leads to a good approximation of one possible spin tune. And again for high enough values of N, each eigenvector of the matrix should usually be a good approximations of one possible spinor Ψ_n and all eigenvectors should then, up to a sign, correspond to the same $\vec{n}$–axis with high accuracy. It has turned out useful to find the eigenvector with the largest zero-Fourier harmonic $|\Psi_{n(0,0,0)}|$ and to determine the spin tune ν from the corresponding eigenvalue.

In fact, it has been shown numerically that the various ν computed with SODOM–2 really do differ by multiples of the orbit tune to a high accuracy [124] and that the

$\vec{n}$–axis and ν obtained by SODOM–2 agree well with those obtained by stroboscopic averaging or anti–damping described in section 4.2 and section 4.3.

For all results which were obtained with the SODOM–2 method and which will be presented below, only vertical motion was considered and 81 Fourier coefficients were used. All spin tunes ν which will be given correspond to the spinor with the largest Fourier coefficient $|\Psi_{n(0,0,0)}|$.

4.1.2 Nonlinear Spin Dynamics for Vertical Particle Motion

To check whether the improvements of spin motion obtained in the framework of linearized spin–orbit motion presented in section 3.1 survive when higher–order effects are considered, P_{lim} and ν has been calculated by the SODOM–2 algorithm with the code SPRINT. For one of the standard Siberian Snake schemes which used to be considered advantageous by a popular opinion the result is shown for the South interaction point of HERA–p in figure 4.1. Four Siberian Snakes were chosen in the $(\frac{\pi}{4}0\frac{\pi}{4}0)6fs$ scheme. Some of the features of P_{lim} were already revealed by linearized spin–orbit motion in figures 2.15 and 3.10. At many higher–order resonances a strong reduction of $P_{\rm lim}$ does along with a strong variation of the amplitude dependent spin tune ν. Especially in the critical energy region where already linearized spin orbit motion in section 3.3 reveled very small P_{lim} due to a coherent spin perturbation in all regular FODO cells. Many higher–order resonances overlap in these critical energy regions of figure 4.1 (top). This goes along with spin tune jumps in figure 4.1 (bottom). The strongest spin tune jumps occur in the critical energy regions, mostly at the second order resonance $\nu = 2Q_y$ which is indicated by the top line [126]. Here only 6 flattening snakes were used and one might think that symmetrizing the ring by 2 additional flattening snakes in the West might reduce the spin tune spread and might lead to an increase of P_{lim}. But since the orbital phase advance between different sections of the ring is not matched by the snake angles in the standard snake schemes like $(\frac{\pi}{4}0\frac{\pi}{4}0)$, the symmetry recovered in the *8fs* scheme does not lead to a significant improvement. Moreover the special choice of the vertical betatron phase advance described in section 3.3.2 together with the $(\frac{\pi}{4}0\frac{\pi}{4}0)$ snake scheme does not lead to a significant improvement of P_{lim} and ν either as shown in figure 4.2. This is not surprising, since this vertical betatron phase advance was custom designed for a snake scheme $(0\frac{\pi}{2}\frac{\pi}{2}\frac{\pi}{2})8fs$.

P_{lim} and ν for higher–order spin dynamics in the snake–matched and phase–advance–matched HERA–p ring are shown in figure 4.3. While the overall behavior of P_{lim} over the complete acceleration range of HERA–p looks similar to the result obtained with linearized spin–orbit motion, which was displayed in figure 3.18, higher–order effects become very strong at high energies, especially in the vicinity of the critical energies where perturbations of spin motion in each FODO cell accumulate. The spin tune spread at momenta below 400GeV/c is small and higher–order effects seem to be benign even at these critical energies. A comparison with figures 4.1 and 4.2 shows that the special scheme obtained by matching orbital phases and snake angles would be a very good choice for HERA–p up to 300 or 400 GeV/c. For linearized spin–orbit motion, this snake–matched scheme does not produce a strong

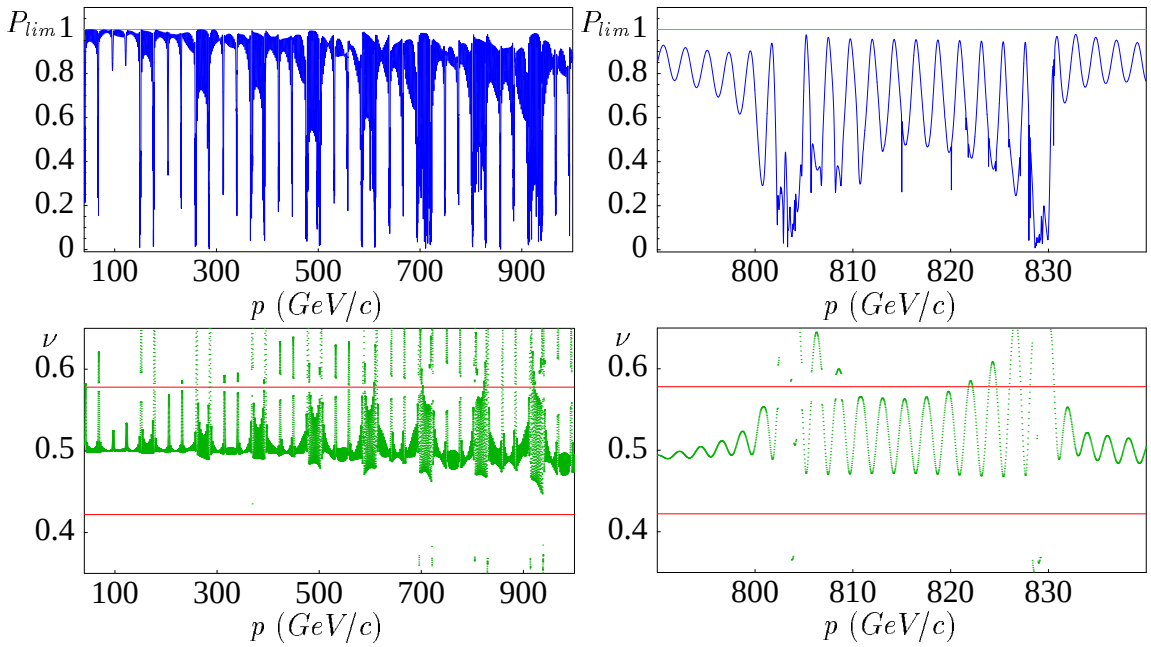

Figure 4.1: P_{lim} and ν for particles with a vertical amplitude corresponding to the 2.5σ emittance in the HERA–p luminosity upgrade lattice with the $(\frac{\pi}{4}0\frac{\pi}{4}0)6fs$ scheme. Top: The maximum time average polarization P_{lim} for the complete acceleration range (left) and for the critical energy range above 800GeV/c which has to be crossed when accelerating to the proposed storage energy of 870GeV/c. Bottom: the corresponding amplitude dependent spin tune $\nu(J_y)$. The second–order resonances $\nu = 2Q_y$ and $\nu = 1 - 2Q_y$ are indicated (red).

reduction of P_{lim} at any critical energy, but the higher–order effects become so dominant at the top energies of HERA–p, that this advantage does not survive. In fact, P_{lim} in figure 4.3 (top–left and middle) shows even more resonant drops than in the previous figures. For the amplitude dependent spin tune ν in figure 4.3 (bottom) an advantage survives however. It comes close to a second order resonance at fewer places and does not exhibit spin tune jumps which are as strong as those in the previous figures.

In this snake–matched scheme, the influence of higher–order effects can be seen very clearly, because the first–order effects have been matched to be very small. Unfortunately this analysis shows that completely snake matching the spin perturbations in the arcs of HERA-p with 4 Siberian Snakes is not advantageous for P_{lim}, since reductions of P_{lim} due to higher–order effects can be increased by this measure and dominate at high energies. Even around 300GeV/c there are resonant dips of P_{lim} in figure 4.3 (middle) but they are less pronounced than those in the previous figures so that the snake matched scheme should be very advantageous at these energies.

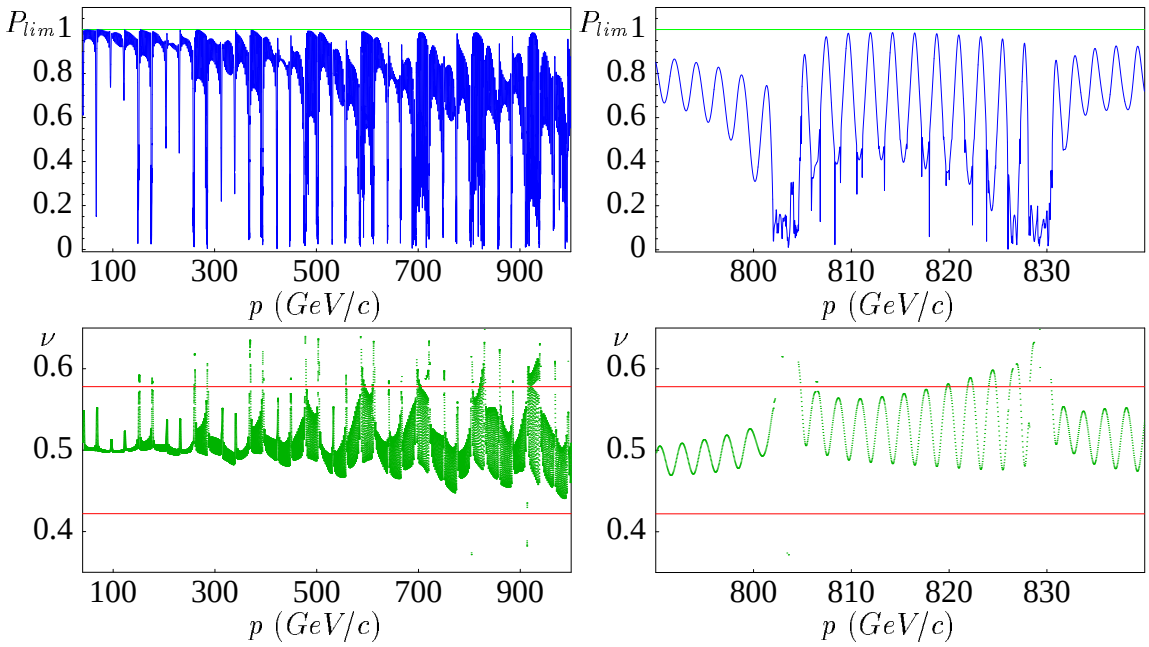

Figure 4.2: P_{lim} and ν for particles with a 2.5σ vertical amplitude in the HERA–p luminosity upgrade lattice after the betatron phase advance between opposite regular arc structures was adjusted to be an odd multiple of π. Together with the snake scheme $(0\frac{\pi}{2}\frac{\pi}{2}\frac{\pi}{2})$, this would lead to a cancelation of the perturbations of linearized spin–orbit motion produced by the arcs. But here results for the standard scheme $(\frac{\pi}{4}0\frac{\pi}{4}0)8fs$ are displayed. Top: The maximum time average polarization P_{lim} for the complete acceleration range (left) and for the critical energy range above 800GeV/c which has to be crossed when accelerating to the proposed storage energy of 870GeV/c. Bottom: the corresponding amplitude dependent spin tune $\nu(J_y)$. The second–order resonances $\nu = 2Q_y$ and $\nu = 1 - 2Q_y$ are indicated (red).

4.1.3 Filtering of Siberian Snake Schemes

When trying to optimize P_{lim} and the spin tune spread of ν one is therefore faced with two problems: The effect of linearized spin–orbit motion has to be minimized while the higher–order effects are not allowed to build up too strongly.

Since there are no analytical methods for comparing the higher–order effects of different snake schemes, an empirical computer algorithm for finding optimal snake schemes has been employed [100, 127].

The Filtering Algorithm

To find out which directions of the rotation axes of Siberian Snakes would be advantageous, the following automated filtering algorithm was introduced:

1. Determine a set of snake angles from which the best snake scheme should be chosen. Over 10^6 schemes were investigated.

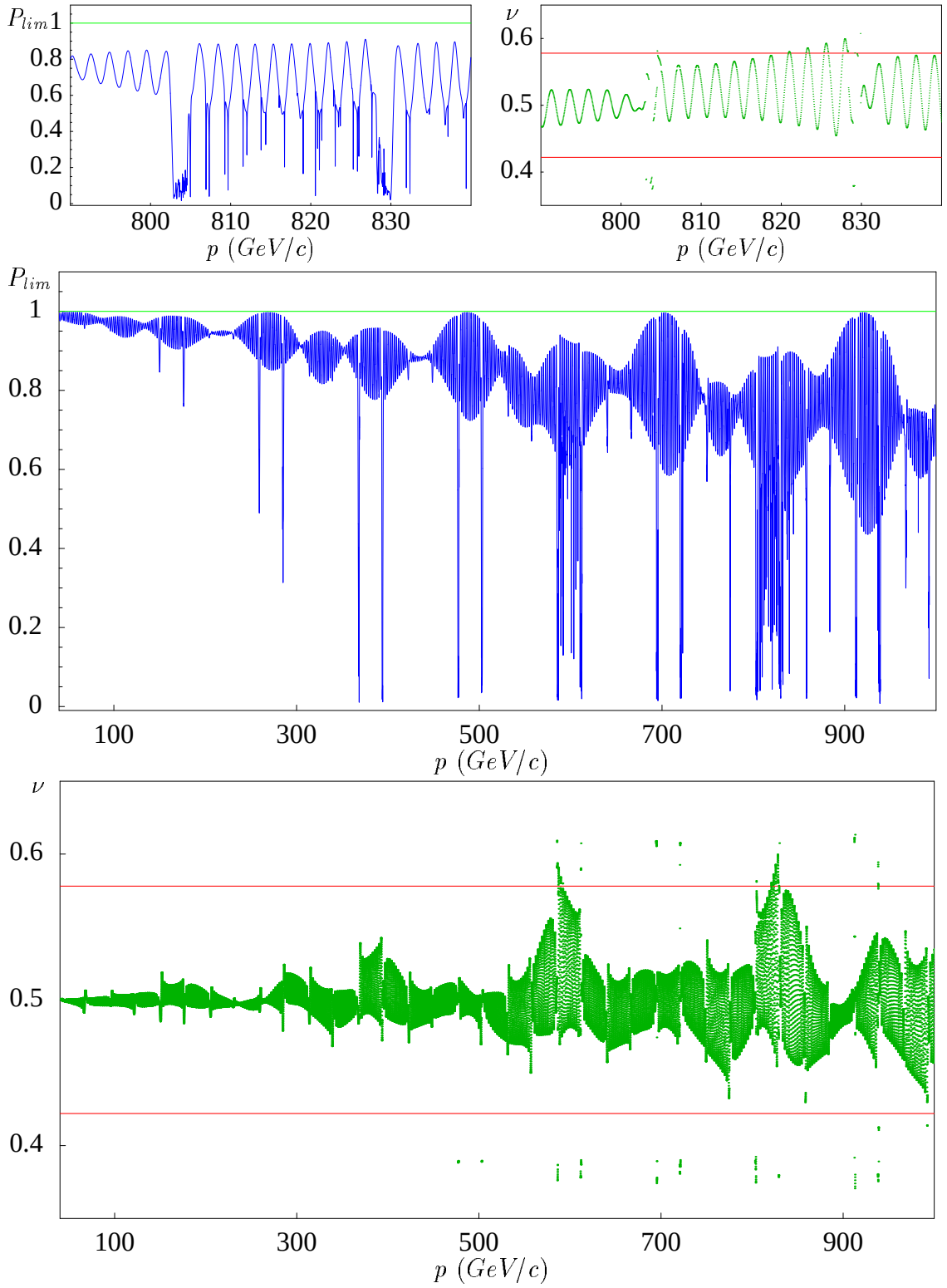

Figure 4.3: P_{lim} and ν a 2.5σ vertical amplitude after the betatron phase advance between opposite regular arc structures was adjusted to be an odd multiple of π. The $(0\frac{\pi}{2}\frac{\pi}{2}\frac{\pi}{2})8fs$ scheme is used. The resonances $\nu = 2Q_y$ and $\nu = 1 - 2Q_y$ are indicated (red).

2. Find all snake combinations for a flat ring which lead to a spin tune of $\nu_0 = \frac{1}{2}$. The requirement for these schemes is given below equation (2.75).

3. Allow only snake combinations with an even number of horizontal Siberian Snakes and therefore vertical $\vec{n}_0$. The use of type III snakes was also investigated [21, 128].

4. Compute the maximum time average polarization $< \vec{n} >$ over the whole energy range of HERA–p using linearized spin–orbit motion and filter on high average values of $P_{lim}^{(1)}$, the approximation of P_{lim} obtained by linearized spin–orbit motion.

5. For the most promising remaining snake schemes, i.e. those with the highest average $P_{lim}^{(1)}$, compute now P_{lim} and ν non–perturbatively for a vertical oscillation amplitude by the SODOM–2 method. I have usually used a 2.5σ vertical amplitude, which contains 95.6% of the beam if it has a Gaussian distribution in the vertical degree of freedom and all longitudinal and radial amplitudes are allowed. The snake scheme which leads to the smallest spin tune spread is then chosen for further analysis.

6. Use stroboscopic averaging, anti–damping, and spin–orbit tacking as described in the next sections for further analysis of the snake scheme.

The steps 1 to 4 of this filtering algorithm have been very efficiently automated in the code SPRINT [112, 100]. During the investigations the snake angle of each of the 4 snakes were allowed to vary in steps of 22.5°. During the filtering analysis in [21] it was found that type III snakes can be helpful and But for reasons already described below equation (3.58), type III snakes will no longer be considered here.

Also schemes with 8 snake were tested but for snake angles which are multiples of 45°. Schemes with 8 Siberian Snakes have been described in [80]. To put Siberian Snakes at the centers of the arcs of HERA–p would be very costly and therefore one should try to avoid schemes with more than 4 Siberian Snakes.

The most destructive energy range which has to be crossed to reach the proposed operation momentum of 870GeV/c is located between 800 and 835 GeV/c. This is due to the very strong resonances corresponding to $G\gamma\Delta_c = 17 \pm \Delta$ in figure 3.7. It should be noted that the result of filtering depends strongly on the energy range over which P_{lim} and the spread of ν are optimized. If one filters snake schemes for an energy range in which there is only one very strong resonance at which the spin phase advance and the orbit phase advance have the relation $-G\gamma\Delta_c \pm \Delta = N_{odd}$ of equation (3.34), then filtering will mostly compensate the perturbation described by the spin–orbit coupling integral responsible for this resonance, either I_y^+ or I_y^-, by adjusting the spin phase advance between sections appropriately. This can be seen in figure 4.4 (left), for which filtering had been performed in the momentum range from 790GeV/c to 820GeV/c. In figure 4.4 (bottom) one sees that for linearized spin–orbit motion the destructive influence of all very strong resonances due to $G\gamma\Delta_c + \Delta = N_{odd}$ have been strongly reduced over the whole of the HERA–p momentum range, while these effects for $G\gamma\Delta_c - \Delta = N_{odd}$ have been increased. Correspondingly,

filtering over an energy range from 820GeV/c to 850 GeV/c reduces the effects due to $G\gamma\Delta_c - \Delta = N_{odd}$ in figure 4.4 (right) while it does not lead to improvements at energies where $G\gamma\Delta_c + \Delta = N_{odd}$.

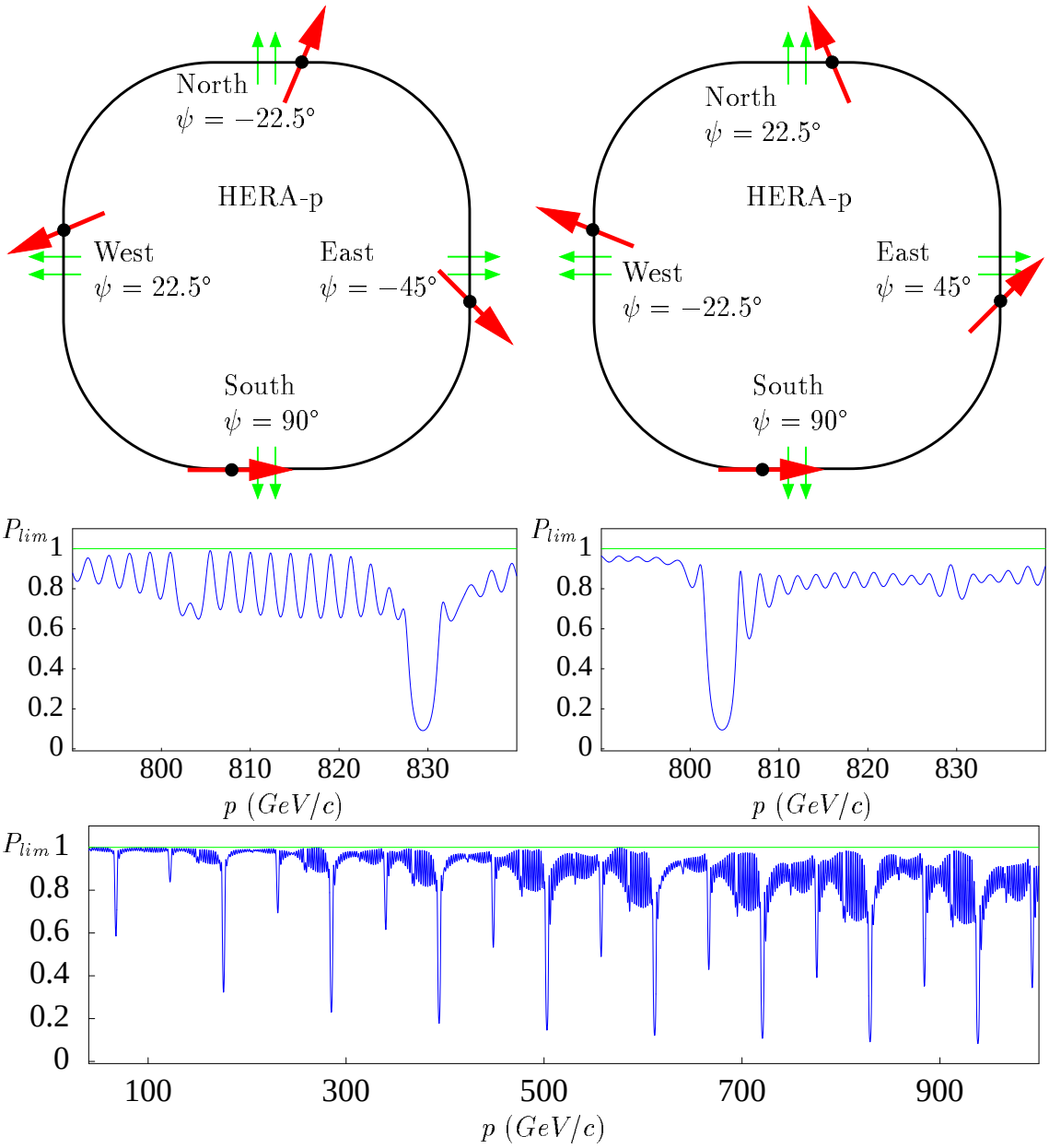

Figure 4.4: P_{lim} and ν for linearized spin motion of particles with a 2.5σ vertical amplitude in the HERA–p luminosity upgrade lattice after implementing filtered 4 snake schemes. Left: Snake angles (top) and P_{lim} (middle) for the snake scheme $(\frac{\pi}{2}\frac{\pi}{4}\frac{\pi}{8}\frac{7\pi}{8})8fs$ found by filtering the $6fs$ scheme in the momentum range from 790GeV/c to 820GeV/c. Right: The $(\frac{\pi}{2}\frac{3\pi}{4}\frac{7\pi}{8}\frac{\pi}{8})8fs$ scheme found by filtering for the energy range from 820GeV/c to 850GeV/c. Bottom: P_{lim} for the $(\frac{\pi}{2}\frac{\pi}{4}\frac{\pi}{8}\frac{7\pi}{8})8fs$ scheme for the complete momentum range.

Filtering therefore has to be performed over sufficiently large energy ranges. After a very efficient implementation of the filtering algorithm in the program SPRINT, filtering was performed for the complete energy range from 40GeV/c to 900GeV/c. Figure 4.5 shows P_{lim} and ν for the best snake schemes found for HERA–p with 6 flattening snakes and with 8 flattening snakes. While both snake schemes perform better than all the standard schemes, the tune spread is a bit smaller in the $8fs$ scheme where the ring is symmetrized by two flattening snakes in the West.

The best snake scheme found by filtering over the complete momentum range from 40 to 920GeV after HERA–p has been symmetrized by 8 flattening snakes is the $(\frac{3\pi}{4}\frac{3\pi}{8}\frac{3\pi}{8}\frac{\pi}{4})8fs$ scheme. P_{lim} and ν obtained with the SODOM–2 method for this scheme are shown in figure 4.6. Compared with the other snake schemes discussed so far, P_{lim} is high and ν has a remarkably small spread around the closed–orbit spin tune $\nu_0 = \frac{1}{2}$ for most energies. However, at the critical energies the spin tune spread is larger than in the snake matched scheme. In particular the small spread of ν is very favorable for polarized proton acceleration, since fever higher–order resonances will be crossed during acceleration. Since the loss of polarization at higher–order resonances can be described by a Froissart-Stora formula for every isolated higher–order resonance crossing as shown in section 2.2.11, the reduction of the spin tune spread can directly lead to less reduction of polarization during the acceleration cycle.

However, the full energy can only be reached by acceleration through the very strong residual resonance structures at around 804GeV/c and around 832GeV/c; and to find out whether the optimized snake schemes can lead to higher polarization at high energy than standard schemes, the process of acceleration through the critical energy regions has to be simulated by a tracking program.

4.1.4 A Note on Spin–Orbit Tracking

The comparison in section 4.1.2 of linearized spin–orbit motion and non–perturbative computations of $\vec{n}(\vec{z})$ for one degree of phase space motion has shown that more accurate simulations of spin dynamics in HERA are required. The more advanced methods which will be described in the following sections evaluate single particle spin–orbit tracking data to determine the invariant spin field and the amplitude dependent spin tune. Various methods of particle tracking have been developed for analyzing properties of particle optical devices in general [129, 130, 131, 132, 133, 134]. For proton storage rings, tracking methods for dynamic aperture and lifetime studies have been brought to a high level of sophistication [135, 136, 137, 138, 139, 140]. If Stern–Gerlach forces are neglected, the orbit motion is not influenced by the spin motion and these established techniques of symplectic particle tracking can be used. While these programs are normally used to analyzed stored beams, for the analysis of polarized proton motion the acceleration process is of particular importance [141].

Since here the average polarization of the beam is being investigated, and since that gets its main contribution from the core of the beam, spin–orbit motion in the tails of the beam does not have to be simulated very well. In fact, the sophisticated tools which were developed to analyze dynamic aperture and lifetime are custom

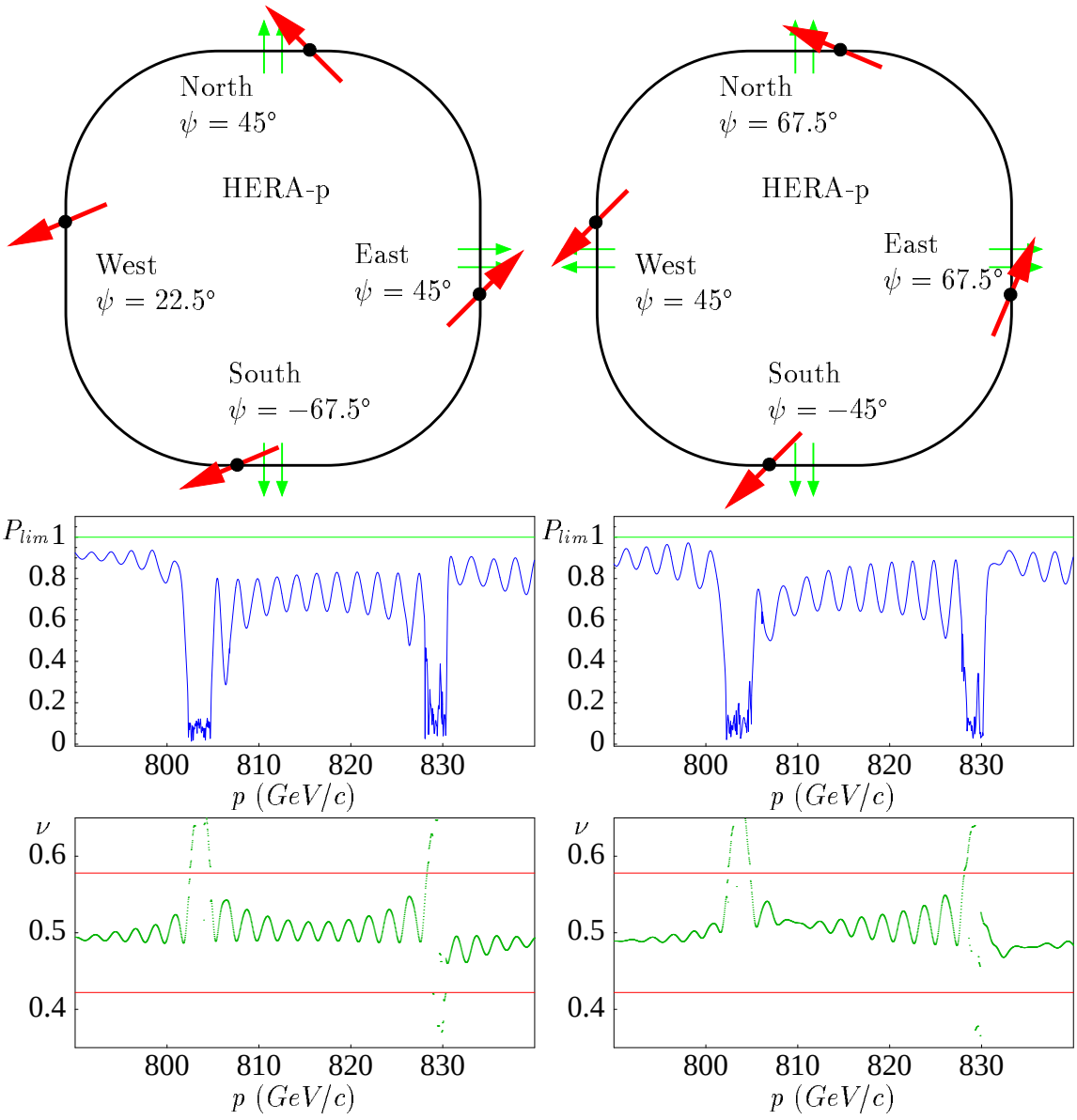

Figure 4.5: P_{lim} and ν of particles with a 2.5σ vertical amplitude in the HERA–p luminosity upgrade lattice after installation of the two best filtered schemes with 4 Siberian Snakes. Left: The snake angles (top) for the $(\frac{5\pi}{8}\frac{\pi}{4}\frac{\pi}{4}\frac{\pi}{8})6fs$ scheme found by filtering when 6 flattening snakes are given lead to a favorable P_{lim} (middle) and ν (bottom). Right: The best snake scheme found by filtering when HERA–p is symmetrized by 8 flattening snakes (top) is $(\frac{3\pi}{4}\frac{3\pi}{8}\frac{3\pi}{8}\frac{\pi}{4})8fs$ and leads on average to an even higher P_{lim} and to an even smaller spread of the amplitude dependent spin tune ν. The second–order resonances $\nu = 2Q_y$ and $\nu = 1 - 2Q_y$ are indicated (red).

designed for particle motion in the tails of the beam and are not necessary when the average beam polarization is studied.

In the HERA–p ring, the 1σ normalized emittances corresponding to one stan-

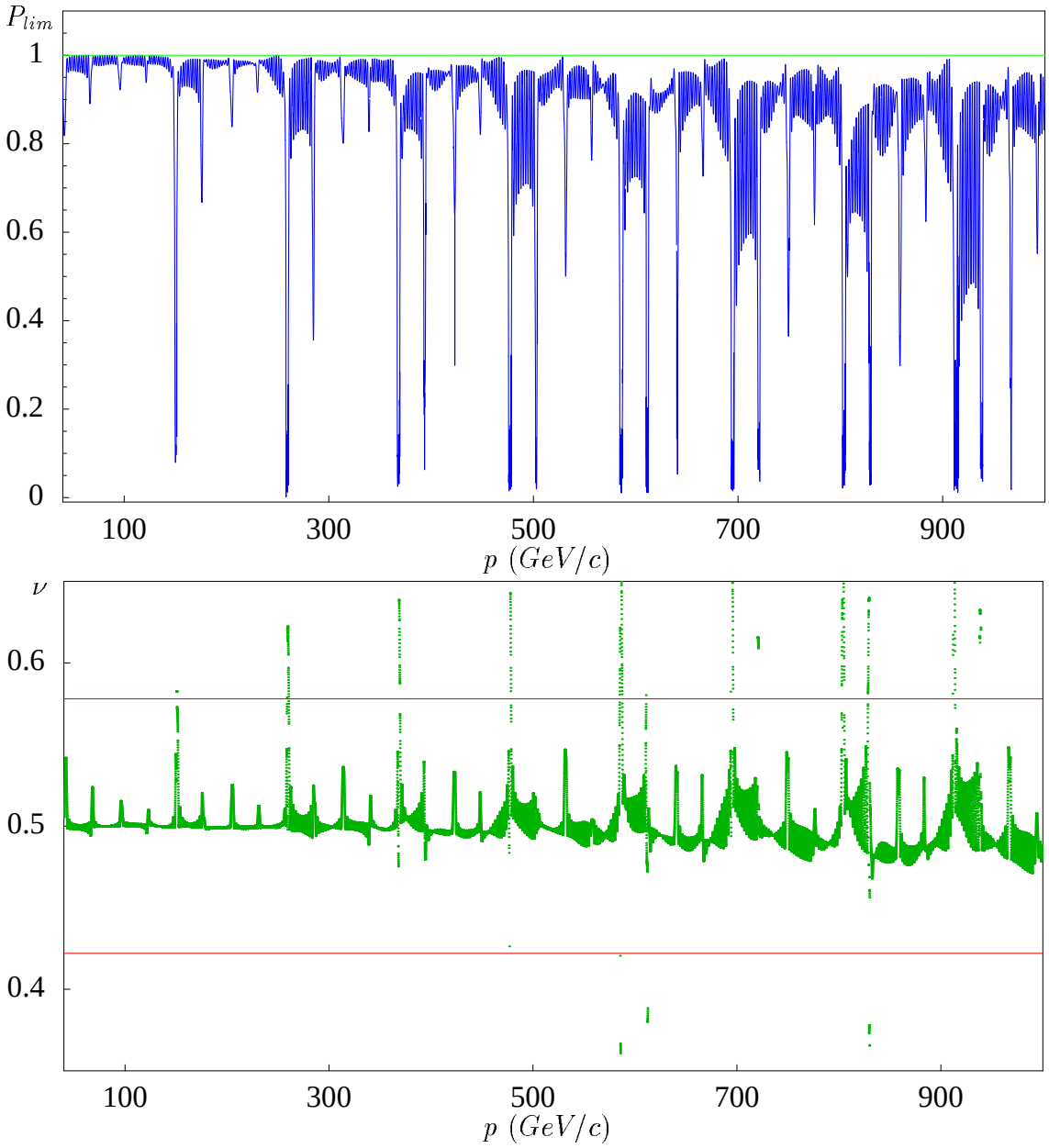

Figure 4.6: P_{lim} (top) and ν (bottom) for the $(\frac{3\pi}{4}\frac{3\pi}{8}\frac{3\pi}{8}\frac{\pi}{4})8fs$ Siberian Snake scheme. Together with the snake–matched scheme, this is the most promising scheme of Siberian Snakes found so far by the filtering algorithm. The second–order resonances $\nu = 2Q_y$ and $\nu = 1 - 2Q_y$ are indicated (red).

dard deviation of the beam size are typically approximately 4πmm mrad in the horizontal and vertical direction and around 17.5πmm rad in the longitudinal direction, which corresponds to 1σ values of $\delta = 1.1 \cdot 10^{-4}$ and $\tau = 16$cm.

For the linearized spin–orbit motion in chapter 3 and when analyzing higher–order effects in chapter 4 up to here, particles with a 2.5σ phase space amplitude were studied. For one degree of freedom, this amplitude contains 95.6% of the beam

if it has a Gaussian distribution and arbitrary phase space amplitudes in the other two degrees of freedom are allowed. One might argue that it would suffice to study smaller phase space amplitudes, since a loss of polarization for 4.4% of the beam can be tolerated. This view has not been adopted here, since (1) computational analysis of an accelerator should leave room for some imperfections in the description of the accelerator and (2) since the polarization can be reduced for particles at large phase space amplitudes in all three degrees of freedom, and only 87% of the particles in a Gaussian beam have phase space amplitudes below 2.5σ in all three degrees of freedom.

As explained in section 2.1, spin is most efficiently propagated along a particle's trajectory using quaternions. This is done by starting the following iterative procedure with an initial phase space point $\vec{z}_0$ at the entrance of the first optical element and with an initial spin transport quaternion of $A_0 = \underline{1}_2$:

$$\vec{z}_n = \vec{M}_n(\vec{z}_{n-1}) \ , \quad A_n = B_n(\vec{z}_{n-1})A_{n-1} \ , \tag{4.10}$$

where $\vec{M}_n(\vec{z})$ is the transport map for the phase space coordinates and $B_n(\vec{z}_{n-1})$ is the transport quaternion of the nth optical element.

Without beam–beam interaction, at 2.5σ the dynamics is often described well by linear phase space motion. Although nonlinear terms in the transport maps $\vec{M}_n(\vec{z})$ of the optical elements are not essential in the core of the beam, the nonlinear dependence of the spin transport quaternions $B_n(\vec{z})$ on phase space coordinates can be important. The spin transfer quaternion of the individual elements can be computed in a power expansion with respect to the phase space variables $\vec{z}$.

The equation of motion for the quaternion (2.36) has the form

$$\frac{d}{d\theta}\vec{A} = \underline{\Omega}(\vec{z}(\theta),\theta)\vec{A} \ , \tag{4.11}$$

where the antisymmetric 4×4 matrix $\underline{\Omega}$ is constructed from the precession vector $\vec{\Omega}$. The starting conditions are $\vec{z}(0) = \vec{z}_0$, $\vec{A} = (1,\vec{0})^T$. The quaternion $\vec{A}(\theta)$ depends on the initial phase space coordinates $\vec{z}_i$ and can be expanded in a Taylor series with respect to these coordinates. In the following I devise an iteration method for A_n, which is the Taylor expansion to order n of A [142].

The precession vector $\vec{\Omega}$ is split into its value on the design curve and its phase space dependent part as $\vec{\Omega}(\vec{z},\theta) = \vec{\Omega}^0(\theta) + \vec{\Omega}^{\geq 1}(\vec{z},\theta)$. The spin motion on the design curve is given by $\frac{d}{d\theta}\vec{A}_0(\theta) = \underline{\Omega}^0\vec{A}_0(\theta)$. Small phase space coordinates will create a rotation which differs little from $\vec{A}_0(\theta)$ and the phase space dependent rotation is written as a concatenation of $\vec{A}_0$ and the $\vec{z}_i$ dependent quaternion $(1+\delta,\vec{\delta})$ which reduces to the identity for $\vec{z}_i = 0$ since the aberrations δ and $\vec{\delta}$ vanish on the design curve. With equation (2.33) one obtains

$$\vec{A} = \underline{A}_0 \begin{pmatrix} 1+\delta \\ \vec{\delta} \end{pmatrix} \ . \tag{4.12}$$

The quaternion A is now inserted in the differential equation (4.11) to obtain

$$\frac{d}{d\theta}\underline{A}_0 \begin{pmatrix} 1+\delta \\ \vec{\delta} \end{pmatrix} + \underline{A}_0 \frac{d}{d\theta} \begin{pmatrix} 1+\delta \\ \vec{\delta} \end{pmatrix} = (\underline{\Omega}^0 + \underline{\Omega}^{\geq 1})\underline{A}_0 \begin{pmatrix} 1+\delta \\ \vec{\delta} \end{pmatrix} \ . \tag{4.13}$$

Taking into account the equation on the design curve and the fact that $\underline{A}_0^T$ describes the inverse rotation of $\underline{A}_0$, one obtains

$$\frac{d}{d\theta}\begin{pmatrix}\delta\\ \vec{\delta}\end{pmatrix} = \underline{\tilde{\Omega}}(\vec{z},\theta)\begin{pmatrix}1+\delta\\ \vec{\delta}\end{pmatrix}\ , \tag{4.14}$$

with $\underline{\tilde{\Omega}} = \underline{A}_0^T\underline{\Omega}^{\geq 1}\underline{A}_0$. Writing the Taylor expansion of $(\delta,\vec{\delta})$ to order n in $\vec{z}_i$ as $(\delta_n,\vec{\delta}_n)$, one finally obtains the iteration equation

$$\begin{pmatrix}\delta_n\\ \vec{\delta}_n\end{pmatrix} =_n \int_0^\theta \underline{\tilde{\Omega}}(\vec{z}_n(\tilde{\theta}),\tilde{\theta})\begin{pmatrix}1+\delta_{n-1}\\ \vec{\delta}_{n-1}\end{pmatrix}d\tilde{\theta}\ ,\quad \begin{pmatrix}\delta_0\\ \vec{\delta}_0\end{pmatrix} = 0\ , \tag{4.15}$$

where $=_n$ describes the equivalence up to order n. The first order of this iteration method was used for the spin transport in the program SPRINT [112, 100] and was evaluated up to second order using MATHEMATICA in [143, 144]. These second–order quaternions are ready to be used for an analysis of nonlinear spin aberrations of individual optical elements. The Taylor coefficients of δ and $\vec{\delta}$ are the spin aberration coefficients. The aberrations are not fully independent but they are related by the equation $(1+\delta)^2 + \vec{\delta}^2 = 1$.

The iteration equation shows that in every iteration order of equation (4.15), $\underline{\tilde{\Omega}}$ is multiplied once. This matrix contains terms which are linear in $G\gamma$, due to the transverse field components in the T–BMT equation (2.5). The matrix $\underline{\tilde{\Omega}}$ additionally contains nonlinear parts in $\vec{z}_i$ due to nonlinear fields which make $\vec{\Omega}(\vec{z},\theta)$ a nonlinear function of $\vec{z}$ and due to the nonlinear phase space motion, which makes $\vec{z}$ itself a nonlinear function of $\vec{z}_i$. After separating the first–order part, $\underline{\tilde{\Omega}} = \underline{\tilde{\Omega}}^1 + \underline{\tilde{\Omega}}^{\geq 2}$, one can observe that the first–order part contributes n times to δ_n, leading to terms of $(G\gamma)^n$. The higher–order terms of $\underline{\tilde{\Omega}}^{\geq 2}$ contribute to aberrations of order n already after fewer iterations and therefore lead to smaller powers in $G\gamma$. For large values of $G\gamma = 1756$ in the case of HERA–p, this observation explains why nonlinear phase space motion and the contribution of nonlinear fields to $\vec{\Omega}$ are not very important when computing the spin-transport quaternion of individual elements. For all the spin–orbit tracking presented here, the higher–order spin motion in the linear fields of $\underline{\tilde{\Omega}}^1$ was included.

4.1.5 Polarization Reduction During Acceleration

It has been observed in section 3.2 that the non–flat regions lead to significant spin perturbations. In fact, when simulating HERA–p without non–flat regions, the destructive spin tune jumps at second order resonances disappear completely. To reduce these perturbations, the East region of HERA–p will now be simulated as flat since the HERMES experiment located in this region does not require that the proton beam is on the level of the electron beam.

When a particle is accelerated across the critical momentum region from 800 to 806GeV/c with a typical acceleration speed of 50keV per turn, the adiabatic invariance of $J_S = \vec{n}\cdot\vec{S}$ can be violated and the level of violation will depend on the

orbital amplitude and the snake scheme. This violation is illustrated in the graphs in figure 4.7 which, for three different snake schemes, show the average spin action $\bar{J}_S$ for three particles at 806GeV/c which had initially $J_S = 1$ at 800GeV/c before they were accelerated.

The change of J_S in the critical energy region depends on the initial phase space angle so that if J_S had been computed only for one particle, it could by chance have had an angle variable for which J_S does not change although it would have changed for other points with the same vertical phase space amplitude. To avoid that J_S seems to be invariant due to such a chance effect, three particles were accelerated and the average $\bar{J}_S$ is displayed in figure 4.7.

At small phase space amplitudes, J_S is nearly invariant and therefore $\bar{J}_S = 1$. For each of the three snake schemes, there is a phase space amplitude J_{ymax} above which $\bar{J}_S < 1$ and the regions of the beam with an amplitude above J_{ymax} lead to a reduction of the beam's polarization during the acceleration process.

For the standard snake scheme $(0\frac{\pi}{4}0\frac{\pi}{4})4fs$, only the part of the beam with less than 1πmm mrad vertical amplitude can remain polarized. For the filtered scheme $(\frac{3\pi}{4}\frac{3\pi}{8}\frac{3\pi}{8}\frac{\pi}{4})8fs$, phase space amplitudes up to 4πmm mrad are allowed. Finally the snake matched scheme has the most stabilizing effect for spin motion and figure 4.7 shows that vertical amplitudes of up to 8πmm mrad are allowed. This shows that

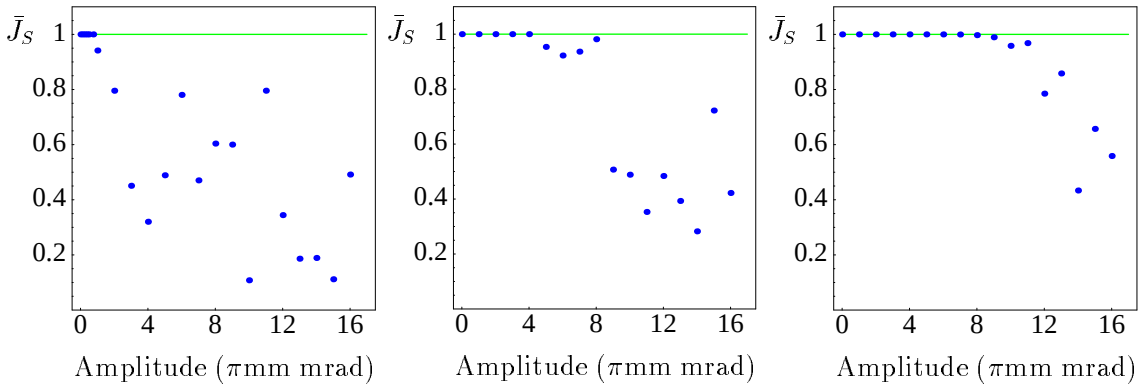

Figure 4.7: The average spin action $\bar{J}_S$ of 3 particles at 806GeV for particles starting with $J_S = 1$ at 800GeV/c for three different snake schemes. Left: $(0\frac{\pi}{4}0\frac{\pi}{4})4fs$, Middle: $(\frac{3\pi}{4}\frac{3\pi}{8}\frac{3\pi}{8}\frac{\pi}{4})8fs$, Right: $(\frac{\pi}{4}0\frac{\pi}{4}\frac{\pi}{4})8fs$ scheme. Particles with an amplitude above 1 (left), 4 (middle), and 8 (right) lead to a reduction of polarization when the beam is accelerated through this critical energy region.

the snake matched scheme is superior to the other four–snake schemes studied so far. It stabilizes spin motion for 10 times larger phase space amplitudes than some other snake schemes. Nevertheless, 8πmm mrad is not enough to allow high polarization at top energies in HERA–p.

I have performed two different snake matches for eight–snake schemes. Snake matching eight–snake schemes for rings with super–periodicity 4 has been illustrated in figure 3.16. Since HERA–p has no super–periodicity, the snake matching has to be modified in a way similar to that for four–snake schemes in section 3.3.3. This

snake match leads to very high P_{lim} and to a very small spin tune spread. But to demonstrate that it is possible to further stabilize spin motion in HERA–p by such schemes, figure 4.8 shows the vertical phase space amplitudes for which J_S remains invariant. The more effective of the two snake scheme stabilizes spin motion up to a vertical amplitude of 14πmm mrad.

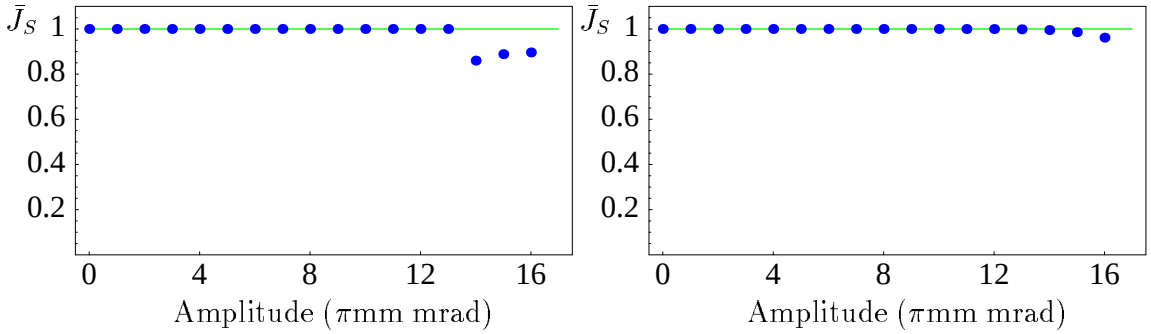

Figure 4.8: The average spin action $\bar{J}_S$ at 806GeV for particles which started with $J_S = 1$ at 800GeV/c for 2 different snake matched eight–snake schemes. Particles with an amplitude above 13 (left) and 14 (right) lead to a reduction of polarization when the beam is accelerated through this critical energy region.

These results for the various snake schemes are collected in figure 4.9, where it becomes clear that snake matching either with 4 or with 8 snakes leads to a significant improvement. But it follows from the discussion in section 4.1.4 that it does not suffice to avoid a reduction of J_S for particles with less than 14πmm mrad amplitude. It would therefore be very helpful to use electron cooling in PETRA [145, 146, 147, 148] so as to reduce the emittance in HERA–p and to allow for an acceleration without loss of polarization for most particles in the beam.

These results show that a simple formula for the number of snakes which are required for a given accelerator cannot be given since different snake schemes lead to very different stability of spin motion.

Such a formula has been sought using the following very simple argument: the Siberian Snakes should dominate the spin precession produced by closed orbit distortions and betatron oscillations. The resonance strength [103] ϵ_κ is a measure for that precession and is shown in figure 3.5 for 1σ vertical betatron oscillations in HERA–p. Then one obtains the rule of thumb that the number of snakes has to be sufficiently larger than $5\epsilon_\kappa$ [149]. This would lead to more than 4 Siberian Snakes in HERA–p. However, it has become apparent that the efficiency of four–snake schemes depends very much on the snake angles of the individual snakes [21]. Furthermore it has been shown that 8 snakes are not necessarily better than 4 snakes for the non–flat HERA–p ring [80]. But if eight–snake schemes are spin–matched, they can produce a significantly larger P_{lim}, reduce the fluctuation of P_{lim} and ν with energy, reduce the overlapping of resonances in the critical regions, and ultimately enable the polarization of particles with larger phase space amplitudes be preserved during the acceleration process.

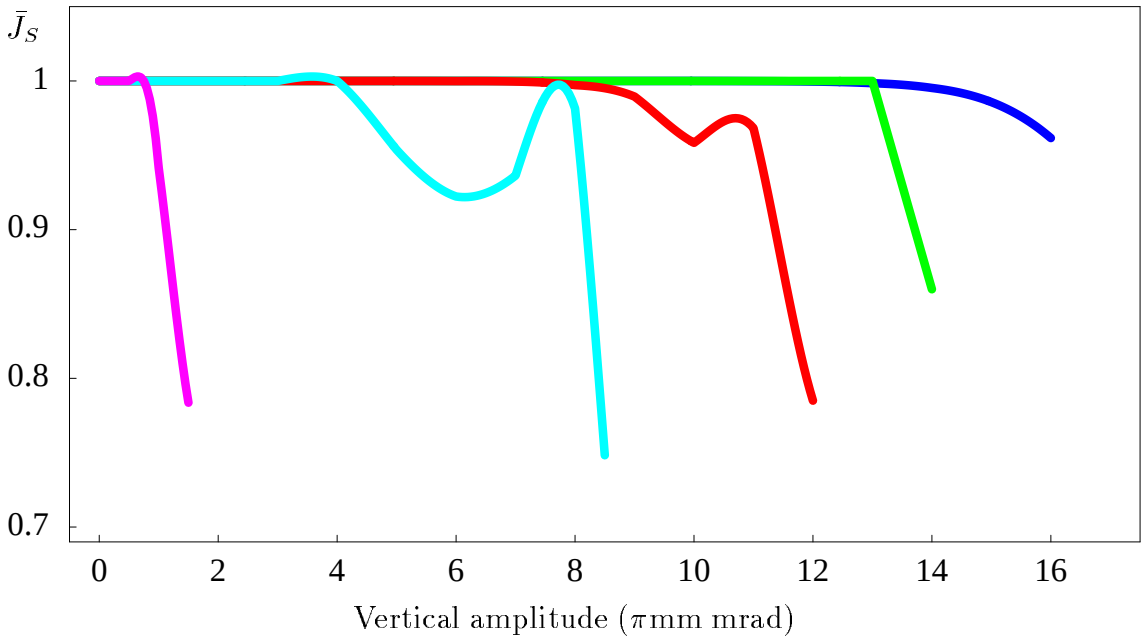

Figure 4.9: The average spin action $\bar{J}_S$ at 806GeV for particles which started initially with $J_S = 1$ at 800GeV/c. Violet: The standard scheme which stabilizes spin motion for particles within 1πmm mrad, Cyan: the filtered four–snake scheme stabilizes 4πmm mrad, Red: the snake–matched four–snake scheme stabilizes 8πmm mrad, Green: the snake-matched eight–snake scheme which stabilizes 13πmm mrad, Blue: and the snake–matched eight–snake scheme which stabilizes 14πmm mrad of vertical phase space amplitude.

4.2 Obtaining $\vec{n}(\vec{z})$ by Stroboscopic Averaging

For linearized spin–orbit motion in flat rings, there is no effect of radial and longitudinal motion on spin dynamics. But it has been observed [123, 27, 80] that these degrees of freedom become important around critical energies when higher–order spin dynamics is taken into account. The SODOM–2 algorithm has been used to analyze vertical motion in optimized snake schemes in section 4.1.3. For one degree of freedom, the use of 83 Fourier coefficients has turned out to be sufficient for amplitudes of up to 2.5σ in HERA–p. For more degrees of freedom, this algorithm requires an extremely large number of Fourier coefficients and then needs large amounts of computing power. For such cases, the following algorithm [100] provides an efficient way to compute an $\vec{n}$–axis for all three degrees of freedom.

Consider a particle beam with a spin field $\vec{f}(\vec{z}, \theta)$. Its initial spin field in the Poincaré section at θ_0 is $\vec{f}_0(\vec{z}) = \vec{f}(\vec{z}, \theta_0)$. In section 2.2.8, it was shown that the time average polarization at a phase space point $\vec{z}_0$ in that Poincaré section has no component perpendicular to the invariant spin field if this field exists. The time averaged polarization is therefore either zero or parallel to $\vec{n}(\vec{z}_0)$. This knowledge can be used to compute the invariant spin field. The infinite sum involved in the

time average polarization at $\vec{z}(\theta_0) = \vec{z}_0$ can be approximated by a sum over N turns,

$$\begin{aligned} \{\vec{f}\}(\vec{z}_0, \theta_0) &\approx \{\vec{f}\}_N(\vec{z}_0, \theta_0) = \frac{1}{N+1} \sum_{j=0}^{N} \vec{f}(\vec{z}_0, \theta_0 + 2\pi j) \\ &= \frac{1}{N+1} \sum_{j=0}^{N} \underline{R}(\vec{z}(\theta_0 - 2\pi j), \theta_0 - 2\pi j; \theta_0) \vec{f}_0(\vec{z}(\theta_0 - 2\pi j)) \ . \end{aligned} \tag{4.16}$$

If $|\{\vec{f}\}_N|$ does not vanish, this yields the following approximation of the $\vec{n}$–axis:

$$\vec{n}(\vec{z}_0, \theta_0) \approx \frac{\{\vec{f}\}_N(\vec{z}_0, \theta_0)}{|\{\vec{f}\}_N(\vec{z}_0, \theta_0)|} \ . \tag{4.17}$$

This method of computing an $\vec{n}$–axis is called stroboscopic averaging [100].

For ease of computation, usually the special choice for the initial spin field is $\vec{f}_0(\vec{z}) = \vec{n}_0$ at azimuth θ_0 and one can simplify $\{\vec{f}\}_N$ to

$$\{\vec{f}\}_N(\vec{z}_0, \theta_0) = \frac{1}{N+1} \sum_{j=0}^{N} \underline{R}(\vec{z}(\theta_0 - 2\pi j), \theta_0 - 2\pi j; \theta_0) \vec{n}_0(\theta_0) \ . \tag{4.18}$$

Equations (4.16) and (4.17) define an algorithm for obtaining an $\vec{n}$–axis. The following two kinds of pathologies can occur:

1. The $\vec{n}$–axis is not unique: if the proposed algorithm converges, then the result could depend on the choice of $\vec{f}_0(\vec{z})$.

2. The stroboscopic average $\{\vec{f}\}_N$ vanishes for $N \to +\infty$ or the sequence in equation (4.16) does not converge.

Both pathologies can be studied with the algorithm. The first situation occurs when the spin tune is in resonance with the orbit tunes and therefore the $\vec{n}$–axis is not unique, as described in section 2.2.7. In almost all examples studied so far, the stroboscopic average seems to converge, implying the existence of a spin field which satisfies the periodicity equation (2.79) to high accuracy. The second case is not only problematic computationally but describes a beam with no polarization usable for experiments. In such a beam the time average polarization is zero and there is little average polarization available for particle physics experiments during most of the approximately 2 billion turns for which protons are typically stored in HERA–p.

In equation (4.18), one can see that the only information needed from tracking is the set of the $N+1$ phase space points $\vec{z}(\theta_0), \vec{z}(\theta_0 - 2\pi), \ldots, \vec{z}(\theta_0 - 2\pi N)$ and the N matrices $\underline{R}(\vec{z}(\theta_0 - 2\pi), \theta_0 - 2\pi; \theta_0), \underline{R}(\vec{z}(\theta_0 - 4\pi), \theta_0 - 4\pi; \theta_0), \ldots, \underline{R}(\vec{z}(\theta_0 - 2\pi N), \theta_0 - 2\pi N; \theta_0)$. Each matrix is a product of one turn spin transport matrices $\underline{R}(\vec{z}, \theta_0; \theta_0 + 2\pi)$ and describes the spin transport for a particle which finally arrives at $\vec{z}_0$.

Since only knowledge of spin and phase space coordinates at θ_0 are required, one can reformulate the algorithm in terms of one turn maps $\vec{M}$ with which $\vec{z}(\theta_0 + 2\pi) = \vec{M}(\vec{z}(\theta_0))$ and one turn spin transport matrices $\underline{R}(\vec{z})$ with $\vec{S}(\theta_0 + 2\pi) =$

$\underline{R}(\vec{z}(\theta_0))\vec{S}(\theta_0)$. All other quantities which depend on θ are also taken at the specified azimuth θ_0. For simplification, this azimuth is not indicated in the following. In terms of the one turn map, the periodicity condition for the invariant spin field

$$\underline{R}(\vec{z})\vec{n}(\vec{z}) = \vec{n}(\vec{M}(\vec{z})) \tag{4.19}$$

has already been stated in equation (2.79). Using the one turn map and the one turn spin transport matrix, the stroboscopic average of equation (4.18) is written as

$$\{\vec{f}\}_N(\vec{z}_0, \theta_0) = \frac{1}{N+1} \sum_{j=0}^{N} \prod_{k=1}^{j} \underline{R}(\vec{M}^{-k}(\vec{z}_0))\vec{n}_0 \ . \tag{4.20}$$

Here the convention $\prod_{k=1}^{0} \underline{R} = \underline{1}$ is used and $\prod_{k=1}^{j} \underline{R}(\vec{M}^{-k}(\vec{z}_0))$ is taken to mean the following order of multiplication: $\underline{R}(\vec{M}^{-1}(\vec{z}_0)) \ldots \underline{R}(\vec{M}^{-j}(\vec{z}_0))$.

The following algorithm shows how an $\vec{n}$–axis at $\vec{z}_0$ and θ_0 can be obtained by evaluating this formula in the case of linear orbit motion:

1. Compute the linearized one turn phase space transport matrix with $\vec{z}(\theta_0 + 2\pi) = \underline{M}\vec{z}(\theta_0)$.

2. Compute the set of $N+1$ phase space points

$$C = \{\vec{c}_j = (\underline{M}^{-1})^j \vec{z}_0 | j \in \{0, \ldots, N\}\} \ . \tag{4.21}$$

3. Compute the rotation matrix $\underline{R}(\vec{z}_{c.o.})$ which describes the one turn spin motion starting at θ_0 for particles on the closed orbit $\vec{z}_{c.o.}(\theta)$ and extract the corresponding rotation vector $\vec{n}_0$.

4. Starting with a spin parallel to $\vec{n}_0$ at every phase space point in C, track until the phase space point $\vec{z}_0$ is reached. For a given j this requires tracking j turns starting at $\vec{c}_j$.

5. Compute the set of spin tracking results as

$$B = \{\vec{b}_0(\vec{z}_0) = \vec{n}_0, \vec{b}_j(\vec{z}_0) = \underline{R}(\vec{c}_1) \ldots \underline{R}(\vec{c}_j)\vec{n}_0 | j \in \{1, \ldots, N\}\} \ . \tag{4.22}$$

6. Compute the average of the elements in B, $\vec{S}_N(\vec{z}_0) = \frac{1}{N+1} \sum_{j=0}^{N} \vec{b}_j(\vec{z}_0)$ and for $|\vec{S}_N| \neq 0$ compute $\vec{n}_N = \vec{S}_N / |\vec{S}_N|$.

The vector $\vec{S}_N(\vec{z}_0)$ is equivalent to $\{\vec{f}\}_N(\vec{z}_0, \theta_0)$ in equation 4.16, if the initial distribution of spins is given by $\vec{n}_0$ as in the equations (4.18) and (4.20).

4.2.1 Convergence properties

The average $\vec{S}_N$ has been defined by

$$\vec{S}_N(\vec{z}_0) = \frac{1}{N+1} \sum_{j=0}^{N} \prod_{k=1}^{j} \underline{R}(\vec{c}_k)\vec{n}_0 \ . \tag{4.23}$$

To check how well $\vec{S}_N$ satisfies the same periodicity condition (4.19) as that for the $\vec{n}$–axis, one can calculate

$$\begin{aligned}
\vec{S}_N(\underline{M}\vec{z}_0) &= \frac{1}{N+1}\sum_{j=0}^{N}\prod_{k=1}^{j}\underline{R}(\vec{c}_{k-1})\vec{n}_0 \\
&= \frac{1}{N+1}(\vec{n}_0+\sum_{j=0}^{N-1}\prod_{k=0}^{j}\underline{R}(\vec{c}_k)\vec{n}_0)\ , \qquad (4.24)\\
\underline{R}(\vec{z}_0)\vec{S}_N(\vec{z}_0) &= \frac{1}{N+1}\sum_{j=0}^{N}\prod_{k=0}^{j}\underline{R}(\vec{c}_k)\vec{n}_0\ , \qquad (4.25)\\
\underline{R}(\vec{z}_0)\vec{S}_N(\vec{z}_0)-\vec{S}_N(\underline{M}\vec{z}_0) &= \frac{1}{N+1}(\underline{R}(\vec{z}_0)\vec{b}_N(\vec{z}_0)-\vec{n}_0) \\
&= \frac{1}{N+1}(\vec{b}_{N+1}(\underline{M}\vec{z}_0)-\vec{n}_0). \qquad (4.26)
\end{aligned}$$

For large N, the error becomes arbitrarily small. But this does not yet establish the accuracy to which the approximation $\vec{n}_N$ of the $\vec{n}$–axis satisfies the periodicity condition. To derive this accuracy, it is assumed that the angles between $\vec{n}_0$ and the vectors $\vec{b}_j(\vec{z}_0)$ are smaller than some positive number $\xi<\pi/2$ for all $j\in\{1,\ldots,N+1\}$. As shown in figure 4.10, the length $|\vec{b}_{N+1}(\underline{M}\vec{z}_0)-\vec{n}_0|$ is then smaller than $2\sin(\xi/2)$. The length of $\vec{S}_N$ is at least $\cos(\xi)$; and here it becomes essential that there is a limit of $\pi/2$ on the angle ξ. The approximation $\vec{n}_N$ of the $\vec{n}$–axis then satisfies the periodicity condition to the following accuracy:

$$\begin{aligned}
\Delta_N &= |\underline{R}(\vec{z}_0)\vec{n}_N(\vec{z}_0)-\vec{n}_N(\underline{M}\vec{z}_0)| = \left|\underline{R}(\vec{z}_0)\frac{\vec{S}_N(\vec{z}_0)}{|\vec{S}_N(\vec{z}_0)|}-\frac{\vec{S}_N(\underline{M}\vec{z}_0)}{|\vec{S}_N(\underline{M}\vec{z}_0)|}\right| \\
&= \frac{1}{|\vec{S}_N(\vec{z}_0)|}\left|\underline{R}(\vec{z}_0)\vec{S}_N(\vec{z}_0)-\vec{S}_N(\underline{M}\vec{z}_0)+\frac{|\vec{S}_N(\underline{M}\vec{z}_0)|-|\vec{S}_N(\vec{z}_0)|}{|\vec{S}_N(\underline{M}\vec{z}_0)|}\vec{S}_N(\underline{M}\vec{z}_0)\right| \\
&\le \frac{1}{|\vec{S}_N(\vec{z}_0)|}(|\underline{R}(\vec{z}_0)\vec{S}_N(\vec{z}_0)-\vec{S}_N(\underline{M}\vec{z}_0)|+||\underline{R}(\vec{z}_0)\vec{S}_N(\vec{z}_0)|-|\vec{S}_N(\underline{M}\vec{z}_0)||) \\
&\le \frac{2}{|\vec{S}_N(\vec{z}_0)|}|\underline{R}(\vec{z}_0)\vec{S}_N(\vec{z}_0)-\vec{S}_N(\underline{M}\vec{z}_0)| \le \frac{4\sin(\xi/2)}{(N+1)\cos(\xi)}\ . \qquad (4.27)
\end{aligned}$$

The error Δ_N by which the vector $\vec{n}_N(\vec{z}_0)$ violates the periodicity condition (4.19) of the $\vec{n}$–axis is therefore smaller than $2\sec(\xi/2)\tan(\xi)/(N+1)$ and converges to 0 for large N.

If one can prove the existence of a suitable number $\xi<\pi/2$ for some spin transport system, then $\vec{n}_N$ satisfies the periodicity condition (4.19) for the $\vec{n}$–axis up to an error which is smaller than or equal to $2\sec(\xi/2)\tan(\xi)/(N+1)$. Since evaluating B by equation 4.22 requires tracking $T=(N+1)N/2$ turns, the accuracy is bounded by $\sqrt{2/T}\sec(\xi/2)\tan(\xi)$. This slow convergence with the square root of T is a very serious limitation and in the next section it will be demonstrated how the rate of convergence can be considerably improved.

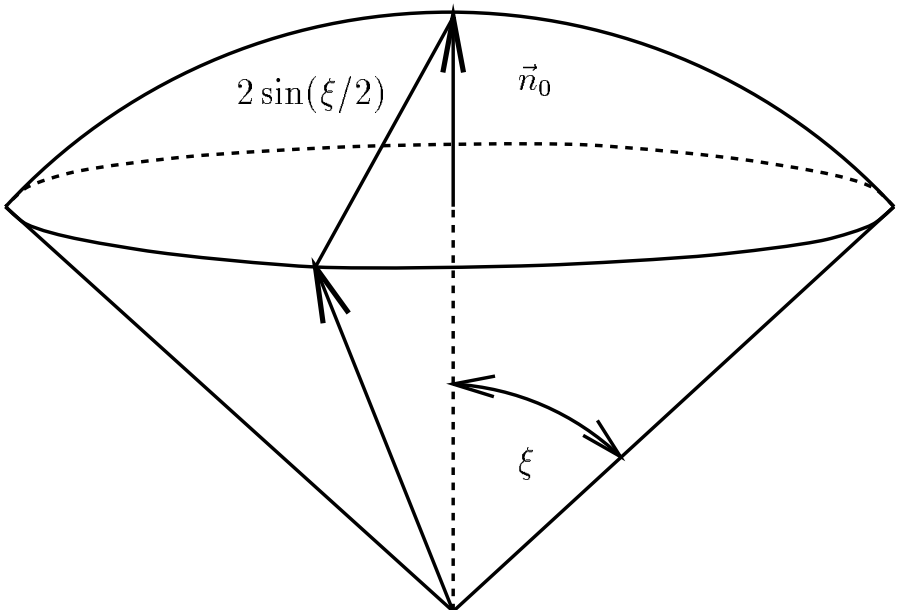

Figure 4.10: Estimation of convergence speed. To guarantee convergence of the stroboscopic average, the angle ξ between the direction of $\vec{n}_0$ and the transported spins has to stay below $\pi/2$.

Having shown that Δ_n converges to 0 linearly with $1/N$, it is interesting to see how $\vec{n}_N$ converges to the $\vec{n}$–axis, if an invariant spin field exists. The following derivation is very similar to that in section 2.2.8 which established that the time average polarization is parallel to $\vec{n}(\vec{z})$. It will be assumed that the phase space motion can be described in terms of action–angle variables and that the motion is strongly non–orbit–resonant and non–spin–orbit–resonant according to the sections 2.2.7 and 2.2.8. The stroboscopic average is now performed in the coordinate system $(\vec{u}_1, \vec{u}_2, \vec{n})$ which has been introduced in section 2.2.7 and in which one writes $\vec{S}_N = s_{N,1}\vec{u}_1 + s_{N,2}\vec{u}_2 + s_{N,3}\vec{n}$. First the tracking points $\vec{c}_j$ are established. Note that the amplitude dependent spin tune $\nu(\vec{J}) = \nu(\vec{c}_j)$ is the same for all tracking points since the action variable $\vec{J}$ is an invariant of motion. In the coordinate system $(\vec{u}_1, \vec{u}_2, \vec{n})$, the vector components of the 2π periodic spin $\vec{n}_0$ on the closed orbit are not constant but depend on the phase space position. This vector is transported from the phase space points $\vec{c}_j$ to $\vec{z}_0 \hat{=} (\vec{\Phi}, \vec{J})$ by the rotation matrix

$$\begin{pmatrix} \cos(j2\pi\nu) & -\sin(j2\pi\nu) & 0 \\ \sin(j2\pi\nu) & \cos(j2\pi\nu) & 0 \\ 0 & 0 & 1 \end{pmatrix} , \tag{4.28}$$

leading to the stroboscopic average

$$\vec{S}_N = \frac{1}{N+1} \sum_{j=0}^{N} \begin{pmatrix} \cos(j2\pi\nu) & -\sin(j2\pi\nu) & 0 \\ \sin(j2\pi\nu) & \cos(j2\pi\nu) & 0 \\ 0 & 0 & 1 \end{pmatrix} \begin{pmatrix} n_{0,1}(\vec{\Phi} - j2\pi\vec{Q}) \\ n_{0,2}(\vec{\Phi} - j2\pi\vec{Q}) \\ n_{0,3}(\vec{\Phi} - j2\pi\vec{Q}) \end{pmatrix} . \tag{4.29}$$

Here the dependence of $\vec{n}_0$ on $\vec{\Phi}$ in the coordinate system $[\vec{u}_1, \vec{u}_2, \vec{n}]$ is explicitly indicated. The dependence on $\vec{J}$ is not indicated since the action variables are constant during the particle tracking. The third component of $\vec{S}_N$ is $\sum_{j=0}^{N} \frac{1}{N+1} n_{0,3}(\vec{\Phi} - j2\pi\vec{Q})$, the first and second components in complex notation are

$$\hat{s}_N = s_{N,1} + is_{N,2} = \frac{1}{N+1} \sum_{j=0}^{N} e^{i(j2\pi\nu)} \hat{n}_0(\vec{\Phi} - j2\pi\vec{Q}) \ , \tag{4.30}$$

where $\hat{n}_0(\vec{\Phi}) = n_{0,1}(\vec{\Phi}) + in_{0,2}(\vec{\Phi})$. In terms of the Fourier components $\breve{n}_0(\vec{k})$ of $\hat{n}_0(\vec{\Phi})$ one obtains the inequality

$$\begin{aligned} |\hat{s}_N| &= \left| \frac{1}{N+1} \sum_{j=0}^{N} e^{ij2\pi(\nu - \vec{k}\cdot\vec{Q})} \sum_{\vec{k}} \breve{n}_0(\vec{k}) e^{i\vec{k}\cdot\vec{\Phi}} \right| \\ &= \frac{1}{N+1} \left| \sum_{\vec{k}} \frac{1 - e^{i(N+1)2\pi(\nu - \vec{k}\cdot\vec{Q})}}{1 - e^{i2\pi(\nu - \vec{k}\cdot\vec{Q})}} \breve{n}_0(\vec{k}) e^{i\vec{k}\cdot\vec{\Phi}} \right| \\ &\leq \frac{1}{N+1} \sum_{\vec{k}} \frac{2}{|1 - e^{i2\pi(\nu - \vec{k}\cdot\vec{Q})}|} |\breve{n}_0(\vec{k})| \ . \end{aligned} \tag{4.31}$$

If the components of $\vec{n}_0$ in the coordinate system $[\vec{u}_1, \vec{u}_2, \vec{n}]$ have an analytic extension in $\vec{\Phi}$, then the sum over $\vec{k}$ is finite due to the assumed strong non–spin–orbit–resonance as has been explained after equation (2.96). Therefore $\hat{s}_N$ converges to 0 linearly with $1/N$. Similarly one obtains the third component of $\vec{S}_N$ as

$$s_{N,3} = \breve{n}_{0,3}(0) + \frac{1}{N+1} \sum_{\vec{k} \neq 0} \frac{1 - e^{-i(N+1)2\pi\vec{k}\cdot\vec{Q}}}{1 - e^{-i2\pi\vec{k}\cdot\vec{Q}}} \breve{n}_{0,3}(\vec{k}) e^{i\vec{k}\cdot\vec{\Phi}} \ , \tag{4.32}$$

were the sum over $\vec{k}$ is finite due to the assumed strong non–orbit–resonance. Therefore $s_{N,3}$ converges to $\breve{n}_{0,3}(0)$ linearly with $1/N$. Here this equation has been re derived for clarity, although it can be obtained directly by setting $f(\vec{z}) = \vec{n}_0$ in equation (2.97). Since $|\vec{S}_N| > \cos(\xi)$ and $\xi < \pi/2$, it is guaranteed that $\vec{S}_N$ does not converge to 0 and therefore $\breve{n}_{0,3}$ does not vanish. Together with the convergence of $\vec{S}_N$ the convergence of $\vec{n}_N$ to either $\vec{n}$ or $-\vec{n}$ follows from

$$\begin{aligned} \mathrm{Min}(|\vec{n}_N \pm \vec{n}|^2) &= \mathrm{Min}\left(\left| \frac{\vec{S}_N}{|\vec{S}_N|} \pm \vec{n} \right|^2 \right) = (1 - \frac{|s_{N,3}|}{|\vec{S}_N|})^2 + (\frac{|\hat{s}_N|}{|\vec{S}_N|})^2 = 2\frac{|\vec{S}_N| - |s_{N,3}|}{|\vec{S}_N|} \\ &< 2\frac{|\vec{S}_N| - |s_{N,3}|}{|s_{N,3}|} = 2(\sqrt{1 + (\frac{|\hat{s}_N|}{|s_{N,3}|})^2} - 1) < 2(\frac{|\hat{s}_N|}{|s_{N,3}|})^2 \ . \end{aligned} \tag{4.33}$$

There is a number N^* such that the absolute value of the N dependent part of $s_{N,3}$ in equation (4.32) is smaller than $\breve{n}_{0,3}(0)/2$. Taking this number of turns N to be bigger than N^*, one finds

$$|\vec{n}_N - \vec{n}| < 2\sqrt{2} \frac{|\hat{s}_N|}{|n_{0,3}(0)|} \tag{4.34}$$

which, together with equation (4.31) finally establishes that $\vec{n}_N$ converges to $\vec{n}$ linearly with $1/N$.

4.2.2 An Algorithm with Faster Convergence

In the previous section, an algorithm was introduced which converged linearly with the inverse square root of the number T of turns tracked. However, it is possible to obtain convergence linear with $1/T$, when one takes advantage of the orthogonality of the spin transport matrix. To illustrate this, again an algorithm is established.

1. Compute $C = \{\vec{c}_j = (\underline{M}^{-1})^j \vec{z}_0 | j \in \{0, \ldots, N\}\}$ as before.

2. Define three orthogonal spins $\{\vec{e}^{(1)}, \vec{e}^{(2)}, \vec{e}^{(3)}\}$.

3. Obtain the sets S_j of the three vectors $\vec{S}_j^{(1)}$, $\vec{S}_j^{(2)}$, and $\vec{S}_j^{(3)}$ by tracking the $\vec{e}^{(k)}$ for $N - j$ turns
$$\vec{S}_j^{(k)} = \underline{R}(\vec{c}_{j+1}) \ldots \underline{R}(\vec{c}_N)\vec{e}^{(k)} \ . \tag{4.35}$$

4. From the set of vectors S_j and the set S_0, one can obtain the spin transport matrix from the phase space point $\vec{c}_j$ to $\vec{z}_0$ denoted by $\bar{\underline{R}}(\vec{c}_j)$. This becomes clear when one realizes that $\vec{S}_0^{(k)} = \bar{\underline{R}}(\vec{c}_j)\vec{S}_j^{(k)}$ for all k. Obtaining these $N + 1$ transport matrices requires the propagation of 3 spins around the circular accelerator for N turns.

5. Now the set $B = \{\bar{\underline{R}}(\vec{c}_j)\vec{n}_0 | j \in \{0, \ldots, N\}\}$ can be computed, which is identical to the set denoted by B in the previous section.

6. The normalized average of B, denoted by $\vec{n}_N$, can now again be computed.

In this approach one only has to track three initial spin directions over N turns, leading to $T = 3N$. The error is therefore bounded by $6 \sec(\xi/2) \tan(\xi)/T$. This implies convergence linear with one over the number T of turns tracked. The following example illustrates the speed of this method: when the angle ξ happens to be 45°, and an accuracy at the 10^{-3} level is required, this linear convergence approach only requires 6500 tracking turns; when the angle ξ is small, fewer iterations are needed.

Backward Tracking

In the two algorithms mentioned above, one needs to find the set C of $N + 1$ backwards tracked phase space points, and then launch spins at these points and track forward so as to compute the set B. In the case of linear motion, it is trivial to obtain these backward tracked phase space points. One simply transforms $\vec{z}_0$ into the action–angle variables of the linear motion and determines the phase advance per turn of the linear motion. Counting back these phase advances and transforming the action–angle variables back into phase space leads to the points $\vec{c}_j$. In the case of nonlinear motion, one would actually in addition have to to track for N turns backwards around the ring.

In the case of the linearly convergent method, this extra effort becomes unnecessary. One can start with the phase space point $\vec{z}_0$ and launch three particles with

spins along $\vec{e}^{(1)}$, $\vec{e}^{(2)}$, and $\vec{e}^{(3)}$. Tracking backward in azimuth defines the $N+1$ sets P_j of the spins $\vec{p}_j^{(1)}$, $\vec{p}_j^{(2)}$, and $\vec{p}_j^{(3)}$ with

$$\vec{p}_j^{(k)} = \underline{R}^T(\vec{c}_j) \ldots \underline{R}^T(\vec{c}_1)\vec{e}^{(k)} \ , \tag{4.36}$$

where advantage is taken of the fact that transposition leads to the inverse of the orthogonal matrices. From the sets P_j and $\{\vec{e}^{(1)}, \vec{e}^{(2)}, \vec{e}^{(3)}\}$ one can again compute the spin transport matrix $\underline{\bar{R}}(\vec{c}_j)$ and with these matrices one obtains the set B with the elements $\vec{b}_j = \underline{\bar{R}}(\vec{c}_j)\vec{n}_0$, which again leads to $\vec{n}_N$ by averaging.

Forward Tracking

There is an even more fundamental problem in the case of nonlinear motion than the computation time. When the lattice or the effect of separate nonlinear elements are computed by nonlinear transport maps, the inverses of these maps might not be known. In this case the required phase space points $\vec{c}_j$ cannot be computed at all. Nevertheless the vector $\vec{n}_N$ can be obtained as follows. The arguments of the section on backward tracking can simply be repeated for tracking forward. One establishes the phase space points $\vec{c}_j = \vec{M}(\vec{c}_{j-1})$ with $\vec{c}_0 = \vec{z}_0$ for $j \in \{1, \ldots, N\}$ and simultaneously the sets S_j by tracking the three unit vectors $\vec{S}_{j-1}^{(k)}$ for one turn with $\vec{S}_0^{(k)} = \vec{e}^{(k)}$. As in the fourth step of the previous algorithm, one can then obtain the spin transport matrix $\underline{\bar{R}}(\vec{c}_j)$ from the phase space point $\vec{z}_0$ to $\vec{c}_j$. The inverse of this transport matrix is simply obtained by transposition leading to the vectors $\vec{b}_j = \underline{\bar{R}}(\vec{c}_j)^T\vec{n}_0$. The normalized average of the vectors $\vec{b}_j$ is then the stroboscopic average $\vec{n}_{inv,N}$ of the inverse motion. For this average the error of the periodicity condition for the inverse motion converges linearly to zero. Fortunately, an $\vec{n}$–axis of the inverse motion $\vec{n}_{inv}(\vec{z})$ is also an $\vec{n}$–axis of the forward motion, since the periodicity condition of the inverse motion is

$$\underline{R}^{-1}(\vec{M}^{-1}(\vec{z}))\vec{n}_{inv}(\vec{z}) = \vec{n}_{inv}(\vec{M}^{-1}(\vec{z})) \ . \tag{4.37}$$

That this leads to the periodicity condition (4.19) of the forward motion for $\vec{n}_{inv}$ can be shown by inserting $\vec{M}(\vec{z})$ for $\vec{z}$ and subsequent multiplication with $\underline{R}(\vec{z})$.

4.2.3 Stoboscopic Average of Linearized Spin–Orbit Motion

In this section, linearized spin–orbit motion is considered as a way to illustrate and to confirm the chief features of stoboscopic averaging. As in equation 3.1, the complex coordinate α is used to describe a spin's components perpendicular to the rotation axis $\vec{n}_0$ for the closed orbit,

$$\vec{S} = \mathrm{Re}\{\alpha\}\vec{m}(\theta) + \mathrm{Im}\{\alpha\}\vec{l}(\theta) + \sqrt{1-|\alpha|^2}\vec{n}_0(\theta) \ . \tag{4.38}$$

The coordinate α is propagated from θ_0 once around the ring by the complex vector $\vec{G}$ which was introduced in equation (3.3),

$$\alpha_{j+1} = \vec{G} \cdot \vec{z}_j + e^{i2\pi\nu_0}\alpha_j \ . \tag{4.39}$$

The complex coordinate of $\vec{n}_0$ is $\alpha = 0$, so that propagating this initial spin at a phase space point $\vec{z}_0$ for j times around the ring leads to the final complex spin component

$$\alpha_j = \sum_{k=1}^{j} e^{i(k-1)2\pi\nu_0} \vec{G} \cdot (\underline{M}^{-k} \vec{z}_0) \ . \tag{4.40}$$

With the column matrix $\underline{A}^{-1}$ of the eigenvectors of the 6×6 dimensional one turn matrix $\underline{M}$, this reduces to

$$\begin{aligned} \alpha_j &= \sum_{k=1}^{j} e^{i(k-1)2\pi\nu_0} \vec{G} \cdot [\underline{A}^{-1} \mathrm{diag}(e^{\mp ik2\pi Q_l}) \underline{A} \vec{z}_0] \\ &= \sum_{k=1}^{j} e^{-i2\pi\nu_0} \vec{G} \cdot [\underline{A}^{-1} \mathrm{diag}(e^{ik2\pi(\nu_0 \mp Q_l)}) \underline{A} \vec{z}_0] \\ &= e^{-i2\pi\nu_0} \vec{G} \cdot [\underline{A}^{-1} \mathrm{diag}(\frac{e^{i2\pi(\nu_0 \mp Q_l)} - e^{i(j+1)2\pi(\nu_0 \mp Q_l)}}{1 - e^{i2\pi(\nu_0 \mp Q_l)}}) \underline{A} \vec{z}_0] \ . \end{aligned} \tag{4.41}$$

The N–turn stroboscopic average of α for linearized spin–orbit motion is given by

$$\begin{aligned} \{\alpha\}_N(\vec{z}_0) &= \frac{1}{N} \sum_{j=1}^{N} \alpha_j \qquad (4.42) \\ &= e^{-i2\pi\nu_0} \vec{G} \cdot [\underline{A}^{-1} \mathrm{diag}(\frac{e^{i2\pi(\nu_0 \mp Q_l)}}{1 - e^{i2\pi(\nu_0 \mp Q_l)}}) \underline{A} \vec{z}_0] (1 - \frac{1}{N} \sum_{j=1}^{N} e^{i(j+1)2\pi(\nu_0 \mp Q_l)}) \ . \end{aligned}$$

For large $N \to \infty$, the fluctuating term averages to small values. With equation (3.15) this leads to $\lim_{N\to\infty} \{\alpha\}_N(\vec{z}_0) = \vec{B} \cdot (\underline{A} \vec{z}_0)$ which agrees with the $\vec{n}$–axis α_n in equation (3.11). For large N, the error $|\{\alpha\}_N - \alpha_n|$ converges to zero linearly with $1/N$ if there are no spin–orbit resonances with $\nu_0 = \pm Q_l$. Equation (4.42) shows that the convergence becomes very slow close to first–order spin–orbit resonances.

4.2.4 Stroboscopic Averaging for the SRM

In order to illustrate which quantities can be computed and how effective stroboscopic averaging can be in numerical computations, it is applied to the single resonance model, where the $\vec{n}$–axis has been derived in equation (2.118) to be

$$\vec{n}(\Phi) = \mathrm{sig}(\delta) \frac{1}{\Lambda} \begin{pmatrix} \epsilon_\kappa \cos\Phi \\ \epsilon_\kappa \sin\Phi \\ \delta \end{pmatrix} \ , \quad \Lambda = \sqrt{\delta^2 + \epsilon_\kappa^2} \ , \quad \delta = \nu_0 - \kappa \ . \tag{4.43}$$

If Λ is not an integer, some tedious manipulations lead to [100]

$$|\vec{n}_N(\Phi, J) - \vec{n}(\Phi, J)| = \sqrt{2}\sqrt{1 - \tau_N} \ , \tag{4.44}$$

$$\tau_{N-1} = [1 + (\frac{\epsilon_\kappa}{N\delta})^2 \frac{1 - \cos(N2\pi\Lambda)}{1 - \cos(2\pi\Lambda)}]^{-1/2} \ . \tag{4.45}$$

One sees that $|\vec{n}_N - \vec{n}|$ is an oscillating function of the resonance strength ϵ_κ and therefore of the orbital amplitude J. The local maxima of $|\vec{n}_N - \vec{n}|$ increase with J, reflecting the fact that large orbital amplitudes reduce the convergence speed. This behavior is plotted in figure 4.11 (top). For all graphs in figure 4.11, the parameters $\nu_0 = 0.3$, $\kappa = 0.23$, and $\Phi = 0.32$ were used. For large N, equations (4.44) and (4.45) predict that the convergence is indeed linear with $1/N$, as illustrated by the slope of -1 in figure 4.11 (middle). Also one sees that $|\vec{n}_N - \vec{n}|$ vanishes for integer values of $N\Lambda$ if Λ is not also an integer. For integer values of Λ, one has

$$\tau_N = \sqrt{1 + (\frac{\epsilon_\kappa}{\delta})^2} = \frac{\Lambda}{|\delta|} \ . \tag{4.46}$$

Therefore in this case $\vec{n}_N$ does not converge to $\vec{n}$. This is no surprise since an integer Λ amounts to the resonance condition $\nu(\vec{J}) + j_0 = 0$ which leads to a non–uniqueness of the $\vec{n}$–axis.

Figure 4.11 (bottom) shows $P_{lim} = \delta/\sqrt{\delta^2 + \epsilon_\kappa^2}$ as a function of the resonance strength (blue curve). Even for N as small as 20, stroboscopic averaging is quite accurate (red points).

4.2.5 Stroboscopic Averaging for HERA–p

In a realistic accelerator, the existence of the $\vec{n}$–axis cannot be guaranteed, but an approximately invariant spin field can be found, if the series $\vec{n}_N$ converges. To indicate the convergence of this series, $|\vec{n}_N - \vec{n}_{20000}|$ is plotted for the phase space point with $y_i = 0.4$mm and $y_i' = 0$ in the East interaction region for the current HERA–p lattice. This corresponds to a vertical amplitude of 69πmm mrad and is therefore a particle at approximately 4σ of the beam distribution. The slope of -1 in the double logarithmic scale of figure 4.12 illustrates clearly that the convergence is linear with $1/N$.

For particles which oscillate only in the kth degree of freedom in phase space, one can easily check that the stroboscopic average $\vec{n}_N$ is a good approximation to an invariant spin field. The phase space points $\vec{z}_j$ in the Poincaré section at θ_0 obtained by tracking a particle with initial phase space coordinates $\vec{z}_0$ for many turns are all on the curve with constant J_k, which is referred to as invariant ellipse. Here this curve is parameterized as $\vec{z}(\varphi)$ with $\varphi \in [0, 2\pi)$. The vectors $\vec{n}(\vec{z}_j)$ are also all on a closed curve which is given by $\vec{n}(\vec{z}(\vec{\varphi}))$. Such closed curves on the unit sphere are invariant curves of spin–orbit motion since these curves are mapped on themselves under the one turn spin–orbit transport.

In order for $\vec{n}_N$ to approximate an $\vec{n}$–axis, the tracked spins $\vec{S}_j$ for $\vec{S}_0 = \vec{n}_N(\vec{z}_0)$ also have to lie approximately on a closed curve on the unit sphere. If the spin of a particle initially has an angle $\vartheta > 0$ with respect to the invariant spin field, the tracked spins would not all be located on a one–parametric closed curve but would wobble around this curve since the angle between the spin and the $\vec{n}$–axis is a constant of motion.

The pictures in figure 4.13 show invariant curves $\vec{n}(\vec{z}(\varphi))$ on the unit sphere for the East interaction point of the current HERA–p lattice at 820GeV/c. The left

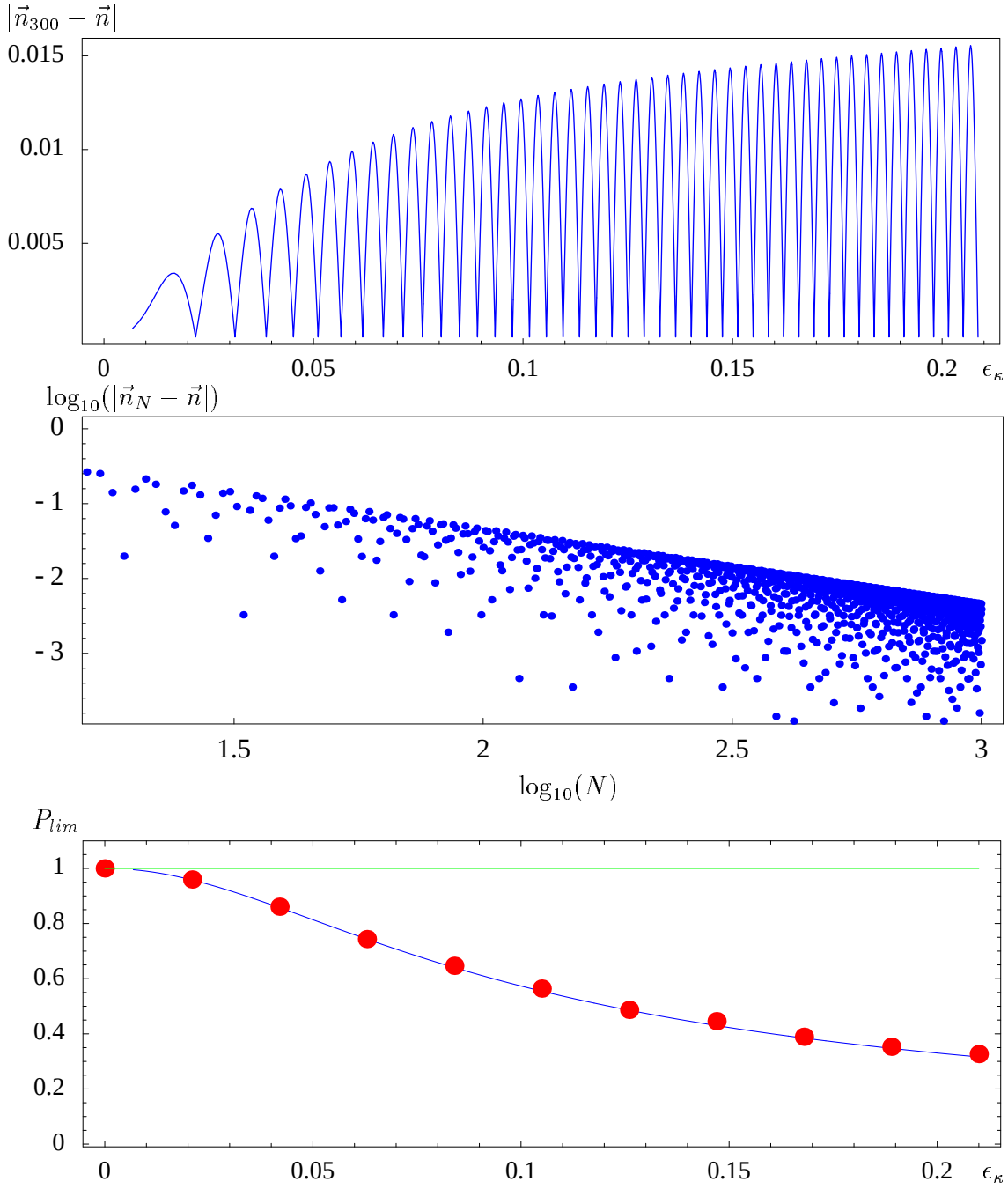

Figure 4.11: All three graphs refer to the SRM with $\kappa = 0.29$, $\nu_0 = 0.36$. The deviation of the stroboscopic average $\vec{n}_N$ from the analytically calculated $\vec{n}$ is shown as a function of ϵ_κ for $N = 300$ (top) and as a function of N for $\epsilon_\kappa = 0.2$ (middle). Bottom: P_{lim} computed by stroboscopic averaging with $N = 20$ (green points) and the analytically calculated P_{lim} (blue curve).

curve was obtained before, and the right curve after, the introduction of 4 Siberian Snakes [21] into the accelerator. Here the standard scheme $(0\frac{\pi}{2}00)fs6$ was used. It can clearly be seen that stroboscopic averaging yielded the $\vec{n}$–axis accurately and

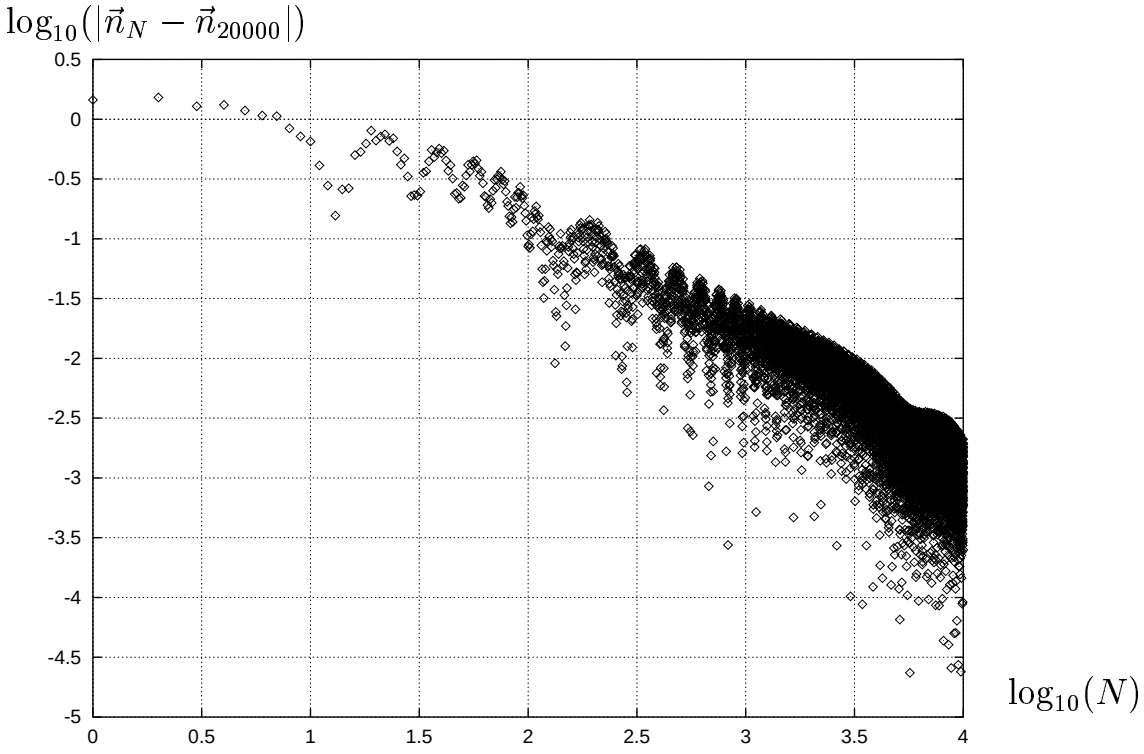

Figure 4.12: The accuracy $|\vec{n}_N - \vec{n}_{20000}|$, where the $\vec{n}$–axis was computed at the the East interaction point of the current HERA–p lattice. The slope of -1 in the double logarithmic scale illustrates that the convergence of $|\vec{n}_N - \vec{n}|$ is linear with $1/N$.

that the variation of the $\vec{n}$–axis over the invariant torus is strongly reduced when Siberian Snakes are used, leading to a $P_{lim} =< \vec{n} >$ which is close to 1.

Distorted Invariants of Spin Motion

For the single resonance model, the $\vec{n}$–axis is given by equation (2.118) as

$$\vec{n}(\Phi) = \mathrm{sig}(\delta)\frac{1}{\Lambda}\begin{pmatrix} \epsilon_\kappa \cos\Phi \\ \epsilon_\kappa \sin\Phi \\ \delta \end{pmatrix} \quad , \quad \Lambda = \sqrt{\delta^2 + \epsilon_\kappa^2} \; . \tag{4.47}$$

The invariant curves $\vec{n}(\Phi)$ are therefore circles on the unit sphere. For linearized spin–orbit motion in the kth degree of freedom, the $\vec{n}$–axis is given by equation (3.27) as

$$\alpha_n = \sqrt{J_k}(B_k^+ e^{i\Phi_k} + B_k^- e^{-i\Phi_k}) \; . \tag{4.48}$$

The real and imaginary part of α_n is therefore a linear combination of trigonometric functions. This can be described by some 2×2 dimensional matrix $\underline{B}$,

$$\begin{pmatrix} \mathrm{Re}\{\alpha_n\} \\ \mathrm{Im}\{\alpha_n\} \end{pmatrix} = \underline{B}\begin{pmatrix} \sin\Phi_k \\ \cos\Phi_k \end{pmatrix} \; , \tag{4.49}$$

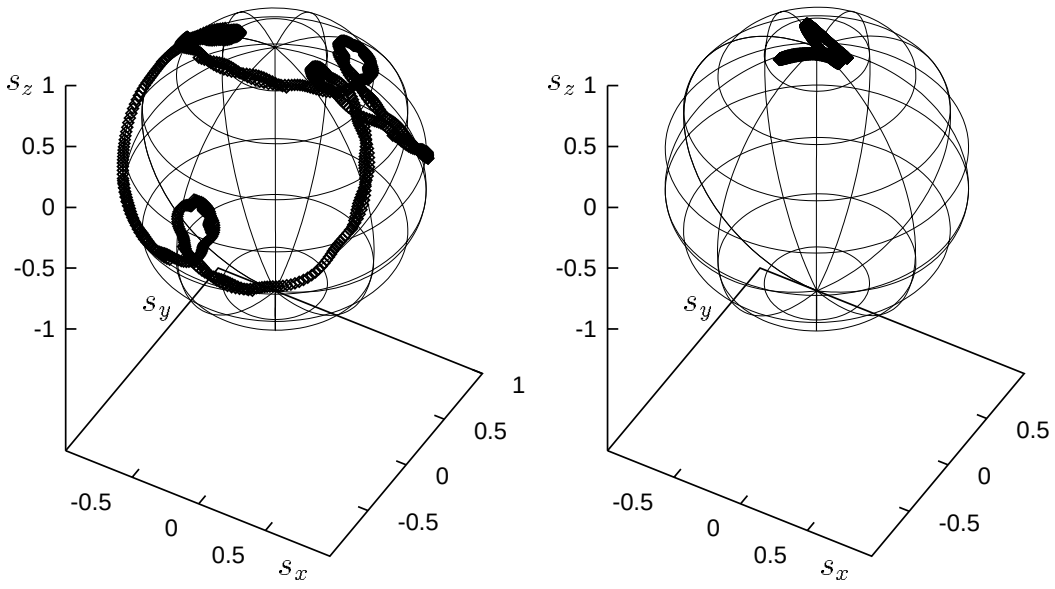

Figure 4.13: Variation of $\vec{n}(\vec{z}(\varphi))$ for the 2σ vertical phase space ellipse of 16πmm mrad in the current HERA–p lattice at 820GeV with 6 flattening snakes. Left: without Siberian Snakes. Right: for the $(0\frac{\pi}{2}00)fs6$ snake scheme.

which leads to the matrix equation of an ellipse,

$$(\mathrm{Re}\{\alpha_n\}, \mathrm{Im}\{\alpha_n\})\underline{B}^T\underline{B}\begin{pmatrix} \mathrm{Re}\{\alpha_n\} \\ \mathrm{Im}\{\alpha_n\} \end{pmatrix} = 1 \ . \tag{4.50}$$

The invariant curves for linearized spin–orbit motion are therefore ellipses around $\vec{n}_0$.

When the invariant spin field is computed non–perturbatively, the invariant curves $\vec{n}(\vec{z}(\varphi))$ are no longer ellipses and their deviation from an elliptical form shows how inaccurate the approximation of linearized spin–orbit motion is. In figure 4.14, such closed curves on the unit sphere are shown for different amplitudes of vertical motion. The initial spin direction $\vec{n}(\vec{z}_i)$ has been obtained by stroboscopic averaging, and subsequent multi–turn spin tracking has lead to the displayed curves. Even for the very complex invariant curves at high amplitudes, stroboscopic averaging leads to accurate results.

The irregularity of the invariant curves of spin–orbit motion at high energy illustrate effects which go beyond first–order resonances [123].

Coupling of the Degrees of Freedom

So far only vertical motion has been considered and for moderate phase space amplitudes the approximation of linearized spin–orbit motion works very well for one degree of freedom even at the very high energies. Figure 4.15 was computed for the current HERA–p lattice after the installation of 6 flattening snakes. It shows that for purely vertical motion phase space amplitude of 4πmm mrad the maximum

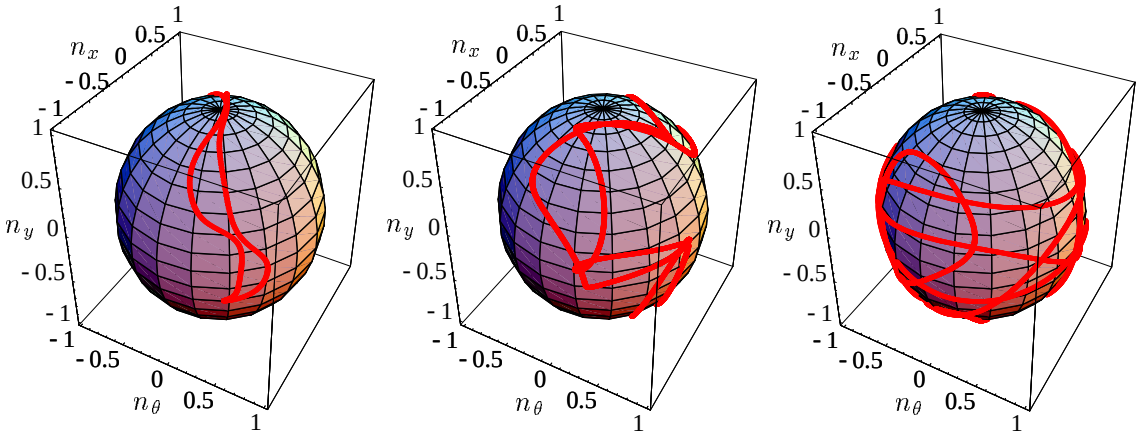

Figure 4.14: The invariant curves $\vec{n}(\vec{z}(\varphi))$ on the unit sphere for various phase space amplitudes in the vertical degree of freedom: Left: 4, middle: 9, and right: 81πmm mrad at the East interaction point of the current HERA–p lattice at 804GeV/c and with the $(0\frac{\pi}{2}00)6fs$ snake scheme.

time average polarization P_{lim} between 818 and 820GeV/c follows very closely the correct curve computed by stroboscopic averaging using the program SPRINT. The linear approximation fails for 16, 36, and 64πmm mrad of vertical amplitude. The location of the resonant reductions of P_{lim} shift with increasing vertical amplitude. This is due to the amplitude dependence of the spin tune $\nu(\vec{J})$.

Purely horizontal and purely longitudinal motion in a flat ring always leads to an invariant spin field which is parallel to the vertical $\vec{n}_0$ since the particles travel only through vertical magnetic fields. When no vertical motion is excited, this result is recovered by linearized spin–orbit motion. But in addition this linear theory does not include any spin coupling between two different degrees of freedom. When a particle in a flat ring has amplitudes in all three degrees of freedom, the P_{lim} of linearized spin–orbit motion only depends on the vertical amplitude and does not change with the horizontal or longitudinal amplitude at all. This is not so when the invariant spin field is computed by stroboscopic averaging of element by element tracking data. When a vertical amplitude is excited, the fields through which a particle propagates vary with the horizontal and longitudinal amplitude, and therefore P_{lim} changes. Thus one observes crosstalk between all degrees of freedom and the spin motion, even when the orbital motion is completely decoupled (linearly as well as nonlinearly) [123]. A decrease of $P_{lim} =< \vec{n} >$ with the horizontal and the longitudinal amplitudes can be seen in figures 4.16 and 4.17, which were computed for the *flat* model of HERA–p where the vertical bends are ignored. Therefore, in the general case it is unfortunately not sufficient to use the linear approximation.

In HERA–p with 6 flattening snakes the situation is quite similar. In this case particles which have no vertical but a horizontal or longitudinal phase space amplitude do travel through horizontal magnetic fields in the vertical bends. Therefore purely horizontal and vertical motion do have a noticeable depolarizing effect even in the linear approximation, as can be seen in the figures 4.18 and 4.19.

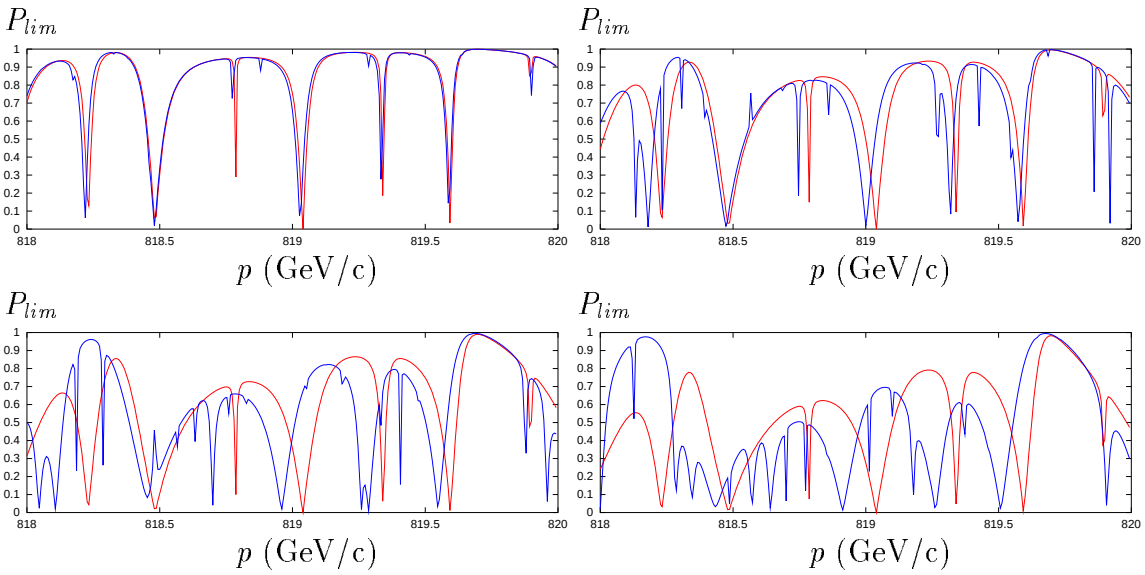

Figure 4.15: P_{lim} for HERA–p with 6 flattening snakes computed with linearized spin–orbit motion (red) and with stroboscopic averaging (blue) for normalized vertical amplitudes of top–left: 4, top–right: 16, bottom–left: 36, and bottom–right: 64πmm mrad.

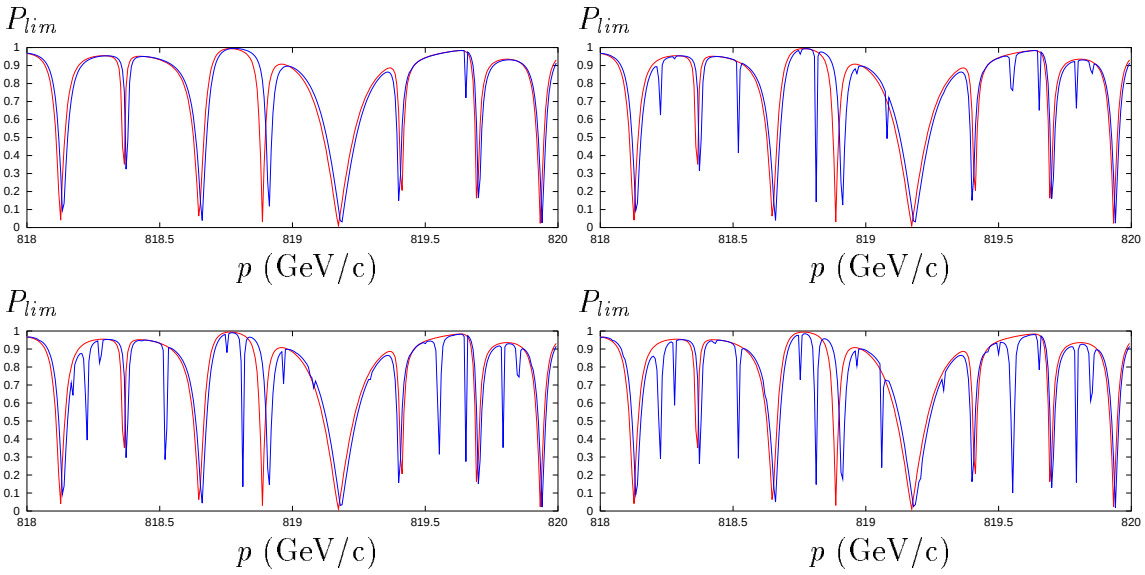

Figure 4.16: $P_{lim} =< \vec{n} >$ for the *flat* model of HERA–p computed with linearized spin–orbit motion (red) and with stroboscopic averaging (blue) for particles with a normalized vertical amplitude of 4πmm mrad and a normalized horizontal amplitude of top–left: 0, top–right: 4, bottom–left: 16, and bottom–right: 36πmm mrad.

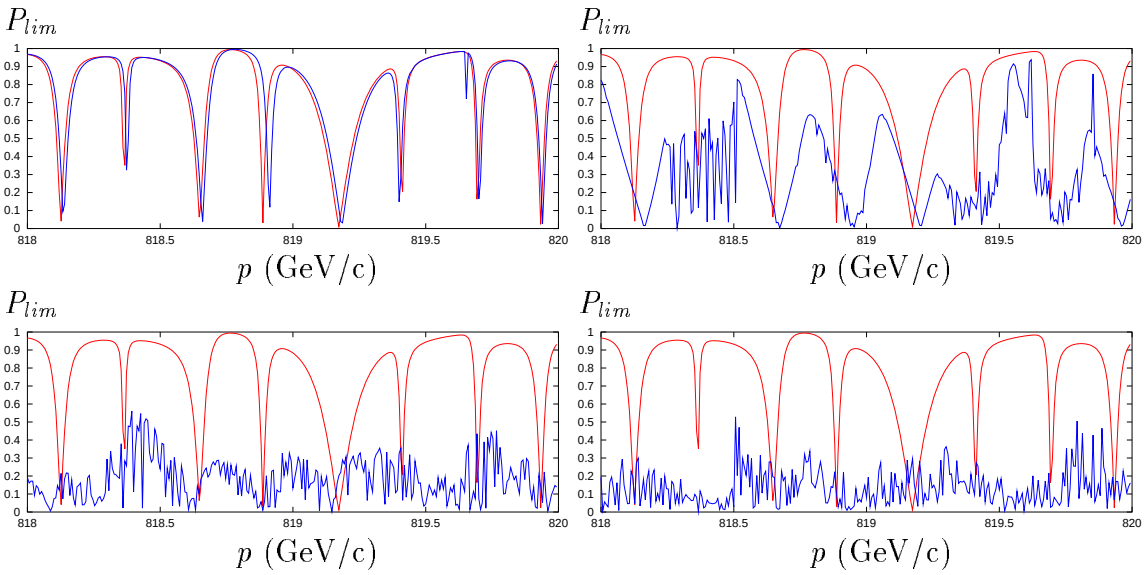

Figure 4.17: $P_{lim} =< \vec{n} >$ for the *flat* model of HERA–p computed with the linearized spin–orbit motion and with stroboscopic averaging (blue) for particles with a normalized vertical amplitude of 4πmm mrad and a normalized longitudinal amplitude of top–left: 0, top–right: 17.5, bottom–left: 70.1, and bottom–right: 157.8πmm rad. These correspond to the one, two, and 4σ emittances for a synchrotron frequency of 30Hz with a 1σ energy spread of $1.1 \cdot 10^{-4}$.

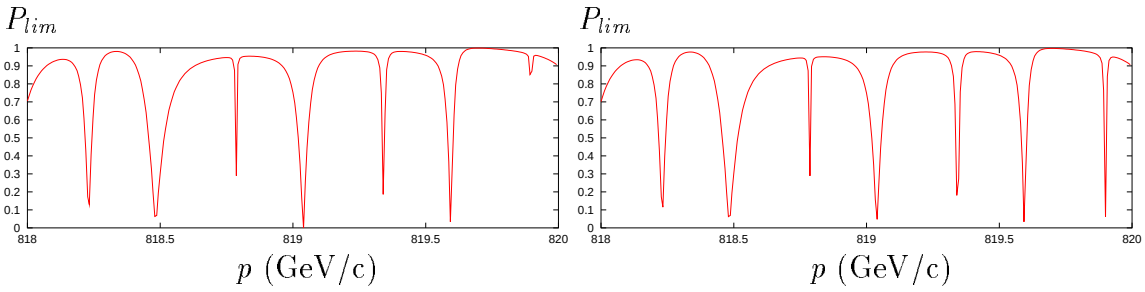

Figure 4.18: P_{lim} for HERA–p with 6 flattening snakes computed with the linearized spin–orbit motion for particles with a normalized vertical amplitude of 4πmm mrad and a normalized horizontal amplitude of 0 (left) and 36πmm mrad (right). Note the resonance at 819.9GeV/c which is excited by horizontal motion.

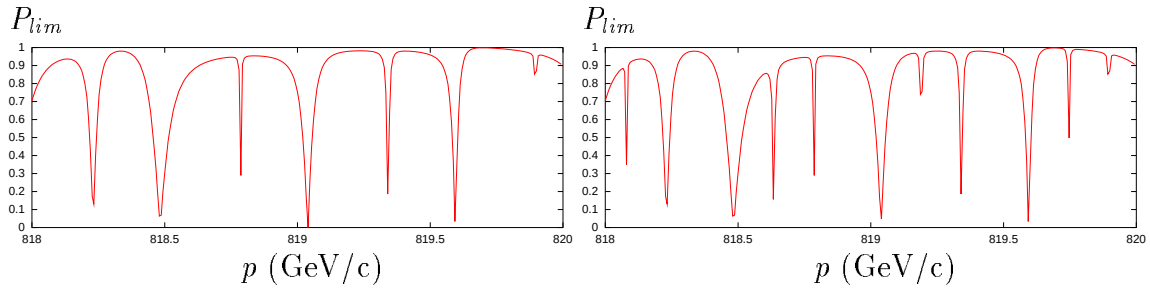

Figure 4.19: $P_{lim} =< \vec{n} >$ for HERA–p with flattening snakes computed with linearized spin–orbit motion for particles with a normalized vertical amplitude of 4πmm mrad and a normalized longitudinal amplitude of 0 (left) and 157.8πmm rad (right). The crosstalk from longitudinal motion to spin motion excites several resonances for this 1σ longitudinal amplitude.

Nevertheless, the small linear coupling between degrees of freedom is completely dominated by the nonlinear coupling which has just been shown for the *flat* model of HERA–p. This can be seen by comparing P_{lim} for linearized spin motion in HERA–p with flattening snakes in figures figure 4.18 and figure 4.19 with P_{lim} from the non–perturbative calculation of stroboscopic averaging in figures 4.20 and 4.21.

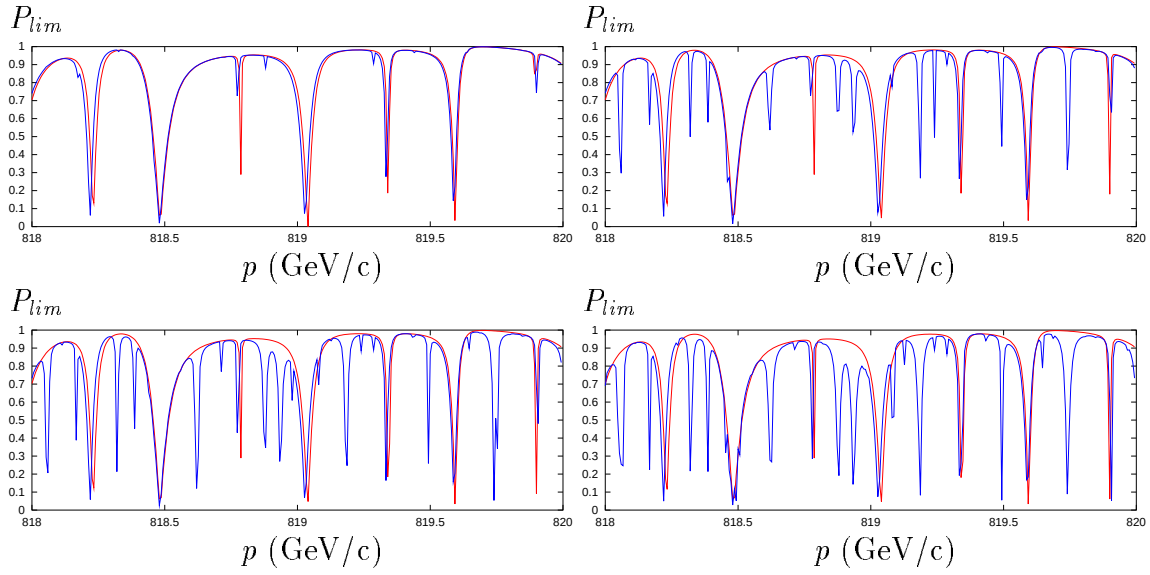

Figure 4.20: $P_{lim} =< \vec{n} >$ for HERA–p with 6 flattening snakes computed with linearized spin–orbit motion (red) and with stroboscopic averaging (blue) for particles with a normalized vertical amplitude of 4πmm mrad and a normalized horizontal amplitude of top–left: 0, top–right: 4, bottom–left: 16, and bottom–right: 36πmm mrad.

The underlying assumption of linearized spin–orbit motion is that $< \angle(\vec{n}, \vec{n}_0) >$ is small so that in addition to the orbit motion the spin motion can also be linearized.

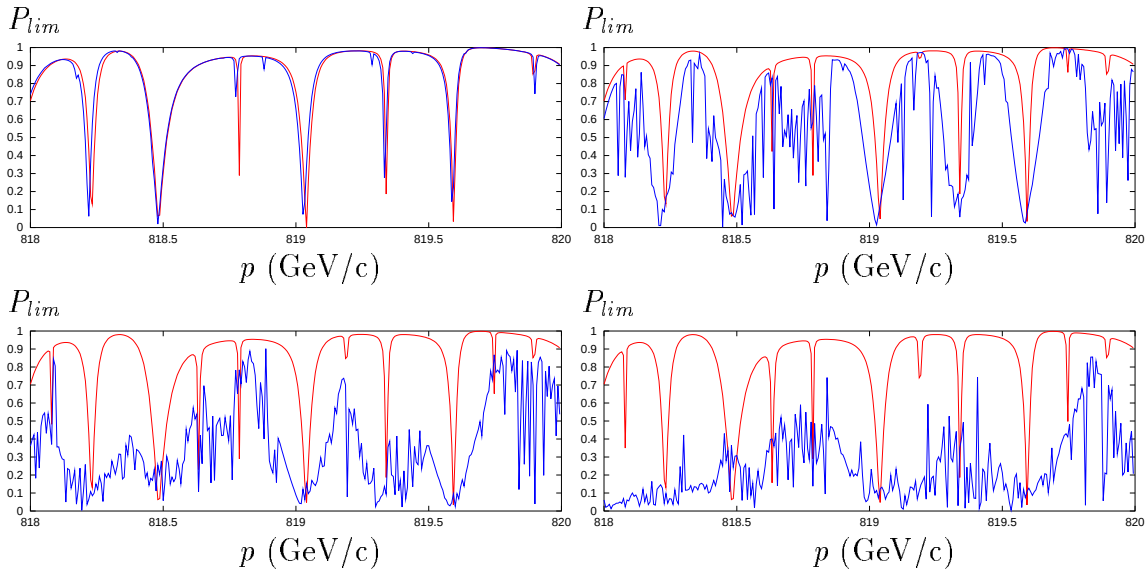

Figure 4.21: $P_{lim} =< \vec{n} >$ for HERA–p with 6 flattening snakes computed with linearized spin–orbit motion (red) and with stroboscopic averaging (blue) for particles with a normalized vertical amplitude of 4πmm mrad and a normalized longitudinal amplitude of top–left: 0, top–right: 17.5, bottom–left: 70.1, and bottom–right: 157.8πmm rad.

However, the linearization does not conserve the length of spin and neglects the non–commutation of spin rotations around different axes. In parameter domains for which this underlying assumption is valid, as for example in the case of low energy electron rings, these weaknesses are not a serious limitation except *very* close to spin–orbit resonances. However, in the proton ring of HERA–p with a $G\gamma$ of about 1756 this approximation can invalidate the calculations. Nevertheless to get a quick estimate on the usefulness of a lattice for polarized proton storage, the linearized spin–orbit motion has turned out to be very helpful in section 3.1.

Figure 4.22 shows an invariant spin curve $\vec{n}(\vec{z}(\varphi))$ on the unit sphere for a relatively large vertical emittance (left). The average polarization is already strongly reduced. When the particle also has a horizontal phase space amplitude then the invariant curves on the unit sphere get washed out and the average polarization is reduced to zero (right). Since the first–order theories neglect any influence of the horizontal motion on the invariant closed curves, figure 4.22 is far out of the range of validity of these theories.

Computing the Derbenev–Kondratenko $\vec{n}$–axis from straight forward spin phase space tracking data by stroboscopic averaging has the following features:

- It has been implemented in the code SPRINT but it can be implemented in any existing spin tracking program.
- For an accuracy on the 10^{-3} level typically less than 3000 turns have to be tracked.
- Since the method is non–perturbative, no resonance denominators appear in

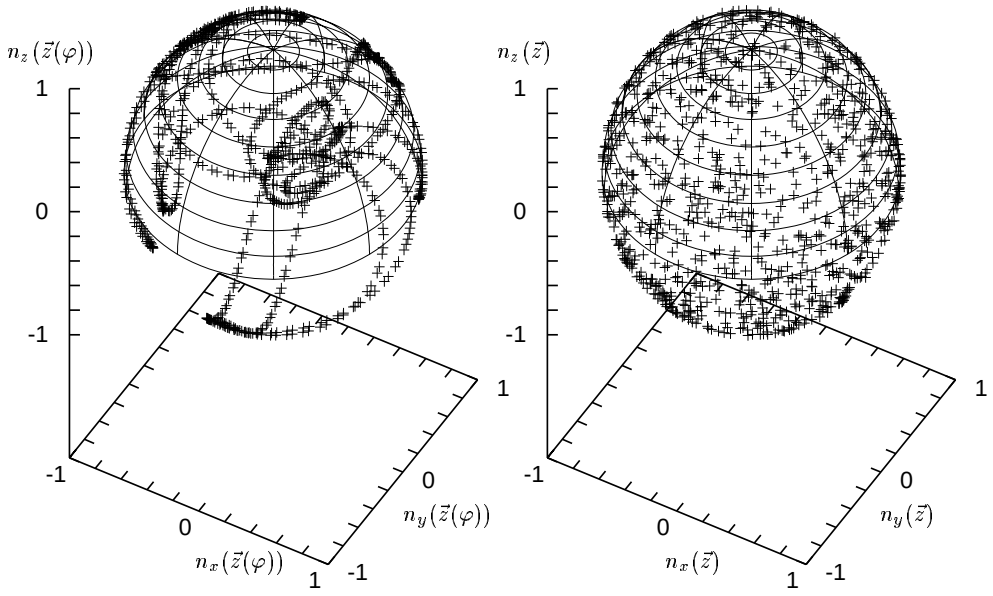

Figure 4.22: Left: An Invariant curve $\vec{n}(\vec{z}(\Phi_y))$ of spin–orbit motion on the unit sphere for particles in HERA–p with a normalized vertical amplitude of 64πmm mrad and no horizontal amplitude. Right: With an additional normalized horizontal amplitude of 4πmm mrad, the phase space points depend two angle variables and spins $\vec{n}(\vec{z}(\Phi_x, \Phi_y))$ are no longer on a one–parametric curve, which illustrates a crosstalk from horizontal motion to spin motion.

the algorithm and it is applicable even close to spin–orbit resonances.

- Since the different degrees of freedom have a coupled influence on the invariant spin field, it is important that stroboscopic averaging can be used for phase space points in all three degrees of freedom.

Since the introduction of stroboscopic averaging in [100] spin tracking in storage rings can now always be initialized with spins parallel to the invariant spin field and much clearer analysis becomes possible.

4.3 Obtaining $\vec{n}(\vec{z})$ by Anti–damping

The $\vec{n}$–axis can also be calculated using the adiabatic invariance of $J_S = \vec{S} \cdot \vec{n}(\vec{z})$, which has been proven in section 2.2.9. There are three possible procedures:

a) One could start a tracking computation with a spin aligned parallel to $\vec{n}_0$ at a low energy far away from any resonance where the invariant spin field $\vec{n}(\vec{z})$ is essentially parallel to $\vec{n}_0$ over all of the relevant phase space. Then one would accelerate the particles slowly up to the energy under investigation. As long as J_S remains nearly invariant the spin would end up parallel to $\vec{n}(\vec{z})$. The disadvantage of this approach is that at HERA–p one would essentially have

to ramp the particle all the way from 40 to 920GeV/c without violating the adiabatic invariance of J_S . This would not only take a lot of computation time but several 100 resonances would have to be crossed, which might lead to a change in J_S . Therefore a slow acceleration is not a suitable method of computing the invariant spin field. Nevertheless this method demonstrates well what actually happens to the polarized beam when it is slowly accelerated in HERA–p.

b) One could start a tracking computation with a particle on the closed orbit polarized parallel to $\vec{n}_0 = \vec{n}(0)$. When the phase space amplitude is increased slowly the spin will stay parallel to $\vec{n}(\vec{z})$ during the complete tracking run until the phase space amplitude of interest is reached. The energy is not changed during this process. This method has been tested and can be performed with practical speed [150]. It has the advantage over the other methods presented so far that one obtains the field $\vec{n}(\vec{z})$ at many phase space amplitudes. One can therefore easily compute the dependence of P_{lim} on $\vec{J}$. When the amplitude dependent spin tune comes in resonance with the orbital tunes for some intermediate particle amplitude, J_S can change and the $\vec{n}$–axis will be determined inaccurately.

c) A third method which has also been tested with success starts a tracking run with a particle at the phase space point $\vec{z}_{-N}$ and a spin parallel to $\vec{n}_0$. In order to make $\vec{n}_0$ parallel to the invariant spin field $\vec{n}(\vec{z})$, the spin–orbit coupling is switched off, i.e. particles all over phase space have the same spin motion as a particle on the closed orbit. Finally the spin–orbit coupling is switched on slowly while tracking the particle for N turns until it arrives at the phase space point $\vec{z}$. This procedure is especially helpful when analyzing the influence of resonance strength on the maximum polarization since one obtains P_{lim} for a variation of resonance strength from 0 to a final value, allowing one to compute the maximally allowed resonance strength for a required average polarization. In fact this technique of anti–damping the spin–orbit coupling is already contained in the SMILE formalism [87]. There it was not exploited numerically but used for deriving a formalism which leads to the required periodicity in azimuth. Also in this algorithm the accuracy can suffer when spin–orbit resonances occur during the calculation.

In the single resonance approximation of spin motion, the maximum time average polarization is given by equation (2.124) as $P_{lim} = |\frac{\delta}{\sqrt{\delta^2+\epsilon_\kappa^2}}|$ where $\kappa = \nu_0 - \delta$ is the frequency of the resonance. The resonance strength ϵ_κ of equation (2.71) is the Fourier coefficient of a linear function of phase space variables $\vec{\omega}(\vec{z}, l)$ and $\kappa = j_0 \pm Q_k$. Therefore ϵ_κ increases with the square root of the action variable J_k of the kth degree of freedom, $\epsilon_\kappa \propto \sqrt{J_k}$. When more than only the first–order effects are taken into account, the polarization depends on the orbital amplitudes in a more complex fashion.

In some cases, as for example in figure 4.23 (left), P_{lim} increases with the phase space amplitude after it has decreased at smaller amplitudes [151]. This is an indica-

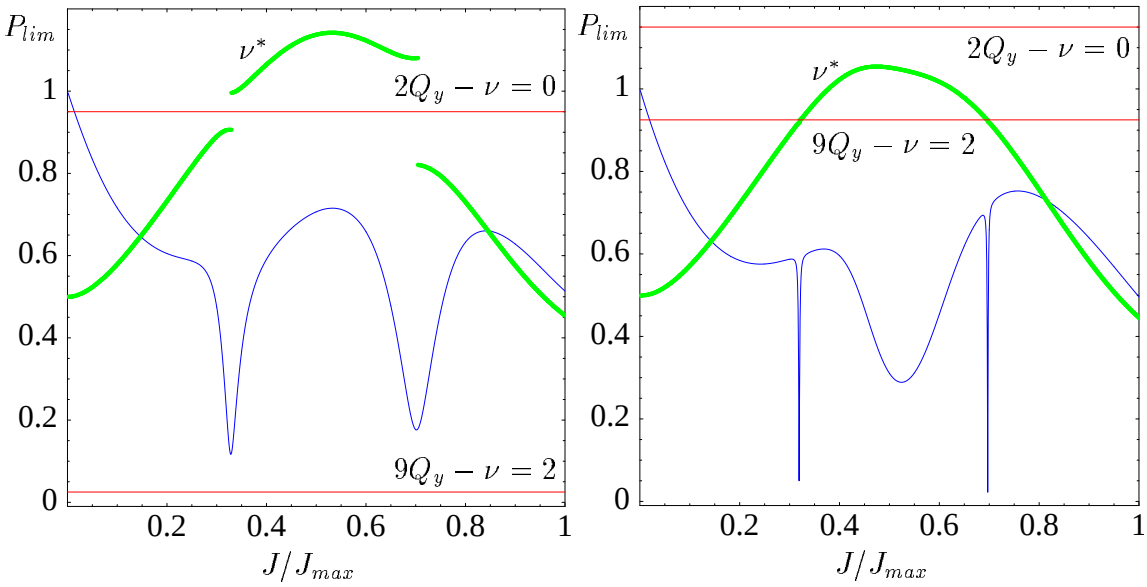

Figure 4.23: P_{lim} (blue) and the magnified spin tune $\nu^* = \frac{1}{2} + 10(\nu - \frac{1}{2})$ (green) as functions of the ratio J/J_{max} between the intermediate vertical action J and the final action J_{max}. The final vertical amplitude was 81πmm mrad which corresponds to 4.5σ of the current proton beam in HERA–p. When the spin tune comes close to one of the resonance lines (red), P_{lim} is reduced. Left: for $Q_y = 0.2725$. Right: for $Q_y = 0.2825$ in the current HERA–p lattice and the $(0\frac{\pi}{2}00)6fs$ snake scheme.

tion for amplitude dependent tunes $\nu(\vec{J})$ and $\vec{Q}(\vec{J})$. While the amplitude changes, the tunes can come close to a resonance condition which causes P_{lim} to drop at some intermediate phase space amplitude. In figure 4.23 (left), it is not the vertical orbit tune which changed, since linear orbit motion is simulated so that $\vec{Q}$ does not depend on the phase space amplitude. The green curves in figure 4.23 show $\nu^* = \frac{1}{2} + 10(\nu - \frac{1}{2})$, the magnified distance of the spin tune from $\nu_0 = \frac{1}{2}$. When this tune comes close to the resonance $\nu = 2Q_y$, then $\vec{n}(\vec{z})$ varies strongly over phase space and P_{lim} becomes small. At intermediate amplitudes where ν has moved away from this resonance condition, P_{lim} is larger. Figure 4.23 (right) shows the amplitude dependence of the spin tune ν and P_{lim} after the vertical tune has been changed from $Q_y = 0.2725$ to $Q_y = 0.2825$. Therefore also the resonant spin tune values $\nu = 2Q_y$ and $\nu = 9Q_y - 2$ (red lines) change, which in turn changes the amplitudes where P_{lim} is reduced. Now the spin tune comes close to the 9th order resonance and narrow dips of P_{lim} can be observed at the corresponding amplitudes.

To study such amplitude dependent depolarizing effects, it is advantageous to have a method which quickly leads to $\vec{n}(\vec{z})$ at various amplitudes. The anti–damping method 2 described above has this feature and was implemented into SPRINT for that purpose. However, it is often not as accurate as stroboscopic averaging, since resonances might be crossed during the slow change of the amplitude, and the adiabatic invariance of $J_S = \vec{S} \cdot \vec{n}(\vec{z})$ can be violated. Therefore figure 4.24, where resonances are crossed, has not been computed by anti–damping but by the SODOM–2

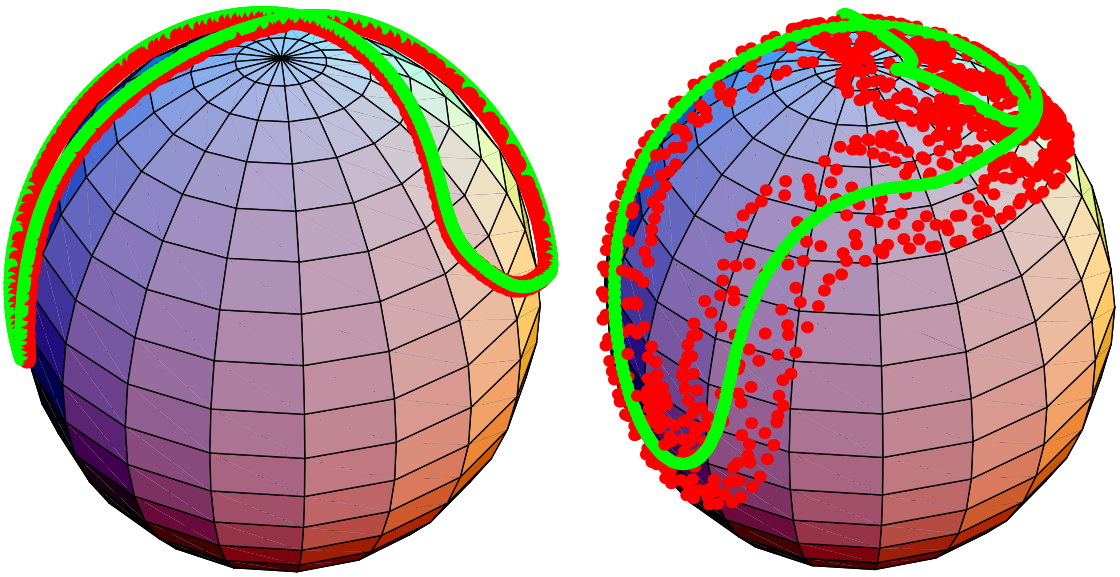

Figure 4.24: Invariant curves $\vec{n}(\vec{z}\vartheta))$ on the unit sphere computed by anti–damping (red) and by stroboscopic averaging (green) for a vertical amplitude of 16πmm mrad (left) and of 64πmm mrad in the current HERA–p lattice and the $(0\frac{\pi}{2}00)6fs$ snake scheme.

method.

Invariant curves on the unit sphere for such a case are shown in figure 4.24. They were computed with the $(0\frac{\pi}{2}00)6fs$ scheme for the current HERA–p lattice at 805GeV/c [150]. While anti–damping (red curves) and stroboscopic averaging (green curves) both allow an accurate computation of the invariant spin field for particles with 16πmm mrad in figure 4.24 (left), the accuracy of anti–damping is strongly reduced at 64πmm mrad in figure 4.24 (right), since a resonance condition had to be crossed during the anti–damping procedure. The accuracy can be increased by reducing the speed with which the phase space amplitude is increased.

4.4 Conclusion

By introducing the invariant spin field $\vec{n}(\vec{z})$ and the amplitude dependent spin tune $\nu(\vec{J})$ and by proving the adiabatic invariance of the spin action $J_S = \vec{S}\cdot\vec{n}$, theoretical concepts have been provided with which it is possible to describe many features of the acceleration of polarized proton beams. Of particular importance among these is the loss of polarization when J_S does not remain invariant.

With the three non–perturbative algorithms for determining $\vec{n}(\vec{z})$ and $\nu(\vec{J})$ which have been introduced: SODOM–2, stroboscopic averaging, and anti–damping, these theoretical concepts can also be numerically evaluated. These three algorithms have become the basis for an analysis of higher–order effects of spin motion in HERA–p and have also been adopted for the analysis of some aspects of polarized proton motion in RHIC.

With these advanced computational techniques it has become possible to determine the strengths of higher–order resonances, and it has been shown that they allow the use of the Froissart–Stora formula to predict the loss of polarization due to higher–order resonances.

In HERA–p, the maximum average polarization is very small at critical energies where the spin perturbations of all FODO cells accumulate. This effect was analyzed in detail with linearized spin orbit motion and the role of the non–flat regions of HERA–p was stressed. This analysis showed that it is helpful to symmetrize the spin perturbations in HERA–p by the use of 8 flattening snakes.

It has been found that different snake schemes have very different abilities to preserve the polarization during the acceleration process in HERA–p and therefore schemes with optimized snake angles had to be found. For this purpose, a filtering algorithm was devised which tests a huge number of potential snake schemes and selects the scheme with the maximum average P_{lim} and the minimum spread of the spin tune over the phase space amplitudes in a polarized proton beam.

In addition, methods have been found to match the snake angles to a suitably modified vertical betatron phase advance in HERA–p so that P_{lim} for linearized spin–orbit motion does not drop strongly at the critical energies where the spin perturbations in all FODO cells accumulate. When higher–order effects were included, these snake–matched lattices with 4 and 8 snakes were shown to reduce the spin tune spread and to allow the acceleration of polarized beams with significantly larger emittances.

However, with the optimal scheme of 4 Siberian Snakes only particles with a vertical phase space amplitude below 11πmm mrad in the luminosity upgrade lattice of HERA–p can be accelerated without a reduction of polarization. And even in snake matched schemes with 8 Siberian Snakes particles with a vertical phase space amplitude above 16πmm mrad will lead to a reduction of polarization.

It would be therefore very advisable to use electron cooling in PETRA so as to reduce the emittance in HERA–p and to allow for an acceleration without loss of polarization for most particles in the beam.

List of References

[1] A. A. Sokolov and I. M. Ternov. On polarization and spin effects in the theory of synchrotron radiation. *Sov. Phys. Doklady*, 8:1203, 1964.

[2] A. A. Sokolov and I. M. Ternov. *Radiation from Relativistic Electrons.* American Institute of Physics, New York, 1986.

[3] A. W. Chao and K. Yokoya. An alternative longitudinal polarization scheme for TRISTAN. KEK–81–7, Tsukuba, 1981.

[4] K. Yokoya. Improvement of radiative polarization in plane storage rings. In *Polarized Electron Acceleration and Storage.* DESY–M–82–09 and KEK–81–19, Tsukuba, 1982.

[5] D. P. Barber, J. Kewisch, G. Ripken, R. Rossmanith, and R. Schmidt. A solenoid spin rotator for large electron storage rings. *Particle Accelerators*, 17:243–262, 1985.

[6] D. P. Barber, M. Böge, H.-D. Bermer, R. Brinkmann, W. Brückner, *et al.* The first achievement of longitudinal spin polarization in a high energy electron storage ring. *Phys. Lett.* B(343):436–443, 1995.

[7] D. P. Barber and G. Ripken. Precession of the polarization of particles moving in a homogeneous electro–magnetic field. In A. W. Chao and M. Tigner, editors. *Handbook of accelerator physics and engineering* World Scientific, 1999.

[8] J. Blümlein and W.-D. Nowak, editors. *Workshop on the Prospects of Spin Physics at HERA.* DESY–95–200, 1995.

[9] J. Blümlein, A. De Roeck, T. Gehrmann, and W.-D. Nowak, editors. *Deep inelastic scattering off polarized targets: Theory meets experiment.* DESY–95–200, 1997.

[10] A. De Roeck and T. Gehrmann, editors. *Physics with polarized protons at HERA.* DESY–Proceedings–1998–01, 1998.

[11] D. P. Barber and A. De Roeck, editors. *Proceedings of Polarized Protons at High Energies*, DESY–Proceedings–1999–03, 1999.

[12] A. W. Chao. Polarization of a stored electron beam. In *Conference proceedings 87*. US Particle Accelerator School, Batavia, USA, American Institute of Physics, 1981.

[13] Bryan W. Montague. Polarized beams in high energy storage rings. *Physics Reports*, 113(1):1–96, 1984.

[14] T. Roser. Polarized proton beam in the AGS. In *Proceedings of SPIN98*, Protvino, 1998.

[15] T. Roser. Acceleration of polarized proton beams. In *Proceedings of SPIN98*, Protvino, 1998.

[16] M. Bai, L. Ahrens, J. Alessi, K. Brown, G. Bunce, P. Cameron, *et al.* Overcoming intrinsic spin resonances with an rf dipole. *Phys. Rev. Lett.* 80(21):4673–4676, 1998.

[17] T. Roser. RHIC spin program: machine aspects and recent progress. In [11].

[18] K. Brown, G. Bunce, E. Courant, R. Fernew, R. Gupta, S. Y. Lee, *et al.* Conceptual design for the acceleration of polarized protons in RHIC. AGS/RHIC/SN 001, Brookhaven, 1995.

[19] SPIN Collaboration. Acceleration of polarized protons to 120 GeV and 1TeV at Fermilab. UM–HE 95–09, University of Michigan, 1995.

[20] D. P. Barber. Possibilities for polarized protons at HERA. In *Prospects of spin physics at HERA*, DESY–95–200, 1995.

[21] G. H. Hoffstaetter. Polarized protons in HERA. In DESY–96–05, 1996.

[22] SPIN Collaboration and the DESY Polarization Team. Acceleration of polarized protons to 820 GeV at HERA. UM–HE–96–20, University of Michigan, 1996.

[23] D. P. Barber, G. H. Hoffstaetter, and M. Vogt. Polarized protons in HERA. In *Future Physics at HERA*, volume 2, p. 1205–1216. DESY, 1996.

[24] G. H. Hoffstaetter. Polarized protons in HERA. In *Proceedings SPIN96*, Amsterdam, 1996.

[25] D. P. Barber, M. Vogt, and G. H. Hoffstaetter. Polarized protons in HERA – the status. In DESY–97–200 (241–246) and DESY–Proceedings–1998–01 (460–465), 1997.

[26] SPIN Collaboration and the DESY Polarization Team. Acceleration of polarized protons to 920 GeV at HERA. UM–HE–99–05, University of Michigan, 1999.

[27] G. H. Hoffstaetter. Polarized protons at HERA: the accelerator issues. In [11].

[28] Ya. S. Derbenev. The Stern–Gerlach method in charge particle storage rings (1) The double–resonance Stern–Gerlach effect. UM-HE-90-30, University of Michigan, 1990.

[29] Ya. S. Derbenev. The Stern–Gerlach method in charged particle storage rings (2) The new–classical Stern–Gerlach effect. UM-HE-90-32, University of Michigan, 1990.

[30] Ya. S. Derbenev. Concepts for Stern–Gerlach polarization in storage rings. DESY Accelerator Physics Seminar, 1995.

[31] M. Conte, A. Penzo, and M. Pusterla. Spin splitting due to longitudinal Stern–Gerlach kicks. *Nuovo Cimento*, 108 A(1):127–136, 1995.

[32] M. Conte, B. E. Norum, A. Penzo, M. Pusterla, and R. Rossmanith. A proposed test of the spin splitter effect in HERA–p. DESY–HERA-96-01, 1996.

[33] C. J. Horowitz and H. O. Meyer. Polarizing stored beams by interaction with polarized electrons. *Phys. Rev. Lett.* 72(25):3981, 1994.

[34] D. P. Barber. Prospects for polarized protons at HERA. In *conference on the spin structure of the nucleon at Erice in 1995*, 1998.

[35] F. Rathmann, C. Montag, D. Fick, J. Tonhäser, W. Brückner, *et al.* New method to polarize protons in a storage ring and implications to polarize antiprotons. *Phys. Rev. Lett.* 71(9):1379–1382, 1993.

[36] C. Montag. Beschleunigerphysikalische Untersuchungen zum FILTEX–Protonen–Testexperiment im Heidelberger Testspeicherring TSR. Diploma thesis, Philipps–Universität, Marburg, 1993.

[37] F. Z. Khiari, P. R. Cameron, G. R. Court, D. G. Crabb, *et al.* Acceleration of polarized protons to 22 GeV/c and the measurement of spin-spin effects in $\vec{p}+\vec{p} \to p+p$. *Phys. Rev.* D 39:45–85, 1989.

[38] A. S. Belov, V. E. Kuzik, Yu. V. Plokhinskii, V. P. Yakushev, and V. G. Dudnikov. A source of polarized negative hydrogen ions with deuterium plasma ionizer. *Nucl. Instr. Meth.* A(333):256–259, 1993.

[39] A. Belov. Atomic beam type polarized ion sources. In [11].

[40] A. Zelenski. Optically pumped polarized ion sources (OPPIS). In [11].

[41] A. N. Zelenski, C. D. P. Levy, K. Jayamanna, M. McDonald, *et al.* The TRIUMF high current DC optically pumped polarized H^- ion source. In *TRIUMF-PP-95-44 and Proceedings of PAC*, Dallas, 1995.

[42] A. N. Zelenski, S. A. Kokhanovskii, V. M. Lobashev, and V. G. Polushkin. A laser source of polarized protons and H^- ions. *Nucl. Instr. Meth.* A(245):223–229, 1986.

[43] L. Buchmann. A proton polarimeter for beam energies below 300-keV. *Nucl. Instr. Meth.* A(301):383–388, 1991.

[44] G. Bunce. Proton polarimetry for RHIC. In [11].

[45] A. D. Krisch. A polarized jet for RHIC polarimetry. In [11].

[46] M. Vogt. Polarized protons in HERA–p. *Dissertation, Universität Hamburg*, 1999. also DESY–Report to be published.

[47] A. Lehrach. Calculation of the invariant spin field by adiabatically blowing up the beam with an rf dipole. In [11].

[48] J. Frenkel. Die Elektrodynamik des rotierenden Elektrons. *Z. Phys.* 37:243–262, 1926.

[49] L. H. Thomas. The kinematics of an electron with an axis. *Phil. Mag.*, 3(13):1–20, 1927.

[50] H. Mendlowitz and K. M. Case. *Phys. Rev.* 97:33, 1955.

[51] V. Bargmann, L. Michel, and V. L. Telegdi. Precession of the polarization of particles moving in a homogeneous electro–magnetic field. *Phys. Rev. Lett.* 2(10):435–436, 1959.

[52] H. Rose. Hamiltonian magnetic optics. *Nucl. Instr. Meth.* A258:374–401, 1987.

[53] G. H. Hoffstaetter. Nonlinear dependence of synchrotron radiation on beam parameters. In *Proceedings of PAC 94, Dallas/TX*, 1995.

[54] E. D. Courant and H. S. Snyder. Theory of the alternating–gradient synchrotron. *Ann. Phys.* 3:1–48, 1958.

[55] M. Berz. Computational aspects of optics design and simulation: COSY INFINITY. *Nucl. Instr. Meth.* A298:473-479, 1990.

[56] A. Luccio. Numerical spin tracking in a synchrotron, computer code SPINK—examples and reference manual. BNL-52481, Brookhaven, 1995.

[57] V. Balandin, M. Berz, and N. Golubeva. Computation and analysis of spin dynamics. In *Fourth Computational Accelerator Physics Conference, AIP Conference Proceedings 391*, p. 276, 1996.

[58] P. Nghiem and A. Tkatchenko. Simulation of proton spin motion in circular accelerators using one–turn spinor transfer maps. *Nucl. Instr. Meth.* A(335):3349–366, 1993.

[59] S. Y. Lee. *Spin dynamics and Snakes in synchrotrons.* World Scientific, 1997.

[60] H. Huang, L. Ahrens, J. G. Alessi, M. Beddo, K. A. Brown, *et al.* Preservation of proton polarization by a partial Siberian Snake. *Phys. Rev. Lett.* 73:2982–2985, 1994.

[61] B. B. Blinov, C. M. Chu, E. D. Courant, D. A. Crandell, *et al.* First test of a partial Siberian Snake during polarized beam acceleration. *Phys. Rev. Lett.* 73(12):1621–1623, 1994.

[62] R. A. Phelps, V. A. Anferov, C. M. Chu, E. D. Courant, *et al.* Adiabatic partial Siberian Snake turn–on with no beam depolarization. *Phys. Rev. Lett.* 72(10):1479–1481, 1994.

[63] A. W. Chao. Evaluation of radiative spin polarization in an electron storage ring. *Nucl. Instr. Meth.*, 180:29, 1981.

[64] H. Mais and G. Ripken. Theory of spin–orbit motion in electron–positron storage rings. DESY–83–062, 1983.

[65] P. Lochak and C. Meunier. *Multiphase averaging for classical systems with applications to adiabatic theorems*, volume 72 of *Applied Mathematical sciences.* Springer, 1988.

[66] V. I. Arnold, editor. *Mathematical Aspects of Classical and Celestial Mechanics, Chapter 5*, volume Dynamical Systems III of *Encyclopedia of mathematical sciences; V.* Springer, 1988.

[67] A. I. Neistadt. Passage through resonance in a two-frequency problem. *Soviet Phys. Doklady*, 20(3):189–191, 1975. English translation of Doklady Akad. Nauk. SSSR Mechanics 221 (2), 301–304, 1975.

[68] D. A. Crandell, V. A. Anferov, B. B. Bilinov, D. D. Caussyn, *et al.* Spin flipping through and intrinsic depolarizing resonance by strengthening it. *Phys. Rev. Lett.* 77(9):1763–1765, 1996.

[69] Ya. S. Derbenev and A. M. Kondratenko. Acceleration of polarized particles. *Sov. Phys. Doklady*, 20:562, 1976. also in russ.: Dokl.Akad.Nauk Ser.Fiz.223:830-833, 1975.

[70] Ya. S. Derbenev, A. M. Kondratenko, S. I. Serednyakov, *et al.* Radiative polarization: obtaining, control, using. *Particle Accelerators*, 8:115–126, 1978.

[71] Ya. S. Derbenev and A. M. Kondratenko. On the possibilities to obtain high-energy polarized particles in accelerators and storage rings. In G. H. Thomas, editor, *High Energy Physics with Polarized Beams and Polarized Targets*, AIP Conference Proceedings 51, p. 292, 1978.

[72] A. D. Krisch, S. R. Mane, R. S. Raymond, T. Roser, *et al.* First test of the Siberian Snake magnet arrangement to overcome depolarizing resonances in a circular accelerator. *Phys. Rev. Lett.* 63(11):1137–1140, 1989.

[73] A. Luccio and T. Roser, editors. Third workshop on Siberian Snakes and spin rotators. BNL–52453, Brookhaven, 1994.

[74] J. E. Goodwin, H-O. Meyer, M. G. Minty, P. V. Pancella, *et al.* Overcoming intrinsic and synchrotron depolarizing resonances with a Siberian Snake. *Phys. Rev. Lett.* 64(23):2779–2782, 1990.

[75] V. Anferov. Siberian Snake design for a high energy ring. In [11].

[76] V. I. Ptitsin and Yu. M. Shatunov. Helical spin rotators and snakes. In *Proc. 3. Workshop on Siberian Snakes and Spin Rotators*, BNL-52453:15, Brookhaven, 1994.

[77] G. H. Hoffstaetter. Snake matching. In UM–HE 99–05, University of Michigan, 1999.

[78] K. Steffen. Strong spin matching with and without snakes, a scheme for preserving polarization in large ring accelerators. DESY–88–068, 1988.

[79] V. A. Anferov. Spin transparent interaction regions for HERA. *Nucl. Instr. Meth.* A398(2-3):423–425, 1997.

[80] D. P. Barber, G. H. Hoffstaetter, and M. Vogt. Spin motion at high energy in HERA-p. In UM–HE 99–05, University of Michigan, 1999.

[81] H. Poincaré. *Les méthodes nouvelles de la méchanique céleste.* Gauthier–Villars, Paris, 1892, 1893, 1899. three volumes.

[82] Ya. S. Derbenev and A. M. Kondratenko. Diffusion of particle spin in storage rings. *Sov. Phys. JETP*, 35:230, 1972.

[83] D. P. Barber, K. Heinemann, G. H. Hoffstaetter, and M. Vogt. The phase space dependent spin polarization direction in the HERA proton ring at high energy. In *Proceedings to EPAC96* and DESY–M–96–14, 1996.

[84] K. Yokoya. The action–angle variables of classical spin motion in circular accelerators. DESY–86–057, 1986.

[85] K. Yokoya. Calculation of the equilibrium polarization of stored electron beams using Lie algebra. *Nucl. Instr. Meth.* A258:149–160, 1987.

[86] K. Yokoya. Non–perturbative calculation of equilibrium polarization of stored electron beams. KEK–92–6, Tsukuba, 1992.

[87] S. R. Mane. Electron-spin polarization in high energy storage rings. II. Evaluation of the equilibrium polarization. *Phys. Rev.* A(36):120–130, 1987.

[88] S. R. Mane. Polarization of electron beams in high-energy storage rings. 1:convergence of perturbation theory. *Nucl. Instr. Meth.* A321:21–41, 1992.

[89] D. P. Barber, K. Heinemann, and G. Ripken. Notes on spin dynamics in storage rings. DESY–M–92–04, 1992.

[90] V. Balandin and N. Golubeva. Hamiltonian methods for the study of polarized proton beam dynamics in accelerators and storage rings. DESY–98–016, 1998.

[91] Yu. Eidelman and V. Yakimenko. The application of Lie methods to the spin motion in nonlinear collider fields. *Particle Accelerators*, 45:17–35, 1994.

[92] V. Balandin and N. Golubeva. Nonlinear spin dynamics. *Proceedings of the XV International Conference on High Energy Particle Accelerators, Hamburg*, p. 998–1000, 1992.

[93] J. Moser. Lectures on Hamiltonian systems. *Mem. Am. Math. Soc. 81*, p. 60, 1968.

[94] J. W. S. Cassels. *An introduction to the theory of Diophantine approximation.* Cambridge University Press, Cambridge U.K., 1957.

[95] K. Yokoya. On multiple Siberian Snakes. SSC–189, SSC Central Design Group, 1988.

[96] A. I. Neistadt. Averaging in multi-frequency systems. *Soviet Phys. Doklady*, 20(7):492–494, 1976. English translation of Doklady Akad. Nauk. SSSR Mechanics 223 (2), 314–317, 1976.

[97] J. A. Ellison and G. H. Hoffstaetter. In preparation. 2000.

[98] K. Abragam. *The principles of nuclear magnetism.* Clarendon, 1961.

[99] S. R. Mane. Exact solution of the Derbenev–Kondratenko $\vec{n}$–axis for a model with one resonance. FERMILAB–TM–1515, 1988.

[100] K. Heinemann and G. H. Hoffstaetter. A tracking algorithm for the stable spin polarization field in storage rings using stroboscopic averaging. *Phys. Rev.* E 54:4240–4255, 1996.

[101] M. Berz. *Differential Algebraic Description and Analysis of Spin Dynamics*, volume 343 of *AIP Conference Proceedings*, p. 321–327, 1995.

[102] M. Froissart and R. Stora. Depolarisation d'un faisceau de protons polarises dans un synchrotron. *Nucl. Instr. Meth.*, 7:297–305, 1960.

[103] E. D. Courant and R. D. Ruth. The acceleration of polarized protons in circular accelerators. BNL–51270 and UC–28 and ISA–80–5, 1980.

[104] M. F. Schlesinger. *The wonderful world of stochastics.* Studies in statistical mechanics 12. North-Holland, p. 382, 1985.

[105] S. Y. Lee and S. Tepikian. Resonance due to a local spin rotator in high–energy accelerators. *Phys. Rev. Lett.* 56(16):1635–1638, 1986.

[106] S. Y Lee. Spin–depolarization mechanisms due to overlapping spin resonances in synchrotrons. *Phys. Rev.* E 47(5):3631–3644, 1993.

[107] V. Ptitsin and Yu. M. Shatunov. The investigation of spin resonances in an accelerator with Siberian Snakes. In C. W. de Jager, T. J. Ketel, P. J. Mulders, J. E. J. Oberski, and M. Oskam-Tamoezer, editors, *Proceedings SPIN96*, p. 516–518. World Scientific, 1996.

[108] M. Vogt, D. P. Barber, and G. H. Hoffstaetter. Introduction to the invariant spin field and update on simulations with polarized protons at HERA–p. In DESY–HERA–98–04, 1998.

[109] L. V. Alexeeva, V. A. Anferov, D. D. Caussyn, C. M. Chu, *et al.* Observation of a second–order spin–depolarizing resonance. *Phys. Rev. Lett.* 75(10):1931–1933, 1995.

[110] V. Balandin, N. Golubeva, and D. P. Barber. Studies of the behavior of proton spin motion in HERA-p at high energies. DESY–M–96–04, 1996.

[111] D. P. Barber, K. Heinemann, G. H. Hoffstaetter, and M. Vogt. The permissible equilibrium polarization distribution in a stored proton beam. In *ICFA Proceedings Quantum Aspects of Beam Physics*, 1998.

[112] G. H. Hoffstaetter and M. Vogt. Sprint users guide and reference manual. DESY, 1999.

[113] A. W. Chao. In *Polarized Electron Acceleration and Storage*, DESY–M–82–09, 1982.

[114] K. Steffen. Sample lattices for polarized proton acceleration in the SSC. In SSC–SR–1036, SSC Central Design Group, 1988.

[115] R. Baiod, C. M. Chu, E. D. Courant, Ya. S. Derbenev, *et al.* A Siberian Snake with overlapping depolarizing resonances. *Phys. Rev. Lett.* 70(17):2557–2560, 1993.

[116] V. Anferov. 820 GeV/c polarized protons in HERA, SPIN@HERA report update. In [11].

[117] A. W. Chao. Workshop summary – accelerator issues. In [11].

[118] E. D. Courant. Hybrid helical snakes and rotators for RHIC. BNL–61920, Brookhaven, 1995.

[119] Ya. S. Derbenev. Private communication, 1998.

[120] R. Degenhardt. *Korrektur von Aberrationen in der Teilchenoptik mit Hilfe von Symmetrien.* Doctoral thesis, Darmstadt University of Technology, 1992.

[121] W. Wan. *A Theory of Arbitrary Order Achromats.* PhD thesis, Michigan State University, 1995.

[122] G. H. Hoffstaetter. Comments on aberration correction in symmetric imaging energy filters. *Nucl. Instr. Meth.* A(427):275–281, 1998.

[123] G. H. Hoffstaetter, M. Vogt, and D. P. Barber. Higher–order effects in polarized proton dynamics. *Phys. Rev. ST–AB*, 2(11):1–15, 1999.

[124] K. Yokoya. An algorithm for calculating the spin tune in circular accelerators. DESY–99–006, 1999.

[125] D. P. Barber, K. Heinemann, G. H. Hoffstaetter, and M. Vogt. Calculations of the equilibrium spin distribution for protons at high energy in HERA. In *Proceedings of SPIN96*, Amsterdam, 1996.

[126] D. P. Barber, G. H. Hoffstaetter, and M. Vogt. Numerical and theoretical spin stability studies for HERA–p. In [11].

[127] G. H. Hoffstaetter. Polarized protons in HERA. In *Proceedings of NUCLEON99, Nucl. Phys.* A, 1999.

[128] D. P. Barber, K. Heinemann, G. Hoffstaetter, and M. Vogt. The polarization at high energy in HERA. DESY–HERA–96–07, 1996.

[129] K. L. Brown. A first– and second–order matrix theory for the design of beam transport systems and charged particle spectrometers. SLAC–75, Menlo Park/CA, 1982.

[130] E. Forest. Canonical integrators as tracking codes (or how to integrate perturbation theory with tracking). SSC–SR–138, SSC Central Design Group, 1987.

[131] E. Forest and K. Ohmi. Symplectic integration for complex wigglers. KEK–92–14, Tsukuba, 1992.

[132] J. S. Berg, R. L. Warnock, R. D. Ruth, and E. Forest. Construction of symplectic maps for nonlinear motion of particles in accelerators. SLAC–PUB–6037, Menlo Park/CA, 1993.

[133] G. H. Hoffstaetter and M. Berz. Accurate and fast computation of high order fringe–field maps via symplectic scaling. *Nucl. Instr. Meth.* A(363):124–127, 1995.

[134] G. H. Hoffstaetter and M. Berz. Symplectic scaling of transfer maps including fringe fields. *Phys. Rev.* E 54(5):5664–5672, 1996.

[135] M. Berz. Symplectic tracking through circular accelerators with high order maps. In *Nonlinear Problems in Future Accelerators*, World Scientific, p. 288–296, 1991.

[136] E. Forest. Lie algebraic maps and invariants produced by tracking codes. *Particle Accelerators*, 22:15, 1987.

[137] Y. Yan. Performance of an implicit algorithm for symplectic one–turn–map tracking. SSCL–Preprint–157, SSC Central Design Group, 1993.

[138] I. M. Gjaja. A comparison of methods for long–term tracking using symplectic maps. In *Nonlinear problems in accelerator physics*, Institute of Physics. Conf. Ser. No. 131, p. 185–192, London, 1993.

[139] L. Schachinger and R. Talman. TEAPOT, a thin element program for optics and tracking. *Particle Accelerators*, 22:35, 1987.

[140] F. Willeke. Tutorial on modern tools of particle tracking. Lecture held at the CERN school on advanced accelerator physics in Rhodos. DESY–M–94–12, 1994.

[141] V. Balandin, N. Golubeva, and D. P. Barber. Studies of the behavior of proton spin motion in HERA-p at high energies. Part II: Acceleration of Polarized Protons in HERA. DESY–M–98–03, 1998.

[142] G. H. Hoffstaetter. Successive approximations for charged particle motion. *Ultramicroscopy*, Accepted, 2000.

[143] Ch. Weißbäcker. Nichtlineare Effekte der Spindynamik in Protonenbeschleunigern. *Diploma thesis, Darmstadt University of Technology*, 1998.

[144] Ch. Weissbaecker and G. H. Hoffstaetter. Nonlinear spin transfer maps. In [11].

[145] K. Balewski, R. Brinkmann, Ya. Derbenev, K. Flöttmann, *et al.* Studies of electron cooling at DESY. In *Proceedings of ECOOL99*, Uppsala, 1999.

[146] P. Wesolowski, K. Balewski, R. Brinkmann, Ya. Derbenev, and K. Flöttmann. An injector study for electron cooling at PETRA using a bunched beam. In *Proceedings of ECOOL99*, Uppsala, 1999.

[147] M. Gentner, D. Husmann, C. Steier, R. Brinkmann, and Ya Derbenev. On the possibilities of electron cooling for HERA. *Nucl. Instr. Meth.* A424:277–295, 1999.

[148] R. Brinkmann for the DESY electron cooling study group. Electron cooling studies for PETRA and HERA. In [11].

[149] S. Y. Lee and E. D. Courant. Tolerance of imperfections in high-energy circular accelerators for polarized protons. *Phys. Rev.* D(41):292–302, 1990.

[150] D. P. Barber, M. Vogt, and G. H. Hoffstaetter. The amplitude dependent spin tune and the invariant spin field in high energy proton accelerators. In *Proceedings EPAC98*, Stockholm, 1998.

[151] D. P. Barber, G. H. Hoffstaetter, and M. Vogt. The amplitude dependent spin tune and the invariant spin field in high energy proton accelerators. In *Proceedings SPIN98*, Protvino, 1998.

List of Figures

ACKNOWLEDGMENTS

I am very much in debt to all my academic teachers. H. Rose has introduced me to the field of nonlinear charged particle optics in electron microscopes, from M. Berz I learned much about the mathematics involved in describing weakly nonlinear systems, especially those which appear in particle accelerators. Many people have contributed to my understanding of accelerator physics, either as teachers, coworkers or friends. Especially I would like to mention D. Barber, R. Brinkmann, K. Brown, Ya. Derbenev, J. Ellison, H. Mais, T. Sen, R. Servranckx, F. Willeke, and K. Yokoya.

D. Barber's, J. Ellison's, K. Heinemann's, M. Vogt's, and K. Yokoya's ideas were very important for the work described here. The program SPRINT which was used for most of the simulations presented has been developed together with M. Vogt who worked with me as a doctoral student. I am thankful for this fruitful collaboration and that he has provided me with the data for the figures 2.11, 4.23, and 4.24. K. Yokoya has provided some essential routines for the implementation of the SODOM–2 algorithm in SPRINT. Some of the sections have an overlap with papers published together with D. Barber, K. Heinemann, and M. Vogt. They can be found in the bibliography. Thanks are due to D. Barber, M. Berglund, J. Ellison, H. Mais, and M. Vogt for their valuable suggestions to the manuscript.

Last not least, I wholeheartedly appreciate the support and patience of my wife Anke Hoffstätter without which much of my research would not have been done.